UNIVERSIDAD COMPLUTENSE DE MADRID
FACULTAD DE CIENCIAS BIOLÓGICAS
Departamento de Bioquímica y Biología Molecular I

INTERRUPTORES MOLECULARES EN LA GÉNESIS DE PRP PATÓGENAS : METIONILSULFÓXIDOS Y SUS MODELOS

MEMORIA PARA OPTAR AL GRADO DE DOCTOR
PRESENTADA POR

Silvia Lisa Ferrer

Bajo la dirección de la doctora

María Gasset Vega

Madrid, 2014

UNIVERSIDAD COMPLUTENSE DE MADRID
FACULTAD DE CIENCIAS BIOLÓGICAS
BIOQUÍMICA Y BIOLOGÍA MOLECULAR I

Interruptores moleculares en la génesis de PrP patógenas: Metionilsulfóxidos y sus modelos

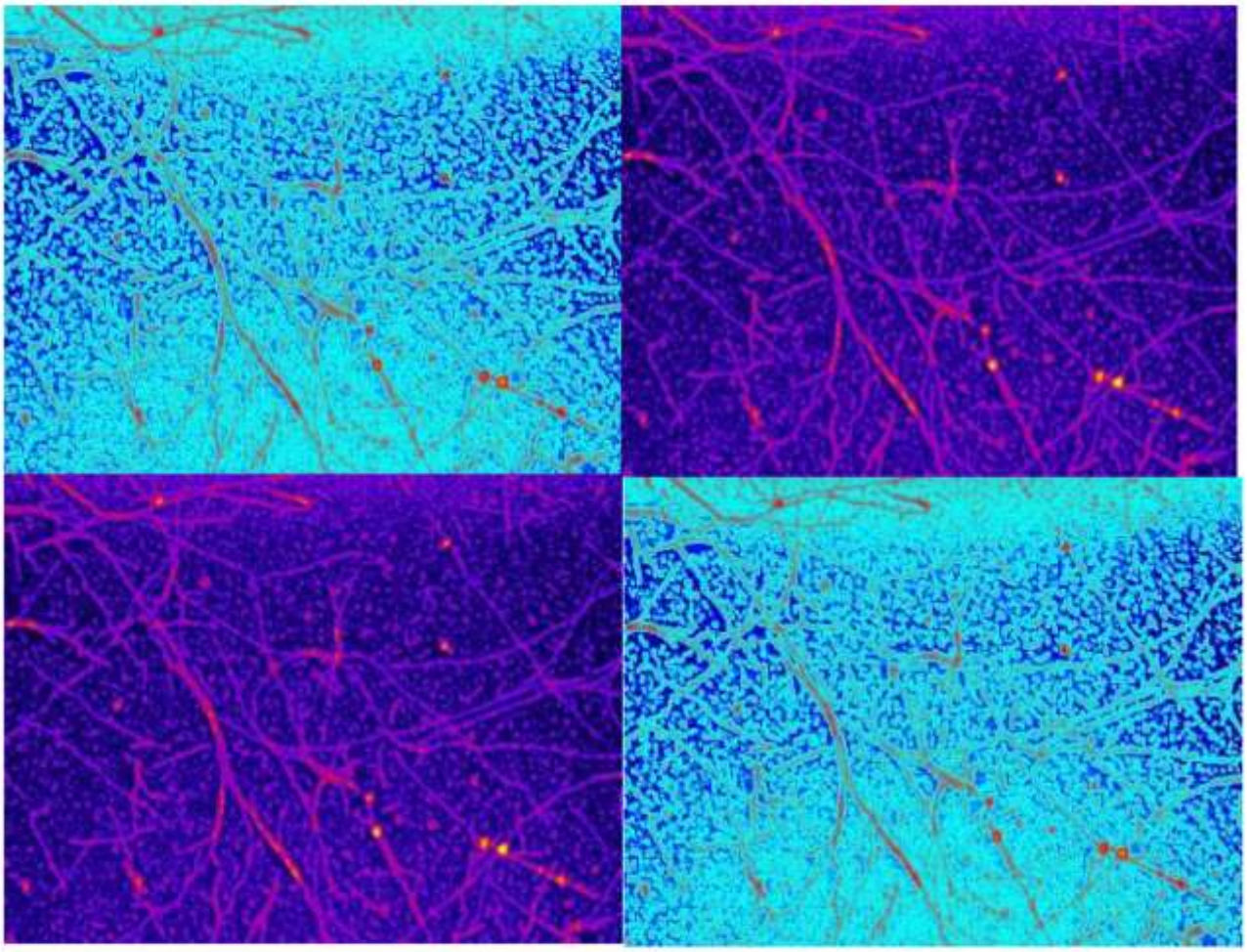

TESIS DOCTORAL
SILVIA LISA FERRER
Madrid 2013

UNIVERSIDAD COMPLUTENSE DE MADRID
FACULTAD DE CIENCIAS BIOLÓGICAS
BIOQUÍMICA Y BIOLOGÍA MOLECULAR I

Interruptores moleculares en la génesis de PrP patógenas: Metionilsulfóxidos y sus modelos

DIRECTOR DE TESIS:
María Gasset Vega

SILVIA LISA FERRER
Madrid 2013

María Gasset Vega, Investigadora Científica del CSIC

CERTIFICA, que el trabajo contenido en esta memoria, titulada "***Interruptores moleculares en la génesis de PrP patógenas: Metionilsulfóxidos y sus modelos***" y presentada por Dña. Silvia Lisa Ferrer, ha sido realizado en el Dpto. de Química-Física Biológica del Instituto de Química-Física "Rocasolano" del CSIC, y financiada por una beca FPI (BES-2007-14431) y por los proyectos SAF2006-00418 (MICINN), BFU2009-07971 (MINECO), una ayuda de la Fundación C.I.E.N-Fundación Reina Sofía y una acción de movilidad en la Universidad de Wyoming (15-04-2010 al 15-07-2010) para la realización de experimentos en el laboratorio del Prof. Hermann Schätzl. Además, los trabajos aquí presentados son originales y la responsabilidad de la autoría ha sido avalada por todos los autores.

En Madrid, a 27 de mayo de 2013

María Gasset, PhD
Investigador Científico del CSIC

A mi familia

El sabio no dice todo lo que piensa pero siempre piensa todo lo que dice

(Aristóteles)

Llegados a este punto, después de tantos años en el mundo de la investigación, ha llegado el momento de agradecer a todos aquellos que me han ayudado y han formado parte de mi vida durante todo este tiempo y que espero, sigan formando parte de la misma haya donde estemos. Espero no olvidarme de nadie.

En primer lugar agradecerle a la Dra. María Gasset todo el empeño que puso en que yo aprendiera y saliera adelante, ya que los inicios fueron duros, pero finalmente dieron sus frutos, y esto no hubiera sido así sin su apoyo, constancia y confianza en mí. ¡GRACIAS!

Agradecer a mis compañeros y amigos, Rosa y Javi, por haberme ayudado cuando necesitaba tener terminado los experimentos para "ayer" y ayudarme en todo momento a poner a punto las cosas y pelearse conmigo para que todo saliera adelante. Además de todo eso, agradeceros la alegría que transmitís todas las mañanas y por aguantarme en mis malos momentos, que no han sido pocos en esta última etapa, pero que gracias a vosotros, se me olvidaban rápido. A Lara, que aunque estuvo poco tiempo, siempre pude contar con ella a la hora de ayudarme en un momento de urgencia. A Maru, por haberme enseñado la parte experimental y haberme llevado de la mano en mis inicios, sin su presencia, todo hubiera sido muy diferente. Y también, al resto de personas que pasaron por el laboratorio antes que yo, Gema, Rene, José, Silvia, Andrea y Juan Carlos, ya que si ellos no hubieran puesto a punto el laboratorio en su momento, mis resultados no serían los mismos. También agradecer a Hermann Schätzl y Sabine Gilch por haberme acogido en Laramie durante tres meses y enseñarme los recursos necesarios para poder seguir adelante en el último periodo de mi tesis. Al igual que a Bea Domingo, por haberme acogido en su casa de una forma tan agradable y desinteresada, y anteponer mis cosas a las suyas, y a Juan Llopis por su amabilidad y paciencia en mis inicios en microscopia confocal. Lo mismo a Ruth cuya colaboración fue de agradecer en los inicios de este trabajo

A todos los que me habéis acompañado en mi etapa del Rocasolano: Laura, Bea, Sheima y Yesi, que se fueron pero siempre han estado ahí; Noe, Cris, Palma y Lupe, por estar al "fondo del pasillo"; Soraya y Flor, por esas comidas tan amenas; a Fer, porque sin él, esta tesis no tendría formato; y a Javi, por acudir siempre a mi llamada quejicosa.

Y qué decir de toda la gente que he conocido en Madrid desde que llegue: a Jacobo, Alexia y Carmen, mis primeros compañeros de piso con los que viví tan buenos momentos y tantas risas; a Raquel, que ha vivido esta tesis como si fuera suya; a Laura, por estar dispuesta siempre a tomar unas cañitas; a Maru, Jorge y a Edu, por sacarme de paseo cuando no tenía ganas; a Fer, por sacarme siempre una sonrisa; a Erica, Elena y Lourdes por estar ahí, y a Anita, por entender los abrazos cortos.

De mi gente de Salamanca, a Bego, Marta, Carmen, Seila y Lucia, por conducirme por este camino, ya que todas terminamos en este mundo, gracias por apoyarme, escucharme y esas reuniones de fin de semana tan amenas que deberíamos repetir todos los años para hacer terapia; a Marta y a Almu, cuyas visitas a Madrid, han amenizado muchas de mis tardes.

A la gente de mi tierra, Ana, Rafa, Vane, Humberto y el pequeño renacuajo, Diego, gracias por preocuparos por mí y por reservarme todos los sábado que yo voy a casa para pasarlo junto a vosotros.

Por ultimo pero no por ello menos importantes, más bien al contrario, a mi familia, y en especial a mis padres, que han aguantado mucho, y siempre se han mostrado compresivos y me han apoyado en todo momento. Sin ellos, esto no hubiera sido posible.

A todos los que me habéis acompañado en este largo camino, solo puedo deciros, gracias por estar ahí.

ÍNDICE

ABREVIATURAS

AG	Aparato de Golgi.
CD	Dicroísmo circular.
CJD	Enfermedad de Creutzfeldt-Jakob.
^{Ctm}PrP	Forma transmembrana de PrP con el dominio C-terminal hacia el lumen del RE.
^{Cyt}PrP	Forma citosólica de PrP
RE	Retículo endoplasmático.
ERAD	Degradación asociada al retículo endoplasmático.
FFI	Insomnio familiar fatal.
FTIR	Espectrometría de infrarrojo por transformada de Fourier.
GdnHcl	Cloruro de guanidina.
GPI	Glicosilfosfatidilinositol.
GSS	Síndrome de Gerstmann-Sträussler-Scheincker.
HC	Segmento hidrofóbico.
HxD	Intercambio hidrógeno por deuterio.
PrP$^{-/-}$ y KO	Ratones knockout para PrP.
Msr	Metionina sulfóxido reductasa.
NMR	Resonancia magnética nuclear
^{Ntm}PrP	Forma transmembrana de PrP con el dominio N-terminal hacia el interior del ER.
OR	Octapéptido repetido.
ORF	Pauta de lectura abierta.
PK	Proteinasa K.
PRNP	Gen de la proteína del prion.
PrP	Proteína del prion.
PrP^{C}	Proteína celular del prion.
PrP^{Sc}	Proteína patógena del prion (Sc de *scrapie*).
QC	Sistema de control de calidad.
ROS	Especies reactivas de oxígeno.
rSHaPrP(23-232)	Proteína recombinante que representa la secuencia madura de la proteína de PrP de hámster sirio.
SDS	Dodecilsulfato sódico.
^{Sec}PrP	Forma de secreción de PrP coincidente con la visión de PrP^{C}.
SeMet, SeM	Selenometionina.
SNC	Sistemas nervioso central.
SS	Secuencia señal.
TSE	Encefalopatía espongiforme transmisible.
UPR	Respuesta a proteínas mal plegadas.

Introducción

Las ideas no duran mucho, hay que hacer algo con ellas

(Santiago Ramón y Cajal)

1.1 LAS ENFERMEDADES CONFORMACIONALES O PROTEINOPATÍAS.

El funcionamiento de una célula y su relación con el entorno, descansa sobre una red compleja de comunicación entre proteínas, en la que sus estructuras desempeñan un papel esencial. La ruta mediante la cual las proteínas adquieren su estructura se denomina plegamiento y, en las células, este proceso está sometido a un control de calidad muy riguroso con el fin de corregir y evitar sus errores. Sin embargo, este proceso no es del todo eficaz y, algunas proteínas plegadas erróneamente agregan y se acumulan dando lugar a estados conocidos como proteinopatías o enfermedades conformacionales (1-4).

Las enfermedades conformacionales fueron descritas hace mucho tiempo, pero hasta 1997 no se enunció su agrupamiento, y es en 2005 cuando se las reconoce como un grupo de trastornos (**Tabla 1**) (1, 5-7). El denominador común a todas estas patologías es la permisividad de una ruta de plegamiento alternativo que permite la adopción de una conformación no nativa estable, con la aparición de una función tóxica y la pérdida de la función biológica de la proteína en cuestión (8-14). A estos estados conformacionales diferentes a los nativos se les denomina coloquialmente "*misfolded*" y su formación está asociada a causas diversas como mutaciones en la secuencia génica, errores en el proceso de traducción, alteraciones en el procesamiento y modificación post-traduccional, en el tráfico y destino subcelular, a cambios inducidos por el entorno, entre otros (4, 9, 13, 15-19).

PATOLOGÍA		PROTEÍNA	PROTEINOPATÍA	Ref
SISTÉMICA		Anticuerpos, transtiretina	Amiloidosis	20, 31
		β2-microglobulina	Amiloidosis asociada a hemodiálisis	5
		CFTR	Fibrosis cística	29
		α1-antitripsina	Deficiencia de α1- antitripsina	6
LOCALIZADAS	ISLOTES PANCREÁTICOS	IAPP	Diabetes tipo II	24
	CRISTALINO	γ-cristalina	Cataratas	4
	SISTEMA NERVIOSO	Pèptido Aβ-amiloide, Tau	Alzheimer	22, 33
		PrP	Encefalopatía espongiforme transmisible	34
		α-sinucleína, LRRK-2, GBA	Parkinson	25, 32, 35
		SOD1, TDP-43, FUS, ubicuitina-2, C9RANT	Esclerosis lateral amiotrófica	21, 26, 27, 28, 30
		Huntintina	Huntington	1
		Ataxina	Ataxia espinocerebelar	23

Tabla 1. Enfermedades conformacionales. Ejemplos clásicos de enfermedades relacionadas con errores de plegamiento de proteínas y acumulación de confórmeros aberrantes, clasificados en función de la localización tisular.

Dentro de las proteinopatías, las patologías neurodegenerativas ocupan una posición especial, dado el crecimiento de su incidencia y la posibilidad de diseñar soluciones preventivas. Las proteínas implicadas en el desarrollo de estas enfermedades son muy diversas en secuencia, en estructura, en función y en localización subcelular, entre otras (13, 14, 34, 36, 37). Sin embargo, todas estas proteínas existen en un estado benigno durante años y agregan en las neuronas longevas produciendo daños tisulares irreversibles que impactan en la integridad estructural y funcional del sistema nervioso (38-44). En el caso de estas proteínas todo indica que la ruta de plegamiento alternativo existe, no es accidental, y es el fallo en la atenuación de su producción durante el envejecimiento, o la desregulación de la proteostasis,

lo que permite la manifestación de los efectos tóxicos (45-50). Por un lado, las chaperonas encargadas de guardar la fidelidad de la ruta disminuyen su eficacia según van envejeciendo (51-58). Por otro lado, las proteínas encargadas de eliminar daños como los causados por las especies reactivas del oxígeno (ROS) pierden efectividad y favorecen la acumulación de productos de oxidación que inciden en la conformación proteica (59-66). La potenciación de estas dos vías de acumulación de errores en las proteínas y la falta de acción de las rutas encargadas de solucionarlos o UPR (*Unfolded Protein Response*) (45), favorecen la aparición y la acumulación de agregados que terminan desencadenando la muerte celular (45, 67-74) (**Figura 1**).

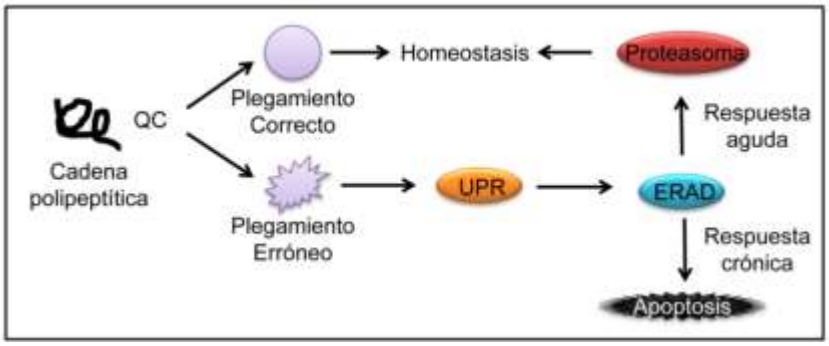

Figura 1. Controles de la ruta de plegamiento de proteínas *in vivo*. Una vez translocada al lumen del retículo endoplasmático (RE) la cadena polipeptídica es sometida a un control de calidad (QC) durante su plegamiento. Si este es correcto, la cadena polipeptídica sigue su curso biológico. Si por el contrario, el plegamiento no es correcto se activa la vía de respuesta de proteínas mal plegadas (UPR) y la activación de una ruta de estrés (ERAD). Si la respuesta es aguda, las proteínas mal plegadas son retrotranslocadas vía ERAD y degradadas por el proteasoma reestableciéndose el equilibrio. En cambio, si es crónica o sostenida, termina provocando la muerte celular por apoptosis.

La aparición de conformaciones alternativas a la nativa en estas proteínas, ya sea por modificaciones covalentes como las oxidaciones, por la unión de ligandos o por cualquier otro motivo, exponen regiones hidrofóbicas que permiten procesos de autoagregación (75). Estas especies reactivas para la agregación pueden inicialmente estabilizarse en forma de oligómeros amorfos o bien oligómeros solubles (1, 2, 13, 76). Estos últimos pueden actuar de núcleos de crecimiento y conducir hacia un proceso de polimerización no covalente con la formación de protofibrillas, que a su vez se ordenan en supraestructuras conocidas como fibras amiloides (1, 2, 13, 77) (**Figura 2**). El término amiloide procede del campo de la botánica, e inicialmente se empleó para describir los acúmulos insolubles, resistentes a SDS y a proteasas de proteínas capaces de teñirse con el Rojo Congo y las Tioflavinas T y S (1, 5, 78-80).

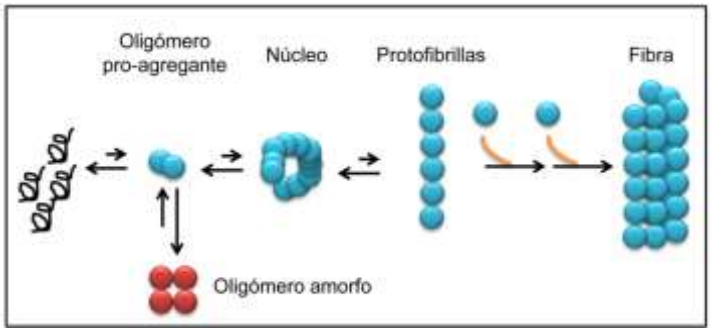

Figura 2. Procesos de autoagregación. Las proteínas con una conformación alternativa a la nativa tienen la capacidad de auto´-agregar y estabilizarse como oligómeros amorfos (rojo) o generar oligómeros solubles (azul). Estos últimos se asocian hasta formar un núcleo que crecerá hasta protofibrillas que, al ensamblarse, conducirán a fibras amiloides.

Estructuralmente, la unidad básica de las fibras amiloides es la lámina-β cruzada definida por un determinado patrón de difracción de rayos X (79). La capacidad de una cadena polipeptídica para adoptar esta supraestructura viene determinada por la presencia en su secuencia de hexapéptidos capaces de adoptar estructuras β y dar lugar a láminas, de forma que el acoplamiento entre dos láminas-β se produce mediante el entrelazamiento de las cadenas laterales como los dientes de una cremallera (*steric zipper*) (81) (**Figura 3**). El conjunto de secuencias de estos hexapéptidos se denomina amiloma, y dado que en una misma proteína pueden existir diversos segmentos y que el ensamblaje de estos no es necesariamente único, una cadena polipeptídica puede formar distintos tipos de fibras (82-86). Esta propiedad, conocida de forma genérica como polimorfismo, se ha correlacionado con diferencias en la estabilidad y la actividad *in vivo* como si se tratase de cepas (87, 88).

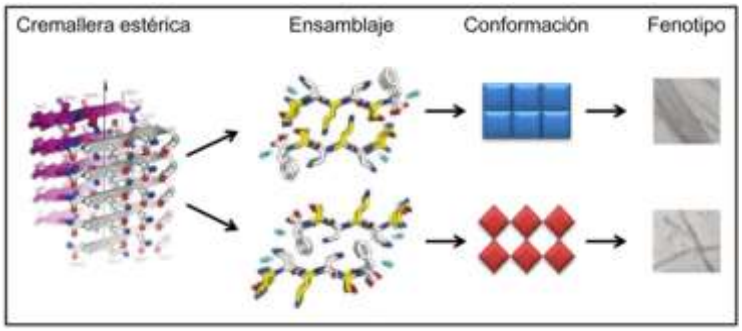

Figura 3. Polimorfismo de las fibras amiloides. La inter-digitación de dos láminas-β no es única, sino que puede producirse de varias formas y dar lugar a diferentes formas fibrilares. (Imágenes tomadas de Wiltzius, Landau y cols 2009 (88) y Eisenberg y Jucker 2012 (89)).

Hay que resaltar que dado que las fibras amiloides representan estados de máxima compactación, estas estructuras no sólo acompañan a estados patológicos sino que tienen su vertiente beneficiosa en los conocidos amiloides funcionales (**Tabla 2**). En estos casos, el ensamblaje/desensamblaje es un proceso regulado que depende de cambios de entorno, de pro-secuencias o de un iniciador heterólogo, entre otros (90-97).

PROTEÍNA	ESPECIE	FUNCIÓN DEL AMILOIDE	Ref.
Curlin	*Escherichia coli*	Colonización de superficies inertes y mediación en la unión a proteínas del hospedador	98
Chaplin	*Streptomyces coelicolor*	Disminución de la tensión superficial del agua y desarrollo de las hifas aereas	93
Ure2p (prion)	*Saccharomyces cerevisiae*	Utilización de fuentes pobres de hidrógeno	99
Sup35p (prion)	*Saccharomyces cerevisiae*	Dotación de nuevos fenotipos [(PSI+)]	94
Rnq1p (prion)	*Saccharomyces cerevisiae*	Desconocida	95, 101
HET-s (prion)	*Podospora anserina*	Iniciación de la muerte celular	97
Proteínas del corion	*Bombix moro*	Protección del oocito y el embrión frente a factores externos	96
Pmel	*Homo sapiens*	Formación de la melanina en los melanosomas	90
Pro-glucagón	*Homo sapiens*	Almacenamiento	100

Tabla 2. Amiloides funcionales. Ejemplos de proteínas cuyos amiloides desempeñan un papel fisiológico.

Para explicar la formación de amiloides se han elaborado diversos modelos cinéticos basados en una reacción de polimerización nucleada por condensación no covalente (**Figura 4**) (102-108). Este proceso consta esencialmente de dos fases: la fase de nucleación y la fase de elongación. En la fase de nucleación (proceso lento) las cadenas polipeptídicas, que se encuentran en un estado de pro-agregación, se unen para dar lugar a un núcleo oligomérico, y el tiempo que transcurre desde un estado soluble en disolución hasta el inicio de la formación del agregado se conoce como fase de retardo (lag) (103). La segunda fase es la de crecimiento o elongación, y en ésta el núcleo crece rápidamente formando polímeros de mayor tamaño que terminan ensamblándose para dar como producto final la fibra amiloide. Además, dado que los distintos polímeros pueden fragmentarse y generar nuevas superficies de crecimiento con propiedades variables, este modelo sencillo puede transformarse incluyendo pasos elementales de rupturas, ramificaciones y crecimientos (9, 109-111).

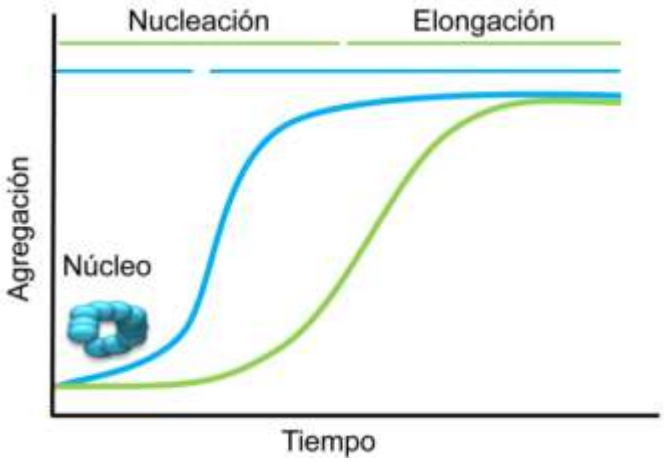

Figura 4. Modelo cinético de polimerización nucleada. La formación del amiloide tiene dos fases temporales. Una primera fase de nucleación es lenta, y la segunda fase, la de elongación es rápida e incluye el crecimiento del núcleo por incorporación de unidades agregantes. En presencia de un núcleo el proceso se acelera.

La propiedad de crecimiento en las fibras amiloides determina sus propiedades de autopropagación y perpetuación *in vivo*. Cuando esta propagación ocurre de forma transcelular (entre células) las fibras amiloides se convierten funcionalmente en prionoides. Cuando la capacidad de transmisión de la estructura y su resultado fisiológico o su fenotipo es de mayor alcance y afecta a una población, entonces las fibras pasan a definirse como priones (112-115).

1.2. LAS PRIONOPATÍAS: UN MODELO COMPLEJO DE ENFERMEDAD CONFORMACIONAL.

Las prionopatías o encefalopatías espongiformes transmisibles (TSE) son el conjunto de neurodegeneraciones letales de mamíferos resultantes de la alteración del metabolismo de la proteína del prion celular (PrP^{C}) y, caracterizadas por la aparición de confórmeros neurotóxicos (^{Ctm}PrP) y autopropagativos o priones (PrP^{Sc}) (116-123). Dentro de estas, se encuentran las encefalopatías espongiformes bovina, de visón y de felinos, la tembladera (o *scrapie*) en ovejas y cabras (124, 125) y la enfermedad del desgaste crónico de ciervos y alces. En humanos se han descrito, Creutzfeldt-Jakob (CJD) y su variante (126, 127), el Kuru (128), el insomnio

familiar fatal (FFI) (129), el síndrome de Gerstmann-Sträussler-Sheinker (GSS) y la prionopatía con sensibilidad variable a proteasa (**Tabla 3**).

Las prionopatías se presentan bajo tres formas: genética, esporádica y adquirida. Las formas genéticas están relacionadas con mutaciones en la línea germinal del gen que codifica para PrP (*PRNP*) (130-133). Las formas adquiridas o infecciosas se originan como resultado de la exposición directa al agente causal (134-136). Por último, las formas esporádicas se atribuyen a exposiciones accidentales y desconocidas al agente causal, a posibles mutaciones genéticas de naturaleza somática, o a fallos en el sistema de control de calidad de la célula favorecidos por el envejecimiento (74, 131-133, 137-145). Desde el punto de vista clínico, estas patologías se caracterizan por la aparición de pequeños cambios en el comportamiento social del individuo que se transforman en cuadros de ataxia y demencia de evolución rápida (146-148). La evaluación post-morten del sistema nervioso central (SNC) muestra una lesión tisular compleja constituida por una combinación variable de gliosis, hipertrofia de los astrocitos, espongiosis con vacuolización de localización variable (en función del tipo de enfermedad, la región del SNC afectada es distinta: córtex en demencias, cerebelo en ataxias, etc) y una pérdida neuronal (149-153).

Tabla 3. Enfermedades priónicas humanas.

Las enfermedades priónicas o prionopatías pueden ser adquiridas, esporádicas o genéticas. En las formas genéticas, distintas mutaciones puntuales conducen a una misma patología y sólo la mutación D178N en función del polimorfismo 129 M/V da lugar a dos fenotipos diferentes.

ENFERMEDAD		SIGLAS	MECANISMO DE PATOGÉNESIS	MUTACIÓN [Ref]
Creutzfeldt-Jakob	Esporádica	sCJD	Mutación somática o conversión espontánea de PrP^{C} en PrP^{Sc}	G114V [157], R148H [161], D178N(MV129) [140], V180I [134], T183A [160], E196K [162], E200K [134], V203I [162], R208H [166], V210I [159], E211Q [162], M232R [134], P238S [155]
	Familiar	fCJD	Mutación de *PRNP*en la línea germinal	
	Iatrogénica	iCJD	Infección por equipo médico contaminado o transplante de órganos contaminados	124
	Nueva Variante	vCJD	Exposición a priones bovinos	126, 127
Síndrome de Gerstmann-Sträusler-Scheinker		GSS	Mutación de *PRNP* en la línea germinal	P102L [165], P105L [167], A117V [158], Y145Stop [156], Q160Stop [154], F198S [164], D202N [163]
Insomnio familiar fatal	Familiar	fFI	Mutación de *PRNP* en la línea germinal	D178N(MM129) [140]
	Esporádica	sFI	Mutación somática o conversión espontánea de PrP^{C} en PrP^{Sc}	
Kurú		-	Rituales de canibalismo	128
Prionopatía con sensibilidad variable a proteasa	Esporádica	VPSP	Desconocido	167

1.2.1. PrP: La proteína del prion.

PrP está codificada en el gen *PRNP* (**Figura 5**), localizado en el cromosoma 20 en humanos y en el 2 en ratones (169-172). Este gen está organizado en varios exones, localizándose la pauta de lectura abierta (ORF) de PrP en el exón 3´ (145, 173-180). *PRNP* se expresa principalmente en neuronas y otras células del SNC, pero también lo hace de forma significativa en el sistema linforreticular y en músculo esquelético (181, 182). El gen *PRNP* se encuentra altamente conservado durante la evolución, presentándose en mamíferos, aves y peces, sugiriendo una cierta esencialidad (183-185). Sin embargo, a pesar de dicha conservación, la eliminación de la expresión de *PRNP* solo ha permitido establecer fenotipos de resistencia a la infección por priones (183, 184) y de inestabilidad de la mielina durante el envejecimiento (186).

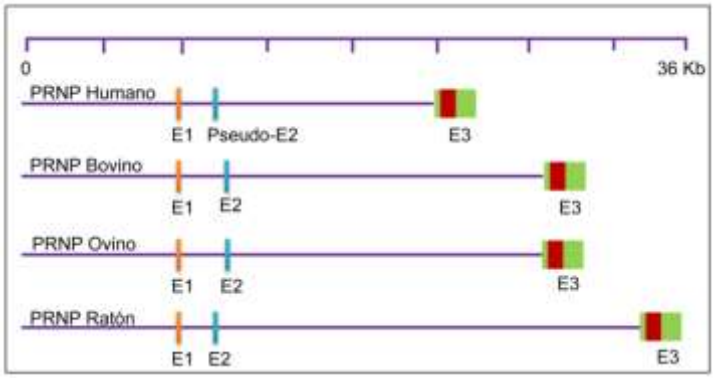

Figura 5. Estructura del gen *PRNP* en mamíferos. *PRNP* contiene dos exones no codificantes, E1 (naranja) y E2 (azul), y un exón codificante (E3), que contiene la pauta abierta de lectura (ORF, rectángulo rojo), separados por intrones de distinta longitud dependiendo de la especie. Los transcritos maduros resultantes del procesamiento consisten en la fusión de E1-E2-E3 (145, 173-180, 187).

La cadena de PrP está constituida por unos 253 aminoácidos, dependiendo de la especie, con una organización muy particular (**Figura 6**). Los primeros 22 aminoácidos N-terminales corresponden a una secuencia señal (SS) de proteínas que se segregan en la ruta de secreción con una estructura tripartita característica (segmentos n, h y c) y que será escindida durante el proceso de translocación cotraduccional (188-191). Entre los residuos 51 y 91 hay un nonapéptido seguido de 4 repeticiones idénticas de un octapéptido (OR) que funciona como sitio de unión de ligandos entre los que destaca el catión Cu^{2+} (192-197). Esta región repetitiva está flanqueada por dos motivos ricos en residuos básicos (CC1 y CC2) que son responsables de la unión de polianiones (198-204). La cadena continúa con un segmento hidrofóbico (HC) que presenta un comportamiento complejo. Este segmento aparece como una región desordenada en los modelos estructurales 3D de PrP^{C}, como hélice transmembrana en las formas integradas en la membrana de PrP (^{Ctm}PrP y ^{Ntm}PrP) y aislado forma agregados fibrilares ricos en estructura β con propiedades de amiloides (205-208).(M129V en humanos, M132L en reno) (210, 211), dos sitios consenso de N-glicosilación (N181, N197) (212) y dos residuos de Cys que forman un puente disulfuro el cual estabiliza la estructura nativa de PrP^{C} (213). La región más distal del extremo C-terminal está constituida por una región altamente hidrofóbica, que es escindida durante el proceso de maduración y remplazada por un grupo GPI (214, 215), que dicta la unión a los dominios lipídicos conocidos como *rafts* (212, 216, 217).

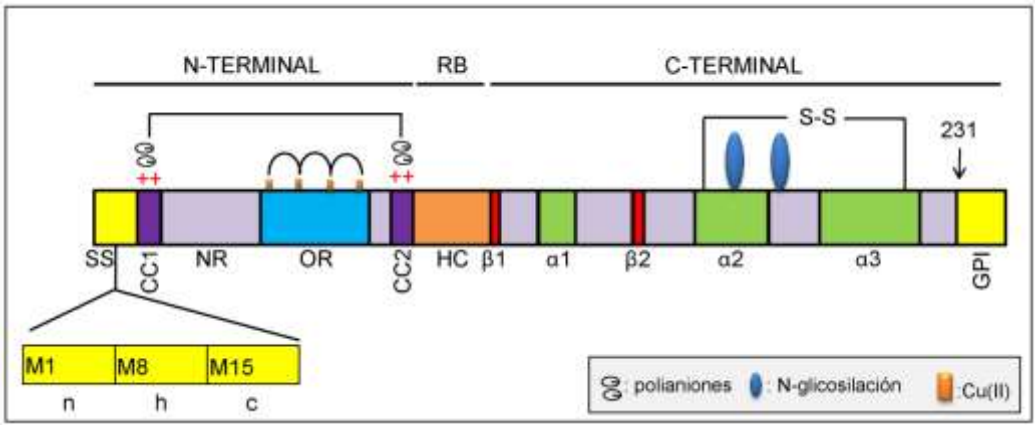

Figura 6. Organización de la cadena polipeptídica de PrP. La cadena polipeptídica de PrP está organizada en dos dominios, N- y C- terminal con una región bisagra (RB) hidrofóbica. El dominio N-terminal incluye la secuencia señal (SS, amarillo) estructurada en las tres regiones, n, h y c, donde, además de la metionina de inicio (M1), hay una Met en la posición 8 en HuPrP y 15 en HaPrP. A continuación, se encuentran dos regiones repetitivas, nona- (NR, lila) y octapeptídos (OR, azul), flanqueadas por dos segmentos ricos en aminoácidos básicos (CC1 y CC2, violeta). La cadena prosigue con una región hidrofóbica HC (naranja) que da entrada al dominio C-terminal. Este dominio contiene varios segmentos altamente conservados, y aloja elementos de estructura secundaria (hélices-α en verde y cadenas β en rojo) y posiciones susceptibles de sufrir modificaciones post-traduccionales (puente disulfuro entre C179 y C214, glicosilaciones en N181 y N179). Al final de la cadena se encuentra una secuencia hidrofóbica de 22 aminoácidos, la cual, al escindirse, permite la incorporación de un grupo GPI en S231.

1.2.2. Diversidad molecular de PrP^C: traducción y translocación.

El diseño de la cadena de PrP, en principio sencillo, contiene encriptada la información para un caso de diversidad molecular complejo. La presencia de una segunda metionina a cualquiera de los lados de la región h de la secuencia señal (M8 en humanos, M15 en roedores) (**Figura 6**) permite un inicio de traducción minoritario y la biosíntesis de una cadena que carece de una secuencia señal funcional (218, 219). Este código es responsable de la biosíntesis de PrPΔ1-7/14 que se distribuye en el núcleo y en el citoplasma y que, en ausencia de la forma mayoritaria, impide la división celular (219).

Por otra parte, la cadena traducida a partir del sitio de inicio canónico (M1) se segrega dentro de la ruta de secreción y, como resultado de la interacción con los componentes de la maquinaria de translocación, da lugar a tres formas que difieren en su topología: ^{Sec}PrP (forma resultante de la translocación completa), ^{Ntm}PrP (forma transmembrana que proyecta la región 22-111 al lumen del RE y la región 121-253 al citosol) y ^{Ctm}PrP (forma transmembrana que proyecta el dominio C-terminal al lumen del RE y la región 22-111 al citosol). Además, los errores de plegamiento de cualquiera de estas tres formas son detectados por sensores de estrés del RE que activan la ruta ERAD lo que provoca la retrotranslocación de estas cadenas al citosol aumentando así la población de PrP citosólica (^{Cyt}PrP) (**Figura 7**) (118, 189, 220-225).

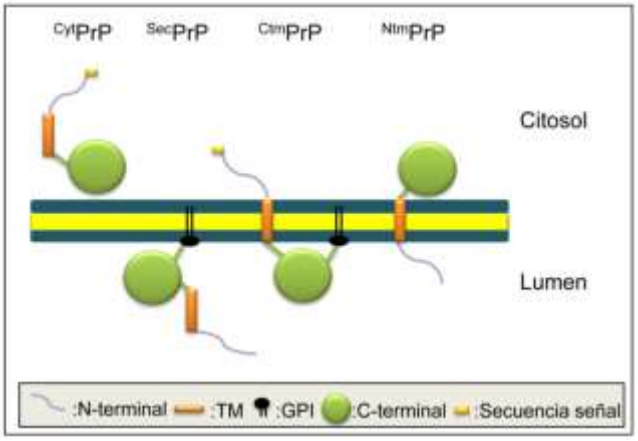

Figura 7. Variabilidad topológica de PrP generada en su biogénesis. La cadena naciente de PrP da lugar a cuatro formas ^{Cyt}PrP, ^{Ctm}PrP, ^{Ntm}PrP y ^{Sec}PrP, diferenciables por su localización, interacción con la membrana y su cadena. La secuencia señal se representa por un rectángulo amarillo, el dominio N-terminal por una línea lila, la región HC por una línea naranja, el dominio C-terminal por un círculo verde, y el grupo GPI por un círculo negro. La presencia de secuencia señal en ^{Ctm}PrP es controvertida (226).

1.2.3. Diversidad covalente de PrP^{C}: modificaciones post-traduccionales y procesamientos proteolíticos.

Debido a la diversidad molecular de PrP, la operatividad de las señales que determinan la posibilidad de una modificación covalente está condicionada a la coincidencia en la localización de la forma de PrP biosintetizada y los sistemas enzimáticos implicados en la modificación y/o procesamiento. Además, dado que algunas modificaciones van a ser dinámicas, la extensión de las mismas es un indicador del estado del tráfico de la proteína.

De forma general, la maduración de las cadenas de PrP nacientes que se segregan en la ruta de secreción se inicia con la escisión de la secuencia señal (SS) por la peptidasa señal en el lumen del RE. A medida que la cadena emerge, los residuos N181 y N197 (numeración de sHaPrP) pueden ser objeto de reacciones de glicosilación, de forma que los núcleos de azúcar sufrirán modificaciones hasta alcanzar su forma madura en el aparato de Golgi (AG) (212, 227, 228). Cerca de los sitios de glicosilación se encuentran los residuos C179 y C214 implicados en la formación de un puente disulfuro intramolecular (213). Finalmente, cuando la cadena ha sido completamente translocada al lumen del RE, se produce una reacción de transesterificación en la S231 de forma que se libera la región C-terminal y se introduce un grupo GPI (215). La presencia de este grupo GPI va a conferir a PrP la capacidad de residir en los dominios de membrana conocidos como balsas lipídicas o rafts (216, 229-231), y de ser liberada enzimáticamente de la superficie celular por la acción de fosfolipasas específicas de GPI y proteasas (*shedding*)). Debido a las restricciones mencionadas, solo ^{Sec}PrP sufrirá todas las modificaciones covalentes detalladas, mientras que ^{Ntm}PrP y ^{Cy}PrP no presentarán las modificaciones covalentes que ocurren en el dominio C-terminal. Por otra parte, el análisis de PrPΔ1-7/14 ha demostrado su capacidad de sufrir sumoilaciones que podrían correlacionarse con estados ON/OFF de su función antiproliferativa (219).

Los estudios realizados con anticuerpos dirigidos frente a los dominios N- y C-terminales han demostrado que la cadena de PrP contiene dos sitios de procesamiento proteolítico (216, 232-240). El sitio de escisión α, localizado entre los residuos 111 y 112 (secuencia de HuPrP), genera los fragmentos N1 y C1 (233). Esta ruptura se asigna a la acción de la α-secretasa (239). Por otra parte, el sitio de escisión β, que tiene lugar entre los residuos

89 y 90, produce los fragmentos N2 y C2 (**Figura 8**) y su origen se asigna a procesos potenciados por las ROS (241). Este procesamiento tiene implicaciones esenciales en las patologías de PrP. Así, la escisión α parece ser beneficiosa ya que genera por un lado el fragmento N1 con propiedades neuroprotectoras (242, 243) y por otro, el fragmento C1, que no pudiendo transformarse en forma PrP^{Sc}, actúa de inhibidor del proceso de amplificación de priones (244). Por el contrario, la escisión β genera formas compatibles con la enfermedad (233). Recientemente se ha descrito un sitio adicional próximo al extremo C-terminal, generando los segmentos N3 y C3, donde están implicadas la acción de metaloproteasas cuyo papel podría estar relacionado con la liberación desde la superficie celular (245, 246).

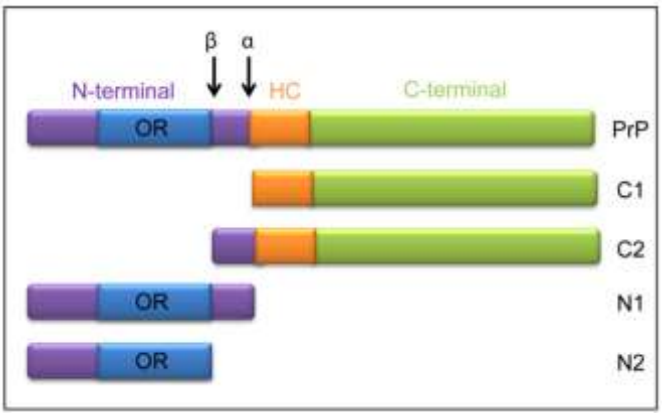

Figura 8. Formas de la cadena de PrP detectadas *in vivo* resultantes de su procesamiento. Esquema de la generación de los fragmentos N1, N2, C1 y C2 y las regiones más significativas de cada uno. El sitio α (111/112) genera los fragmentos N1 y C1 que comienza en la región hidrofóbica (HC) y el sitio β (89/90), que da lugar a los fragmentos N2 y C2 que comienza en la región de las octarepeticiones (OR).

1.2.4. La función de PrP^{C}.

Los estudios funcionales de PrP^{C} se iniciaron en la década de los 80 mediante el empleo de transgénesis. Los estudios pioneros del grupo de Prusiner (173, 247-249) permitieron relacionar la secuencia con la aparición espontánea de patología y con la susceptibilidad a la infección por priones. Más tarde, en 1992 la generación de la primera línea de ratones transgénicos $PrP^{-/-}$ sorprendentemente no permitió observar ningún fenotipo de alteración compatible con el grado de conservación del gen (184). No obstante, esta línea de ratones junto con otras similares se convirtieron en herramientas fundamentales para los estudios de la relación estructura-función (181). En este sentido, los estudios de transgénesis han sido esenciales para determinar el papel de PrP^{C} como iniciador y elongador de los priones tipo PrP^{Sc}, como determinante de la integridad estructural y funcional de la mielina en el envejecimiento, y como receptor de oligómero neurotóxicos (183, 186, 250, 251). Por otra parte, la generación de modelos recombinantes y celulares ha permitido avanzar en la funcionalidad de PrP en reacciones de reconocimiento molecular y sus repercusiones en el metabolismo celular (**Tabla 4**).

Tabla 4. Funciones asignadas a PrP.
Resumen de las funciones atribuidas a PrP^{C} desde los puntos de vista: fisiológico, celular e interacción molecular.

FUNCIÓN	PROCESO	REF.
Fisiológica	Interacción con PrP^{Sc} y regulación de su perpetuación	183
	Protección de la integridad estructural y funcional de la mielina durante el envejecimiento	186
	Regulación de las convulsiones inducidas por kainato	266
	Regulación de los ritmos circadianos	267
	Regulación en el desarrollo del bulbo olfatorio	259
	Regulación en el desarrollo de las células T y STEM	258, 272
Celular	Diferenciación neuronal	261
	Transmisión sináptica	254
	Función antiapoptótica por unión a Bcl-2	259
	Protección frente al estrés oxidativo	265
	Neuroprotección	262, 264
	Recepción de oligómeros tóxicos (Aβ, PrP, Sup35, péptidos β)	250, 251
Molecular (Interacción)	Cationes (Cu^{2+}, Zn^{2+})	270, 271
	Polianiones (GAGs, ácidos nucleicos, fosfolípidos, cromatina)	252, 253, 255, 263
	Proteínas (BiP, GFAP, NCAM, Grb2, LRP, laminina)	256, 257, 266, 269

1.2.5. PrP y su diversidad estructural: priones, amiloides y otras formas tóxicas.

El proceso molecular central de las proteinopatías de PrP es la conversión estructural de PrP^{C} en un conjunto de confórmeros alternativos con propiedades autopropagativas (infecciosas) y/o neurotóxicas que de forma colectiva se agrupan bajo el término PrP^{Sc} (273). PrP^{Sc} tiene la capacidad de actuar como molde e imponer su conformación sobre PrP^{C} que actúa de precursor y amplifica la forma de PrP^{Sc} inicial (273, 274) (Ver más adelante). Esta reacción de amplificación *in vivo* produce lesiones histológicas y se caracteriza por su tiempo de incubación y la región del SNC afectada (273). Estos dos parámetros junto con el comportamiento frente al tratamiento con proteinasa K (PK) (sensibilidad, resistencia y los fragmentos de resistencia), la solubilidad en detergentes aniónicos no desnaturalizantes, y la exposición diferencial de epítopos en los tratamientos con concentraciones crecientes de desnaturalizantes permiten clasificar PrP^{Sc} en diversos subconjuntos conocidos como "cepas" (87, 275, 276) (**Figura 9**). El resto de formas neurotóxicas comparten con las formas infecciosas algunas características como la agregación y la insolubilidad en detergentes pero generalmente son sensibles a la acción de la PK e incapaces de nuclear su amplificación tanto *in vitro* como *in vivo* (277, 278).

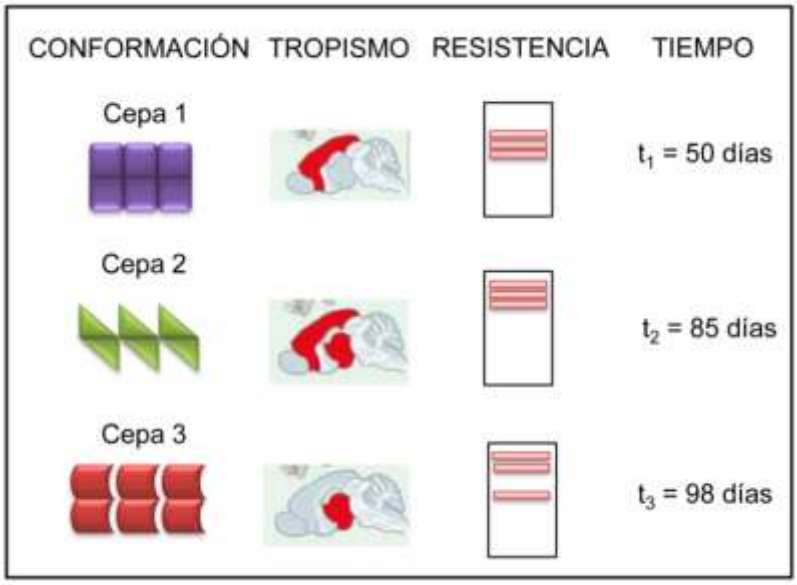

Figura 9. Las cepas de priones y sus propiedades diferenciales. Representación de las características más específicas que definen a cada una de las cepas priónicas: conformación, tropismo, tamaño de los fragmentos resistentes a la digestión con PK y tiempo de incubación. Las cepas más agresivas son las que tienen tiempos de incubación cortos debido a que son menos estables y, por lo tanto, se fragmentan con mayor facilidad aumentando la población de núcleos de PrP^{Sc} (279-281). (Imágenes tomadas de Collinge y Clarke 2007 (282))

1.2.5.1 PrP^{C} y PrP^{Sc}.

La producción de modelos recombinantes de PrP^{C} basados en cadenas maduras, libres de las secuencias señales N- y C- terminales, y conteniendo el puente disulfuro intramolecular, permitió establecer un modelo de estructura 3D (283, 284). Este modelo muestra a PrP^{C} como una proteína con dos dominios, la mitad N-terminal no estructurada y el dominio C-terminal conformado por tres hélices-α y dos láminas-β (**Figura 6**) corroborando la composición obtenida a partir de medidas de CD y FTIR (284-287). Esta estructura básica se conserva en todas las cadenas de PrP de mamíferos, si bien existen diferencias en la longitud de las hélices y en el grado de flexibilidad de algunos loops (209, 288-295). En ausencia de indicadores funcionales, estos modelos estructurales son considerados por consenso como el plegamiento α de PrP^{C}. No obstante, la ausencia de estructura en el dominio N-terminal es dudosa. En este sentido, el análisis de las esferas de coordinación de Cu (II) unido a esta región ha demostrado la existencia de distintas estructuras intra- e intermoleculares (296-299).

A diferencia de PrP^{C}, la forma PrP^{Sc} presenta una estructura secundaria caracterizada por un mayor contenido de lámina-β que, en algunos casos llega al 40% (286, 300). Los estudios de intercambio HxD, dirigidos a determinar la exposición diferencial de regiones de la cadena al solvente, han apuntado que la estructura fibrilar de PrP^{Sc} es una lámina-β cruzada cuyo núcleo se localiza en la región 218-224 (301). Por otra parte, el establecimiento de modelos recombinantes de PrP^{Sc} y su caracterización mediante NMR de estado sólido sugiere que su formación, al igual que en otros amiloides, se produce por el apilamiento en paralelo de las hojas-β (*in-register parallel β-sheet*) (302-311). Además, dichos estudios han sugerido que el núcleo está constituido por la región 173-224 y la formación de las láminas-β está dirigida por dos regiones de residuos: 182-184 y 222-224 (302).

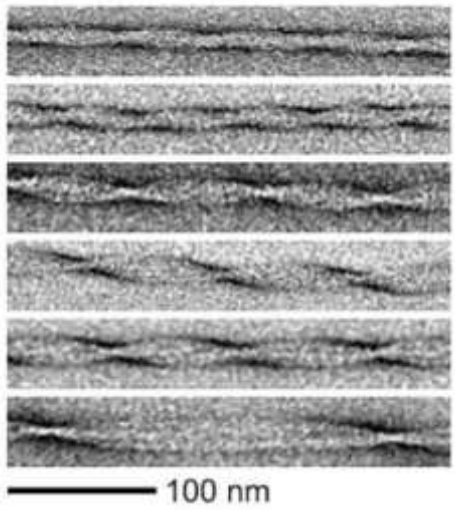

Figura 10. Polimorfismo estructural de las fibras amiloides. Caracterización mediante microscopia electrónica del conjunto de fibras de PrP generadas *in vitro* (Imagen tomada de Fandrich, Meinhardt y cols 2009 (312)).

A pesar de todo, PrP^{Sc} no es un estado conformacional único, si no que posee un polimorfismo funcional y estructural conocido como "cepas" o "inóculos" (87). Estas formas que muestras patrones de actividad distintos (tiempo de incubación de la infección, localización de la lesión, etc), difieren en la solubilidad en detergentes, en la resistencia a proteasas y en los perfiles de desnaturalización frente a agentes tales como GdnHCl (**Figura 9**). Este polimorfismo puede reproducirse in vitro a partir de un mismo lote de proteína empleando condiciones de ensamblaje por alteraciones del entorno (agitación, temperatura, pH, iones, etc) (312, 313) (**Figura 10**).

Los estados PrP^{C} y PrP^{Sc} están vinculados mediante el proceso denominado "conversión", que de acuerdo con la hipótesis de "sólo proteína" puede explicarse atendiendo a dos modelos: el modelo "*replegamiento asistido por cebador*" (314) y el modelo de "*polimerización nucleada por condensación no covalente*" (315). En el primer modelo, PrP^{Sc} es exógena y PrP^{C} endógena, y como producto de la interacción se induce un cambio conformacional de forma que PrP^{C} se transforme en más PrP^{Sc} (**Figura 11A**). Por el contrario, el segundo modelo establece la existencia de ambas formas en equilibrio y sólo cuando PrP^{Sc} alcanza una concentración crítica el proceso avanza (**Figura 11B**). Si bien ambos modelos son igualmente válidos, el desarrollo del método de amplificación *in vitro* conocido como PMCA ha permitido validar el proceso de polimerización nucleada y resaltar el papel central de los oligómeros de PrP^{Sc} como unidad replicativa fundamental (103, 316-322). Sin embargo, hay que subrayar que PrP^{Sc} no parece ser la causa única de la enfermedad, ya que en ausencia de PrP^{C} y del proceso de amplificación, no se produce patología alguna (183, 323). En este sentido, los datos existentes apoyan que el proceso patógeno de PrP^{Sc} está relacionada con algún proceso dependiente de PrP^{C} que culmina en disfunción y muerte neuronal (324-330).

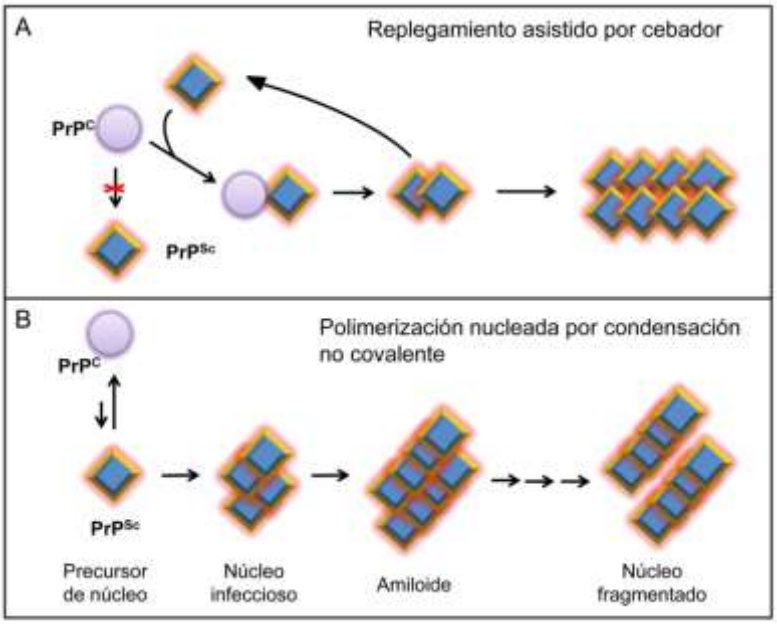

Figura 11. Modelos cinéticos de la conversión de PrP^C. Representación de los dos modelos de conversión: (A) replegamiento asistido por cebador, donde la conversión de PrP^C en PrP^{Sc} se produce por la interacción entre PrP^{Sc} (rombo azul) exógena y PrP^C endógena (círculo lila). (B) Polimerización nucleada por condensación no covalente, en el cual PrP^C y un precursor de PrP^{Sc} están en equilibrio y sólo si la concentración de este precursor incrementa y forma un núcleo de polimerización, PrP^{Sc} se estabiliza.

1.2.5.2 Formas citoplasmáticas: ^{Cyt}PrP y ^{Ctm}PrP.

Aunque la formación de PrP^{Sc} desempeña un papel principal en las prionopatías, una mayor presencia de las formas ^{Ctm}PrP y ^{Cyt}PrP se correlaciona directamente con estados neurodegenerativos (118, 119, 331, 332). Estas formas, que aparecen como agregados intracelulares, son sensible a la digestión con PK y no transmisibles (no favorecen la conversión a PrP^{Sc}) (119, 333). La aparición y acumulación de ambas formas se relaciona con la presencia de mutaciones, artificiales y asociadas a enfermedades genéticas (**Tabla 5**), y a alteraciones o disfunciones metabólicas (118, 119, 123, 134, 188, 189, 223, 225, 257, 334-341).

Tabla 5. Efectos de las mutaciones patógenas de HuPrP sobre la conversión. El empleo de mutantes de PrP asociados a patologías genéticas humanas han sido los modelos básicos para elucidar las bases del proceso de conversión.

REGIÓN		MUTACIÓN	TEJIDO	CÉLULAS	ESTUDIOS IN VITRO
N-terminal		P102L	PrP^{Res} [360]	↑^{Ctm}PrP (MoPrP) [359]	Sin diferencias significativas [363]
		P105L	356	↑ ^{Ctm}PrP (HuPrP) [118]	
HC		G114V	PrP^{Res} [362]	↑^{Ctm}PrP (HuPrP) [123]	
		A117V	↑ % ^{Ctm}PrP [353]	↑% ^{Ctm}PrP (HuPrP) [118]	Ligero aumento de la exposición al medio de residuos hidrofóbicos [345]
C-terminal	α1	Y145Stop	134	↑^{Cyt}PrP (HuPrP) [225]	Sin diferencias significativas [367]
		R148H	PrP^{Sc} [357]		
	β2	Q160Stop		↑^{Cyt}PrP (MoPrP) [352]	Sin diferencias significativas [367]
	α2	D178N	PrP^{Res} [344]	PrP^{Res} (HuPrP) [361]	Sin diferencias significativas [349]
		V180I	PrP^{Res} [343]	PrP^{Sen} (HuPrP) [343]	Sin diferencias significativas [364]
		T183A	PrP^{Res} [348]	PrP^{Res} (MoPrP) [355]	Sin diferencias significativas [364]
		E196K	PrP^{Res} [346]	347	Sin diferencias significativas [347] aunque predicen disminución de la estabilidad [162]
		F198S	PrP^{Res} [163]	PrP^{Res} (MoPrP) [355])	Sin diferencias significativas [365]
	α3	E200K	PrP^{Res} 342]	PrP^{Res} (HuPrP) [342]	Ligera diferencia no significativa [363]
		D202N	PrP^{Res} [163]	Agregados intracelulares (HuPrP) [350]	Sin diferencias significativas pero energéticamente es menos estable que wt [351]
		V203I	PrP^{Res} [354]	Agregados intracelulares (MoPrP) [358]	Sin diferencias significativas [364]
		R208H	PrP^{Res} [166]	347	Variación en la estabilidad a pH ácido [368]
		V210I	159	PrP^{Sen} (HuPrP) [366]	Sin diferencias significativas [364]
		E211Q	162	PrP^{Res}? (HuPrP) [358]	Sin diferencias significativas aunque energéticamente es menos estable que wt [351]

La forma ^{Cyt}PrP, por definición, es la conformada por las cadenas no translocadas al RE (**Figura 7**) (219, 224), lo que determina la conservación de las secuencias señales y la ausencia de las glicosilaciones y del puente disulfuro intramolecular además de un ambiente de plegamiento distinto al de la ruta de secreción. Además, esta forma puede distribuirse en el núcleo y cuando lo hace presenta sumoilaciones (219, 224). La población de ^{Cyt}PrP se alimenta también de cadenas retrotranslocadas desde el RE, cuyas secuencias señales han podido ser procesadas (223, 225, 257, 334, 335, 369). La descripción de los mutantes HuPrP Y145Stop y Q160Stop como formas ^{Cyt}PrP permitió generar cadenas HuPrP 23-145 y 23-160 (225, 352), cuya caracterización determinó su ensamblaje en fibras amiloides dependientes de la región 139-144 (367, 370-373). Del mismo modo, el empleo de cadenas MoPrP 90-231 reducidas, pH ácidos y oxidaciones lentas (aire) revelaron la formación de fibras amiloides (374).

Con respecto a ^{Ctm}PrP, su naturaleza transmembrana ha concentrado el interés en el conocimiento de su estructura. Los estudios de traducción-translocación *in vitro* y su acoplamiento a ensayos de protección frente a proteasas y la identificación inmunológica de los fragmentos producidos, estableció que el anclaje a la membrana se produce mediante la región 105-140 de la cadena (118) (**Figura 7**). La producción de ^{Ctm}PrP está asociada tanto a mutaciones que incrementan la hidrofobicidad de la región 105-140, como a algunas mutaciones del dominio globular y a condiciones de reducción del puente disulfuro (118, 119, 155, 340, 375). Este anclaje condiciona la proyección del dominio N-terminal al citosol, donde pueden manifestarse sus propiedades de unión de cationes y polianiones. Del mismo modo, el dominio C-terminal queda expuesto al lumen del RE donde puede sufrir glicosilaciones, el anclaje del GPI y la formación del puente disulfuro (336, 340, 375-377). De forma importante, la segregación de los dominios en dos compartimentos diferentes favorece sus oligomerizaciones homólogas (199, 200, 296, 378-382). En este sentido, estudios metabólicos recientes sugieren, además, que la acumulación de esta forma está asociada a un proceso de agregación (383). No obstante, a diferencia de los agregados de PrP^{Sc}, los oligómeros de ^{Ctm}PrP son sensibles a la digestión proteolítica (118)

1.2.6. PrP y sus metioninas: posibles interruptores moleculares.

Una de las características más notables de la cadena de PrP es el elevado número de metioninas (Met) en su secuencia y su grado de conservación (**Figura 12**). Además de su papel iniciador en la traducción, la presencia de metioninas se asocia con funciones antioxidantes y como interruptores conformacionales a través de su ciclo de óxido-reducción (219, 384-388).

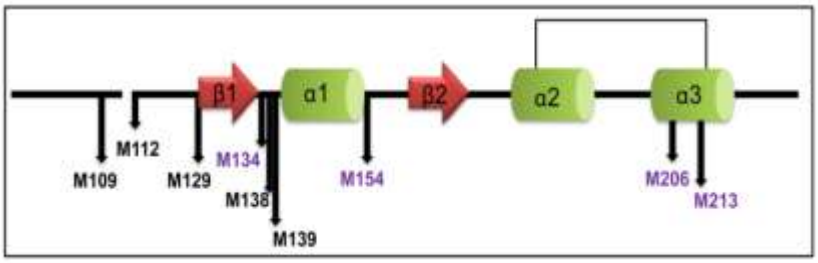

Figura 12. Localización de los residuos de metionina en rHaPrP (23-231). Las regiones que corresponden a estructuras secundarias se representan por cilindros (α-hélice) y flechas (cadenas-β) y sus posiciones son: β1(129-133), α1(145-153), β2(160-163), α2(171-194) y α3(200-226). Las metioninas se representan con el código de una letra y las conservadas en todas las especies se señalan en violeta.

Las metioninas son aminoácidos hidrofóbicos fácilmente oxidables por ROS. Esta oxidación da lugar a una de las dos formas sulfóxido de la metionina (MetO): R o S, isómeros conformacionales (389) (**Figura 13**). Esta reacción altera la polaridad de la cadena lateral pudiendo revertirse al ser reducida por un sistema enzimático denominado metioninas sulfóxido reductasas (Msr) con especificidad de isómero (Msr A, específica para los isómeros S y MsrB, para los isómeros R) (390-393). Aunque no es muy común en condiciones fisiológicas, la reacción de oxidación de las metioninas puede avanzar hasta el estado sulfona ($MetO_2$), que supone un estado irreversible (389, 393, 394). De forma genérica la susceptibilidad de las Met a la oxidación depende de su grado de exposición al solvente (mayor exposición, mayor susceptibilidad a la oxidación/reducción) (391, 395)

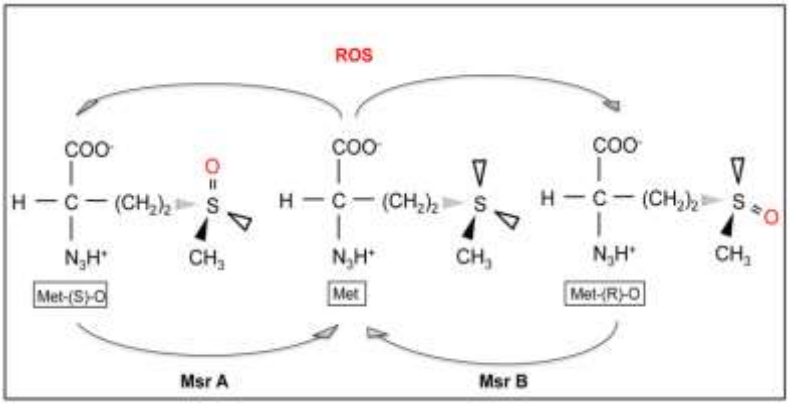

Figura 13. Ciclo de óxido-reducción de la metionina. La oxidación de la cadena de metionina por la acción de ROS es una reacción química y genera el sulfóxido y en un estado posterior de oxidación la sulfona. La oxidación a sulfóxido da lugar a dos isómeros S y R, cuya reducción está catalizada por las metioninas sulfóxido reductasas A y B (MsrA y MsrB). La oxidación a sulfona es irreversible *in vivo*.

El hecho de que la metionina sea uno de los residuos que se oxidan con mayor facilidad y de forma reversible, determina que esta modificación actúe como defensa antioxidante (387). Por otra parte, dado el cambio en las propiedades de la cadena lateral también hace las veces de regulador funcional (396-398). En este sentido, la calmodulina, una proteína intracelular estable de bajo peso molecular, actúa como receptor para el calcio modificando su conformación y alterando su espectro de interacciones con otras proteínas (399, 400). La calmodulina tiene 9 Met en su secuencia y su oxidación reduce drásticamente su afinidad por el calcio y, como consecuencia, el reconocimiento de otras proteínas (401-403).

Estructuralmente, la oxidación de las Met altera la conformación, disminuyendo el contenido helicoidal y reorganizando la estructura terciaria (404).

Al igual que la calmodulina, la cadena de PrP es rica en Met y por ello una de las hipotéticas funciones es la antioxidante (265, 405-413) El uso conjunto de metodologías inmunológicas y de proteómica permitió diferencias en el estado de oxidación de alguna de las Met en los estados PrP^{C} y PrP^{Sc} (414-416). En particular MetO213, el sulfóxido de una de las Met más enterradas y por ello menos susceptible a priori (**Figura 14A**), se reveló como una firma covalente del estado PrP^{Sc} y como un posible efector del proceso de conversión (414-416).

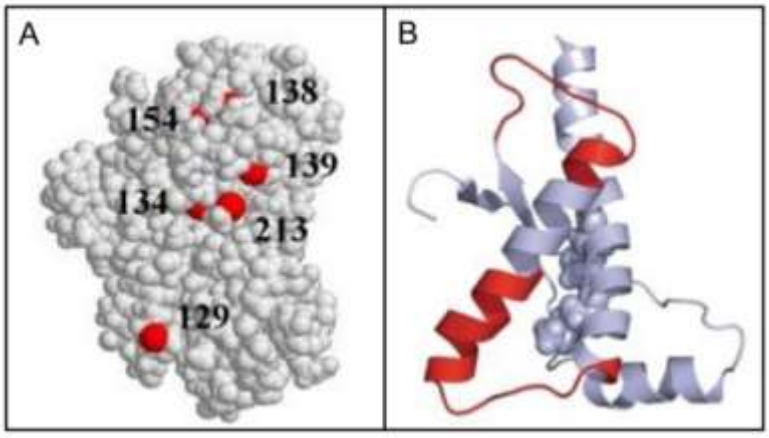

Figura 14. Disposición y efecto de la oxidación de las metioninas de α3. (A) Representación 3D de SHaPrP(90-231) donde los átomos de azufre de las metioninas se simbolizan como círculos rojos (imagen tomada de Requena , Dimitrova y cols 2004). B) Mapa 3D de las regiones cuya flexibilidad se altera al sustituir M206 y M213 por sus sulfóxidos de acuerdo con los cálculos de dinámica molecular. (imagen tomada de Colombo, Meli y cols. 2009 (417)).

El estudio del papel que tiene esta modificación covalente en el proceso de conversión se comenzó con un estudio de dinámica molecular utilizando como modelo la estructura 3D de HuPrP(121-229) (417). Esta aproximación teórica, que permite determinar el sitio de modificación de manera controlada y observar sus efectos a nivel atómico, reveló que la oxidación de la cadena lateral de cualquiera de las Met de α3, solas o en combinación, incrementa drásticamente la flexibilidad de la molécula en una región alejada secuencia (región que une α3 con α2, en los extremos de la α2 y en la región que conecta α2 con β1) (**Figura 14B**). La región afectada engloba residuos que aparecen mutados en enfermedades genéticas de priones o bien cuya mutación artificial favorece la transformación (418-420). Las alteraciones observadas permitieron proponer la formación de estos sulfóxidos como posible interruptor molecular en el proceso de conversión, sin diferenciar entre un papel causal o simplemente una consecuencia del mismo.

Objetivos

Lo que sabemos es una gota de agua, lo que ignoramos es el océano.

(Isaac Newton)

A pesar de los avances realizados en el campo de las prionopatías, el proceso elemental que determina la conversión de PrP^{C} en PrP^{Sc} y el nacimiento de un prion todavía sigue siendo un gran interrogante. Según la hipótesis del prion, la única diferencia entre PrP^{C} y PrP^{Sc} es la conformación (198, 207, 286, 421). No obstante, dicha diferencia, que define los estados extremos, podría estar condicionada a la existencia de un interruptor desconocido (unión de un ligando, modificación covalente lábil en uno de los dos estados). En este sentido, en el único estudio de secuenciación de PrP^{Sc} empleando espectrometría de masas, *Stahl y cols* observaron estados oxidados en las metioninas contenidas en la región que forma la hélice α3 (416). Dadas las limitaciones impuestas por la ausencia de controles adecuados basados en PrP^{C}, dicha observación pasó a considerarse como posible artefacto técnico. En 2008, como resultado de un estudio dirigido a la generación de anticuerpos empleando rMoPrP(23-231) como antígeno sobre Tg PrP-/- , *Canello y cols* obtuvieron uno que reconocía PrP^{C} pero no así PrP^{Sc} de forma interespecífica. La búsqueda del origen de dicha diferencia en el reconocimiento permitió demostrar que la metionina M213, localizada en la α3, en las formas PrP^{Sc} se encontraba en forma de sulfóxido (415). En un estudio posterior, *Colombo y cols* demostraron mediante un análisis exhaustivo de dinámica molecular que la sustitución individual o conjunta de los residuos M206 y M213 por sus sulfóxidos en el dominio globular de HuPrP (región 121-229) produce un conjunto de alteraciones tales que convergen hacia un estado flexible que facilitaría la conversión estructural (417). Este hallazgo permitió postular que la oxidación de dichas metioninas, las más internas, podría ser el desencadenante necesario para el proceso de conversión y explicar su dependencia del envejecimiento.

En este contexto, se plantearon los siguientes objetivos:

1. **Diseñar y generar reactivos inmunológicos para la determinación *in vivo* del momento metabólico, dentro del proceso de conversión de PrP^{C} en PrP^{Sc}, en el cual ocurre la oxidación.**

2. **Diseñar y generar modelos de sulfóxido de metionina (MetO) que permitan sustituciones puntuales en cadenas recombinantes y determinar, experimentalmente, el efecto de dichas oxidaciones en las metioninas de α3 sobre la estructura y estabilidad de PrP.**

3. **Diseñar y generar modelos que permitan evaluar el efecto de las mutaciones metabólicas Met/SeMet sobre la formación de amiloides.**

4. **Diseñar y generar modelos de PrP con estructuras lábiles para determinar el papel de la ruta de plegamiento *in vivo* en el proceso de formación de PrP tóxicas**.

Resultados

No basta saber, se debe también aplicar. No es suficiente querer, se debe también hacer

(Johann Wolfgang von Goethe)

Artículo 1. Oxidation of helix-3 methionines precedes the formation of PK resistant PrP.

La hipótesis central de la biología de priones establece que la única diferencia entre PrP^{C} y PrP^{Sc} es un cambio conformacional en el dominio globular, desde un estado helicoidal a uno con mayor presencia de láminas-β (207, 286, 421). El estudio de secuenciación pionero de la cadena de PrP^{Sc} realizado por *Stahl y cols* en 1993 describió la presencia de MetO en los péptidos correspondientes a la región α3. Sin embargo, en ausencia de controles adecuados basados en PrP^{C}, esta descripción se asignó a un posible artefacto instrumental y se olvidó (416). En 2008 *Canello y cols* usando un anticuerpo dirigido frente a α-PrP, describen la falta de reconocimiento de la forma PrP^{Sc} debido a la presencia de MetO en la posición 213 (415). Un año más tarde, *Oien y cols* (2009) corroboran la presencia de esta modificación oxidativa en homogeneizados tisulares que contenían PrP^{Sc} empleando un anticuerpo generado contra una proteína rica en MetO (422). Dado que la formación de MetO es una oxidación química, que PrP tiene en su cadena un número elevado de Met y que los MetO que diferencian a PrP^{C} y PrP^{Sc} ocurren en la metioninas más enterradas y por ello con menor probabilidad de oxidación, la formación de sulfóxidos podría ser la causa o la consecuencia de la conversión estructural. En un primer estudio teórico *Colombo y cols* (2009) describieron que la oxidación de las metioninas de α3, solas o en combinación, cambian dramáticamente la dinámica global de la proteína, aumentando la flexibilidad de determinadas regiones y alterando los enlaces de estabilización del estado nativo, indicando que su formación puede constituir un efector crucial para la activación de los primeros pasos de la formación de PrP^{Sc} y la necesidad de determinar *in vivo* la temporalidad de este proceso (417).

En este trabajo, ampliando la batería de anticuerpos y los modelos de conversión, se persigue determinar el momento, durante el proceso de conversión, en el cual se produce la oxidación de la metionina de α3. Mi contribución en este trabajo ha sido el diseño, producción y caracterización de las proteínas recombinantes y la realización de controles ciegos.

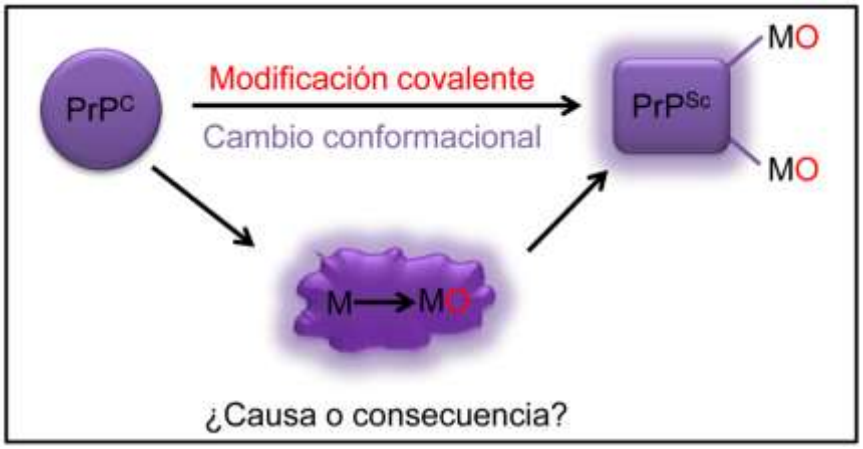

OPEN ACCESS Freely available online

PLoS PATHOGENS

Oxidation of Helix-3 Methionines Precedes the Formation of PK Resistant PrP^{Sc}

Tamar Canello[1], Kati Frid[1], Ronen Gabizon[2], Silvia Lisa[3], Assaf Friedler[2], Jackob Moskovitz[4], María Gasset[3], Ruth Gabizon[1]*

1 Department of Neurology, The Agnes Ginges Center for Human Neurogenetics, Hadassah University Hospital, Jerusalem, Israel, **2** Institute of Chemistry, The Hebrew University of Jerusalem, Safra Campus, Jerusalem, Israel, **3** Instituto Química-Física Rocasolano, Consejo Superior de Investigaciones Científicas, Madrid, Spain, **4** Department of Pharmacology and Toxicology, School of Pharmacy, University of Kansas, Lawrence, United States of America

Abstract

While elucidating the peculiar epitope of the α-PrP mAb IPC2, we found that PrP^{Sc} exhibits the sulfoxidation of residue M213 as a covalent signature. Subsequent computational analysis predicted that the presence of sulfoxide groups at both Met residues 206 and 213 destabilize the α-fold, suggesting oxidation may facilitate the conversion of PrP^{C} into PrP^{Sc}. To further study the effect of oxidation on prion formation, we generated pAbs to linear PrP peptides encompassing the Helix-3 region, as opposed to the non-linear complexed epitope of IPC2. We now show that pAbs, whose epitopes comprise Met residues, readily detected PrP^{C}, but could not recognize most PrP^{Sc} bands unless they were vigorously reduced. Next, we showed that the α-Met pAbs did not recognize newly formed PrP^{Sc}, as is the case for the PK resistant PrP present in lines of prion infected cells. In addition, these reagents did not detect intermediate forms such as PK sensitive and partially aggregated PrPs present in infected brains. Finally, we show that PrP molecules harboring the pathogenic mutation E200K, which is linked to the most common form of familial CJD, may be spontaneously oxidized. We conclude that the oxidation of methionine residues in Helix-3 represents an early and important event in the conversion of PrP^{C} to PrP^{Sc}. We believe that further investigation into the mechanism and role of PrP oxidation will be central in finally elucidating the mechanism by which a normal cell protein converts into a pathogenic entity that causes fatal brain degeneration.

Citation: Canello T, Frid K, Gabizon R, Lisa S, Friedler A, et al. (2010) Oxidation of Helix-3 Methionines Precedes the Formation of PK Resistant PrP^{Sc}. PLoS Pathog 6(7): e1000977. doi:10.1371/journal.ppat.1000977

Editor: Umberto Agrimi, Istituto Superiore di Sanità, Italy

Received January 21, 2010; **Accepted** May 28, 2010; **Published** July 1, 2010

Funding: This work has been supported by grants from the Israeli Science foundation and The Israeli Ministry of Health (RG) as well as grants BFU2009-07971 from the Ministerio de Ciencia e Innovación (MG) and PI101209 from the Fundación Cien (MG). The funders had no role in study design, data collection and analysis, decision to publish, or preparation of the manuscript.

Competing Interests: The authors have declared that no competing interests exist.

* E-mail: gabizonr@hadassah.org.il

Introduction

Prions are infectious agents that cause neurodegenerative diseases, such as scrapie, bovine spongiform encephalopathy (BSE) and CJD. They are believed to be composed mainly of PrP^{Sc}, a misfolded form of the GPI-anchored glycoprotein termed PrP^{C}[1]. While the function of PrP^{C} has not been fully elucidated, it has been suggested that this protein plays a role in the protection of cells from copper-induced oxidative stress [2–5]. Until recently, and mainly in the absence of convincing data to the contrary, the two PrP isoforms were believed to differ from each other only by their high-order structures; mostly an α-helical fold for PrP^{C}, and largely a β-sheet assembly for PrP^{Sc}[6]. Nevertheless, while investigating the epitope of an α-PrP monoclonal antibody (mAb) with an uncommon recognition pattern (IPC2), we came to the conclusion that at least one of the Helix-3 methionine residues of PrP^{Sc}, M213, is differentially oxidized [7]. The oxidation of PrP^{Sc} was also confirmed by chemical reduction experiments, state of the art mass spectrometry and detection by an antibody generated against a MetO rich maize protein [8]. The finding that M213 as well as the other conserved Helix-3 Met residue, M206, were oxidized in PrP^{Sc} was first reported in the seminal work of Stahl et al. following sequencing of the PrP27-30 endoLysC peptides [9]. The fact that these specific Met residues are oxidized in PrP^{Sc} is particularly intriguing since they are the most buried residues among methionines in the 3D PrP α-fold and thus are less accessible to reactive oxygen species (ROS) [10]. So is the case for Met 205, present in PrP proteins from some species, which when mutated to both Ser or Arg destabilizes the protein structure [11]. However, if and when they are oxidized, Helix-3 Met residues may not be targeted by the methionine reductase (Msr) system, which reverses oxidation of accessible Met residues [12,13]. Indeed, it was shown that while mice overexpressing superoxide dismutase (SOD), which inhibits oxidation, presented prolonged incubation periods upon RML infection, ablation of the MsrA system did not reduce the time from infection to disease outbreak [14].

The time course of Helix-3 Met oxidation as related to PrP conformational conversion is of great mechanistic importance. If this specific oxidation takes place after PrP^{Sc} is formed and accumulated in brain cells, then Met oxidation, while being an interesting covalent marker of PrP^{Sc}, may not participate in the sequence of events leading to prion formation and disease manifestation. Conversely, if Met oxidation occurs on the PrP^{C} form and mediates the subsequent conformational change, then methionine oxidation may constitute an early and important step in prion formation. Along these lines, theoretical investigations have predicted that the polarity increase of Met 206 and 213 residues upon sulfoxidation may induce destabilization of the PrP

Author Summary

The protein only theory, a widely accepted model describing the prion agent, assumes that the mechanism underlying prion disease pathogenesis includes a conformational change of the α-helix rich, soluble and protease sensitive PrP^{C} into an aggregated and protease resistant β-sheet rich PrP^{Sc} form. Until recently, no covalent modification was known to be associated with such a conversion, making it difficult to follow the individual fate of each PrP form or to associate cellular events as stress-response or inflammation with the formation of prions. We now show that before PrP^{C} initiates its conversion from proteinase K sensitive to resistant and from soluble to aggregated in the pathway to becoming PrP^{Sc}, it first undergoes oxidation of the most hidden Met residues located in a protein region exhibiting sequence identity for all species. While the cellular events promoting such oxidation in this transmissible disease remain unclear, we present evidence that PrP molecules carrying a mutation ascribed to the most common familial prion disease spontaneously oxidizes at these same Met residues. Our data provide new insights into the mechanism underlying familial Creutzfeld Jacob disease (CJD) and contribute to our general understanding of the fundamental processes related to prion pathogenesis.

helical conformation [15]. This prediction agrees with the destabilization of the native α-fold and the appearance of proaggregating properties observed in PrP chains with either methoxinine or serine substitutions of Helix-3 Met residues [16,17]. To further establish the role sulfoxidation in PrP^{Sc} formation, we aimed to generate pAb antibodies against linear PrP human/mouse sequences, which include reduced and oxidized Helix-3 Met residues. As opposed to the complex IPC2 epitope, which precludes simple recognition of most PrP forms upon disulfide bond reduction [7], an antibody raised against a linear sequence should detect all denatured PrP forms unless a covalent modification in the amino acid chain interferes with such recognition. Furthermore, the use of such antibodies would allow quantitative investigation of the different PrP forms under similar conditions, avoiding the need for distinct purification protocols, which alone may change the properties of the tested proteins.

Consistent with this prediction, we now show that all human PrP^{Sc} and most mouse PrP^{Sc} chains were not detected by antibodies generated against reduced PrP Helix-3 Met residues unless these brain proteins were previously reduced by strong chemical reagents. In addition, our antibodies did not detect PrP^{Sc} expressed in prion-infected cells or partially aggregated PrPs present in gradient fractions of prion-infected brains, indicating that both newly formed PrP^{Sc} as well as intermediate PrP forms could be oxidized. Intriguingly, this was also the case for a PK-sensitive mutant PrP form linked to the most prevalent familial prion disease rHuPrP(23–231) E200K[18]. Our results establish the presence of sulfoxides in the Helix3 methionines in all pathogenic forms of the prion protein and indicate that such oxidation most probably precedes the conversion of PrP^{C} into proteinase K (PK) resistant PrP^{Sc}.

Results

Tailoring antibodies against PrP Helix-3 epitopes

Figure 1A shows the sequences of the PrP Helix-3 region for various species. These sequences are very similar for all species listed and even identical for the 206–214 regions, which includes both Met206 and Met213. Some species (such as human, mouse and cow) also present a Met residue at position 205. To generate specific Ab to reduced and sulfoxidized Helix-3 PrP forms, we immunized rabbits with several KLH-coupled peptides (Figure 1B). These peptides include KLH coupled to the Hu/Mo 203–214 sequence, which covers the three Met residues in these species. As oxidized antigens, we inoculated rabbits with two peptides prepared by different methods, including Hu/MoPrP 201–214 coupled to KLH, synthesized with MetO residues, and KLH-C-204-213, which was oxidized with H_2O_2 after synthesis and coupling. Following several rounds of immunization (see Methods), the rabbits (two for each peptide) were bled, and isolated serum was tested against normal brain homogenates from different species. Next, positive homogenates were immunoblotted with the designated antiserum preincubated with an array of small PrP peptides (Figure 1C) to determine the recognition site of each antibody on the protein sequence by competition. Finally, the characterized serum samples were tested against prion-infected samples.

No reactivity against any form of PrP was detected using the serum from the rabbits immunized with the oxidized KLH-KM peptide (not shown). Properties of the other serum samples are described in Figure 2. As shown in panel A, both the antiserum raised against the KLH-conjugated and oxidized TC peptide (pAb RTC) and the antiserum raised against the reduced VC peptide (pAb RVC) clearly recognized Mo and Hu PrP^{C}, although they did not recognize Ha and Bo PrPs. Indeed, while the Mo and Hu PrP sequences are identical in this region, other species present slight individual differences in the 203–205 sequence (Figure 1a).

As opposed to the similarity in species reactivity of the pAbs RTC and RVC, the RTC and RVC epitopes on the PrP sequence were found to be different, as determined by the inhibition of the PrP immunoblotting signal with an array of peptides. While the activity of the pAb RVC was inhibited by the KM peptide, which includes the three Met residues, this same peptide did not affect recognition of PrP by the pAb RTC in either the reduced or H_2O_2-oxidized form. In contrast, the activity of RTC was inhibited by the TM peptide (201–205), suggesting that this pAb recognizes the TVDK or TVDKM sequence (present in Hu and Mo PrP), N-terminally to the relevant Met residues. This finding implies that both oxidized PrP peptides failed to generate an immune response to the oxidized Met rich region, consistent with investigations in other fields indicating that charged and oxidized epitopes are mostly unrecognized by T-cell receptors [19,20].

Antibodies designed to recognize Helix 3 Met residues may not recognize PrP^{Sc}

Next, we examined the capacity of the RTC and RVC pAbs to recognize PrP^{Sc} forms. To this effect, we immunoblotted brain samples from normal and prion infected brains (digested in the presence or absence of proteinase K at 37°C) with a panel of antibodies generated against PrP epitopes upstream and downstream of the helix 3 Met area to ensure that PrP^{Sc} was present in its full length under these conditions. Figure 2C shows that the α-PrP mAb 6H4 (Prionics), which recognizes PrP in all species (at residues 145–152), the pAb RTC and also the recombinant R1 antibody (at residues 225–231 in rodent PrP [21]) detected PrP isoforms in normal and prion-infected brain samples. However, the PrP recognition pattern of the pAb RVC was significantly different. While this reagent recognized PrP from normal brain samples as well as from undigested brain samples of RML-infected mice and genetic and sporadic CJD patients (believed to comprise both PrP^{Sc} and PrP^{C}) the pAb RVC could not detect all of

A

	206 ——— 214		
Bo	HTVTTTTKGENFTETD	IKM	MERVVEQMC	ITQYQ RESQAYYQ
Ha	HTVTTTTKGENFTETD	IKI	MERVVEQMC	TTQYQ RESQAYYQ
Hu	HTVTTTTKGENFTETD	VKM	MERVVEQMC	ITQYE RESQAYYQ
Mo	HTVTTTTKGENFTETD	VKM	MERVVEQMC	VTQYQ RESQAYYQ
Ov	HTVTTTTKGENFTETD	IKI	MERVVEQMC	ITQYQ RESQAYYQ
Ra	HTVTTTTKGENFTETD	IKI	MERVVEQMC	ITQYQ QESQAAYQ

B

KLH-conjugates	Rabbit pAb
VKMMERVVEQMC-***KLH***	pAb RVC
TDVK**MoMo**ERVVEQ**MoC**-***KLH***	pAb RTC
KLH-CK**MoMo**ERVVEQ**Mo**	none
GENFTETDVKMMERVVEQMC-***KLH***	pAb RGM

C

Region	Name	Sequence
V203-E211	VE	VKMMERVVE
V203-M213	VM	VKMMERVVEQM
K204-M213	KM	KMMERVVEQM
T201-M205	TM	TDVKM
K204-Mo213	KMox	KMoMoERVVEQMo

Figure 1. Helix-3 sequences. (**A**) Helix-3 sequences in different PrP species. The 206–214 region, comprising M206 and M213, is completely conserved in all species. (**B**) PrP peptides used for the generation of α Helix-3 antibodies. (**C**) PrP peptides used for the inhibition of α Helix 3 antibodies.
doi:10.1371/journal.ppat.1000977.g001

HuPrP^{Sc} and detected only low levels of MoPrP^{Sc} after PK digestion.

To confirm that the recognition pattern of the pAb RVC vis a vis proteinase K resistant PrP^{Sc} forms indeed resulted from Met oxidation, we subjected PK digested extracts from prion-infected human and mouse brains to N-methylmercaptoacetamide (MMA), a specific MetO reducing agent [22]. Figure 2D shows that following MMA treatment, the pAb RVC easily recognized both human and mouse PrP^{Sc} at detection levels similar to those of the α-PrP mAb 6H4 both before and after MMA treatment. Similar but less striking results were obtained for detection of the reduced samples by IPC2 because, as described in our previous publication [7], full detection of reduced PrP forms by this mAb requires deglycosylation of PrP forms by PNGase.

Oxidation of newly formed PrP^{Sc}

To establish whether oxidation of Met residues is essential for the conversion of PrP^{C} to PrP^{Sc}, we asked whether Met oxidation occurs first on PrP^{C} or whether oxidation is a delayed effect related to the long-term accumulation and reduced clearance of proteinase K resistant and misfolded prion protein in the brains of the affected subjects. To separate these mechanistic possibilities, we studied by pAb RCV the oxidation status of newly formed PK resistant PrP^{Sc} generated in cells permanently infected with prions, such as ScN2a [23] and ScGT1 cells [24]. Since these cells constantly proliferate, PrP^{Sc} produced by them can be considered relatively new, as opposed to the PrP^{Sc} molecules that accumulate in infected brains.

For this experiment, extracts from ScN2a cells (infected with the RML mouse prion strain) and from the ScGT1 cell line (infected with both the RML and the 22L prion strains) [25] were treated in the presence or absence of proteinase K and immunoblotted with the anti-PrP IPC1mAb, which recognizes all forms of Mo and Ha PrP ([7], Sigma), and the pAb RVC, which properties were described above. Extracts from the uninfected cell lines (N2a and GT1) and brain samples from normal and scrapie-infected mice were included in this study. Figure 3a shows that while the IPC1 mAb recognized all forms of PrP in cells and brains, the pAb RVC failed to detect proteinase K resistant PrP forms in any of the infected cell systems and barely detected bands characteristic for PrP^{Sc} before proteinase K digestion. These results indicate that newly made PrP^{Sc} may be quantitatively oxidized, as was shown here for PrP from two different cell lines and for two prion stains (ScN2a-RML, ScGT1-RML and ScGT1- 22L). Similar results were obtained for an RML infected GT1 line expressing chimeric Mo-Ha PrP [26,27] (not shown here for the pAb RVC, see bellow for a similar antibody). Contrary to PK resistant PrP^{Sc} in the cells, and as depicted also in Figure 2, pAb RVC could detect low levels of PrP^{Sc} in infected mouse brains as well as some prion-related bands in the undigested parallel samples. Therefore, we conclude that in infected murine brains, as opposed to infected human brains or infected mouse cells, low levels of proteinase K resistant PrP are present in a fully or partially reduced form. Whether such PrP^{Sc} molecules are formed independently or join a seed of oxidized PrP^{Sc} molecules after formation is currently unknown.

Similar to brain PrP^{Sc}, detection of cell PrP^{Sc} by the pAb RVC could be restored in both cell lines when samples were reduced by MMA before being subjected to immunoblotting (Fig. 3B). This finding is consistent with the notion that the lack of PrP^{Sc} recognition by RVC indeed relates to the oxidative state.

Met oxidation of intermediate PrP states

Previous studies on prion-infected cells demonstrated that the formation of PrP^{Sc} from PrP^{C} is a slow multistep process, which may include a variety of intermediate PrP states [28,29]. To investigate whether PrP Helix-3 Met oxidation occurs before the acquisition of PK resistance, we examined the oxidation state of putative PK sensitive intermediate forms. Several experimental approaches indicated the presence of such intermediates, denominated either PrP^{Sc}-sen (from PK sensitive) or PrP* [30–32]. While

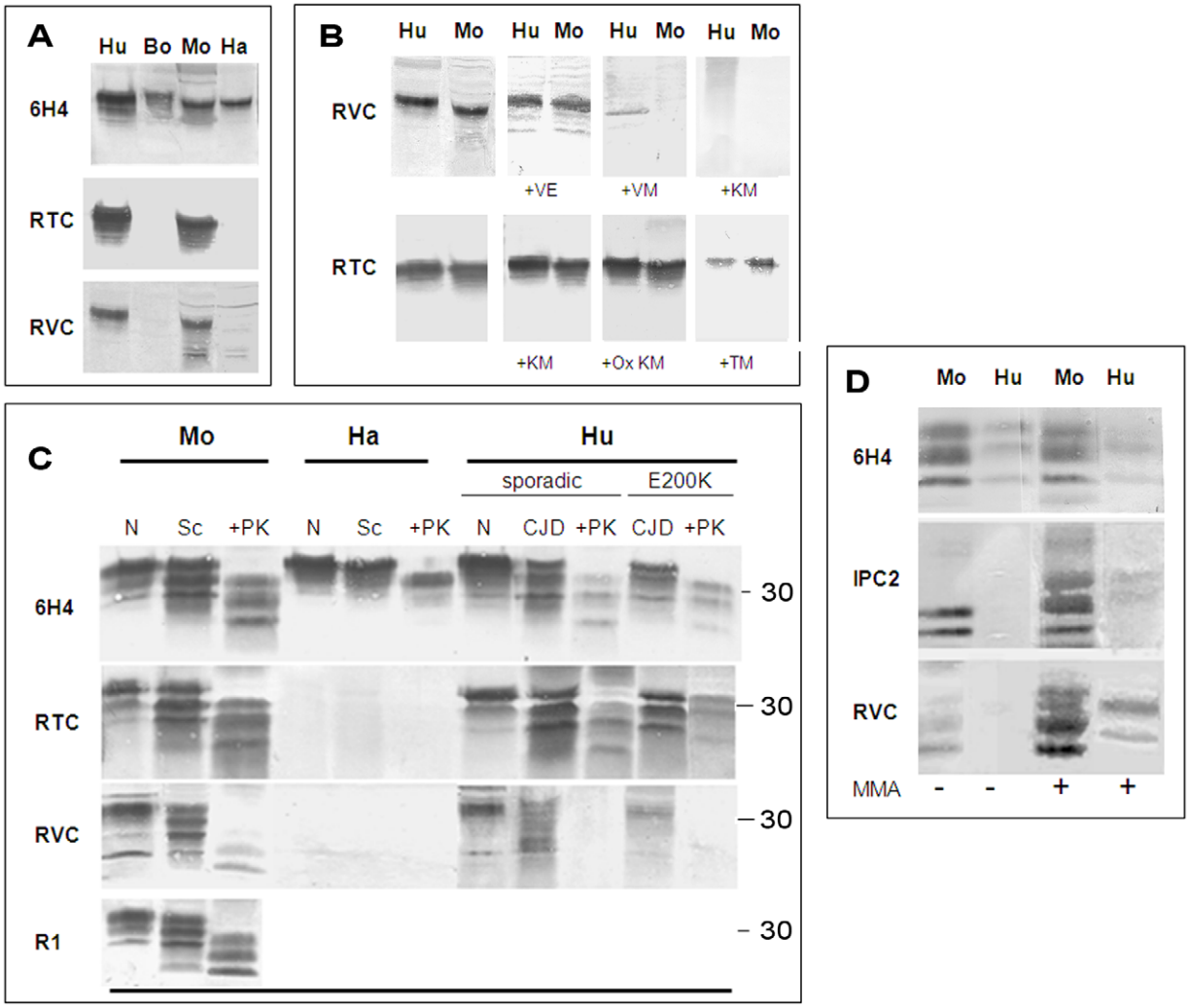

Figure 2. Testing for the activity of anti-Helix-3 antibodies: pAb RVC does not recognize PrP^{Sc} generated in prion infected brains. (**A**) Activity of pAb RVC and RTC, as compared to the established mAb 6H4, against normal brain homogenates from bovine, mouse, humans and hamster. (**B**) Human and mouse normal brain homogenates were immunoblotted with pAb RVC and RTC alone or in the presence of diverse Helix-3 PrP peptides (see Figure 1C for the peptide sequences) (**C**) Brain homogenates from mice, hamster and humans (normal, prion-infected and prion-infected digested with proteinase K), were immunoblotted with mAb 6H4, with pAb RTC or RVC, or with rec Ab R1. D) Mouse scrapie (RML) and human CJD brains (E200K) were digested with PK, processed for MMA reduction as described in the methods and immunoblotted with α PrP mAb 6H4, IPC2, or pAb RVC.
doi:10.1371/journal.ppat.1000977.g002

these forms were never proven directly to be infectious, they were shown to present characteristic PrP^{Sc} properties. Intermediate PK sensitive PrP forms may be present as aggregates and require extensive or partial denaturation to be recognized by anti-PrP antibodies, as is the case for PrP^{Sc} [33]. To determine the oxidation state of intermediate forms of PrP, we subjected Sarkosyl extracted control and prion-infected brain samples from murine and human subjects to sucrose gradients, as previously described for PrP* [30]. Fractions of the centrifuged gradients (light to heavy) were collected and digested in the presence or absence of PK before immunoblotting with either the mAb 6H4 or pAb RVC. As shown in Figure 4, while PrP was similarly detected by both antibodies in the lighter gradient fractions of control samples (normal mouse and normal human brains), immunoblots of the prion-infected samples (RML infected mouse and CJD E200K heterozygous familial cases) with each of the antibodies showed very different results. Before proteinase K digestion, PrP was recognized by mAb 6H4 in most fractions of both human and mouse gradients, although the banding pattern of the protein resembled PrP^{C} in the lighter fractions (1–3) and PrP^{Sc} in the heavier fractions. After proteinase K digestion, only the heaviest gradient fractions (mostly fractions 9–10) presented any form of PrP signal, indicating that while proteinase K resistant PrP^{Sc} is the most aggregated, partially aggregated PrP-sen forms (fractions 4–7) may also present the PrP^{Sc} banding pattern [22]. In contrast, when the undigested gradient fractions from the prion-infected brains were immunoblotted with the pAb RVC, the pattern of PrP recognition mostly resembled that of the normal brain homogenates. No PrP forms were detected in any of the intermediate or heavy fractions, except low levels of mouse PrP^{Sc} in the heaviest fraction. Following proteinase K digestion, the PrP signal mostly disappeared form all infected fractions, except traces in the last fraction of the mouse gradient, consistent with the experiments described in Figures 2 and 3. Similar results were obtained for brain samples from sporadic CJD patients (data not shown). Since the lack of recognition of PrP by the pAb RVC in the intermediate

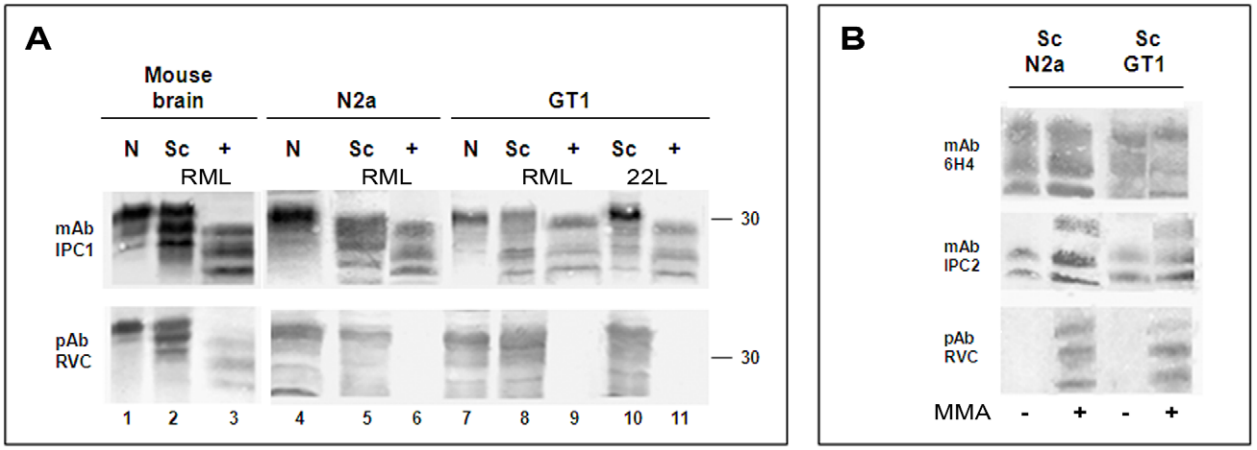

Figure 3. pAb RVC does not recognize PrP^{Sc} generated in prion infected cells. (**A**) Brain (normal, scrapie infected, as well as scrapie infected digested with PK) as well as normal and prion-infected cells, (N2a and GT1 infected either with the RML or the 22L prion strains) were extracted and immunoblotted with mAb IPC1 as compared to pAb RVC. (**B**): Effect of the MMA chemical reduction of proteinase K digested ScGT1 and Sc N2a cells on the PrP recognition by mAb IPC1, mAb IPC2 and pAb RVC.
doi:10.1371/journal.ppat.1000977.g003

gradient fractions indicates that PrP^{Sc}-sen forms are as oxidized as the PrP^{Sc}-res forms, we conclude that oxidation of PrP accompanies the conformational change required for PrP aggregation and precedes the acquisition of proteinase K resistance during PrP^{Sc} formation. The fact that the low levels of reduced mouse PrP^{Sc} were detected by PVC only in the most aggregated fraction, both before and after PK digestion, further suggests that non-oxidized mouse PrP may join the prion seed following its formation from oxidized PrP molecules.

Spontaneous oxidation of proteinase K sensitive E200K PrP

Figure 2C shows that as opposed to PrP^{C} in normal human brains and undigested PrP in the brains of sporadic CJD patients, PrP was poorly detected in brains of heterozygous E200K PrP fCJD patients [18]. This finding indicates that the mutant E200K PrP molecules may be oxidized in these brains even in their initial conformational state. Indeed, the Met rich area of PrP Helix-3 is located C-terminally to the residue 200, which mutated form,

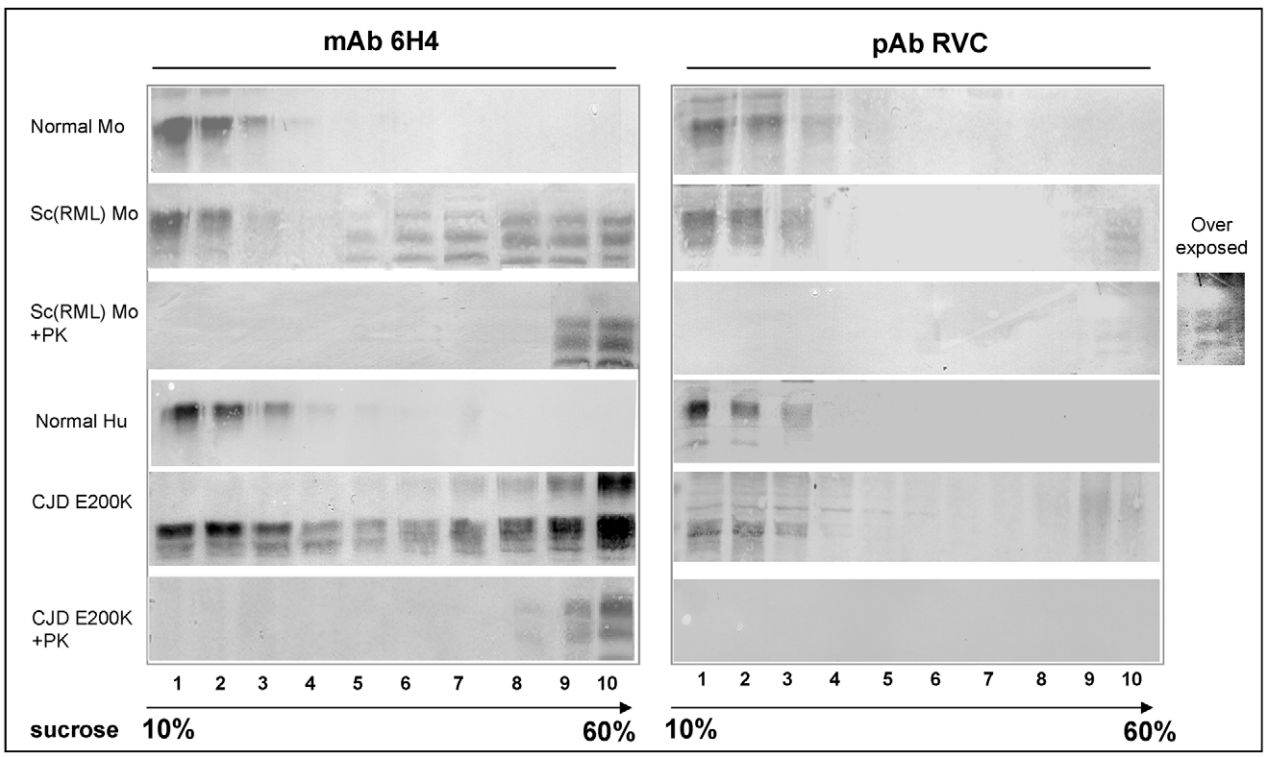

Figure 4. Intermediate PrP forms are oxidized as PrP^{Sc}. Sarkosyl extracted brain samples from normal and prion infected mice and humans were subjected to sucrose gradient centrifugation. Fractions from these gradients were digested in the presence or absence of proteinase K and immunoblotted with both mAb 6H4 and pAb RVC.
doi:10.1371/journal.ppat.1000977.g004

E200K, is the most abundant among familial CJD patients. In fact, peptides embracing this region and comprising either E (peptide 195–213) or K (peptide 185–205) at position 200 were used more than a decade ago for the generation of specific (to wt or mutant) anti- PrP pAbs [34]. The pAb raised against the HuPrP peptide containing E at position 200 (designated in Figure 1b as the pAb RGM) did not recognize proteinase K sensitive PrP forms expressed in fibroblasts from homozygous E200K patients, suggesting that the pAb RGM specifically detected wt PrP as opposed to the mutant E200K form [34]. Next, brain extracts from heterozygous CJD E200K patients were immunoblotted with this antiserum. The results showed convincingly that the pAb RGM did not detect proteinase K-resistant PrP forms. Due to the general belief at the time that no covalent modification separates PrP^{C} from PrP^{Sc} and that the only difference between the mutant and wt PrP proteins could be the mutation itself, it was concluded that in heterozygous E200K patients only the mutant protein (K at codon 200) acquires the proteinase K resistance property during disease [34]. This conclusion was then generalized using other methods and additional PrP mutations [35].

Based on the results described above for the pAb RVC, demonstrating that antibodies directed against Helix-3 methionines may not recognize PrP^{Sc} and since the peptide used for generation of the RGM antibody comprised both the 200 residue and the Helix-3 methionines, we now investigated whether this reagent does not recognize E200K PrP^{Sc} specifically or otherwise cannot detect all forms of human PrP^{Sc}, as described above for pAb RVC. To this effect, we immunoblotted brain homogenates from RML infected-mice as well as from sporadic or familial E200K CJD human cases and analyzed them in parallel with both anti-PrP mAb 6H4 and pAb RGM. As depicted in Figure 5a, pAb RGM, similarly to pAb RVC, did not recognize proteinase K resistant HuPrP in both sporadic and E200K familial CJD samples, and in addition detected poorly undigested forms of HuPrP E200K. Consistent with the results obtained with pAb RVC, pAb RGM detected low levels of $MoPrP^{Sc}$ from infected brains, but did not detect PrP^{Sc} from infected cells lines, as depicted here for GT1 cells expressing chimeric Mo-Ha PrP. Similar results were obtained for PrP^{Sc} from ScN2a cells (not shown).

To assess whether pAb RGM has separate recognition sites for E at position 200 and for the Helix 3 Met residues, which may explain why this antibody did not detect 200K PrP in fibroblasts from E200K homozygous subjects [34], we repeated the inhibition experiments described for RTC and RVC in Figure 2 using pAb RGM. We found that the activity of pAb RGM, which detected

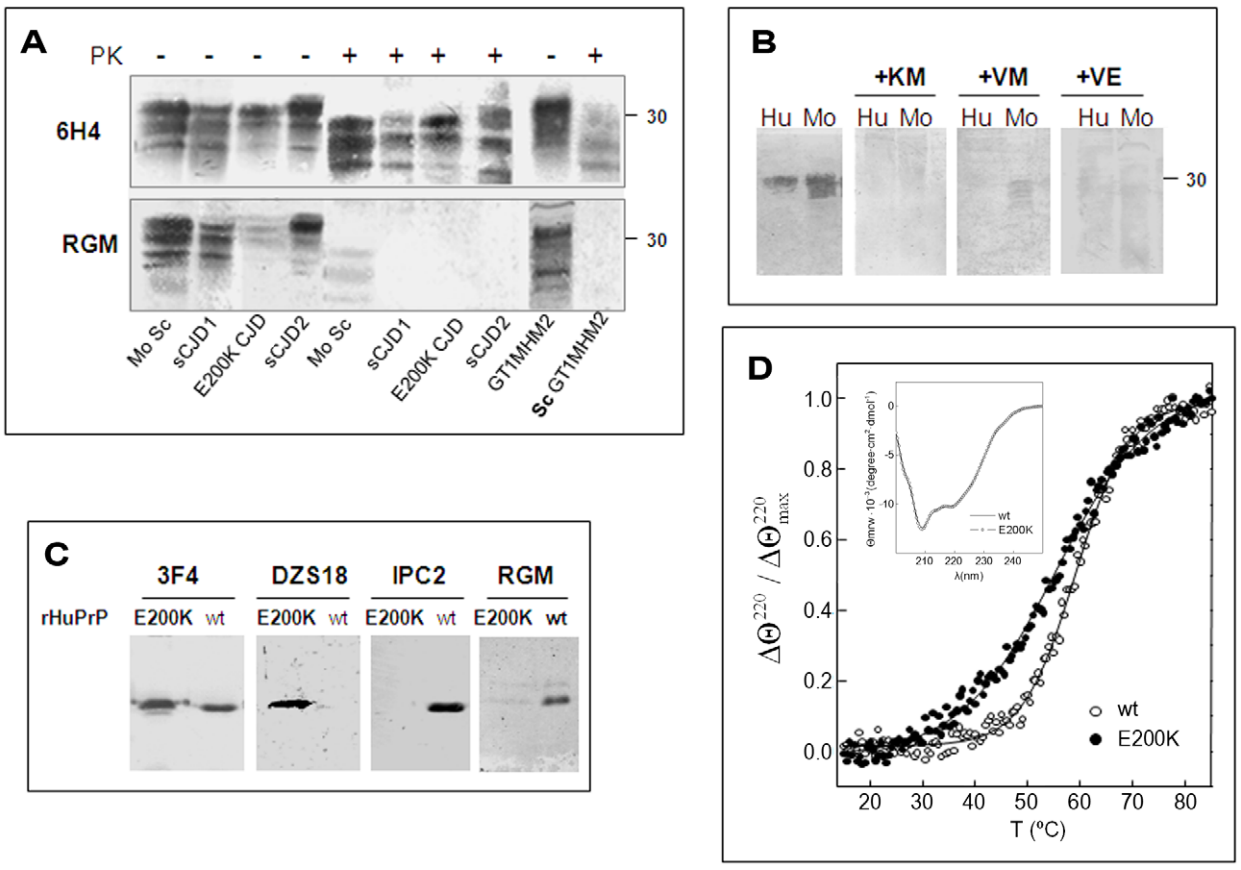

Figure 5. HuPrP E200K is spontaneously oxidized. (**A**) Brain samples from scrapie infected mice and from humans suffering from familial E200K or sporadic CJD, were digested in the presence or absence of proteinase K and subsequently immunoblotted with mAb 6H4 or pAb RGM. The last 2 lanes of each gel comprise normal GT1 and proteinase K digested ScGT1 cells expressing a chimera Mo/Ha PrP form. (**B**) Human and mouse normal brain homogenates were immunoblotted with the RGM antibody alone or preincubated with several PrP peptides in the Helix-3 Met area. (**C**) Immunoblots of HuPrP(23–230) wt and E200K with 3F4 (recognizing the 109–112 region), DZS18 (recognizing oxidized Met residues in different proteins), IPC2 (recognizing non-oxidized M213) and RGM (recognizing non-oxidized M206). Blots were prepared in the absence of β-mercaptoethanol. (D) Thermal stability of HuPrP(23–230) wt and E200K probed by the relative change in the ellipticity at 220 nm as a function of temperature. Insert: Far-UV CD spectrum of HuPrP(23–230) wt and E200K.
doi:10.1371/journal.ppat.1000977.g005

only mouse and human PrP (not shown), was totally inhibited by several peptides covering the Helix-3 Met residues, including the one comprising the 203–211 PrP sequence. This prevents the residue at codon 200, regardless E or K, from forming part of the pAb RGM epitope (Figure 5b), indicating that the lack of recognition of the mutant PrP by pAb RGM is not related to the presence of K instead of E at position 200. In addition, and since the epitope of this antibody does not comprise M213, these results constitute the first direct evidence that oxidation of M206 (and/or M205) can also be considered as a covalent signature of PrP^{Sc}, as predicted by the theoretical studies.

To investigate why pAb RGM was unable to recognize the mutated PrP even though its epitope does not include the 200 residue, we examined the recognition of wt and rHuPrP E200K by RGM as well as by a panel of antibodies designed to detect oxidized and non-oxidized PrP forms. As shown in Figure 5C, while α-PrP mAb 3F4 recognized the wt and mutant rHuPrP chains equally, pAb RGM did not detect the mutant recombinant protein, as described before for mutant PrP expressed in fibroblasts from E200K homozygous patients [34]. Similar results were obtained when wt and mutant recombinant PrPs were immunoblotted with α-PrP mAb IPC2, the epitope of which includes Met 213 and the adjacent disulfide bond, both distant from the site of the E200K mutation. In contrast, only the rHuPrP E200K was recognized by pAb DZS18, a pAb raised against a MetO rich maize repetitive sequence, which was shown to recognize enriched PrP^{Sc} as well as other oxidized proteins [8]. These results suggest that Helix-3 methionines in PrP E200K may undergo facilitated or spontaneous oxidation both in cells [34] and in its α-folded recombinant form. Indeed, Figure 5D shows that the monomers of wt and E200K HuPrP (23–231) are indistinguishable by far-ultraviolet CD spectroscopy at 25°C and pH 4.5, but they differ in their thermal denaturation profile. Curve fitting yielded Tm values of 60±0.5°C and 54.5±1°C for the wt and E200K chains, which agrees with previously reported destabilization of this mutant PrP under a different setup [36]. These results, as well as previous experiments showing charged-induced alterations of E200K PrP [37] suggest that changed dynamics of Helix-3 in the mutated protein might favor transient exposures of the contained methionines to ROS. The spontaneous oxidation of E200K PrP also explains the poor recognition of undigested PrP from E200K patients brain by both RGM and RVC pAbs (Fig. 2, 5).

Discussion

We have shown here that antibodies generated against reduced Helix-3 PrP Met residues could not recognize the majority of PrP^{Sc} forms. This finding applied to most PrP^{Sc} accumulated in scrapie-infected mouse brains and for all PrP^{Sc} accumulated in human CJD brains, as well as for all newly formed PrP^{Sc} in several prion-infected cell lines. Since reduction by MMA restored the recognition of brain and cell's PrP^{Sc} by these antibodies, we conclude that most Helix 3 Met residues in PrP^{Sc}, both as newly made in cells, or as long term accumulated in infected brains are oxidized. Our results also indicate that Met oxidation is also present in intermediate PrP forms, such as proteinase K sensitive and partially aggregated PrPs found in human and mouse infected brains, indicating that oxidation accompanies aggregation and precedes acquisition of proteinase K resistance by the nascent PrP^{Sc} molecules. In addition, we show here that pathogenic mutant PrP forms, as is the case for E200K PrP [18], are mostly oxidized even in the monomeric state. Taken together, our results are consistent with the conclusion that Helix-3 Met oxidation is an early event in the conversion of PrP^{C} into proteinase K resistant PrP^{Sc} and thus in prion formation and subsequent disease pathogenesis.

From a structural point of view, Met oxidation involves the transformation from a moderated hydrophobic to a hydrophilic side chain. While in protein exposed residues this chemical change may not have major structural effects, sulfoxidation of buried Met may impact the stabilization interactions maintaining the proteins 3D fold. Indeed, this intuitive prediction is in agreement with our theoretical studies, which showed that changing the sulfur atom of Met206 and M213, both single or in combination, by a sulfoxide destabilizes the native α-folded [15], thereby allowing for a conformational conversion. Indeed, increasing the polarity side chain at any of the conserved Helix-3 Met residues (Met205, Met206 and M213) impedes the native state folding and the appearance of proaggregating states [11,16,17,38,39]. Then, from these studies it can be proposed that the tolerance for the PrP α-fold is determined by the redox state of the Helix-3 Met residues and that the intolerance for the native state increases the probability of the productive conversion pathway.

Surprisingly, our results suggest that raising antibodies specific for PrP^{C} is not a difficult task. The Met rich area in Helix-3 appears to be quite immunogenic, as deduced by the fact that even immunization of rabbits with the relatively large peptide spanning amino acids 195–213 yielded antibodies against the Met rich area (see Figure 6). So was the case for the mAb IPC2, which was produced following the immunization of mice with full length recombinant mouse PrP [7]. Reagents similar to pAb RGM and RVC may have been produced in many laboratories, but their true meaning not understood. In contrast, raising antibodies against oxidized PrP peptides that may be specific for proteinase K sensitive and resistant forms of PrP^{Sc} has been unsuccessful thus far. This difficulty may relate to the well-established immunological barrier that precludes recognition of oxidized peptides by T-cell receptors [19,20]. Such immunological phenomena may partially explain the apparent lack of immune response against PrP^{Sc} in all species.

While the failure of our antibodies to recognize aberrant forms of mouse and human PrP was mostly quantitative, a recent MS study failed to detect high levels of Met213 oxidation in hamster PrP^{Sc} [40]. Indeed, while MS may be the method of choice to establish the presence of covalent modifications in proteins, its use for quantification of oxidation in this specific case may be limited. First, the labile character of sulfoxidation of Met residues does not allow for accurate separation of *in vivo* and *in vitro* modifications [41]. Furthermore, as opposed to detection of full length mature proteins by specific antibodies, MS detection operates on soluble peptides produced by proteolysis, each of which has different recovery pattern efficiencies, even in the same protein. Indeed, it was previously shown that recovery of the PrP tryptic peptide including M213 is quite poor, and that the recovery is even less efficient for the peptide including M206 [42]. In this study, we

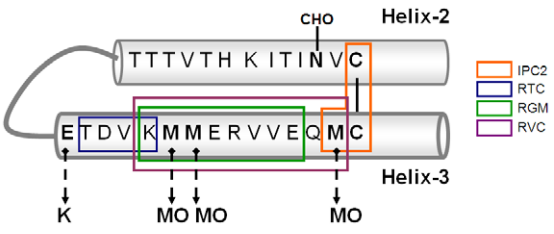

Figure 6. Scheme of Helix 2 and 3 of PrP including epitopes of α Helix 3 antibodies.
doi:10.1371/journal.ppat.1000977.g006

were unsuccessful in recovering the Helix3 area of HuPrP (23–230) E200K for MS analysis, likely because the mutation, which adds a digestion site for trypsin, generated labile peptides that could not be identified with significant yield. Eventhough, and given the right conditions, we assume that a combination of immunological reagent sand MS are the right methods to look for modifications in this and other proteins.

We also describe in this study how an antibody believed to detect E at codon 200 of wtPrP actually recognized a reduced Met Helix-3 sequence [34]. The reason for such misconception was that, if, as generally believed, no covalent modifications separated between the different forms of PrP, than the epitope of an antibody that recognizes wt PrP (E at codon 200) but not mutant PrP (K at codon 200) should include E at codon 200. We have shown here that despite the accuracy of the old results, the previous interpretation, suggesting that only mutant PrP converts into proteinase K resistant PrP in the brains of heterozygous patients may be mistaken in view of our new knowledge. While pAb RGM indeed did not detect PrP^{Sc} in brains from heterozygous E200K CJD patients (Figure 5), similar results were obtained for PK resistant PrP^{Sc} in brains from sporadic CJD patients, which comprise E at position 200. In addition, our results suggest that pAb RGM did not recognize E200K PrP in cells from homozygous subjects not because it carries K at codon 200, but because this mutant PrP form may be present in an oxidized form, as shown here for rHuPrP E200K. Most importantly, the finding that E200K PrP can undergo spontaneous oxidation at Helix-3 Met residues constitutes the first mechanistic clue explaining the late onset spontaneous appearance of CJD in carriers of pathogenic PrP mutations. Once oxidized, the conformation of the mutant PrP may be irreversibly impaired. We speculate that oxidative events may facilitate spontaneous CJD outbreaks in subjects carrying designated PrP mutations, as is the case for E200K mutation carriers. Indeed, the prevalence of familial CJD increases with age [43,44], as in the case for oxidative insults [45]. Whether oxidized mutant PrP can serve as a template for wt PrP conversion in heterozygous cases remains to be established.

While our results suggest that the oxidation of PrP forms may play a role in the formation of PrP^{Sc}, we have still to elucidate the conditions, kinetics and mechanism that lead to the initial irreversible oxidation of wt PrP Helix 3 Met residues. Interestingly, it has recently been shown that when fibrillar assemblies of recombinant PrP chains are annealed (by heat), they can transmit prion infectivity to wt animals [46], a result that could not be obtained with other recombinant PrP preparations [47]. It would be interesting to test whether synthetic prions as well as prions arising from diverse PMCA protocols [48–50] include oxidized PrP forms.

Based mainly on the fact that PrP ablated mice did not suffer from severe neurological damage [51], it was generally assumed that the function of PrP^{C} is not associated with prion disease pathogenesis. However, we show here that oxidation of Met residues on PrP^{C}, which may relate to its proposed antioxidative function [5], may be an essential step in acquisition of the aberrant PrP^{Sc} conformation. In fact, the association between oxidative stress and PrP conversion may link the activity of the prion proteins with other neurodegenerative conditions affected by stress and oxidation, such as ALS, AD and Parkinson's diseases [2,52,53], as well as to normal aging [45].

Materials and Methods

Ethical statement

Animal experiments were conducted under the guidelines and supervision of the Hebrew University Ethical Committee, which approved the methods employed in this project. Brain human samples were received following postmortem examinations from the Pathology Department of the Hadassah University Hospital. Immunobloting analysis, as that described in this manuscript (in search of PrPSc), is part of the routine pathological protocol applied on brains from suspected CJD cases. Our laboratory in the Hadassah Department of Neurology is the national referral center for CJD diagnosis (genetic and biochemical testing). The testing of these samples was approved by both the safety and ethical authorities of the Hadassah University Hospital. Since all cases of CJD and alike negative controls are unable to sign for such tests long before their death due to their medical condition, the relatives of these patients provided informed written consent for PM studies. Enabling close relatives to provide such consent is the standard policy of the Israeli Ministry of Health.

Peptide and protein productions

PrP peptides were synthesized on a Liberty peptide synthesizer with a Discover single mode microwave module, using standard Fmoc chemistry. Amino acids were purchased from Luxembourg Bio Technologies, except for Fmoc-Met(O)-OH, which was purchased from Novabiochem. Peptides were cleaved from the resin by treatment with a mixture 95% trifluoroacetic acid, 2.5% water, 2.5% triisopropylsilane, and precipitation with cold diethylether. The peptides were purified on a Vydac C8 semipreparative column using gradients of 5% to 60% acetonitrile in water, with 0.1% trifluoroacetic acid (TFA) in both solvents. The mass of the peptides was measured using an Applied Biosystems Voyager-DE Pro MALDI TOF mass spectrometer and verified to be within ± 1 Da of the theoretical mass. The purified peptides were lyophilized with 30% acetic acid to remove residual TFA.

Recombinant HuPrP(23–230) wt (with M129) and E200K chains were produced, purified and refolded into the α-form from their pET11a constructs using oxidized glutathione for disulfide bond formation and including 2 mM Met in refolding buffers [54,55]. The mutant chain was generated by site-directed mutagenesis using QuickChange protocols with the following primers: 5′-GAAGTTCACCAAGACCGACGTTAAG-3′ (forward) and 5′–CTTAACGT CGGTCTTGGTGAACTTC-3′ (reverse). Before their use, proteins were equilibrated by dialysis in 10 mM NaAc pH 4.5 containing 50 mM NaCl and 0.5 mM citrate and characterized both as monomers by dynamic light scattering using DynaPro Titan spectroscatter (Wyatt Technology). CD spectra were recorded using a Jasco-810 spectropolarimeter operating at 25°C, and using 0.1 cm pathlength cuvettes and about 13 μM protein concentration solutions. Thermal denaturation experiments were performed by following the changes in the ellipticity at 220 nm as the samples were heated from 15°C to 85°C at the rate of 1 degree/min.

Generation of α-PrP pAb

Designated PrP peptides were coupled to activated KLH (Sigma) and inoculated into rabbits while emulsified into Complete Freund's Adjuvant for the first immunization and Incomplete Freund's Adjuvant for subsequent injections. Most peptide immuniziations were performed at the animal facility of the Hebrew University-Medical School, except the ones for the RVC antibody which was produced by GenScript Inc (NJ, USA). KLH coupled with the Cys-KM peptide was first oxidized with 20 mM H_2O_2. After 15 min incubation at 37°C, the reaction was quenched by addition of 20 mM of free methionine before addition to the adjuvant. Following 3 lines of immunization, serum samples from all immunized rabbits were tested for their anti-PrP

activity. Rabbits with positive sera were immunized once again before final collection of blood. Antisera were purified by affinity chromatography, using for retention either peptides (RVC antibody) or Protein A (RTC and RGM antibodies).

Tissue sources and brain homogenate preparation

Brain samples of normal humans and patients with confirmed sporadic and genetic E200K CJD were obtained from Hadassah University Hospital Pathology department. Brains from mice infected with the RML scrapie prions and from golden hamsters inoculated with Sc237 prions were provided by the Animal Facility of the Hebrew University-Medical school. Brain homogenates (10% w/v) were prepared by repeated extrusion through an 18-gauge followed by a 21-gauge needle in phosphate-buffered saline (PBS), aliquoted and maintained at −70°C until use.

Cell lines

Naïve and scrapie infected ScN2a[23] and ScGT1 cells [24] were washed, collected and lysed in 1 ml lysis buffer (100 mM Tris pH 7.4, 100 mM NaCl, 1% NP40, 1 mM EDTA) for 10 min. Samples were then centrifuged at 2000 rpm for 15 min at 4°C, and the supernatant was concentrated by methanol precipitation. Pellets were resuspended in 2% sarkosyl/STE buffer (10 mM Tris–HCl, pH 7.5, 10 mm NaCl, 1 mM EDTA). Protein content was determined by a BCA kit (Pierce). Equal amounts of protein were treated in the presence and absence of 40 μg/ml proteinase K for 30 minutes in 37°C. Digestion was stopped by the addition of a protease inhibitor complex (Complete Protease Inhibitor Cocktail Tablets, Roche) before subjecting the samples to denaturation by boiling in the presence of sample buffer. Samples were then immunoblotted with the designated anti-PrP antibodies.

Immunoblotting experiments

Normal and prion-containing brain samples were homogenated at 10% (W/V) in 10 mM Tris, pH 7.4 and 0.3 M sucrose. Proteinase K digestions were performed by incubating 30 μl of 10% prion-infected brain homogenates with 2% sarkosyl for 30 min at 37°C with 40 μg/ml protease. Control samples were incubated at 37°C in the absence of proteinase K). After boiling in sample buffer, samples were subjected to SDS PAGE and immunoblotting with the diverse anti-PrP antibodies. For the inhibition experiments, nitrocellulose sheets comprising the transferred proteins were subjected either to a 1:2000 dilution of the designated antibody alone or preincubated for at least 2 hours with the appropriate synthetic peptide (2 μg/ml). Immunoblots were developed with α mouse or α rabbit antibodies AP or HRP-conjugated secondary antibodies (Promega, Madison WI).

N-methylmercaptoacetamide reduction

Proteinase K digested prion-infected cells or brain homogenates were treated with 6 M N-methylmercaptoacetamide (MMA) [22]. After 15 h of incubation at 37°C, samples were precipitated with 9 volumes of methanol (1 h, −80°C) and then centrifuged (10000 rpm, 30 min, 4°C). Pellets were washed twice with methanol and processed for SDS-PAGE analysis. When immunoblotting with IPC2, sample buffer was devoid of β-mercaptoethanol [7].

Sucrose gradient centrifugation experiments

Sarkosyl extracted brain extracts from human and mouse (normal and prion infected were subjected to a sucrose gradient as previously described [30]. Shortly, 140 μl of 10% brain homogenates (mouse:normal and scrapie infected; human: normal and CJD), extracted in the presence of 2% Sarkosyl were overlaid on a sucrose gradient composed of layers of increasing concentrations of sucrose (10–60%). Gradients were then centrifuged for 1 h at 55000 rpm in a Sorval mini-ultracentrifuge and subsequently 11 samples of 120 μl were collected from the top to the bottom. In the prion infected gradient fractions were digested in the presence and absence of 40 μg/ml proteinase K before immunobloting with either α PrP mAb 6H4 or pAb RVC.

Accession numbers/ID numbers

Human Prion Protein: P04156 (PRIO_HUMAN), Mouse Prion Protein: P04925 (PRIO_MOUSE), Hamster Prion Protein: P04273 (PRIO_MESAU).

Author Contributions

Conceived and designed the experiments: Tamar Canello, Ruth Gabizon. Performed the experiments: Tamar Canello, Kati Frid, Ronen Gabizon, Silvia Lisa, Ruth Gabizon. Analyzed the data: Tamar Canello, Kati Frid, Assaf Friedler, María Gasset, Ruth Gabizon. Contributed reagents/materials/analysis tools: Ronen Gabizon, Silvia Lisa, Assaf Friedler, Jackob Moskovitz, María Gasset. Wrote the paper: Tamar Canello, Ronen Gabizon, Jackob Moskovitz, María Gasset, Ruth Gabizon.

References

1. Prusiner SB, Scott MR, DeArmond SJ, Cohen FE (1998) Prion protein biology. Cell 93(3): 337–348.
2. Brown DR (2005) Neurodegeneration and oxidative stress: prion disease results from loss of antioxidant defence. Folia Neuropathol 43: 229–243.
3. Nadal RC, Abdelraheim SR, Brazier MW, Rigby SE, Brown DR, et al. (2007) Prion protein does not redox-silence Cu2+, but is a sacrificial quencher of hydroxyl radicals. Free Radic Biol Med 42: 79–89.
4. Brown DR, Clive C, Haswell SJ (2001) Antioxidant activity related to copper binding of native prion protein. J Neurochem 76: 69–76.
5. Brown DR, Sassoon J (2002) Copper-dependent functions for the prion protein. Mol Biotechnol 22: 165–178.
6. Pan KM, Baldwin M, Nguyen J, Gasset M, Serban A, et al. (1993) Conversion of alpha-helices into beta-sheets features in the formation of the scrapie prion proteins. Proc Natl Acad Sci U S A 90(23): 10962–10966.
7. Canello T, Engelstein R, Moshel O, Xanthopoulos K, Juanes ME, et al. (2008) Methionine sulfoxides on PrPSc: a prion-specific covalent signature. Biochemistry 47: 8866–8873.
8. Oien DB, Canello T, Gabizon R, Gasset M, Lundquist BL, et al. (2009) Detection of oxidized methionine in selected proteins, cellular extracts and blood serums by novel anti-methionine sulfoxide antibodies. Arch Biochem Biophys 485: 35–40.
9. Stahl N, Baldwin MA, Teplow DB, Hood L, Gibson BW, et al. (1993) Structural studies of the scrapie prion protein using mass spectrometry and amino acid sequencing. Biochemistry 32: 1991–2002.
10. Requena JR, Groth D, Legname G, Stadtman ER, Prusiner SB, et al. (2001) Copper-catalyzed oxidation of the recombinant SHa(29-231) prion protein. Proc Natl Acad Sci U S A 98: 7170–7175.
11. Hirschberger T, Stork M, Schropp B, Winklhofer KF, Tatzelt J, et al. (2006) Structural instability of the prion protein upon M205S/R mutations revealed by molecular dynamics simulations. Biophys J 90: 3908–3918.
12. Moskovitz J, Bar-Noy S, Williams WM, Requena J, Berlett BS, et al. (2001) Methionine sulfoxide reductase (MsrA) is a regulator of antioxidant defense and lifespan in mammals. Proc Natl Acad Sci U S A 98: 12920–12925.
13. Binger KJ, Griffin MD, Heinemann SH, Howlett GJ () Methionine-oxidized amyloid fibrils are poor substrates for human methionine sulfoxide reductases A and B2. Biochemistry 49: 2981–2983.
14. Tamguney G, Giles K, Glidden DV, Lessard P, Wille H, et al. (2008) Genes contributing to prion pathogenesis. J Gen Virol 89: 1777–1788.
15. Colombo G, Meli M, Morra G, Gabizon R, Gasset M (2009) Methionine sulfoxides on prion protein Helix-3 switch on the alpha-fold destabilization required for conversion. PLoS ONE 4: e4296.
16. Wolschner C, Giese A, Kretzschmar HA, Huber R, Moroder L, et al. (2009) Design of anti- and pro-aggregation variants to assess the effects of methionine oxidation in human prion protein. Proc Natl Acad Sci U S A 106: 7756–7761.
17. Lisa S, Meli M, Cabello G, Gabizon R, Colombo G, et al. (2010) The structural intolerance of the.PrP a-fold for polar substitution of the helix-3 methionines. Cell Mol Life Sci in press.

18. Hsiao K, Meiner Z, Kahana E, Cass C, Kahana I, et al. (1991) Mutation of the prion protein in Libyan Jews with Creutzfeldt-Jakob disease. N Engl J Med 324: 1091–1097.
19. Weiskopf D, Schwanninger A, Weinberger B, Almanzar G, Parson W, et al. (2010) Oxidative stress can alter the antigenicity of immunodominant peptides. J Leukoc Biol 87: 165–172.
20. Sulzer B, Perelson AS (1997) Immunons revisited: binding of multivalent antigens to B cells. Mol Immunol 34: 63–74.
21. Williamson RA, Peretz D, Pinilla C, Ball H, Bastidas RB, et al. (1998) Mapping the prion protein using recombinant antibodies. J Virol 72: 9413–9418.
22. Houghten RA, Li CH (1979) Reduction of sulfoxides in peptides and proteins. Anal Biochem 98: 36–46.
23. Butler DA, Scott MR, Bockman JM, Borchelt DR, Taraboulos A, et al. (1988) Scrapie-infected murine neuroblastoma cells produce protease-resistant prion proteins. J Virol 62: 1558–1564.
24. Leucht C, Simoneau S, Rey C, Vana K, Rieger R, et al. (2003) The 37 kDa/67 kDa laminin receptor is required for PrP(Sc) propagation in scrapie-infected neuronal cells. EMBO Rep 4: 290–295.
25. Liu Y, Sun R, Chakrabarty T, Manuelidis L (2008) A rapid accurate culture assay for infectivity in Transmissible Encephalopathies. J Neurovirol 14: 352–361.
26. Scott MR, Kohler R, Foster D, Prusiner SB (1992) Chimeric prion protein expression in cultured cells and transgenic mice. Protein Sci 1: 986–997.
27. Caspi S, Halimi M, Yanai A, Sasson SB, Taraboulos A, et al. (1998) The anti-prion activity of Congo red. Putative mechanism. J Biol Chem 273: 3484–3489.
28. Borchelt DR, Scott M, Taraboulos A, Stahl N, Prusiner SB (1990) Scrapie and cellular prion proteins differ in their kinetics of synthesis and topology in cultured cells. J Cell Biol 110: 743–752.
29. Caughey B, Race RE, Ernst D, Buchmeier MJ, Chesebro B (1989) Prion protein biosynthesis in scrapie-infected and uninfected neuroblastoma cells. J Virol 63: 175–181.
30. Tzaban S, Friedlander G, Schonberger O, Horonchik L, Yedidia Y, et al. (2002) Protease-sensitive scrapie prion protein in aggregates of heterogeneous sizes. Biochemistry 41: 12868–12875.
31. Safar J, Ceroni M, Piccardo P, Liberski PP, Miyazaki M, et al. (1990) Subcellular distribution and physicochemical properties of scrapie-associated precursor protein and relationship with scrapie agent. Neurology 40: 503–508.
32. Safar J, Wille H, Itri V, Groth D, Serban H, et al. (1998) Eight prion strains have PrP(Sc) molecules with different conformations. Nat Med 4: 1157–1165.
33. Serban D, Taraboulos A, DeArmond SJ, Prusiner SB (1990) Rapid detection of Creutzfeldt-Jakob disease and scrapie prion proteins. Neurology 40: 110–117.
34. Gabizon R, Telling G, Meiner Z, Halimi M, Kahana I, et al. (1996) Insoluble wild-type and protease-resistant mutant prion protein in brains of patients with inherited prion disease. Nat Med 2: 59–64.
35. Chen SG, Parchi P, Brown P, Capellari S, Zou W, et al. (1997) Allelic origin of the abnormal prion protein isoform in familial prion diseases. Nat Med 3: 1009–1015.
36. Swietnicki W, Petersen RB, Gambetti P, Surewicz WK (1998) Familial mutations and the thermodynamic stability of the recombinant human prion protein. J Biol Chem 273: 31048–31052.
37. Zhang Y, Swietnicki W, Zagorski MG, Surewicz WK, Sonnichsen FD (2000) Solution structure of the E200K variant of human prion protein. Implications for the mechanism of pathogenesis in familial prion diseases. J Biol Chem 275: 33650–33654.
38. Winklhofer KF, Heske J, Heller U, Reintjes A, Muranyi W, et al. (2003) Determinants of the in vivo folding of the prion protein. A bipartite function of helix 1 in folding and aggregation. J Biol Chem 278: 14961–14970.
39. Hart T, Hosszu LL, Trevitt CR, Jackson GS, Waltho JP, et al. (2009) Folding kinetics of the human prion protein probed by temperature jump. Proc Natl Acad Sci U S A 106: 5651–5656.
40. Silva CJ, Onisko BC, Dynin I, Erickson ML, Vensel WH, et al. Assessing the role of oxidized methionine at position 213 in the formation of prions in hamsters. Biochemistry 49: 1854–1861.
41. Froelich JM, Reid GE (2008) The origin and control of ex vivo oxidative peptide modifications prior to mass spectrometry analysis. Proteomics 8: 1334–1345.
42. Onisko B, Dynin I, Requena JR, Silva CJ, Erickson M, et al. (2007) Mass spectrometric detection of attomole amounts of the prion protein by nanoLC/MS/MS. J Am Soc Mass Spectrom 18: 1070–1079.
43. Spudich S, Mastrianni JA, Wrensch M, Gabizon R, Meiner Z, et al. (1995) Complete penetrance of Creutzfeldt-Jakob disease in Libyan Jews carrying the E200K mutation in the prion protein gene. Mol Med 1: 607–613.
44. Chapman J, Ben-Israel J, Goldhammer Y, Korczyn AD (1994) The risk of developing Creutzfeldt-Jakob disease in subjects with the PRNP gene codon 200 point mutation. Neurology 44: 1683–1686.
45. Stadtman ER, Berlett BS (1997) Reactive oxygen-mediated protein oxidation in aging and disease. Chem Res Toxicol 10: 485–494.
46. Makarava N, Kovacs GG, Bocharova O, Savtchenko R, Alexeeva I, et al. (2010) Recombinant prion protein induces a new transmissible prion disease in wild-type animals. Acta Neuropathol 119: 177–187.
47. Legname G, Baskakov IV, Nguyen HO, Riesner D, Cohen FE, et al. (2004) Synthetic mammalian prions. Science 305: 673–676.
48. Saborio GP, Permanne B, Soto C (2001) Sensitive detection of pathological prion protein by cyclic amplification of protein misfolding. Nature 411: 810–813.
49. Atarashi R, Moore RA, Sim VL, Hughson AG, Dorward DW, et al. (2007) Ultrasensitive detection of scrapie prion protein using seeded conversion of recombinant prion protein. Nat Methods 4: 645–650.
50. Wang F, Wang X, Yuan CG, Ma J Generating a prion with bacterially expressed recombinant prion protein. Science 327: 1132–1135.
51. Bueler H, Fischer M, Lang Y, Bluethmann H, Lipp HP, et al. (1992) Normal development and behaviour of mice lacking the neuronal cell-surface PrP protein [see comments]. Nature 356: 577–582.
52. Varadarajan S, Yatin S, Aksenova M, Butterfield DA (2000) Review: Alzheimer's amyloid beta-peptide-associated free radical oxidative stress and neurotoxicity. J Struct Biol 130: 184–208.
53. Chi L, Ke Y, Luo C, Gozal D, Liu R (2007) Depletion of reduced glutathione enhances motor neuron degeneration in vitro and in vivo. Neuroscience 144: 991–1003.
54. Gonzalez-Iglesias R, Pajares MA, Ocal C, Espinosa JC, Oesch B, et al. (2002) Prion protein interaction with glycosaminoglycan occurs with the formation of oligomeric complexes stabilized by Cu(II) bridges. J Mol Biol 319: 527–540.
55. Makarava N, Baskakov IV (2008) Expression and purification of full-length recombinant PrP of high purity. Methods Mol Biol 459: 131–143.

Artículo 2. The structural intolerance of PrP alpha-fold for polar substitution of the helix-3 methionines.

La conversión estructural de PrP^{C} en PrP^{Sc}, que supone una transición desde un estado monomérico principalmente helicoidal hasta uno polimérico rico en estructura-β, es un proceso complejo en el que participan etapas de desestabilización de la conformación nativa, replegamiento y ensamblaje (77). A raíz de los resultados de *Colombo y cols* (2009) y *Canello y cols* (2010), la sulfoxidación irreversible de M206 y M213 en la cadena de PrP^{C} se posiciona como un interruptor covalente pro-conversor (417, 423). No obstante, el mecanismo de acción estructural de este interruptor requiere el uso de sistemas modelo. Los estudios teóricos de *Colombo y cols* 2009, que permiten la sustitución de metionina por MetO con especificidad de secuencia, demuestran que la sulfoxidación impone un incremento de flexibilidad del estado nativo. Sin embargo estos estudios tienen como limitaciones el uso de la región 121-231 y la escala temporal (las simulaciones son de 80 ns) (417).

El empleo de la cadena completa de PrP y el estudio experimental del efecto de esta modificación plantea una serie de problemas. Por un lado, la oxidación de Met es una reacción química inespecífica y la susceptibilidad a esta reacción viene dada por el grado de exposición. En PrP, que contiene 9 Met y M206 y M213 las más enterradas, la oxidación química generaría un conjunto de especies con menor representación de las deseadas requiriendo estrategias de especificidad de sitio. Para ello, las Met cuya oxidación no es deseable pueden sustituirse por Leu y, a continuación realizar una oxidación química (393). Alternativamente, puede recurrirse a modelos de MetO mediante mutagénesis dirigida. De estos modelos, la sustitución Met por Gln reproduce los cambios de polaridad asociados a la sulfoxidación y respeta las condiciones de tamaño de la cadena, sin embargo, es un residuo altamente representado en secuencias que forman amiloides y por ello puede provocar reacciones adicionales. Por el contrario, la sustitución por Ser, que conlleva una reducción del tamaño de la cadena, respeta la tendencia helicoidal y polaridad de MetO (454). En este trabajo, empleando modelos de MetO basados en la sustitución de metionina por serina, se persigue determinar el mecanismo estructural de acción de las MetO de α3 de PrP empleando estudios teóricos y biofísicos. Mi contribución en este trabajo ha sido la producción y caracterización de las cadenas recombinantes de PrP.

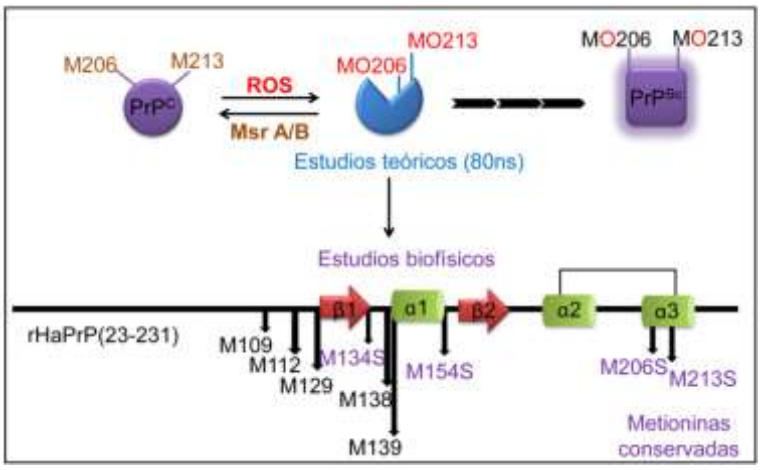

Cell. Mol. Life Sci. (2010) 67:2825–2838
DOI 10.1007/s00018-010-0363-1

Cellular and Molecular Life Sciences

RESEARCH ARTICLE

The structural intolerance of the PrP α-fold for polar substitution of the helix-3 methionines

Silvia Lisa · Massimiliano Meli · Gema Cabello · Ruth Gabizon · Giorgio Colombo · María Gasset

Received: 21 February 2010 / Revised: 17 March 2010 / Accepted: 19 March 2010 / Published online: 9 May 2010

Abstract The conversion of the cellular prion protein (PrP^C) into its disease-associated form (PrP^{Sc}) involves a major conformational change and the accumulation of sulfoxidized methionines. Computational and synthetic approaches have shown that this change in the polarity of M206 and M213 impacts the C-terminal domain native α-fold allowing the flexibility required for the structural conversion. To test the effect in the full-length molecule with site-specificity, we have generated M-to-S mutations. Molecular dynamics simulations show that the replacement indeed perturbs the native state. When this mutation is placed at the conserved methionines of HaPrP(23–231), only substitutions at the Helix-3 impair the α-fold, stabilizing a non-native state with perturbed secondary structure, loss of native tertiary contacts, increased surface hydrophobicity, reduced thermal stability and an enhanced tendency to aggregate into protofibrillar polymers. Our work supports that M206 and M213 function as α-fold gatekeepers and suggests that their redox state regulate misfolding routes.

Keywords Protein conformational switches · Methionine oxidation · Prion protein conversion · Amyloids

Abbreviations

PrP^C	Cellular prion protein
PrP^{Sc}	Disease-related form of PrP
HuPrP(125–229)	Polypeptide chain representing the globular domain of the human PrP
HaPrP(23–231)	Polypeptide chain representing the mature chain of the hamster PrP
MD	Molecular dynamics
RWISP	Root weighted square inner product
CP	Communication propensity
CD	Circular dichroism
DLS	Dynamic light scattering
R_h	Hydrodynamic radius
ThT	Thioflavin T
AFM	Atomic force microscopy

Introduction

Prions are infectious proteins that use a conformational code for self-perpetuation. In mammals, prions causing transmissible neurodegenerative disorders are composed mainly of PrP^{Sc}, an altered form of the cellular prion protein (PrP^C) [1, 2]. The long-standing hypothesis of prion biology is that the distinct biological and physicochemical properties separating PrP^C and PrP^{Sc} relate only to the conformational differences of the C-terminal domain, which adopts a major globular α-fold in PrP^C and displays a high content of β-sheet structure in PrP^{Sc} [3–11]. However, the populations of PrP^C and PrP^{Sc} also differ in the

S. Lisa and M. Meli contributed equally to this work.

S. Lisa · G. Cabello · M. Gasset (✉)
Instto Química-Física "Rocasolano", CSIC,
Serrano 119, 28006 Madrid, Spain
e-mail: mgasset@iqfr.csic.es

M. Meli · G. Colombo
Istituto di Chimica del Riconoscimento Molecolare,
Consiglio Nazionale delle Ricerche, Via Mario Bianco 9,
20131 Milan, Italy

R. Gabizon
Department of Neurology, The Agnes Ginges Center for Human Neurogenetics, Hadassah University Hospital,
91120 Jerusalem, Israel

redox state the methionines of Helix-3, suggesting a possible role for these residues in facilitating the structural change [12–15].

The chain reorganization accompanying the conversion of PrP^{C} to PrP^{Sc} proceeds through a complex pathway involving the obligatory initial destabilization of the PrP^{C} α-fold for its subsequent refolding and assembly into PrP^{Sc} [1, 9, 16–19]. Similarly to tau, the hyperphosphorylation of which impairs function and provokes accumulation, sulfoxidation of PrP methionines could also regulate the folding repertoire through the reorganization of intra- and intermolecular bonds [9, 20–22]. As opposed to the enzymatic nature of phosphorylation, methionine sulfoxidation is a chemical modification that takes place in response to oxidative insults and lacks sequence specificity [23–26]. The oxidation product, a mixture of *R,S*-sulfoxide isomers, is reversed by the action of the isomer-specific methionine sulfoxide reductases (MrsA and MsrB), both of which are impaired on ageing [23, 24].

The theoretical analysis of the structural and dynamic impact of the sulfoxidation of any of the Helix-3 methionines conserved within all mammalian species studied has suggested its potential as a destabilizing switch [14]. These modifications alter the stability of the α-fold by disrupting the network of inter-residue interactions responsible for its stability. This destabilization in turn determines a decrease in the internal dynamic coordination of the native state, favoring the transition to alternative conformational states. Synthetic approaches focused on this region of the protein have shown that site-specific substitution of these Met residues with either the more hydrophobic norleucine or the highly hydrophilic methoxinine does in fact modulate the conformation of the chain and its aggregation behavior [15]. However, PrP^{Sc} formation requires a larger polypeptide chain than that accessible to conventional solid-phase synthesis and its high number of Met residues precludes the control in the residue number and position of the covalent modification using chemical oxidative approaches [4, 23–27].

To test the theoretical predictions on experimental grounds, we have used the full-length PrP, the mature chain without signal peptides, and employed mutagenesis to confer site-specificity in the changes [4, 28, 29]. We chose Ser to replace Met since, while it is shorter than Met and chemically different from the sulfoxidized version of Met (MetO), Ser retains the helical propensity and polarity of the MetO [29]. The other possibility previously used for such substitution would be Gln. However, while this amino acid also retains some helical propensity and reproduces the length of the chain, its polarity arises from an amide bond, not only oxygen [30]. In addition, Gln is over-represented in prion-forming sequences, therefore possibly leading to other effects [31]. This strategy, based on providing a property of the covalent modification by mutagenesis (here, the polarity of MetO mimicked with Ser replacement) has been previously used in mimicking Ser/Thr phosphorylation by Asp substitution in the study of the independent and site effects in proteins containing multiple modification sites [22].

Using wt HaPrP(23–231) as the template for mutagenesis, biophysical studies show that the M-to-S replacement of any of the conserved methionines of Helix-3, singly or in combination, prevents the formation of the α-fold and stabilizes a non-native intermediate state with an increased tendency for aggregation and amyloid formation tendency.

Materials and methods

Molecular dynamics

Molecular dynamics (MD) simulations were performed using the 3D structure of HuPrP(125–229) (PDB entry 1QLZ) as a starting point essentially as described [14]. M-to-S mutations were generated at the desired positions by side chain replacement using the MUTATE command of the WHATIF package [14, 32]. Oxidation variants were generated by replacing the sulfur atoms of M206, M213, or both by an (*S*)-sulfoxide group as reported previously [14]. For each system, two independent long-time scale all-atom MD simulations were performed in explicit water at 310 K. Each 100-ns simulation was run independently using different sets of initial velocities as described previously [14]. The two simulations for each system were combined and analyzed in terms of the dynamic subspace spanned and the internal dynamics using different approaches to identify structural and dynamic similarities/differences introduced in the α-fold. Structural comparison of HuPrP and HaPrP α-folds was performed using the overlapped region of their 3D structures (PDB entries 1QLZ and 1B10) [14, 33]. The similarities/differences in the environments of M206 or M213 in the two species were evaluated by calculating all the residues in non-bonded contact with either of them using the Maestro Software package from Schrödinger Inc.

Mutation, production, and folding of the HaPrP(23–231) chains

HaPrP(23–231) chains were produced, purified, and refolded into the α-form from their pET11a constructs using oxidized glutathione for disulfide bond formation and including 2 mM Met in the refolding buffers [27, 34]. The protein concentrations were determined spectrophotometrically as described [34]. All proteins were used within 2 weeks after their production. The different mutants were produced by site-directed mutagenesis using QuickChange

protocols with the following primers (only the forward primers are given): M134S: 5′-CTGGGGAGTGCCTC CTCTAGACCCATG-3′; M154S: 5′-CTACCGTGAAAA CTCCAATCATACCC-3′; M206S: 5′-GACATCAAGA TATCCGAGCGCGTGG-3′; M213S: 5′-GTGGTGGAGC AGTCCTGTACCACCCAG-3′; M213L: 5′-GTGGTGAG CAGCTCTGTACCACCCAG-3′. The chain integrity of the different proteins was assessed during the experiments by SDS-PAGE using 15% acrylamide gels and Coomassie Blue staining procedures.

Dynamic light scattering

Dynamic light scattering (DLS) measurements were carried out using the DynaPro Titan spectroscatter (Wyatt Technology) with controlled temperature and Dynamics software was used for data acquisition and analysis. All solutions (protein and buffers) were filtered through 0.22-μm Millex-GV filters. The samples (20 μl) were placed in a quartz cuvette and measured at a constant temperature of 15 or 25 °C, accumulating 20 measurements per sample. Values for the species hydrodynamic radius (R_h) and proportion (%) were derived from the autocorrelation data assuming a model of n-monodisperse globular proteins and using the software provided by the manufacturer. The data were compared by one-way ANOVA with Bonferroni′s post-test analysis using GraphPad Prism v 4.0.

Circular dichroism

CD spectra were recorded using a Jasco-810 spectropolarimeter operating at 15°C and with 0.1 (far-UV, 250–200 nm) and 1 (near-UV, 320–250 nm) cm pathlength cuvettes. Approximately 13 μM (far-UV) and 30 μM (near-UV) protein concentration solutions were used. For each measurement, we averaged six scans. The data were corrected for the buffer components and then transformed into Θ_{mrw} using 110 as the mean residue molecular weight. Thermal denaturation experiments were performed by following the changes in the ellipticity (Θ) at 222 nm as the samples were heated from 15 to 90°C at the rate of 1°/min. The reversibility of the secondary structure changes was assessed by comparing the spectra to those recorded after cooling to 15°C from 90°C. The changes in Θ^{222} with temperatures were normalized to the fraction of unfolded protein (f_U) using:

$$f_U = \left(\Theta^{222} - \Theta_N^{222}\right)/\left(\Theta_U^{222} - \Theta_N^{222}\right) \quad (1)$$

Here N and U refer to the native and unfolded states, respectively. The value of f_U was plotted as a function of temperature for the calculation of Tm and ΔHm [35]. The experimental Tm values were converted into the apparent relative changes in free energy with respect to the wt protein ($\Delta\Delta G°_{MS/wt}$) using the equation:

$$\Delta\Delta G_{MS/wt} = \Delta Hm_{wt} \times [1 - Tm_{wt}/Tm_{MS}] \quad (2)$$

Tm_{wt} and Tm_{MS} are the Tm values for the wt and mutant protein, respectively, and ΔHm_{wt} is the denaturation enthalpy of the wt protein [36, 37].

Bis-ANS binding

Fluorescence emission spectra of bis-ANS (30 μM) were recorded in the presence and absence of 10–13 μM HaPrP(23–231) wt and its mutants using an SLM 8100 spectrofluorimeter equipped with a thermostated cell-holder. Spectra were recorded using 0.5-cm square cuvettes and an excitation wavelength of 380 nm. After correction for the buffer contribution and instrumental factors, we plotted the intensity at 470 nm as a function of temperature.

Protein aggregation analysis

Protein solutions at various concentrations were prepared in 20 mM MES pH 6.5, 50 mM NaCl, 0.1 mM citrate and 0.03% NaN_3. After increasing the salt concentration to 0.35 M NaCl on ice, the solutions were incubated at 37°C under continuous orbital agitation at 100 rpm (unless stated otherwise). The samples were then analyzed for turbidity and protein solubility at different times. The turbidity was determined from absorbance readings at 450 nm using 0.5-cm quartz cuvettes in an Ultrospec 3000Pro equipped with a thermostated cell holder [34]. Protein solubility was determined from the partition of the protein between the supernatant and the soluble phase during centrifugation at 13,000 × *g* for 10 min at 4°C [38].

Thioflavin T binding

The kinetics of thioflavin T (ThT) binding were monitored by bottom reading of fluorescence intensity in a POLARstar microplate reader (BMG Labtech) using 450-nm excitation and 480-nm emission filters, 0.20-ml samples and 15 μM ThT concentration. For best reproducibility, the reaction mixtures were prepared at 4°C into wells of black 96-well plates (Corning), sealed with foiled film and placed into the reader at 37°C to start the measurement. The measurement program consisted of ten flashes reading every 10 min with 1-min of orbital 1-mm diameter shaking at 100 rpm. The dead time between the preparation of the protein and the start of the measurement was usually 10 min. All measurements were done in triplicate and the experiments were repeated at least twice using two different protein batches. When required, the lag-phase was determined as described [39].

Atomic force microscopy

Typically, 2 µl of the protein solutions was diluted 1:50 with H_2O after 24 h of polymerization reaction and deposited onto freshly cleaved mica surfaces. The samples were allowed to adsorb for 15 min and then were washed extensively with H_2O and dried with a gentle stream of N_2. Atomic force microscopy (AFM) studies were performed using a PicoSPM LE AFM scanner (Molecular Imaging, Phoenix, AZ, USA) in acoustic alternating current mode with Si,N-ACT type cantilevers (ScienTec) that had a tip radius <10 nm and a spring constant of 25–75 N/m. The images (1 × 1 µm scans) were collected at a scan rate of 0.7–1 lines/s and analyzed using WSxM 5.0 Nanotec software.

Results

MD simulations reveal that the M-to-S replacements perturb the PrP native state

Despite the chemical differences of the side-chain functional groups, M-to-S mutations provide the polar change of the sulfoxidation of methionine side chains while retaining the secondary structure propensities [27, 28]. To determine whether this polar substitution also behaves as a structural destabilizer, we first analyzed the impact of the mutations on the dynamic evolution of the C-terminal domain α-fold via MD simulations (Fig. 1). To compare the results with those previously obtained for the sulfoxide-variants, we performed this analysis using the 3D structure of HuPrP(125–229) and with its M206S, M213S, and M206S-M213S mutants [14].

First, we investigated the effect on the global dynamic properties. To this end we used essential dynamics (ED) analysis to identify concerted, non-random structural fluctuations in the proteins [40]. The analysis is based on the covariance-matrix of the positions of pairs of residues that can be extracted from each simulation. By focusing on the subset of the principal eigenvalues and eigenvectors of the covariance matrix, it is possible to define the "essential subspace" of the protein (generally correlated with the functional aspects of the conformational dynamics) and use the RWSIP (root weighted square inner product) parameter to calculate variations ([41], Table 1). A RWSIP value of 1 between two simulations would indicate that they are spanning identical conformational spaces, whereas a value

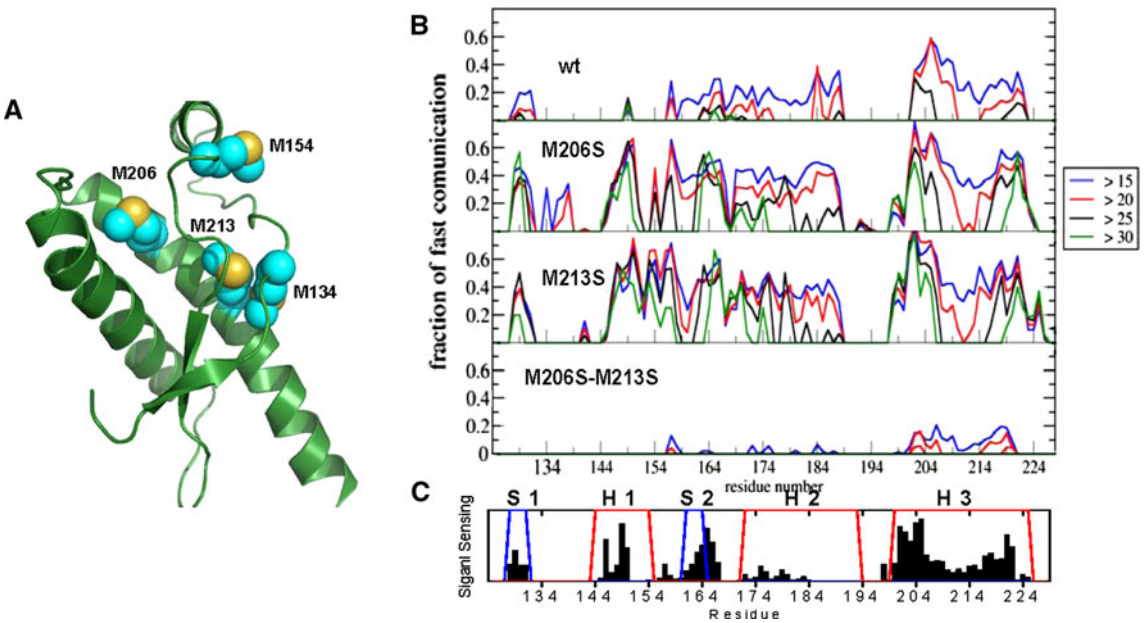

Fig. 1 The relative dynamic effects of the substitution of the conserved Helix-3 Met by Ser in the HuPrP(125–229) α-fold, as analyzed by using MD. **a** The location of M134, M154, M206, and M213, the conserved methionines within all mammalian species studied, in the 3D structure of the HuPrP(125–229) α-fold. **b** The effects of the M-to-S mutations on the internal dynamic of the protein followed by the communication efficiency of all residues at increasing distances. Each bin refers to a residue and shows the fraction of residues of the whole protein that are highly prone to communicate with it (CP < 0.025). In each histogram, only communications at distances greater than a given threshold (>15, >20, >25, and >30 Å) are considered. **c** The signal sensing of the Helix-3 on M206 and M213 sulfoxidation. The variation of the fraction of residues with high CP in the M206 and M213 sulfoxidated chain with the residue number was taken from [14] and averaged for the distances. The regions corresponding to native strands (*blue*, S1,S2) and helices (*red*, H1,H2,H3) are highlighted. The unmodified protein is indicated as wt, whereas the mutated and oxidized forms are indicated as M-to-S or MO, respectively, together with the location (position 206, 213, or both)

Table 1 Similarities and differences between the essential subspaces spanned by sulfoxidized (MO) and M-to-S mutant HuPrP (125–229) chains analyzed with the RWSIP values

	wt	MO206	MO213	MO206, MO213	M206S	M213S	M206S, M213S
wt	1	0.65	0.63	0.51	0.65	0.70	0.51
MO206		1	0.42	0.54	0.68	0.61	0.50
MO213			1	0.25	0.63	0.75	0.70
MO206, MO213				1	0.51	0.65	0.45
M206S					1	0.77	0.65
M213S						1	0.63
M206S, M213S							1

Values refer to the RWSIP parameter calculated as described [41]. A value equal to 1 indicates that the two dynamic subspaces are identical, while a parameter value equal to 0 indicates absence of any superposition. The calculations were carried out on the combined trajectories for each of the mutants. Site of modification or mutation is indicated with the residue number

of 0 indicates the absence of superposition in the dynamic evolution of the systems. According to these metrics, the introduction of a single M-to-S mutation at positions 206 or 213 or a single sulfoxidation occurs with a comparable reduction in the similarity of the dynamic subspaces with the wt protein, with RWSIP values around 0.65 (Table 1). Interestingly, very similar low RWSIP values are observed for the double M-to-S mutation and for the double sulfoxidation variants. These results support that single and double M-to-S mutations perturb the conformational dynamic evolution of the native fold, a property previously found for the sulfoxidated forms [14].

To further determine whether the mutation can actually mimic the global dynamic effects of the oxidation, we calculated the RWSIP-based similarities of the essential subspaces spanned by the mutants and the sulfoxidized variants on the combined trajectories. Indeed, the RWSIP between the dynamics of the single variants at position 206 (M206S and M206MO) yielded a value of 0.68, and the RWSIP value calculated between the dynamics of the single variants at position 213 (M213S and M213MO) yielded a value of 0.75. The superposition of the essential subspaces of the double mutants is lower than for the previous cases, with an RWSIP value of 0.45. These latter results indicate that the perturbation introduced by double mutations forces the protein to sample different regions of the conformational space. In either case, M-to-MO or M-to-S substitutions, the double substitution variants span essential dynamic spaces that diverge from the native one. As a caveat, it should be considered that the simulation length, while being long compared to those currently run, may not be fully converged or may not have fully sampled all the relevant regions of the phase space. Taken together, these results show that M-to-S replacement, as M-to-MO, reduce the similarity of the dynamic subspaces to those of the wt protein, and that, for changes at the same positions, the similarity between the mutation and the oxidation decreases in the order from 213 > 206 > 206–213.

We next analyzed the differential effects on the internal dynamics of the protein (Fig. 1b). For this purpose, we calculated the communication propensity (CP) histograms of the different mutants of the protein according to the method described [14]. Each bin in the histogram represents the fraction of residues that have high communication efficiency with a given residue (CP < 0.025) among those with a distance higher than a certain threshold (i.e., 15, 20, 25 or 30 Å) from that residue. The value associated with each bin indicates the degree of coordination of that specific residue with the rest of the protein. It must be noted that the number of residues that communicate efficiently (y-axis) with a certain target residue (x-axis) represents a reverberation of the degree of internal coordination of the residue–residue pairs in a protein structure and it reports on the possible diffusion of dynamic effects due to specific perturbations. In this context, these calculations provide a qualitative view of the role of a region as a signal sensor, the signal being in this case a change in the chemical group. Interestingly, single M-to-S mutations at positions 206 and 213 increase the communication propensity mainly at longer distances of residues located at the N-terminal flank of the Helix-3, at the residues connecting the Strand-2 with Helix-2, and at the residues forming Helix-1. Strikingly, the double mutation to S in the M206S-M213S variant results in an almost complete abrogation of the native communication propensities among pairs of residues. Even at short threshold distances, communication is lost and no residue pairs are found to communicate efficiently. These results indicate that the double mutation severely perturbs the coordinated dynamics of the native fold, compared to the wt case, allowing the protein to visit alternative dynamic states, characterized by the lack of long-range communications between residue pairs. The latter data should, however, not be considered as a reverberation of the additive effect of the double M-to-S mutations: the perturbation introduced by the double mutation has an effect that is not limited to a "linear

combination" of the effects of the single mutations. As shown in the case of the RWSIP calculations, the double mutation determines a complex modulation of the dynamics that can be (partially) captured by investigating the degree of correlated and coordinated motions that characterize the mutated proteins. Summarizing, these data show that the M-to-S substitutions indeed trigger transmissible structural signals as found for the oxidative modifications [14].

Then, the emerging picture is that the polarity increase in the side chain provided by the M-to-S replacement perturbs the global coordination and essential dynamics of the α-fold native state. However, its destabilizing potency differs from that observed for the sulfoxidation of equivalent methionines.

M-to-S mutations in Helix-3 distort the HaPrP(23–231) α-fold

The 3D structures of the globular domain of both HuPrP and HaPrP, and in particular the environments of M206 and M213, are highly conserved (Fig. 2a). The root mean squared deviation (RMSD) between the two 3D structures is 1.5 Å. The residues in Van der Waals contact with M213 [208-VVEQ-CITQ-217; 158-PNQV-161; 134-MSRP-136 in HuPrP(125–229)] are identical in both protein structures. The residues in contact with M206 [202-DVKM-ERVVE-211; F198; H187; I184 and 157-YP-158 in HuPrP(125–229)] differ only in respect to residues 203 (V/I Hu/Ha) and 205 (M/I Hu/Ha). It can therefore be assumed that the general trend of the structural perturbations induced by the polarity increase in the Helix-3-conserved Met residues should be species-independent.

Based on the previous considerations, we generated the full-length M206S, M213S, and M206S-M213S mutants using the HaPrP(23–231) wt chain as a template (Fig. 2a). We included the M134S and M154S mutations, as these residues are also conserved and flank secondary structure elements (Strand-1 and Helix-1, respectively). In addition, we prepared the mutant M213L as a control for site substitution (Figs. 1a, 2c). All these chains were produced in *E. coli* inclusion bodies, isolated under denaturing conditions and folded to the α-form [29, 34]. The chain integrity was assessed during experiments by SDS-PAGE (Fig. 2d).

We began the study of the effect of the M-to-S mutations on the conformation and stability of the HaPrP(23–231) α-fold using dynamic light scattering (DLS). In general, DLS provides information on the homogeneity and particle size of the protein solutions that can be transformed into molecular-sized species provided that hydrodynamic models are available. Despite the structural divergence of α-HaPrP(23–231) wt from classical globular

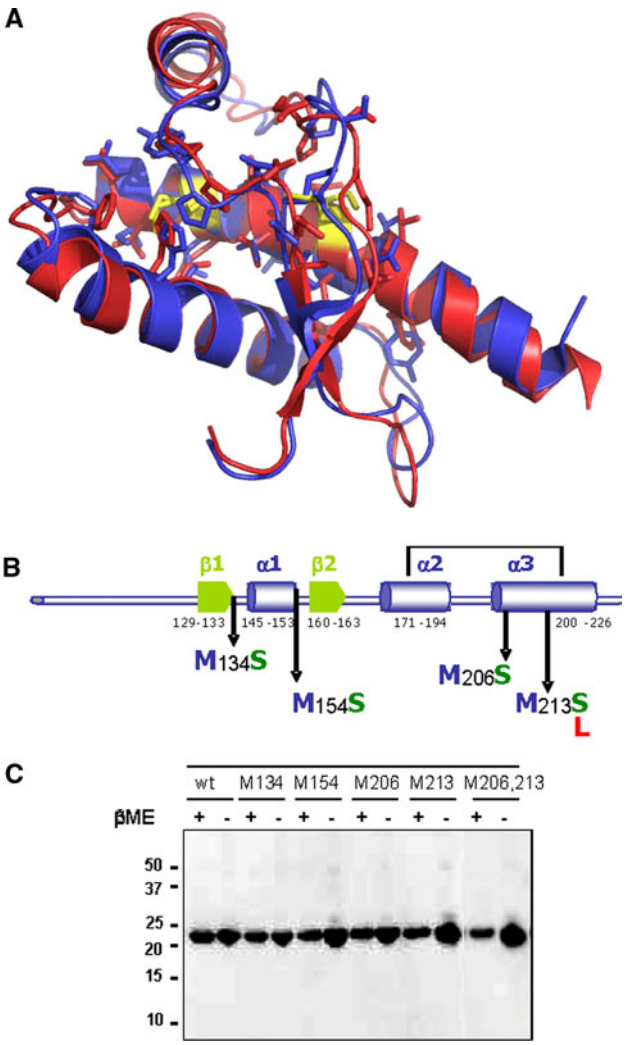

Fig. 2 Pseudosulfoxidation mutants of HaPrP(23–231). **a** Overlapped 3D structures of the HuPrP (*red*) and HaPrP (*blue*) globular domains. Residues in Van der Waals contact with M206 and M213 are highlighted. **b** The HaPrP(23–231) mutant design. **c** PAGE-SDS analysis of HaPrP(23–231) wt and its M134S, M154S, M206S, M213S, and M206S-M213S used in the study, both in the absence and presence of *β*-mercaptoethanol. The M213L mutant yielded identical results

proteins and flexible polymers (the N-terminal domain is flexible and the C-terminal domain is globular), its monomeric behavior at pH 4.5 at protein concentrations up to 0.8 mM allows the determination of the R_h for the monomer. This can be used as an internal control for variations ([42] and references therein). As depicted in Table 2, and at pH 4.5 and at 15°C, all proteins being studied yield an R_h of about 3.7 ± 0.5 nm. Therefore, they can be described essentially as monomers. However, only the M206S, M213S, and M206S-M213S mutants permit the detection of an additional minor species (amounting to about 15% of the total) featured by a higher R_h (9.2 ± 0.4 nm), suggesting the presence of soluble

Table 2 Particle sizing of α-HaPrP(23–231) wt and of its mutants by dynamic light scattering

Temperature	15 (°C)				25 (°C)			
HaPrP(23–231)	$R_{h1}^{a,c}$ (nm)	%	$R_{h2}^{b,c}$ (nm)	%	$R_{h1}^{a,c}$ (nm)	%	$R_{h2}^{b,c}$ (nm)	%
wt	3.2 ± 0.2	95 ± 5			3.9 ± 0.5	95 ± 4		
M134S	4.0 ± 0.6	94 ± 5			4.4 ± 0.2	89 ± 2	9.6 ± 0.6	11 ± 4
M154S	3.3 ± 0.5	95 ± 5			3.3 ± 0.2	80 ± 5	9.5 ± 0.4	20 ± 7
M206S	4.5 ± 0.5	91 ± 6	9.0 ± 0.6	9 ± 6	4.5 ± 0.2	24 ± 10	9.5 ± 0.3	76 ± 8
M213S	3.3 ± 0.2	85 ± 6	9.0 ± 0.2	15 ± 7			8.8 ± 0.2	98 ± 4
M206S, M213S	3.6 ± 0.3	87 ± 7	9.1 ± 0.2	13 ± 6			9.0 ± 0.1	97 ± 4
M213L	3.3 ± 0.3	96 ± 5			3.6 ± 0.4	96 ± 4		

Displayed data correspond to measurements performed at pH 4.5. The values of the hydrodynamic radius (R_h) and the related proportion (%) were derived from the scattered function using the model of n-globular monodisperse particles provided by the manufacturer's software. Data collected at pH 6.5 were essentially similar to that at pH 4.5. Data were compared by one-way ANOVA with Bonferroni's post-test analysis

[a] Differences in the values of R_{h1} were not statistically significant

[b] Differences in the values of R_{h2} were not statistically significant

[c] Differences between R_{h1} and R_{h2} are statistically significant ($p < 0.01$)

oligomers (see below). Experiments performed at pH 6.5 yielded essentially similar results (data not shown).

The conformational features of HaPrP(23–231) wt and its M-to-S mutants were then studied by far- and near-UV CD to probe the secondary and tertiary structures, respectively (Fig. 3). At pH 4.5 and pH 6.5, a comparison of the far-UV CD spectra shows that only M206S and M213S mutations, singly or in combination, cause a drastic change (Fig. 3a, b). This change is characterized by an increase in the $\Theta^{205}/\Theta^{220}$ ratio (from 1.07 up to 2.0) and indicates the presence of non-native secondary structures. As in the previous spectral region, the M206S and M213S mutations, both singly or combined, also altered the near-UV spectrum. This is not true for the M134S and M154S mutations. Here the observed spectral changes, in which the aromatic bands but not the disulfide bond region (around 260 nm) are affected, show the disruption of the native tertiary structure (Fig. 3c). The CD studies taken together indicate that the replacement of M by S at positions 206, 213, and both, but not at positions M134 or M154, preclude the adoption of the conventional α-fold and induce partially unstructured states. Interestingly, replacing M213 by L rather than S retains the conformational features of the wt supporting the importance of the polarity of the side chain for the observed perturbations (Fig. 3a, b, and c).

To gain insight into the partially unfolded state induced upon mutation of the M-to-S in Helix-3, we characterized the bis-ANS binding properties, a probe that is used to titrate surface hydrophobicity [43]. Figure 3d shows that as opposed to HaPrP(23–231) wt, M134S, M154S, and M213L, the Helix-3 M-to-S mutants displayed an enhanced binding of bis-ANS, indicating an increase in their solvent-exposed hydrophobic surfaces and again their partially structured state.

Thermal unfolding reveals the M-to-S replacements in Helix-3 cause a drastic reduction in thermal stability

Given that structural changes have large impacts on stability, we further probed the effect of the M-to-S substitutions using thermal denaturation experiments. Under the conditions used, the thermal unfolding of the wt, M134S, M154S, and M213L proteins, as followed by the variation of Θ^{222} as a function of temperature, was essentially reversible as judged from the recovering of approximately 95% of the initial signal on cooling from the highest temperature. The thermal unfolding curves for these proteins denote identical two-state processes with Tm′s of about 57 ± 1 at pH 6.5, whereas at pH 4.5 the M134S and M154S mutants unfold at a lower Tm than the wt (56 ± 0.5 and 61 ± 0.5°C, respectively) (Fig. 4; Table 3). Conversely, the thermal denaturation of M206S, M213S, and the M206S-M213S HaPrP(23–232) was only partially reversible (75% of the signal was recovered after cooling from the highest temperature), involved a lower $\Delta\Theta^{222}$, was less cooperative and occurred at significantly lower temperatures (38 and 40°C at both pH 6.5 and 4.5, respectively) (Fig. 4; Table 3).

All the features found for the Helix-3 M-to-S mutants follow the pattern for the thermal unfolding of partially unstructured states involving pro-aggregating species [44]. To assess this process, we studied the temperature dependence of bis-ANS binding and of the hydrodynamic radius (Figs. 2, 4c). In addition to the previously described differences in the temperature dependence of Θ^{222}, the chains bearing M-to-S mutations at the Helix-3 methionines also displayed a temperature-dependent ANS binding and R_h changes at low temperatures. These are not observed in HaPrP(23–231) wt, M134S, M154S, and M213L. In this

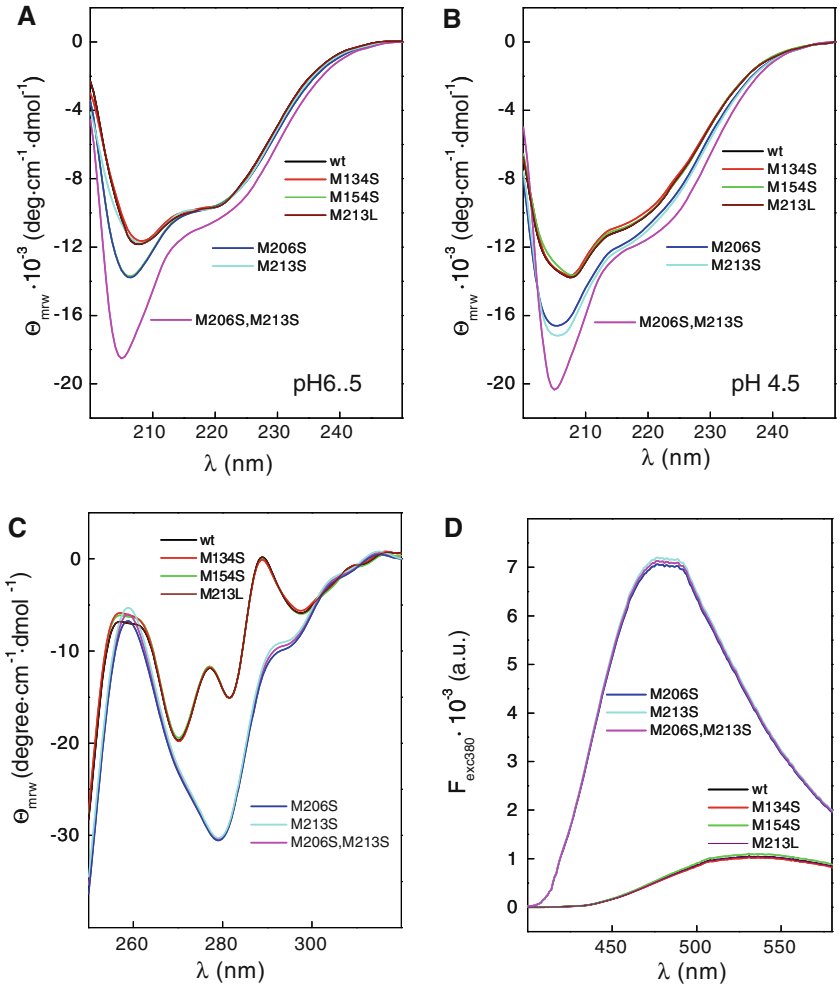

Fig. 3 Conformational features of HaPrP(23–231) wt and of its mutants as probed by circular dichroism in the far-UV region (**a**, **b**) and near-UV region (**c**) and by their bis-ANS binding properties (**d**). Far-UV CD spectra of HaPrP(23–231) wt and of its mutants **a** in 20 mM MES pH 6.5 containing 50 mM NaCl and 0.1 mM citrate, and **b** 20 mM NaAc pH 4.5 containing 50 mM NaCl and 0.1 mM citrate. Spectra were recorded at 15°C using protein at 11 μM. **c** Near-UV CD spectra of the different HaPrP(23–231) chains. The spectra were recorded at 15°C using protein solutions at 22 μM. **d** The effect of HaPrP(23–231) wt and its mutants on the bis-ANS fluorescence emission spectrum at 15°C. The displayed data are the averaged of three independent measurements using at least two different protein batches The trace color or symbol codes are indicated in each of the panels

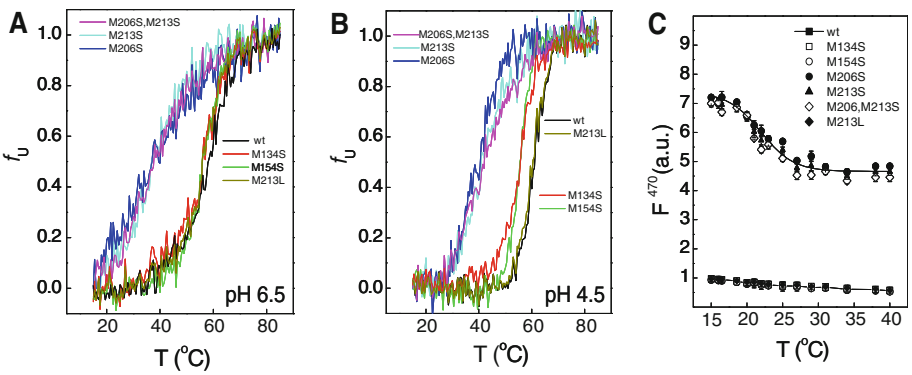

Fig. 4 The thermal unfolding profiles of HaPrP(23–231) wt and of its mutants as monitored by circular dichroism and ANS-binding. The temperature dependence of the Θ_{222} for HaPrP(23–231) wt and of its mutants, at pHs: **a** 6.5 and **b** 4.5. The trace color code is indicated in each of the panels. **c** The temperature dependence of the ANS emission intensity in the presence of HaPrP(23–231) wt and its mutants

sense, the bis-ANS-binding profiles show sigmoidal decays with inflection points at approximately 21 ± 1.5°C, indicating that the Helix-3 methionine mutants undergo a transition involving the reduction in the hydrophobic surface. This transition is accompanied by a threefold increase in the R_h value and precedes the temperature-dependent changes in the secondary structure (Table 2; Fig. 4). These data suggest the presence of pro-aggregating folding intermediates.

The differences in the reversibility of the thermal unfolding processes preclude any formal equilibrium thermodynamic analysis. However, given the reversibility of the HaPrP(23–231) wt thermal denaturation at both pHs allows the calculation of the thermodynamic parameters at equilibrium (ΔHm). Given this fact, the experimental Tm values for the denaturation of the different mutants can be converted into the apparent relative changes in the free energy with respect to the wt protein [36, 37]. Table 3

Table 3 Parameters of the thermal unfolding of HaPrP(23–231) wt and of its mutants followed by the variation of Θ^{222} with temperature

	pH	Tm (°C)	Θ_{15}^{222} (deg cm^{-1} dmol^{-1})	Θ_{90}^{222} (deg cm^{-1} dmol^{-1})	ΔT (°C)	$\Delta G^*_{MS/wt}$ (kcal mol^{-1})
wt	6.5	57.8 ± 0.5	−9.3 ± 0.2	−5.7 ± 0.1	5 ± 1	
	4.5	60.9 ± 0.4	−9.4 ± 0.3	−7.3 ± 0.1	3 ± 0.5	
M134S	6.5	57.0 ± 0.5	−9.2 ± 0.5	−5.5 ± 0.2	5 ± 1	−0.10 ± 0.09
	4.5	55.4 ± 0.5	−9.1 ± 0.5	−6.7 ± 0.2	3 ± 0.5	−1.11 ± 0.06
M154S	6.5	56.3 ± 0.4	−9.2 ± 0.3	−5.5 ± 0.2	4 ± 1	−0.20 ± 0.10
	4.5	55.5 ± 0.6	−9.3 ± 0.3	−6.7 ± 0.3	2 ± 0.6	−1.05 ± 0.06
M206S	6.5	37.9 ± 0.2	−9.5 ± 0.4	−7.4 ± 0.5	10 ± 0.5	−3.30 ± 0.12
	4.5	39.5 ± 0.3	−10 ± 0.2	−7.9 ± 0.5	5 ± 0.4	−4.45 ± 0.09
M213S	6.5	38.1 ± 0.9	−9.4 ± 0.4	−7.2 ± 0.4	7 ± 0.6	−3.20 ± 0.11
	4.5	41.0 ± 1.0	−10.2 ± 0.2	−8.7 ± 0.4	5 ± 0.4	−4.13 ± 0.09
M206S,M213S	6.5	36.7 ± 0.9	−10.0 ± 0.2	−7.4 ± 0.4	10 ± 0.5	−3.50 ± 0.10
	4.5	42.0 ± 1.0	−11.0 ± 0.2	−9.4 ± 0.4	10 ± 0.5	−3.93 ± 0.04
M213L	6.5	58.8 ± 1.0	−9.4 ± 0.3	−5.6 ± 0.2	3 ± 0.5	0.15 ± 0.09
	4.5	60.5 ± 0.4	−9.2 ± 0.3	−7.3 ± 0.1	3 ± 0.5	−0.08 ± 0.07

Thermal unfolding curves were analyzed as described in the experimental section. $\Delta G^*_{MS/wt}$ were calculated using the ΔH_{vH} (50.8 kcal/mol and 65.5 kcal/mol for pH 6.5 and 4.5, respectively) calculated from the thermal denaturation curves of HaPrP(23–231) wt analyzed according to a two-state transition. Θ_{15}^{222} and Θ_{90}^{222} represent the values of ellipticity at 15 and 90°C, respectively. ΔT was derived from the fit to sigmoidal curves to estimate changes in the cooperativity of the transitions

shows that all the M-to-S replacements cause changes in stability, ranging from −0.20 ± 0.10 to −4.45 ± 0.09 kcal mol^{-1}. For the M134S and M154S mutants, the destabilization of the secondary structure is only significant at pH 4.5. For the Helix-3 methionine mutants, the destabilization is larger and involves relative changes in the apparent free energy of −3.20 and −4.5 kcal mol^{-1}, respectively. Contrarily, the M213L mutation causes negligible effects. Taken together, these results indicate that the M-to-S substitutions in Helix-3 do indeed prevent the adoption of the conventional α-fold and induce a partially structured state.

Helix-3 M-to-S mutants of HaPrP(23–231) undergo facilitated aggregation and fibrillation

Bearing in mind that partially structured states are key precursors for the formation of amyloid fibrils through their allowance for rearrangement of "amyloid-prone sequence regions" [9, 11, 16, 18, 45], we then asked whether the structural states formed by M-to-S replacement in Helix 3 could permit or facilitate oligomerization pathways that are impeded to the native fold. For this purpose, we incubated HaPrP(23–231) wt and its mutants in 20 mM MES pH 6.5, 0.1 mM citrate and 0.01% NaN_3 in the absence and presence of 0.35 M NaCl at 37°C with orbital agitation. The samples were analyzed for the occurrence of polymerization processes (Fig. 5).

The aggregation kinetics, followed by turbidity measurements, show that all proteins at concentrations above 13 μM undergo a time-dependent aggregation upon increasing the ionic strength to 0.35 M NaCl (Fig. 5a). However, the turbidity increase was significantly larger for the Helix-3 methionine mutants than for the wt, M134S, M154S, and M213L mutants. The turbidity changes paralleled the formation of insoluble aggregates. The solubility, measured after 24 h of incubation, shows that aggregation was significantly larger for the Helix-3 methionine mutants than for the wt, M134S, and M154S HaPrP(23–231) proteins (Fig. 5c). Under similar conditions, the kinetics of ThT binding reveal the occurrence of a significant fibrillation process in the M206S, M213S, and M206S-M213S mutants. This process was negligible in the wt, M134S, M154S, and M213L HaPrP(23–231) forms (Fig. 5b). The degree of probe binding in the isolated insoluble polymers was essentially similar to the three different M-to-S Helix-3 mutants (Fig. 5d). Similarly, the lag-phase for this process, calculated using three independent experiments with protein concentrations of about 14 ± 1 μM, yielded values of 2.5 ± 0.5 h for the three different M-to-S Helix-3 mutants.

To assess the nature of the protein polymers formed after 24 h of incubation, we analyzed the morphology using AFM. Analyzing the topographical images of the Helix-3 methionine mutants revealed the presence of aggregates constituted by irregular rod-like structures with diameters of about 25–50 nm and typical lengths of a few hundreds of nanometers (Fig. 6). These formations appeared heterogeneous, and included single straight rods, laterally associated rods, doughnut, and hairpin-like shapes. This precluded the detection of clear-cut differences among the distinct Helix-3 methionine mutants and

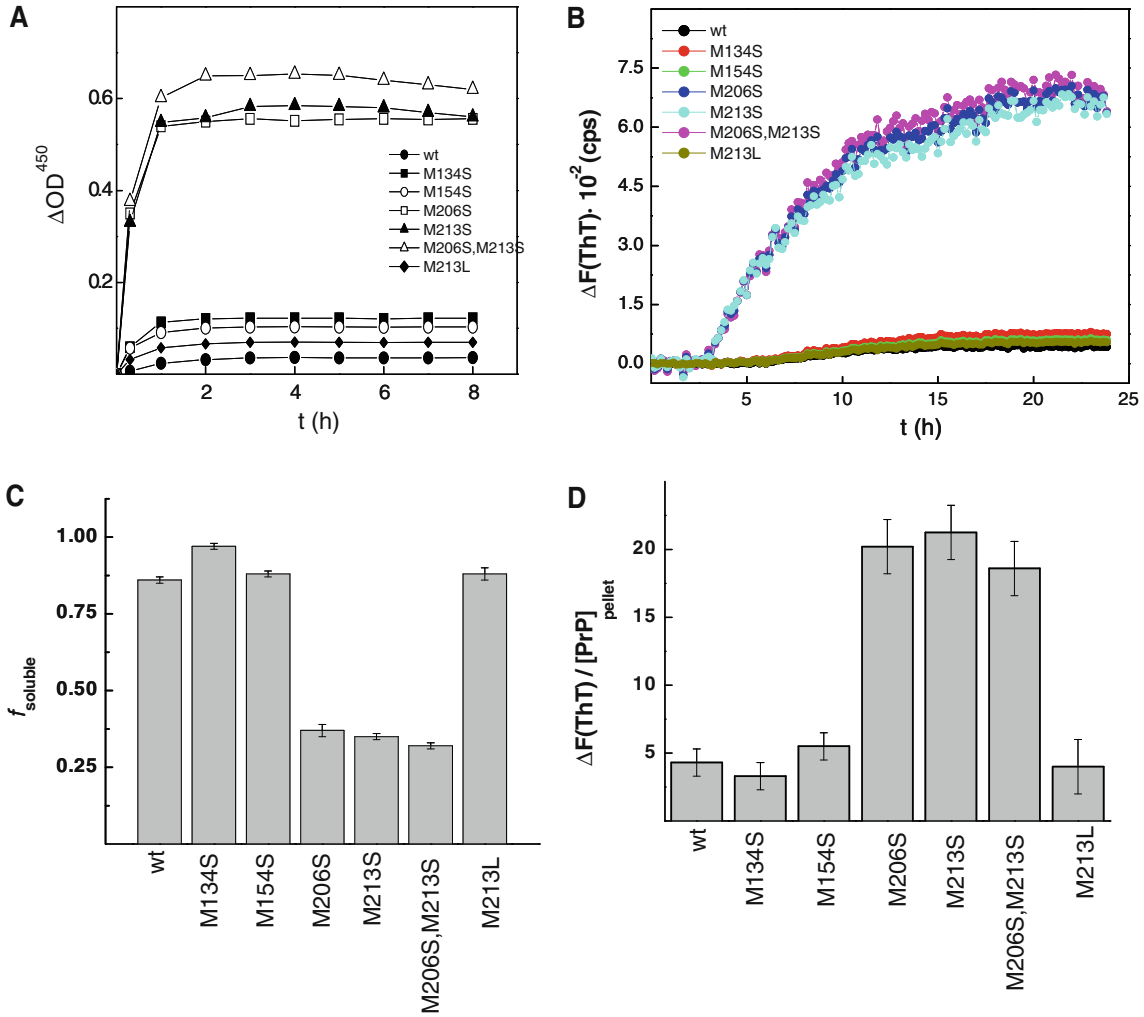

Fig. 5 The aggregation properties of HaPrP(23–231) wt and its M-to-S mutants. **a** The time-dependence of the turbidity increase of the different protein solution solutions prepared in 20 mM MES, 0.35 M NaCl, 0.1 mM citrate, and 0.01% NaN_3 at pH 6.5, upon incubation at 37°C under agitation. **b** Typical kinetics of the ThT binding of HaPrP(23–231) wt and its mutants. The displayed traces are the averaged of three independent experiments performed in triplicate. **c** The partition of HaPrP(23–231) wt and its mutants into the soluble fraction during a 10,000 × g centrifugation for 20 min after a 24-h incubation under aggregating conditions (37°C, 0.35 M NaCl). Solubility is expressed as the molar fraction of the total protein concentration (approximately 13–14 μM) and represents the average of two independent determinations with different protein batches using duplicates. **d** The extent of ThT in isolated insoluble aggregates. The insoluble aggregates formed after 24-h incubation were isolated by centrifugation, resuspended in the same buffer, and the ThT fluorescence was referred to the protein concentration. The data are displayed as the average of three independent measurements performed in triplicate

suggested similarity with prefibrillar states [46, 47]. It must be stressed that despite the polymorphism of the assemblies formed by the M206S, M213S, and M206S-M213S mutants, their shapes were clearly different from the amorphous patches formed by HaPrP(23–231) wt, used as control for adherence. Measurements from cross sections of the isolated assemblies of the mutants yielded averaged values of 4.0 ± 0.4 nm for the height (Fig. 6). Correction of these values for the dehydration effect (multiplying by a factor of 1.4 [47]). the heights of the assemblies (5.6 nm) agree with the diameters of protofibrils, which are typically of 2–6 nm [46, 47].

In conclusion, these results indicate that under denaturant-free conditions, the partially structured state that is induced by the M-to-S substitution in Helix-3 undergoes a polymerization process leading to the formation of amyloid protofibrils.

Discussion

The conversion of PrP^C into its propagative PrP^{Sc} form involves a drastic structural change that requires the remodeling of the noncovalent bonds of at least its

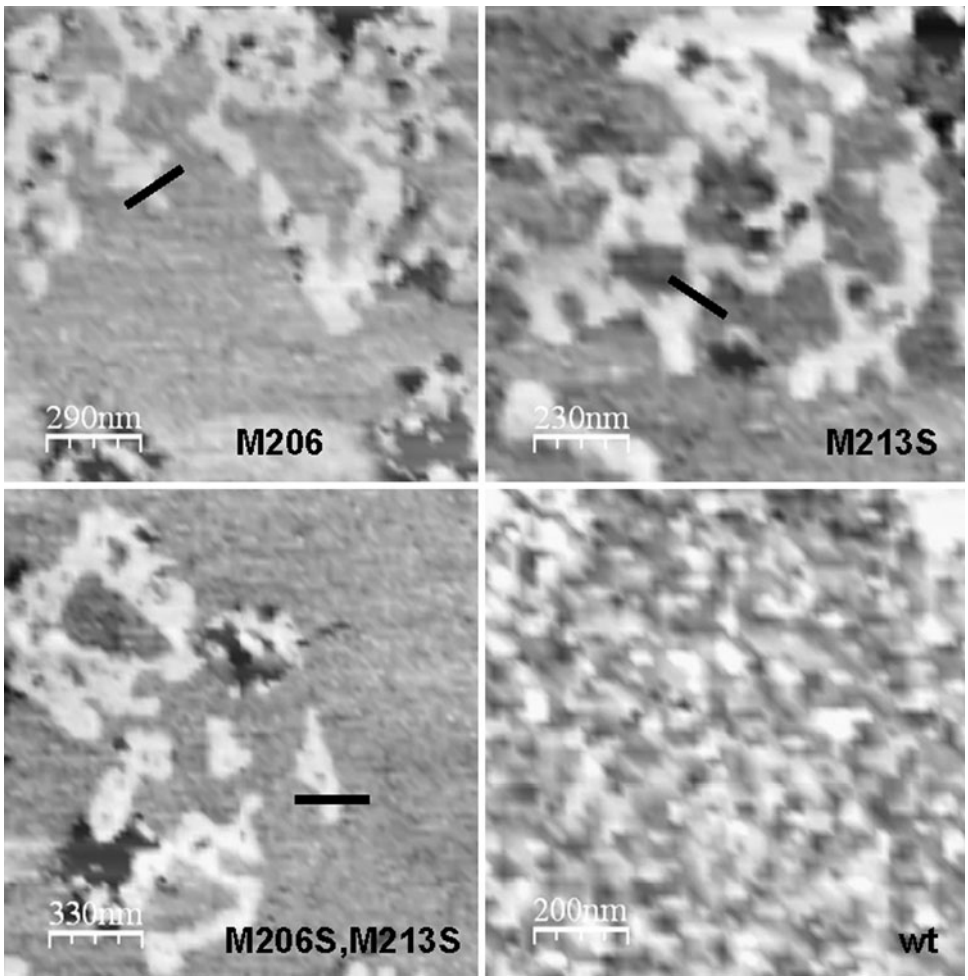

Fig. 6 AFM topographical images of amyloid polymers adsorbed onto mica surfaces. The AC-AFM topographic image of aggregates formed by **a** M206S, **b** M213S, **c** M206-M213S mutants and **d** wt chains of HaPrP(23–231) after 24-h incubation at 0.4 mg/ml at 37°C in 20 mM MES, 0.35 M NaCl, 0.1 mM citrate, and 0.01% NaN_3, at pH 6.5, under agitation at 100 rpm. Scans were registered at 1 × 1 μm. Z range (black to white) is 10 nm on average. *Black bars* indicate example of regions selected as cross sections for height determinations

C-terminal domain. To do so, the α-fold of PrP must undergo an obligatory destabilization (i.e., breakage of noncovalent bonds) and accommodate into an aggregation-prone state (or ensemble of states) that may allow the efficient formation of new noncovalent bonds [9, 18]. Within this picture, the finding of sulfoxides at the Helix-3 methionines in PrP^{Sc}, which provide an increase in local polarity with transmissible structural effects, offered an adequate covalent feature for switching on either the formation or stabilization of the obligatory folding intermediate [12–14]. If transient, this intermediate can be a physiological form of PrP^{C} (for example, as a species on the pathway to degradation). However, if accumulated, the intermediate could evolve to PrP^{Sc}. Using mutagenesis to provide a side-chain polarity increase with site specificity, our work shows that M-to-S replacements at Helix-3 disrupt the native protein fold. This forces the full-length chain to adopt a partially structured fold that forms amyloid protofibrils through its pro-aggregation properties. Interestingly, such structural effects are not observed when the replacement is performed at the conserved M134 and M154 residues or when M213 is replaced by L rather than S. This supports the specificity of the target sites and of the polarity change.

The analysis by MD simulations shows that the M-to-S mutations perturb both the global and internal dynamics of the native state. Single M-to-S substitutions determine effects on the global dynamics and on the internal coordination of the α-fold that are similar to the effects observed for the sulfoxidation of the respective methionines. This qualitatively supports the possibility to mimic methionine sulfoxidation by serine substitution. The effect of the double M-to-S mutations is more complex and determines a perturbation of the native state dynamics that reverberates in a different sampling of essential spaces and in a complete abrogation of internal residue-pair coordination. These results should not be considered as fully quantitative, given the inherent limitations of the force-fields and of the sampling. However, they indicate that the insertion of an electronegative oxygen atom in an otherwise mainly hydrophobic environment may act as a possible switch for the control of the conformational stability of the protein. The differences in the outcomes of methionine sulfoxidation or M-to-S substitutions can be

explained in terms of the disparity in the chemical groups and of the trajectory length for each of the groups required to display the effect. However, the fact that the M-to-S substitution in Helix-3, which theoretically is less perturbing than sulfoxidation experimentally impairs the adoption of the native state in the full-length chain, also argues for alternative destabilizing sources eluded in the theoretical approach. This means that the effect of the substitutions on stability factors provided by other protein regions, by alternative dynamic states or by both, that are not computed, are indeed playing a critical role in the final outcome. In this sense, it must be noted that the unstructured N-terminal region plays an important role in the structure and stability of PrP^C and of its conversion capacity and it is not included in the structure of the native state [27, 48]. It must also be considered that the effects of the substitutions could a priori differ in the effects on the native-state properties but could converge in stabilizing folding intermediates [49, 50].

Folding intermediates or partially structured species are usually very short-lived and less stable than the fully folded form, and so they are not significantly populated at equilibrium. Conversely, stable conformations of proteins that are not fully folded or unfolded can be found under several non-native conditions, for example at extreme pHs, mild denaturant concentrations, loss of cofactors, and upon engineering certain residues [22, 49, 50]. Most of these states retain considerable native-like secondary structure but have disrupted tertiary structure [47, 49]. In general, these partially structured states allow the expansion of the structural and functional repertoire through their increased flexibility. Loss of the cation cofactor and acid pHs permits α-lactalbumin to adopt a folding intermediate that yields the antitumoral form referred to as HAMLET upon oleic acid binding [51]. Similarly, mild denaturing conditions permit Rop-dimer interconversion between two opposed native structures [52]. From this work, it can be proposed that the pseudosulfoxidation mutations in Helix-3 act as trapdoors for the formation of partially structured states that can easily evolve to protofibrils. However, it could be possible that such intermediates could be either degraded or rescued by ligand binding and yield novel functions in the cellular milieu [23, 24, 53].

In general, the accumulation of covalent modifications appears to be both the cause and a consequence of ageing and a crucial factor contributing to neurodegenerative disease pathogenesis through either the impairment of their reversibility or their occurrence at alternative sites [21, 23, 25]. In the case of tau-related dementias, hyperphosphorylation impairs microtubule-binding function and causes the protein to accumulate as neurofibrillary tangles [20, 21]. Importantly, the changes in the properties of tau that occur on hyperphosphorylation can be reproduced or mimicked using S/T-to-E mutations [22]. For Aβ-peptides and ApoC-II, methionine sulfoxidation favors the formation of non-amyloid oligomeric states [30, 51, 52]. In the case of PrP, the use of site-specificity for the polarity replacement shows that only the oxidation of hidden methionines, M206 and M213, would have deleterious consequences for the α-fold. Assuming that these methionines can be transiently exposed through the perturbation of Helix-3 (as shown by high-pressure studies [54] or in states populated in pathways to degradation), the sulfoxide-stabilized state could be then considered as a physiological folding intermediate. Its accumulation would then favor the pathway of conversion through the impairments of its reversion and degradation [23, 24].

The work with synthetic peptides has shown that the redox cycle of methionine side chains involves an amphipathic code that can function as a structural switch regulating not only the secondary structure but also the shape of the peptide oligomers [27, 28, 55, 56]. Given the high content of methionine residues in the PrP chain and their differences in location and conservation degree, it may be possible that these residues participate in a general evolutionary mechanism involved in the regulation of the folding basin. In this sense, the site-specificity conferred by the mutational approach described here, which is in contrast to the lack of specificity of the chemical oxidation and the variability of its effect [57, 58], indicates that the polarity increase linked to the oxidation of M206 and M213, but not that of M134 and M154, is critical for the permissibility of the native α-fold. The polarity effect also plays a role in polymer sculpturing, as pseudosulfoxidation of the Helix-3 methionines stalls the polymerization process at the protofibril stage. In addition to M206 and M213, some species contain an extra Met residue in Helix-3 (M205, in human and mouse, among others) that is essential for proper folding and that when mutated switches on the aggregation propensity of the C-terminal domain, reinforcing the α-fold gatekeeper role of Helix-3 methionines [59]. On the other hand, M129 which is highly conserved, but polymorphic in human (M129V) and deer (M132L), was found as easily oxidized as M134 [57]. Preventing such oxidation sensitivity as in the polymorphic variant V129 does not cause major conformational effects or preclude succumbing to diseases but indeed modulates the risk and phenotype of prion disorders in humans in agreement with the previous hypothesis [59]. In cervid PrP the polymorphism M132L, which dictates the oxidation capacity of the position, determines the strain susceptibility [60].

Then, deciphering this as yet unresolved code may be of essential importance for understanding the regulation of the folding basin of proteins in relation to their misfolding in terms of both the permissibility of conformational transitions and the properties of their assemblies.

Acknowledgments This work was supported by grants SAF2006-00418 (MG) and BFU2009-07971 (MG) from the Ministerio de Ciencia e Innovación, FOOD-CT-2004-506579 (MG, RG) from the EC and PI101209 (MG) from the Fundación Cien. SL is supported by a FPI-PhD fellowship from the Ministerio de Ciencia e Innovación. We gratefully acknowledge the advice of Dr. Angel Cuesta in relation to the AFM experiments and the technical support of Lara Reviejo and Rosa Sánchez.

References

1. Prusiner SB (2001) Shattuck lecture: neurodegenerative diseases and prions. N Engl J Med 344:1516–1526
2. Aguzzi A, Baumann F, Bremer J (2008) The prion's elusive reason for being. Annu Rev Neurosci 31:439–477
3. Oesch B, Westaway D, Wälchli M, McKinley MP, Kent SB, Aebersold R, Barry RA, Tempst P, Teplow DB, Hood LE, Prusiner SB, Weissmann C (1985) A cellular gene encodes scrapie PrP 27–30 protein. Cell 40:735–746
4. Meyer RK, McKinley MP, Bowman KA, Braunfeld MB, Barry RA, Prusiner SB (1986) Separation and properties of cellular and scrapie prion proteins. Proc Natl Acad Sci USA 83:2310–2314
5. Caughey BW, Dong A, Bhat KS, Ernst D, Hayes SF, Caughey WS (1991) Secondary structure analysis of the scrapie-associated protein PrP 27–30 in water by infrared spectroscopy. Biochemistry 30:7672–7680
6. McKinley MP, Meyer RK, Kenaga L, Rahbar F, Cotter R, Serban A, Prusiner SB (1991) Scrapie prion rod formation in vitro requires both detergent extraction and limited proteolysis. J Virol 65:1340–1351
7. Gasset M, Baldwin MA, Lloyd DH, Gabriel JM, Holtzman DM, Cohen F, Fletterick R, Prusiner SB (1992) Predicted alpha-helical regions of the prion protein when synthesized as peptides form amyloid. Proc Natl Acad Sci USA 189:10940–10944
8. Pan KM, Baldwin M, Nguyen J, Gasset M, Serban A, Groth D, Mehlhorn I, Huang Z, Fletterick R, Cohen F, Prusiner SB (1993) Conversion of alpha-helices into beta-sheets features in the formation of the scrapie prion proteins. Proc Natl Acad Sci USA 90:10962–10966
9. Baskakov IV, Breydo L (2007) Converting the prion protein: what makes the protein infectious. Biochim Biophys Acta 1772:692–703
10. Sigurdson CJ, Nilsson KP, Hornemann S, Heikenwalder M, Manco G, Schwarz P, Ott D, Rülicke T, Liberski PP, Julius C, Falsig J, Stitz L, Wüthrich K, Aguzzi A (2009) De novo generation of a transmissible spongiform encephalopathy by mouse transgenesis. Proc Natl Acad Sci USA 106:304–309
11. Colby DW, Giles K, Legname G, Wille H, Baskakov IV, Dearmond SJ, Prusiner SB (2009) Design and construction of diverse mammalian prion strains. Proc Natl Acad Sci USA 106:20417–20422
12. Stahl N, Baldwin MA, Teplow DB, Hood L, Gibson BW, Burlingame AL, Prusiner SB (1993) Structural studies of the scrapie prion protein using mass spectrometry and amino acid sequencing. Biochemistry 32:1991–2002
13. Canello T, Engelstein R, Moshel O, Xanthopoulos K, Juanes ME, Langeveld J, Sklaviadis T, Gasset M, Gabizon R (2008) Methionine sulfoxides on PrPSc: a prion-specific covalent signatura. Biochemistry 47:8866–8873
14. Colombo G, Meli M, Morra G, Gabizon R, Gasset M (2009) Methionine sulfoxides on prion protein Helix-3 switch on the alpha-fold destabilization required for conversion. PLoS One 4(1):e4296
15. Wolschner C, Giese A, Kretzschmar HA, Huber R, Moroder L, Budisa N (2009) Design of anti- and pro-aggregation variants to assess the effects of methionine oxidation in human prion protein. Proc Natl Acad Sci USA 106:7756–7761
16. Kelly JW (1998) The alternative conformations of amyloidogenic proteins and their multi-step assembly pathways. Curr Opin Struct Biol 8:101–106
17. Eisenberg D, Nelson R, Sawaya MR, Balbirnie M, Sambashivan S, Ivanova MI, Madsen AØ, Riekel C (2006) The structural biology of protein aggregation diseases: fundamental questions and some answers. Acc Chem Res 39:568–575
18. Nelson R, Eisenberg D (2006) Structural models of amyloid-like fibrils. Adv Protein Chem 73:235–282
19. Sawaya MR, Sambashivan S, Nelson R, Ivanova MI, Sievers SA, Apostol MI, Thompson MJ, Balbirnie M, Wiltzius JJ, McFarlane HT, Madsen AØ, Riekel C, Eisenberg D (2007) Atomic structures of amyloid cross-beta spines reveal varied steric zippers. Nature 447:453–457
20. Kopke E, Tung YC, Shaikh S, Alonso AC, Iqbal K, Grundke-Iqbal I (1993) Microtubule-associated protein tau: abnormal phosphorylation of a non-paired helical filament pool in Alzheimer disease. J Biol Chem 268:24374–24384
21. Iqbal K, Liu F, Gong CX, Alonso AC, Grundke-Iqbal I (2009) Mechanisms of tau-induced neurodegeneration. Acta Neuropathol 118:53–69
22. Sun Q, Gamblin TC (2009) Pseudohyperphosphorylation causing AD-like changes in tau has significant effects on its polymerization. Biochemistry 48:6002–6011
23. Stadtman ER (2006) Protein oxidation and aging. Free Radic Res 40:1250–1258
24. Oien DB, Moskovitz J (2008) Substrates of the methionine sulfoxide reductase system and their physiological relevance. Curr Top Dev Biol 80:93–133
25. Hernández F, Nido JD, Avila J, Villanueva N (2009) GSK3 inhibitors and disease. Mini Rev Med Chem 9:1024–1029
26. Virshup DM, Shenolikar S (2009) From promiscuity to precision: protein phosphatases get a makeover. Mol Cell 33:537–545
27. Ostapchenko VG, Makarava N, Savtchenko R, Baskakov IV (2008) The polybasic N-terminal region of the prion protein controls the physical properties of both the cellular and fibrillar forms of PrP. J Mol Biol 383:1210–1224
28. Dado GP, Gellman SH (1993) Redox control of secondary structure in a designed peptide. J Am Chem Soc 115:12609–12610
29. Schenck HL, Schenck HL, Dado GP, Gellman SH (1996) Redox-triggered secondary structure changes in the aggregated states of a designed methionine-rich peptide. J Am Chem Soc 118: 12487–12494
30. Binger KJ, Griffin MD, Howlett GJ (2008) Methionine oxidation inhibits assembly and promotes disassembly of apolipoprotein C-II amyloid fibrils. Biochemistry 47:10208–10217
31. Wiltzius JJ, Landau M, Nelson R, Sawaya MR, Apostol MI, Goldschmidt L, Soriaga AB, Cascio D, Rajashankar K, Eisenberg D (2009) Molecular mechanisms for protein-encoded inheritance. Nat Struct Mol Biol 16:973–978
32. Vriend G (1990) What if: a molecular modeling and drug design program. J Mol Graph 8:52–56
33. James TL, Liu H, Ulyanov NB, Farr-Jones S, Zhang H, Donne DG, Kaneko K, Groth D, Mehlhorn I, Prusiner SB, Cohen FE (1997) Solution structure of a 142-residue recombinant prion protein corresponding to the infectious fragment of the scrapie isoform. Proc Natl Acad Sci USA 94:10086–10091
34. González-Iglesias R, Pajares MA, Ocal C, Espinosa JC, Oesch B, Gasset M (2002) Prion protein interaction with glycosaminoglycan occurs with the formation of oligomeric complexes stabilized by Cu(II) bridges. J Mol Biol 319:527–540

35. Pace CN, Scholtz JM (1997) Measuring the conformational stability of a protein. In: Creighton (ed) Protein structure, a practical approach. IRL Press, Oxford, pp 299–321
36. Becktel WJ, Schellman JA (1987) Protein stability curves. Biopolymers 26:1859–1877
37. Tadeo X, López-Méndez B, Castaño D, Trigueros T, Millet O (2009) Protein stabilization and the Hofmeister effect: the role of hydrophobic solvation. Biophys J 97:2595–2603
38. González-Iglesias R, Elvira G, Rodríguez-Navarro JA, Vélez M, Calero M, Pajares MA, Gasset M (2004) Cu^{2+} binding triggers alphaBoPrP assembly into insoluble laminar polymers. FEBS Lett 556:161–166
39. Bishop MF, Ferrone FA (1984) Kinetics of nucleation-controlled polymerization: a perturbation treatment for use with a secondary pathway. Biophys J 46:631–644
40. Amadei A, Linssen ABM, Berendsen HJC (1993) Essential dynamics of proteins. Proteins 17:412–425
41. Carnevale V, Pontiggia F, Micheletti C (2007) Structural and dynamical alignment of enzymes with partial structural similarity. J Phys Condens Matter 19. doi:10.1088/0953-8984/19/28/285206
42. Lysek DA, Schorn C, Nivon LG, Esteve-Moya V, Christen B, Calzolai L, von Schroetter C, Fiorito F, Herrmann T, Güntert P, Wüthrich K (2005) Prion protein NMR structures of cats, dogs, pigs, and sheep. Proc Natl Acad Sci USA 102:640–645
43. Hawe A, Sutter M, Jiskoot W (2008) Extrinsic fluorescent dyes as tools for protein characterization. Pharm Res 25:1487–1499
44. Creighton TE (1990) Protein folding. Biochem J 270:1–16
45. Jahn TR, Parker MJ, Homans SW, Radford SE (2006) Amyloid formation under physiological conditions proceeds via a native-like folding intermediate. Nat Struct Mol Biol 13:195–201
46. Goldsbury C, Green J (2005) Time-lapse atomic force microscopy in the characterization of amyloid-like fibril assembly and oligomeric intermediates. Methods Mol Biol 299:103–128
47. Campioni S, Mossuto MF, Torrassa S, Calloni G, de Laureto PP, Relini A, Fontana A, Chiti F (2008) Conformational properties of the aggregation precursor state of HypF-N. J Mol Biol 379:554–567
48. Kaimann T, Metzger S, Kuhlmann K, Brandt B, Birkmann E, Höltje HD, Riesner D (2008) Molecular model of an alpha-helical prion protein dimer and its monomeric subunits as derived from chemical cross-linking and molecular modeling calculations. J Mol Biol 376:582–596
49. Kuwajima K (1989) The molten globule state as a clue for understanding the folding and cooperativity of globular-protein structure. Proteins 6:87–103
50. Sanz JM, Fersht AR (1993) Rationally designing the accumulation of a folding intermediate of barnase by protein engineering. Biochemistry 32:13584–13592
51. Pettersson-Kastberg J, Aits S, Gustafsson L, Mossberg A, Storm P, Trulsson M, Persson F, Mok KH, Svanborg C (2009) Can misfolded proteins be beneficial? The HAMLET case. Ann Med 41:162–176
52. Gambin Y, Schug A, Lemke EA, Lavinder JJ, Ferreon AC, Magliery TJ, Onuchic JN, Deniz AA (2009) Direct single-molecule observation of a protein living in two opposed native structures. Proc Natl Acad Sci USA 106:10153–10158
53. Silva JL, Vieira TC, Gomes MP, Bom AP, Lima LM, Freitas MS, Ishimaru D, Cordeiro Y, Foguel D (2009) Ligand binding and hydration in protein misfolding: insights from studies of prion and p53 tumor suppressor proteins (dagger). Acc Chem Res 43:271–279
54. Kremer W, Kachel N, Kuwata K, Akasaka K, Kalbitzer HR (2007) Species-specific differences in the intermediate states of human and Syrian hamster prion protein detected by high pressure NMR spectroscopy. J Biol Chem 282:22689–22698
55. Hou L, Kang I, Marchant RE, Zagorski MG (2002) Methionine 35 oxidation reduces fibril assembly of the amyloid abeta-(1–42) peptide of Alzheimer's disease. J Biol Chem 277:40173–40176
56. Bitan G, Tarus B, Vollers SS, Lashuel HA, Condron MM, Straub JE, Teplow DB (2003) A molecular switch in amyloid assembly: Met35 and amyloid beta-protein oligomerization. J Am Chem Soc 125:15359–15365
57. Requena JR, Dimitrova MN, Legname G, Teijeira S, Prusiner SB, Levine RL (2004) Oxidation of methionine residues in the prion protein by hydrogen peroxide. Arch Biochem Biophys 432:188–195
58. Breydo L, Bocharova OV, Makarava N, Salnikov VV, Anderson M, Baskakov IV (2005) Methionine oxidation interferes with conversion of the prion protein into the fibrillar proteinase K-resistant conformation. Biochemistry 44:15534–15543
59. Hart T, Hosszu LL, Trevitt CR, Jackson GS, Waltho JP, Collinge J, Clarke AR (2009) Folding kinetics of the human prion protein probed by temperature jump. Proc Natl Acad Sci USA 106:5651–5656
60. Lee S, Antony L, Hartmann R, Knaus KJ, Surewicz K, Surewicz WK, Yee VC (2010) Conformational diversity in prion protein variants influences intermolecular beta-sheet formation. EMBO J 29:251–262
61. Green KM, Browning SR, Seward TS, Jewell JE, Ross DL, Green MA, Williams ES, Hoover EA, Telling GC (2008) The elk PRNP codon 132 polymorphism controls cervid and scrapie prion propagation. J Gen Virol 89:598–608

Artículo 3. Selenomethionine incorporation into amyloid sequences regulates fibrillogenesis and toxicity.

Los cambios conformacionales que definen las proteinopatías con formación de amiloides, pueden estar supeditados a modificaciones covalentes que hagan las veces de interruptores (81, 417, 424). En proteínas tales como PrP y Aβ, los estados estructurales asociados a enfermedad se caracterizan por la presencia de residuos de metionina esenciales cuya oxidación actúa como posible elemento regulador (414, 415, 425-430).

Los residuos de metionina están sujetos a una sustitución metabólica por seleniometionina (SeMet), que difiere en tamaño e hidrofobicidad (431-436). Tanto metionina como seleniometionina son aminoácidos esenciales para el ser humano y su aporte relativo depende únicamente de la dieta, por ello esta sustitución se considera una mutación metabólica (437-440). La cadena lateral de la seleniometionina también puede experimentar una oxidación, modificando drásticamente la función de la proteína (425, 427, 428, 430, 441, 442), y es reducida por GSH (443, 444).

Dado que la formación de amiloides es una reacción de ensamblaje intermolecular en la que cambios de tamaño y polaridad pueden alterar significativamente el proceso, en este trabajo abordamos el efecto de la sustitución de metionina por seleniometionina empleando síntesis química y péptidos amiloides con distinto número de metioninas. Mi aportación en este trabajo consistió en los experimentos de dicroísmo circular y el análisis de los estudios de viabilidad celular.

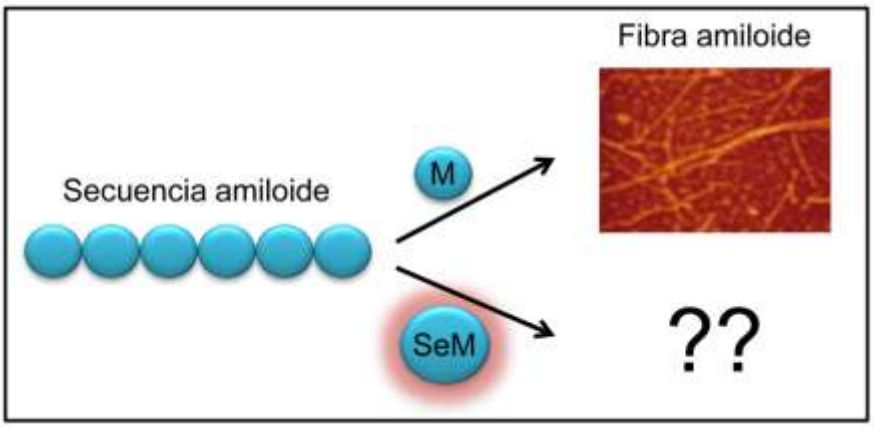

OPEN ACCESS Freely available online

PLoS one

Selenomethionine Incorporation into Amyloid Sequences Regulates Fibrillogenesis and Toxicity

Javier Martínez[1], Silvia Lisa[1], Rosa Sánchez[1], Wioleta Kowalczyk[2], Esther Zurita[3], Meritxell Teixidó[3], Ernest Giralt[3,4], David Andreu[2], Jesús Avila[5], María Gasset[1]*

1 Instituto de Química-Física Rocasolano, Consejo Superior de Investigaciones Científicas, Madrid, Spain, **2** Department of Experimental and Health Sciences, Pompeu Fabra University, Barcelona Biomedical Research Park, Barcelona, Spain, **3** Institute for Research in Biomedicine, Barcelona, Spain, **4** Department of Organic Chemistry, University of Barcelona, Barcelona, Spain, **5** Centro de Biologia Molecular Severo Ochoa, Consejo Superior de Investigaciones Científicas-Universidad Autónoma de Madrid, Madrid, Spain

Abstract

Background: The capacity of a polypeptide chain to engage in an amyloid formation process and cause a conformational disease is contained in its sequence. Some of the sequences undergoing fibrillation contain critical methionine (Met) residues which in vivo can be synthetically substituted by selenomethionine (SeM) and alter their properties.

Methodology/Principal Findings: Using peptide synthesis, biophysical techniques and cell viability determinations we have studied the effect of the substitution of methionine (Met) by selenomethionine (SeM) on the fibrillogenesis and toxic properties of Aβ40 and HuPrP(106–140). We have found that the effects display site-specificity and vary from inhibition of fibrillation and decreased toxicity ([SeM^{35}]Aβ40, [SeM^{129}]HuPrP(106–140) and [SeM^{134}]HuPrP(106–140)), retarded assembly, modulation of polymer shape and retention of toxicity ([SeM^{112}]HuPrP(106–140) to absence of effects ([SeM^{109}]HuPrP(106–140)).

Conclusions/Significance: This work provides direct evidence that the substitution of Met by SeM in proamyloid sequences has a major impact on their self-assembly and toxic properties, suggesting that the SeM pool can play a major role in dictating the allowance and efficiency of a polypeptide chain to undergo toxic polymerization.

Citation: Martínez J, Lisa S, Sánchez R, Kowalczyk W, Zurita E, et al. (2011) Selenomethionine Incorporation into Amyloid Sequences Regulates Fibrillogenesis and Toxicity. PLoS ONE 6(11): e27999. doi:10.1371/journal.pone.0027999

Editor: Andrew Francis Hill, University of Melbourne, Australia

Received July 13, 2011; **Accepted** October 30, 2011; **Published** November 22, 2011

Funding: This work was supported in part by gra'ts BFU2009-07975 (MG), BIO2008-04487-CO3-02 (DA) and BIO2008-00799 (EG) from the Spanish Ministry of Science and Innovation, from the Fundación Cien-Fundación Reina Sofia, and from Generalitat de Catalunya (XRB and Grups Consolidats). Wioleta Kowalczyk is supported by a Juan de la Cierva fellowship from the Spanish Ministry of Science and Innovation. The funders had no role in study design, data collection and analysis, decision to publish, or preparation of the manuscript.

Competing Interests: The authors have declared that no competing interests exist.

* E-mail: mgasset@iqfr.csic.es

Introduction

Protein conformational diseases share the occurrence of a basic misfolding event that leads to the accumulation of proteins or fragments thereof as distinct oligomeric self-assemblies with gained toxic functions [1–3]. Among the various assemblies, amyloids refer to highly ordered cross β-sheet fibrillar aggregates resulting from tight interfacing of complementary β-sheets [4–7]. Despite the regulation by covalent modifications such as proteolytic cleavage, glycosilation and oxidation, among others, the gross information dictating the capacity of a polypeptide chain to form an amyloid is contained in its sequence [4,5,8]. Therefore, deciphering the rules for modulating these sequences, their conformation and their self-assembly preferences is fundamental for the design of preventive therapies.

Among the different strategies for modifying protein sequences, the replacement of Met residues by SeM is unique in that it occurs in the absence of changes at the nucleic acid level [9,10]. Like Met, SeM is an essential amino acid for humans and its availability is strictly related to diet [9,11,12]. SeM incorporates non-specifically into proteins in competition with Met [12]. As an organic part of the Se pool, the reduction of its levels has been correlated with an enhanced risk of aging disorders [13–15]. In principle, Met substitution by SeM is regarded as a structurally inert change that is exploited for the phasing of macromolecular structures in X-ray crystallography [10]. However, some reports indicate changes in the stability of proteins due to the increased hydrophobicity and distinct oxidation susceptibility of SeM compared to Met [16–21]. Thus, changes in the Met/SeM ratio can be considered as a source of transient, metabolic or non-coded mutations and their effect on proteins may vary as a function of residue location.

Of the various amyloid-forming sequences, the amyloid β peptides (Aβ40 and Aβ42) and the PrP(106–140) region are essential components of protein deposits in degenerative dementias and share the presence of regulatory Met residues [22–32]. Aβ40 and Aβ42, produced by sequential proteolytic cleavage of the amyloid β-protein precursor (APP) by β- and γ-secretase, accumulate both as extracellular amyloid deposits and synaptic oligomers in Alzheimer disease (AD) [27]. In both Aβ peptides, Met^{35}, through the oxidation of its side chain, modulates the oligomerization kinetics, the shape of the final polymer (oligomer vs amyloid fibril) and the neurotoxic function [26,33–37]. In prion

protein amyloidoses such as Gerstmann-Straussler-Scheinker syndrome and cerebral amyloid angiopathy, fragments overlapping the 106–140 region of the cellular prion protein (PrP^C) form the specific amyloid deposits [23,29,38]. This sequence (HuPrP) contains four Met residues (Met^{109}, Met^{112}, Met^{129}, Met^{134}) flanking either side of the palindromic AGAAAAGA region essential for assembly [38]. Of those, Met^{109} and Met^{112} are not conserved in mammalian PrP sequences and their mutation to Val does not impede fibrillation while it regulates the processing at the α-cleavage site [29,30,39]. On the other hand Met^{129} and Met^{132} are polymorphic positions in human and deer, respectively, and their substitution by Val or Leu regulates the disease phenotype and the ability to recognize and amplify exogenous prions [22,28,29,32,40].

To establish the role of Se intake as related to its specific incorporation as SeM into amyloid forming sequences, we have synthesized Aβ40 and HuPrP(106–140) sequences containing SeM as a replacement for Met. In contrast to the single Met^{35} substitution in Aβ40, the presence of four methionines in HuPrP(106–140) allows to investigate the role of the replacement site on fibril formation. Herein we show that the substitution of Met by SeM in Aβ40 and HuPrP(106–140) regulates both amyloid formation and toxicity. For HuPrP(106–140), the inhibitory effect displays site-specificity, with the activity varying from inhibition of fibrillation and decrease in toxicity ([SeM^{35}]Aβ40 and [SeM^{129}]-HuPrP(106–140)) to accelerated fibrillation and modulation of the polymer shape with retention of toxicity ([SeM^{109}]HuPrP(106–140) and [SeM^{112}]HuPrP(106–140)).

Results

SeM incorporation to amyloid sequences

Figure 1 shows the sequences of Aβ40 and HuPrP(106–140), both with amyloid-forming capacity and with one or more Met residues with relevant roles [27,29]. The single methionine (Met^{35}) in Aβ40 allowed an unambiguous SeM replacement, while the four (Met^{109}, Met^{112}, Met^{129}, Met^{134}) in HuPrP(106–140) required a more extensive investigation of the site-specificity of SeM replacement. Hence, the wt HuPrP(106–140) sequence with four SeM residues (all-M), a non-oxidizable variant sequence (all-V) with all four Met residues mutated to Val, plus four analogs with single SeM replacements at either position 109, 112, 129 or 134, and Val at the other positions, were prepared. While all seven peptide sequences are of a size generally regarded as viable for solid phase synthesis methodologies, their well-known tendency to aggregate clearly placed them in the "synthetically difficult" category [41]. This fact, plus the need for cost-effective handling of the high-priced Fmoc-SeM building block, called for highly optimized, state of the art synthetic strategies. Thus, for [SeM^{35}]Aβ40, the O-acyl isopeptide approach [42] to difficult sequences was applied, whereby a soluble precursor, 26-O-isoacyl-[SeM^{35}]Aβ(1–40), was prepared and purified to near-homogeneity, then incubated at pH 7.4 to give the target peptide in precipitate form. For its part, [$SeM^{109,112,129,134}$]HuPrP(106–140) (all-M), its all-Val counterpart and the four site-specifically SeM-substituted analogs were efficiently assembled by microwave-assisted solid phase synthesis on ChemMatrix®, a resin proven successful in preventing aggregation during the synthesis of large, complex peptides [43]. Peptides were successfully purified from the crude material and their identity and homogeneity confirmed by mass spectrometry [44]. Full details on the synthesis, purification and analytical documentation of all peptides are given in the **Supporting Information S1** file.

SeM^{35} impedes Aβ40 fibrillation

To investigate the ability of SeM to modify the aggregation properties of Aβ40 we set up a ThT binding kinetics assay. To this end, either wt Aβ40 (Met^{35}) or [SeM^{35}]Aβ40 were incubated at 20–40 μM concentration in PBS in the presence of 15 μM ThT and the increase in fluorescence emission as consequence of its binding to cross β-sheets was monitored (see methods). **Figure 2A** shows that wt Aβ40 at 20 μM and 30°C provokes a time-dependent increase in ThT fluorescence compatible with the known fibrillation process [45]. Importantly, the kinetic trace was reproducible in independent experiments with different batches, with an average lag-phase of 13±2 h. In contrast, incubation of [SeM^{35}]Aβ40 under similar conditions did not cause any detectable change in ThT fluorescence. Increasing [SeM^{35}]Aβ40 concentration up to 200 μM and the incubation time up to 1 week did not provoke any significant or additional change. These results suggest that the substitution of Met by SeM has a clear deleterious impact on amyloid formation.

To confirm the previous findings we analyzed the reaction products by Atomic Force Microscopy (AFM). **Figure 2C** shows that, as expected from the ThT fluorescence readings, Aβ40 assembles into long (>200 nm length) and thin (7 nm height and about 2×40 nm diameter) fibrils that appear decorated by globular particles of about 4 nm in height and 40–80 nm in diameter [**Figure 2C insert**]. In contrast, [SeM^{35}]Aβ40 uniquely yields globular aggregates characterized by 3.5–7 nm height and 35 nm average diameter, corroborating the impairment of the fibrillation process. On the other hand, [SeM^{35}]Aβ40 aggregates yielded electrophoretic patterns different from those of toxic Aβ40 oligomers [**Figure 2B**] [46].

SeM effect on fibrillation displays site-specificity

To ascertain whether the previous findings are uniquely related to the Aβ40 sequence and the essential role played by Met^{35}, or can take place also in other sequences, we analyzed the effect of this substitution on the fibrillation properties of HuPrP(106–140). In this case, given the presence of four Met residues and the possible interference of undesired oxidations in long time incubations, we investigated a non-oxidizable version (all-V, all four Met replaced by Val), as well as single SeM replacements with Val at the other positions [**Figure 1**].

Figure 3A shows that, at 30°C, 20 μM concentration in PBS and with mild orbital shaking, both all-M and all-V HuPrP(106–140) undergo fibrillation, though with notable kinetic differences. Thus, all-M HuPrP(106–140) exhibits the kinetic profile of a highly cooperative process, characterized by an average lag time of 33.8±2.0 h and a final arbitrary ThT fluorescence intensity of 60±5, whereas fibrillation of the all-V variant is characterized by a lag-phase of about 16.4±2.0 h and a final ThT intensity reading of 40±4 [**Figures 3A and 3B**]. These differences found here for the (106–140) sequence regions agree with previous findings reporting the faster polymerization of [Val^{129}]PrP compared to [Met^{129}]PrP and the higher propensity of [Met^{129}]PrP(109–135) over its Val^{129} variant to form β-sheet stabilized fibers [40,47]. Placing SeM at position 109 slightly reduces both the lag phase and the final ThT intensity of the fibrillation kinetics. However, the absence of a clear statistical significance in these changes suggests that SeM^{109} behaves as an all-Val variant. On the contrary, placing SeM at position 112 significantly increases the lag time to 19.7±1.2 h with no effects in the maximum ThT intensity. Surprisingly, the introduction of SeM at position 129 drastically impairs the fibrillation process. Prolonged incubations (up to 1 week) yielded ThT intensity increases below 2.5 with averaged lag phases of >72 h. Along similar lines but to a lesser extent, placing SeM at position 134 allowed a slight fibrillation

PEPTIDE	SEQUENCE
Aβ 40 M35	DAEFRHDSGY EVHHQKLVFF AEDVGSNKGA IIGL MVGGVV
Aβ 40 SeM35	DAEFRHDSGY EVHHQKLVFF AEDVGSNKGA IIGLSeMVGGVV
Aβ 42 M35	DAEFRHDSGY EVHHQKLVFF AEDVGSNKGA IIGL MVGGVVIA
PrP M	KTNMKHM AGAAAAGAVVGGLGGY MLGSA MSRPIIH
PrP V	KTNVKHV AGAAAAGAVVGGLGGY VLGSA VSRPIIH
PrPSeM109	KTNSeMKHV AGAAAAGAVVGGLGGY VLGSA VSRPIIH
PrPSeM112	KTNVKHSeM AGAAAAGAVVGGLGGY VLGSA VSRPIIH
PrPSeM129	KTNVKHV AGAAAAGAVVGGLGGY SeMLGSA VSRPIIH
PrPSeM134	KTNVKHV AGAAAAGAVVGGLGGY VLGSASeMSRPIIH

Figure 1. Proamyloid sequences used as templates for the substitution of Met by SeM. Residues are depicted following one-letter code except for selenomethionine that is abbreviated as SeM.
doi:10.1371/journal.pone.0027999.g001

process featured by a final ThT intensity of 8 and a lag time of 31.5±2.0 h.

To confirm these findings we analyzed by AFM the products of the aggregation reactions [**Figure 3C**]. In agreement with the ThT kinetics, the all-M, all-V, SeM^{109} and SeM^{112} versions of HuPrP(106–140) yielded fibrillar structures, of which those formed by SeM^{112} differed notably from the others by appearing as regular straight rods with a high homogeneity in length. On the contrary, the reaction product of the SeM^{129} analog yielded mainly amorphous aggregates with rarely the presence of fibrillar aggregates. The SeM^{134} peptide displayed an intermediate behaviour, showing few but detectable fibrillar assemblies. The aggregation profile was also studied by SDS-PAGE. **Figure 4A** shows that on aggregation all-M, all-V, SeM^{109} and SeM^{112} versions of PrP(106–140) yielded bands of SDS-resistant aggregated species, whereas SeM^{129} and SeM^{134} ran mainly as monomers.

Taken together these data indicate that, as for the case of Aβ40, SeM incorporation also impairs HuPrP(106–140) fibrillation, but in this case the inhibitory process is highly dependent on the replacement site, with position 129 and to a lesser extent 134 being essential in this respect.

SeM modulates fibril shape

As noted above, [SeM^{112}]HuPrP(106–140) forms fibrillar aggregates that differ notably from those obtained from all-M,

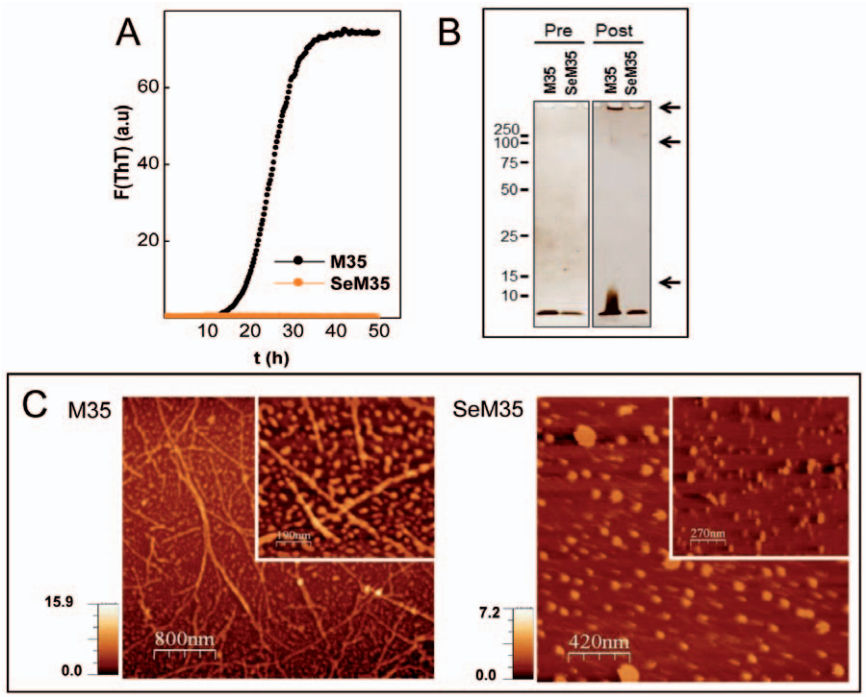

Figure 2. Effect of the incorporation of SeM on the Aβ40 amyloid formation. (**A**) Fibrillation kinetics followed by ThT binding. The displayed curves were obtained by continuous incubation of 20 μM peptide solutions in PBS containing 15 μM ThT at 30°C run in triplicate, and represent the average of three independent experiments. (**B**) Representative silver-stained SDS-PAGE gel of [Met^{35}]Aβ40 and [SeM^{35}]Aβ40 before (pre) and after 80 h (post) of incubation under aggregating conditions. Arrows indicate the distinct oligomers. (**C**) AFM topography imaging of the aggregation reaction products of [Met^{35}]Aβ40 and [SeM^{35}]Aβ40 after 80 h of incubation. Inserts displayed the magnification of a representative area of each case.
doi:10.1371/journal.pone.0027999.g002

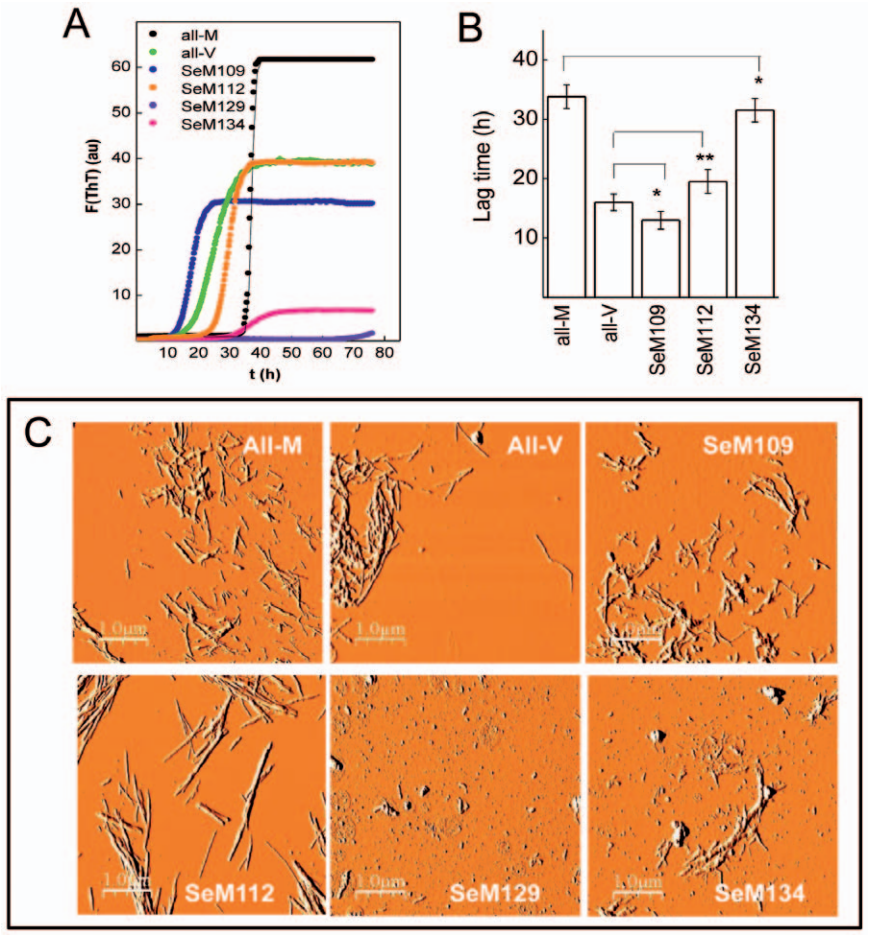

Figure 3. Effect of the incorporation of SeM in HuPrP(106–140) on its amyloid formation. (**A**) Representative fibrillation kinetics of HuPrP(106–140) sequences followed by ThT binding. The color code of the traces is depicted as an insert in each panel. The displayed curves were obtained by continuous incubation of 20 μM peptide solutions in PBS containing 15 μM ThT at 30°C run in triplicate, and represent the average of three independent experiments. (**B**) Lag times of the fibrillation kinetics of HuPrP(106–140) and of its variants. Lag times were calculated independently from each curve and analyzed statistically using the Student's t-test tool provided by Origin 6 software: *, non-significant; **, $P<0.05$. (**C**) Phase images of the molecular species formed after 80 h incubation of HuPrP(106–140) sequences. The displayed fields for all-V, all-M, SeM^{109} and SeM^{112} sequences represent most frequent areas (9 out 10 analyzed 1 μm×1 μm regions). For SeM^{129} and SeM^{134} the displayed fields represent the minor hits (1 out of 20 analyzed 1 μm×1 μm regions).
doi:10.1371/journal.pone.0027999.g003

all-V and SeM^{109} peptides. To gain an insight on the basis of this polymorphism, the fibrils were isolated from the aggregation reactions by centrifugation and, after resuspension, were characterized for their ThT binding on fibril molar basis and by far-UV CD for comparison with previous reports [48]. It must be noted that SeM^{129} and SeM^{134} peptides were not considered in this study given their failure to form fibrils with minimal efficiency.

Figure 4B shows that the fibrillar aggregates of all-M, all-V, SeM^{109} and SeM^{112} recovered by centrifugation from the aggregation reactions and resuspended to similar molar concentration yield similar ThT intensity, and the minor variations are not statistically significant. **Figure 4C** shows that the all-M, all-V and SeM^{109} peptides shared a common spectrum, featured by a double minimum at 208 and 220 nm suggesting an altered β-sheet structure. On the contrary, the spectrum of the SeM^{112} analog displayed the features of a pure β-sheet structure. The results thus support that, depending on its incorporation site, SeM can modulate the secondary structure and subsequently sculpture its self-assembly shape.

Interestingly, these distinct spectral features have been previously reported for the R- and S-fibrils formed by the full length PrP resulting from the aggregation using two different conditions [48]. In fact the morphological and spectral features herein found for the aggregates formed by the SeM^{112} analog resemble those described for S-fibrils, which can be formed with the HaPrP but not with the MoPrP [48,49]. Similarly, the features of the fibrils formed by the all-M, all-V and SeM^{109} peptides resemble the properties described for the R-fibrils which can be formed by both HaPrP and MoPrP [48,49]. Among other sequence differences, HaPrP and MoPrP differ in the residue at position 112, Met in HaPrP and Val in MoPrP. Since Met though not Val can be metabolically replaced by SeM, it is tempting to speculate that the formation of S-fibrils could be dictated at least in part by the presence of chains containing SeM in position 112, which can uniquely occur with HaPrP, not with MoPrP.

SeM effects on fibrillation are unrelated to oxidation

As with Met, the SeM side chain can undergo oxidation to selenoxide and selenone, and if so could drastically modify the

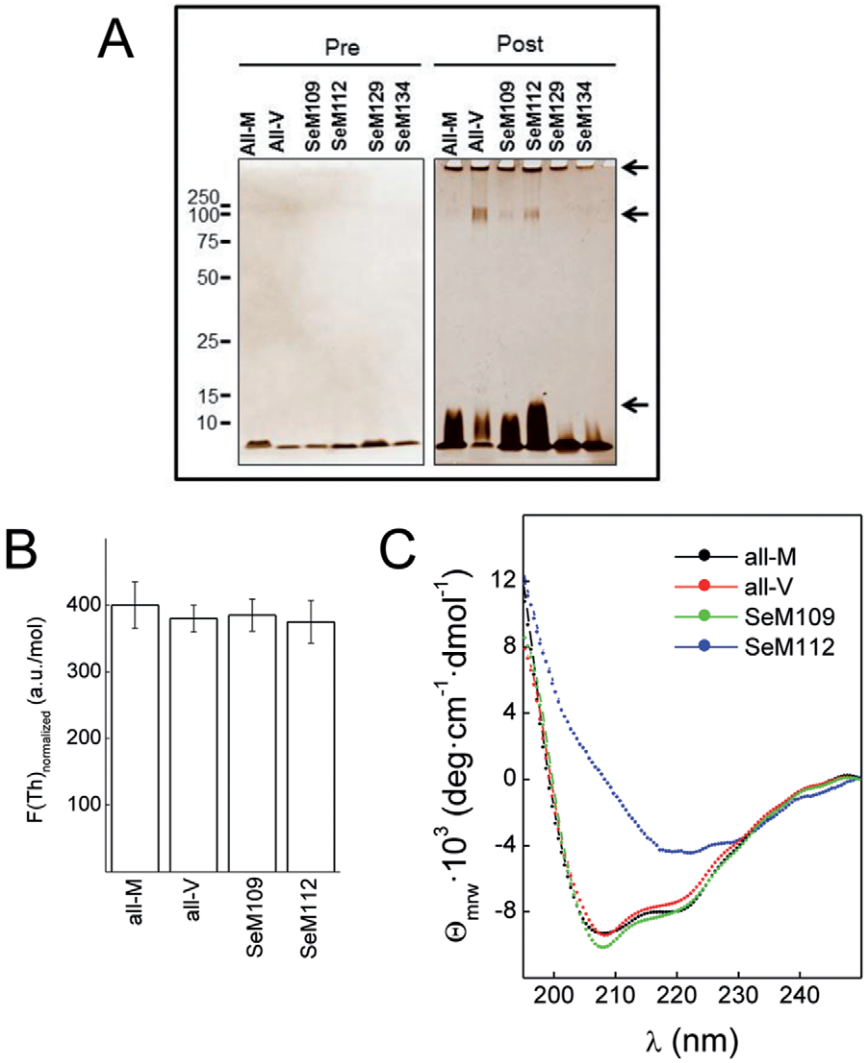

Figure 4. Aggregation profiles of HuPrP(106–140) sequence variants. (**A**) Typical aggregation pattern of HuPrP(106–140) and of its variants probed by silver-stained SDS-PAGE. Peptide aliquots (1 μg) before (pre) and after 80 h (post) of aggregation were separated in TGX-Precast BioRad gels and then silver stained. (**B**) Normalized ThT binding of the insoluble aggregates formed by HuPrP(106–140) peptides. Aggregated peptides were isolated as insoluble pellets of 30 min centrifugations at 15000 rpm, resuspended in PBS at 60 μM concentration. ThT binding of the resuspended aggregates was measured by fluorescence at 20 μM peptide and 15 μM ThT concentrations. (**C**) Far-UV CD spectral features of the insoluble aggregates formed by HuPrP(106–140) peptides. Insoluble pellets were prepared as in panel B in PBS and the spectra recorded at 60 μM. At least three separate experiments were performed to confirm these results.
doi:10.1371/journal.pone.0027999.g004

process of amyloid formation [26,33–37]. To investigate whether the observed differences in fibrillation were related to SeM oxidation we analyzed by MALDI FT-ICR the peptides before and after the aggregation reaction. In all cases, m/z patterns of pre-aggregated and post-aggregated samples were superimposable and peaks reproduced the theoretical predicted charged masses [**Figure 5, Supporting Information**]. Importantly, no peaks at +16/+32 Da expected for the oxidized variants were detected [**Figure 5**]. Despite the non-quantitative nature of the mass spectrometry method, it plausible discards that undesired side chain oxidations play a role in the amyloid formation traits.

SeM containing sequences also function as exogenous fibrillation regulators

Consistent with the previous findings and with the fact that Met substitution by SeM would be hardly ever quantitative under physiological conditions, we next tested the capacity of the SeM-containing sequences to modulate the amyloid formation process of the unlabelled sequences. As amyloid formation can be essentially view as a seeded-polymerization in which nucleation, elongation and polymer fragmentation are critical steps, the SeM effects could also provide mechanistic information [1–7]. The results are shown in **Figure 6**.

Co-incubation of [SeM^{35}]Aβ40 with Aβ40 and with its longer and more fibrillogenic form Aβ42 impaired their fibrillation process [**Figure 6A**]. These impairments could not be attributed to dilution since, in the absence of [SeM^{35}]Aβ40 and at equal concentration, both Aβ40 and Aβ42 undergo fibrillation. Rather, the results agreed with an inhibition process and suggested that [SeM^{35}]Aβ40 interacts with Met^{35}-bearing peptides, and halts their productive aggregation through the formation of growth-impaired oligomers.

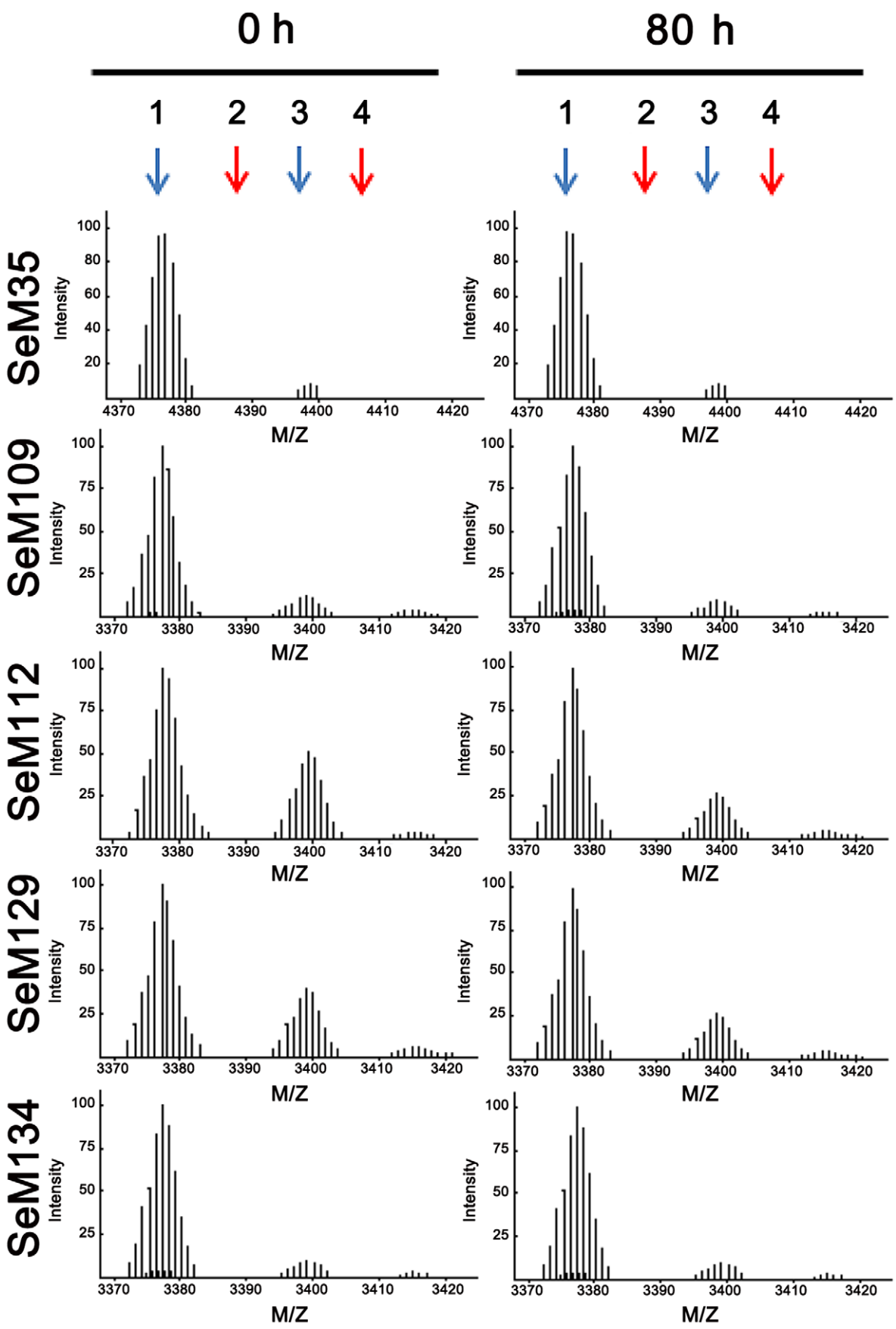
0 h
80 h
1
2
3
4
SeM35
SeM109
SeM112
SeM129
SeM134
Intensity
M/Z

Figure 5. MALDI FT-ICR profiles of SeM-containing Aβ40 and HuPrP(106–140) peptides. Representative m/z patterns of the distinct peptides after 80 h of incubation under aggregating conditions. Measurements were performed using samples of at least two separate experiments. Arrows indicate the theoretical positions for the m/z values of: 1) +1, 2) +16 (selenoxide), 3) +23 (Na+-adduct) and 4) +32 (selenone). For SeM35 the values are: 4376.1, 4381.1, 4388.1, 4408.1. For SeM analogs of HuPrP(106–140) the values are: 3377.2, 3393.2, 3399.2, 3409,2. The peak complexity arises from the Se isotopic distribution [20].
doi:10.1371/journal.pone.0027999.g005

Similarly, in the HuPrP(106–140) case, co-incubation of 10 μM SeM^{129} analog with 10 μM of either all-M [**Figure 6B**] or all-V [**Figure 6C**] peptides inhibited amyloid formation. Again, such inhibitions could not be attributed to dilution effects, since the latter peptides, at 10 μM and in the absence of the SeM^{129} analog, yielded ThT binding kinetics compatible with fibrillation reactions. Hence, the inhibition trend suggests that [SeM^{129}]-HuPrP(106–140), acting like a quencher, interacts with either all-M or all-V HuPrP(106–140), giving rise to oligoheteromeric species that do not sustain growth. This data agreed with previous findings indicating the essential role of identity in position 129 for the allowance of formation of a stable steric zipper [50].

On the contrary, [SeM^{134}]HuPrP(106–140), of very low efficiency in fibrillogenesis, when mixed with either all-M or all-V does not alter significantly the ThT binding pattern of the previous peptides [**Figure 6B and 6C**]. These results suggest that SeM^{134} precludes stable interaction and therefore causes its segregation. Since position 134 has not been found to play a fundamental role in amyloid formation, then the segregating behavior seems related to SeM hydrophobic properties and their provoked reactions [5,51,52].

On the other hand, SeM^{109} and SeM^{112} when mixed 1:1 with either all-V or all-M peptides altered the ThT binding kinetics, imposing their characteristic lag-phase and allowing the final ThT intensity of the SeM-free peptide [**Figure 6B and 6C**]. This observation strongly suggests that positions 109 and 112 determine the efficiency of seed formation and therefore the speed of the polymerization reaction [1–7].

SeM-containing sequences can ameliorate toxicity

To investigate the structure–activity relationship of the SeM substitutions we analyzed the effect of the aggregation reaction products on the viability of rodent primary cortical neurons [**Figure 7**]. For this purposes, the different peptides and their combination were incubated for 80 h at 30°C at 0.10–0.15 mM in PBS and then diluted to a final concentration of 10 μM in the cell medium and allowed to incubate for 48 h. Under the assay conditions, all peptides except [SeM^{35}]Aβ40 and the SeM^{129} and SeM^{134}-analogs of HuPrP(106–140) and their mixtures have completed their fibrillation process as judged by parallel ThT reading, and the untreated cells yielded cell viability values that amounted to 97.5±1%.

Aβ40 was found to cause 11±1% cell death, in agreement with previous reports [27,37,53]. Interestingly, [SeM^{35}]Aβ40 reduced cell death to 3±1.5%, thereby excluding any relationship between its assemblies and the highly neurotoxic nonfibrillar oligomers formed by Aβ peptides [27]. This reduction pattern was maintained for its 1:1 mixture with Aβ40, which cannot be explained solely on the basis of [Met^{35}]Aβ40 dilution as judged from the concentration control.

As for HuPrP(106–140), the aggregation reaction products of all-M and all-V caused about 20±2% of cell death, in agreement with the toxicity levels described for the polymers formed by HuPrP(82–146) [54]. SeM^{109} and SeM^{112} analogs caused cell death to a similar extent, in agreement with their similar amyloid forming ability at long incubation times [**Figure 3A**]. On the contrary, SeM^{129} and to a lesser extent SeM^{134} caused minor effects on cell viability (1.1±0.5 and 4±0.6, respectively). As in the case of [SeM^{35}]Aβ40, these statistically significant reductions in the extent of cell death compared to that caused by the amyloid-assembled sequences discards active oligomeric species. Moreover, the aggregation products of the all-M and all-V peptides mixed with SeM^{129} and SeM^{134} reproduced the profiles observed in kinetic experiments [**Figure 6B and 6C**]. Mixing SeM^{129} 1:1 with either all-M or all-V decreases cell death extent to almost abrogation, and the effect cannot be explained solely in terms of

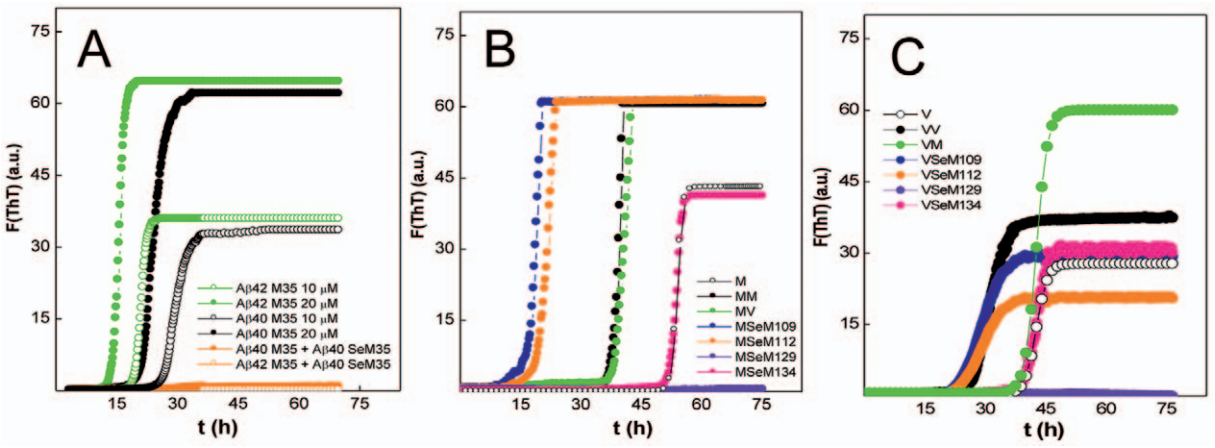

Figure 6. Analysis of the regulatory cross-talk between SeM-tagged and wt sequences. (**A**) ThT binding kinetics of Aβ40 and Aβ42 in the absence (10 and 20 μM) and presence of [SeM^{35}]Aβ40 (10 μM of each peptide). (**B**) Time evolution of the ThT binding of mixtures of 10 μM all-M HuPrP(106–126) in the absence and presence of 10 μM of HuPrP(106–126) sequence variants. (**C**) ThT binding kinetics of mixtures of 10 μM all-M HuPrP(106–126) in the absence and presence of 10 μM of HuPrP 106–126 sequence variants. The color code of the different traces is indicated at the right hand side of each panel. The displayed curves were obtained by continuous incubation of the different peptide solutions in PBS containing 15 μM ThT at 30°C in duplicate, and represent the average of three independent experiments.
doi:10.1371/journal.pone.0027999.g006

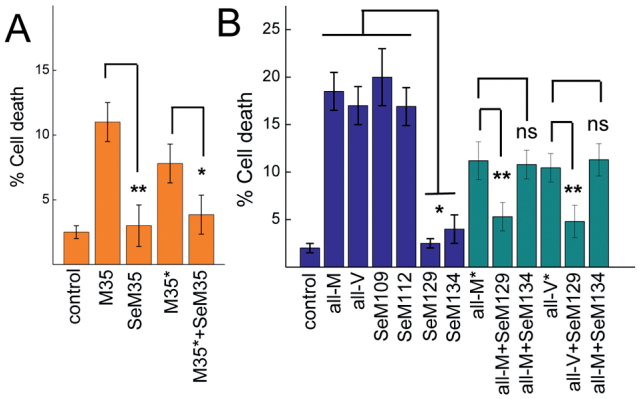

Figure 7. Cytotoxic potential of SeM containing sequences and of their mixtures. Rodent primary cortical neurons were cultured for 7 days on poly-D-lysine-coated coverslips and treated with 10 μM of each peptide or 1:1 molar ratio mixture of peptides for 48 h. The cells were then probed with LIVE/DEAD kit. The percentage of dead cells was obtained dividing the number of dead cells by the total (live and dead) number of cells. The results are the means ± SD of three independent experiments ran in duplicate. Statistical analysis was performed with the Student's *t* test tool of Origin software. ns, non-significant. *, $P<0.05$; **, $P<0.005$.
doi:10.1371/journal.pone.0027999.g007

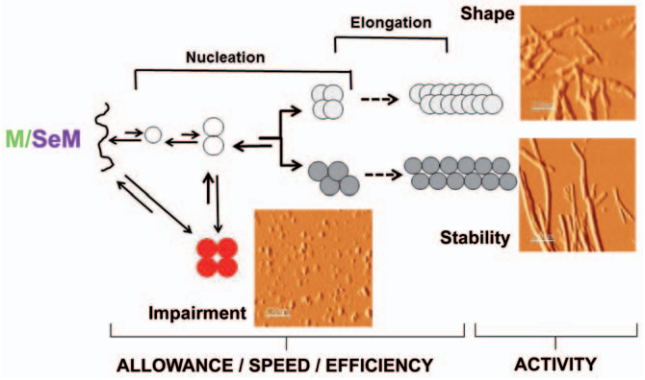

Figure 8. Summary of the effects of SeM introduction in amyloid forming sequences. Replacement of methionine (M) residues by its metabolic competitor selenomethionine (SeM) in proamyloid sequences involves changes in local hydrophobicity and steric factors. With a site-dependence, the replacement can promote side association reaction that either decrease the efficiency and speed or impair amyloid formation. In other cases, by regulating the seed packing can generate distinct fibrilar assemblies.
doi:10.1371/journal.pone.0027999.g008

the reduction all-M and all-V concentration as shown by the concentration controls. On the contrary, mixing the SeM^{134} analog 1:1 with either all-M or all-V reproduces the cell death percentage of diluted all-M and all-V peptides.

Discussion

Unveiling the ways proamyloid sequences can be modulated to impede their productive engagement into self-assembly processes yielding toxic events is essential for designing preventing strategies for conformational diseases. The pioneer study of Goldschmidt et al [5] has solidly established as general principle that the capacity of a protein to form the β-sheet based fibrillar amyloid structures is coded in its sequence, although its display may depend on structural and environmental regulatory factors [55]. One possible modulatory event is that involving metabolic changes of Met and SeM pools and consequently of their competitive incorporation in proteins through the AUG codon. Taking the advantage of synthetic approaches we have substituted Met by SeM in amyloid forming sequences and we have found dramatic effects on their polymerization and toxicity. These effects varied from inhibition ([SeM^{35}]Aβ40 and [SeM^{129}]PrP(106–140)), polymerization kinetics perturbation to polymer shape determination ([SeM^{112}]PrP(106–140)) [**Figure 8**].

Despite the consideration of Met and SeM as structurally equivalent, the change of a sulfur by a selenium atom involves major steric and reactivity differences. Se is slightly larger than S (atomic radius of 1.17 vs 1.04 Å) and has also a larger van der Waals radius (1.90 vs 1.80 Å).Since the spines of amyloid fibrils consist in steric zippers formed by the interdigitation of β-sheets through their side chains, any steric perturbation may lead to clashes which may reduce the stability of this unit or even preclude its formation [5,50]. This might be the case of the fibrillation impairments of [SeM^{35}]Aβ40 and [SeM^{129}]PrP(106–140) peptides, for which the crystal structure of shorter fragments have shown Met^{35} and Met^{129} actively participating in the inter-sheet packing [50,56]. Also, since the interdigitations are not unique but can involve distinct patterns, the side chain size increase together with its position can dictate the preference for specific stacking patterns over others that as seeds will produce distinct fibril shapes as for SeM^{109} and SeM^{112} analogs of PrP(106–140) [5,50,56]. The larger size of Se than S also causes SeM to have a larger surface area and hence hydrophobicity than Met. Since amyloid formation is a complex process involving the construction of oligomeric species undergoing growth, fragmentation and quenching or arrest, minor changes in hydrophobicity may trigger significant alterations in the solubility of the distinct oligomeric species as well as in the the features of the interacting surfaces [1–7,50]. For instance, by its increased hydrophobicity SeM can decrease the efficiency of amyloid formation in [SeM^{134}]PrP(106–140), which retains the ability to engage in the process but does it with a very low efficiency.

SeM also differs from Met in its side chain oxidation process. SeM can undergo oxidation by peroxynitrites to selenoxide but, unlike the sulfoxide, the selenoxide is easily reduced by organic thiols as glutathione and does not required enzymatic assistance [20,52,57]. Although SeM oxidation is not a major event in our experimental setup, since sulfoxide formation is known to impair fibrillation in Aβ40 and PrP(106–126), the chemical differences of the reaction could add novel regulatory steps to the polymerization [24–26,34,35,58]. To address this possibility, improved basic knowledge is required on reaction conditions and product characterization of SeM oxidation as a part of a protein and free in solution [52,57].

For Aβ40 the Met35SeM non-coded or metabolic mutation impairs amyloid formation but stabilizes oligomeric assemblies as shown by AFM. Based on shape considerations, the oligomers might be suspected to act as the actual neurotoxins. However, both PAGE-SDS analysis and toxicity evaluation discard such assemblies being deleterious and support the importance of the amyloid pathway as a source of toxic species. This rationale can be extended to the [SeM^{129}]HuPrP(106–140) analog, which in addition to its impaired fibrillation and lack of toxic activity, prevents the fibrillation and toxicity of all-V and all-M. For these two cases, the incorporation of SeM into an essential position functions as a physiological anti-amyloid metabolic defense. However, the effect of SeM incorporation is not homogeneous. For instance, the SeM^{109} and SeM^{112} analogs of HuPrP(106–140) displayed differences in kinetics and in fibril shape, and such morphological differences can have important functional implica-

tions [59]. In this sense, fibrils of the SeM^{112} –shape are expected to be more toxic that fibrils with shapes of the SeM^{109}-analog, whereas if fragmented the toxicity profile inverts [59]. In our set up, both assemblies yielded statistical similar toxicity traits suggesting that SeM substitution could also play a role in the in vivo stability (fragmentation or recycling) of the polymers so activity differences in the 48 h assay become averaged. In this line, H/D exchange experiments have shown that isolated fibrils can display significant distinct recycling properties, with changes in fibril dissolution rate constant of about two orders of magnitude (0.6 s^{-1} and 1.0×10^{-2} s^{-1} for Aβ40 and Aβ42, respectively) [60].

As summarized in **Figure 8**, these evidences clearly indicate that SeM incorporation into pro-amyloid sequences results in various effects as a function of its location and suggest that metabolic changes in the Met/SeM pool can exert important modulatory effects in amyloid diseases.

Materials and Methods

Peptides and aggregation reactions

The SeM-substituted versions of Aβ40 and HuPrP(106–140) (Figure 1A) were synthesized by solid phase methods, purified by HPLC and characterized by mass spectrometry. Details are given in the **Supporting Information S1** file. For control studies, Aβ40 and Aβ42 were obtained from GenScript. Lyophilized peptide stocks were dissolved in HFIP, aliquoted and dried under N_2 for storage at −80°C. Samples were reconstituted in 5 mM NH_4OH pH 8.0 at about 2 mg/ml concentration and filtered through 0.2 μm membranes before use. Peptide concentrations were determined by UV spectroscopy and by amino acid analysis. Peptide stock solutions were diluted with PBS at 100–200 μM concentrations and kept at 4°C for less than 30 min. The aggregation reactions were performed both in eppendorf tubes and in wells of a 96-well plate by incubating 20–200 μM peptide monomers in PBS at 30°C with orbital shaking (100 rpm).

Thioflavin T binding kinetics

The kinetics of thioflavin T (ThT) binding was monitored by bottom reading of fluorescence intensity in a POLARstar microplate reader (BMG Labtech) as described [51]. Measurements were performed using 450 nm excitation and 480 nm emission filters, 0.20 ml samples and 15 μM ThT concentration. The measurement program consisted of 10 flashes reading every 10 min with 1-min of orbital 1-mm diameter shaking at 100 rpm with the temperature controller set at 30°C. All measurements were done in triplicate and the experiments were repeated at least twice using two different peptide batches. When required, the lag-phase was determined as described [61].

PAGE analysis

Peptide samples before and after 80 h of aggregation were removed and diluted 1:1 in β-mercaptoethanol-free Laemmli buffer and, omotting the thermal denaturation step, loaded in BioRad precastTGX-gels. After silver staining, gel images were captured and analyzed using the Molecular Imager ChemiDoc^{TM} XRS+ Imaging system and ImageLab 3.0.1 (beta2) software (BioRad).

Mass spectrometry analysis

Aliquots of the peptide solutions before and after aggregation were removed, treated with HFIP for aggregate disruption and analyzed using α-hydroxy-cinnamic acid matrix and a MALDI FT-ICR 930-MS (Varian) instrument operating at 7 T and 10^{-9} Torr and with OMEGA software.

Atomic force microscopy (AFM)

Ten μl-samples of peptide solution after 70 h incubation were diluted to 2 μM with ddH_2O and applied onto freshly cleaved mica surfaces to adhere for 15 min. After washing with ddH_2O, samples were dried with N_2. AFM imaging was then performed using a PicoSPM^{TM} (Molecular Imaging, Phoenix, AZ), operating the AFM scanner in acoustic alternating current mode with Si,N-ACT type cantilevers (ScienTec) with a tip radius <10 nm and a spring constant of 25–75 N/m [51]. The images (1×1 μm scans) were collected at a scan rate of 1 line per second and analyzed using WSxM 5.0 Nanotec software.

Circular dichroism (CD) spectroscopy

CD spectra were recorded in the far-UV region with a Jasco J-810 spectropolarimeter in continuous scan mode (250−190 nm) and a 0.1 cm path length quartz cuvette (Hellma) as described previously [51].

Citotoxicity assays

Mice were obtained from the Centro de Biología Molecular and treated following the guidelines of Council of Europe Convention ETS123, recently revised as indicated in the Directive 86/609/EEC. Animal experiments were performed under protocols (P22/P23) approved by the Centro de Biología Molecular Severo Ochoa Institutional Animal Care and Utilization Committee (CEEA-CBM, Madrid, Spain). Primary cortical neurons were obtained from the cerebral cortex of C57B16 E18 rat embryos, by enzymatic dissociation with papain (Worthington Biochemical) in EBSS for 45 min at 37°C. Cells were resuspended in Neurobasal medium with 2% B27, 0.25% 200 mM Gln, 1% Glutamax and 1% penicillin/streptomycin and seeded on cover slips pre-coated with poly-D-Lys (10 μg/ml). Two days later, 5 μM Ara-C was added to the medium. Seven days later, peptides preincubated in PBS were added at a final concentration of 25 μM. After 48 h incubation at 37°C, neuronal cell death was determined using the LIVE/DEAD kit (Invitrogen) for mammalian cells. Live cells (stained with calcein-AM) and dead cells (stained with red-fluorescent ethidium homodimer-1) were counted and the percentage of dead cells calculated.

Supporting Information

Supporting Information S1
(DOCX)

Acknowledgments

Angel Cuesta, Natalia Carulla, Juan Dávalos and Javier González are acknowledged for their advice on AFM and MALDI FT-ICR measurements.

Author Contributions

Conceived and designed the experiments: MG JA DA EG. Performed the experiments: JM SL RS WK EZ MT MG. Analyzed the data: MG JM SL. Contributed reagents/materials/analysis tools: WK EZ MT EG DA JA. Wrote the paper: MG DA.

References

1. Carrell RW, Lomas DA (1997) Conformational disease. Lancet 350: 134–138.
2. Stefani M, Dobson CM (2003) Protein aggregation and aggregate toxicity: new insights into protein folding, misfolding diseases and biological evolution. J Mol Med 81: 678–699.
3. Chiti F, Dobson CM (2006) Protein misfolding, functional amyloid, and human disease. Annu Rev Biochem 75: 333–366.
4. Maji SK, Wang L, Greenwald J, Riek R (2009) Structure-activity relationship of amyloid fibrils. FEBS Lett 583: 2610–217.
5. Goldschmidt L, Teng PK, Riek R, Eisenberg D (2010) Identifying the amylome, proteins capable of forming amyloid-like fibrils. Proc Natl Acad Sci U S A 107: 3487–3492.
6. Toyama BH, Weissman JS (2010) Amyloid Structure: conformational diversity and consequences. Annu Rev Biochem 80: 557–585.
7. Shewmaker F, McGlinchey RP, Wickner RB (2011) Structural insights into functional and pathological amyloid. J Biol Chem 286: 16533–16540.
8. Wiltzius JJ, Landau M, Nelson R, Sawaya MR, Apostol MI, et al. (2009) Molecular mechanisms for protein-encoded inheritance. Nat Struct Mol Biol 16: 973–978.
9. Schrauzer GN (2000) Selenomethionine: a review of its nutritional significance, metabolism and toxicity. J Nutr 130: 1653–1656.
10. Yokoyama S (2003) Protein expression systems for structural genomics and proteomics. Curr Opin Chem Biol 7: 39–43.
11. Griffiths NM, Stewart RDH, Robinson MF (1976) The metabolism of (75Se)selenomethinine in four women. Br J Nutr 35: 373–382.
12. Rayman MP (2008) Food-chain selenium and human health: emphasis on intake. Br J Nutr 100: 254–268.
13. Méplan C (2011) Trace elements and ageing, a genomic perspective using selenium as an example. J Trace Elements Med Biol 255: 511–516.
14. McCann JC, Ames BN (2011) Adaptative dysfunction of selenoproteins from the perspective of the triage theory: why modest deficiency may increase risk of diseases of aging. FASEB J 25: 1793–1814.
15. Shahar A, Patel KV, Semba RD, Bandinelli S, Shahar DR, et al. (2010) Plasma selenium is positively related to performance in neurological tasks assessing coordination and motor speed. Mov Disord 25: 1909–1915.
16. Budisa N, Huber R, Golbik R, Minks C, Weyher E, et al. (1998) Atomic mutations in annexin V: thermodynamic studies of isomorphous protein variants. Eur J Biochem 253: 1–9.
17. Gassner NC, Baase WA, Hausrath AC, Matthews BW (1999) Substitution with selenomethionine can enhance the stability of methionine-rich proteins. J Mol Biol 294: 17–20.
18. Håkansson K, Broder D, Wang AH, Miller CG (2000) Crystallization of peptidase T from Salmonella typhimurium. Acta Crystallogr D Biol Crystallogr 56: 924–926.
19. Wernimont AK, Huffman DL, Finney LA, Demeler B, O'Halloran TV, et al. (2003) Crystal structure and dimerization equilibria of PcoC, a methionine-rich copper resistance protein from Escherichia coli. J Biol Inorg Chem 8: 185–194.
20. Le DT, Liang X, Fomenko DE, Raza AS, Chong CK, et al. (2008) Analysis of methionine/selenomethionine oxidation and methionine sulfoxide reductase function using methionine-rich proteins and antibodies against their oxidized forms. Biochemistry 47: 6685–6694.
21. Yamniuk AP, Ishida H, Lippert D, Vogel HJ (2009) Thermodynamic effects of noncoded and coded methionine substitutions in calmodulin. Biophys J 96: 1495–1507.
22. Collinge J, Palmer MS, Dryden AJ (1991) Genetic predisposition to iatrogenic Creutzfeldt-Jakob disease. Lancet 337: 1441–1442.
23. Ghetti B, Piccardo P, Spillantini MG, Ichimiya Y, Porro M, et al. (1996) Vascular variant of prion protein cerebral amyloidosis with tau-positive neurofibrillary tangles: the phenotype of the stop codon 145 mutation in PRNP. Proc Natl Acad Sci U S A 93: 744–748.
24. Palmblad M, Westlind-Danielsson A, Bergquist J (2002) Oxidation of methionine 35 attenuates formation of amyloid β-peptide 1–40 oligomers. J Biol Chem 277: 19506–19510.
25. Bitan G, Tarus B, Vollers SS, Lashuel HA, Condron MM, et al. (2003) A molecular switch in amyloid assembly: Met35 and amyloid β-protein oligomerization. J Am Chem Soc 125: 15359–15365.
26. Butterfield DA, Boyd-Kimball D (2005) The critical role of methionine 35 in Alzheimer's amyloid β-peptide (1–42)-induced oxidative stress and neurotoxicity. Biochim Biophys Acta 1703: 149–156.
27. Haass C, Selkoe DJ (2007) Soluble protein oligomers in neurodegeneration: lessons from the Alzheimer's amyloid beta-peptide. Nat Rev Mol Cell Biol 8: 101–112.
28. Green KM, Browning SR, Seward TS, Jewell JE, Ross DL, et al. (2008) The elk PRNP codon 132 polymorphism controls cervid and scrapie prion propagation. J Gen Virol 89: 598–608.
29. Aguzzi A, Calella AM (2009) Prions: protein aggregation and infectious diseases. Physiol Rev 89: 1105–1152.
30. Haigh CL, Lewis VA, Vella LJ, Masters CL, Hill AF, et al. (2009) PrPC-related signal transduction is influenced by copper, membrane integrity and the alpha cleavage site. Cell Res 19: 1062–1078.
31. Lee S, Antony L, Hartmann R, Knaus KJ, Surewicz K, et al. (2010) Conformational diversity in prion protein variants influences intermolecular beta-sheet formation. EMBO J 29: 251–262.
32. Parchi P, Strammiello R, Giese A, Kretzschmar H (2011) Phenotypic variability of sporadic human prion disease and its molecular basis: past, present, and future. Acta Neuropathol 121: 91–112.
33. Näslund J, Schierhorn A, Hellman U, Lannfelt L, Roses AD, et al. (1994) Relative abundance of Alzheimer Aβ amyloid peptide variants in Alzheimer disease and normal aging. Proc Natl Acad Sci USA 91: 8378–8382.
34. Butterfield DA, Bush AI (2004) Alzheimer's amyloid beta-peptide (1–42): involvement of methionine residue 35 in the oxidative stress and neurotoxicity properties of this peptide. Neurobiol Aging 25: 563–568.
35. Clementi ME, Marini S, Coletta M, Orsini F, Giardina B, et al. (2005) Abeta(31–35) and Abeta(25–35) fragments of amyloid beta-protein induce cellular death through apoptotic signals: Role of the redox state of methionine-35. FEBS Lett 579: 2913–2918.
36. Johansson AS, Bergquist J, Volbracht C, Päiviö A, Leist M, et al. (2007) Attenuated amyloid-beta aggregation and neurotoxicity owing to methionine oxidation. Neuroreport 18: 559–563.
37. Maiti P, Piacentini R, Ripoli C, Grassi C, Bitan G (2010) Surprising toxicity and assembly behaviour of amyloid β-protein oxidized to sulfone. Biochem J 433: 323–332.
38. Gasset M, Baldwin MA, Lloyd DH, Gabriel JM, Holtzman DM, et al. (1992) Predicted alpha-helical regions of the prion protein when synthesized as peptides form amyloid. Proc Natl Acad Sci U S A 89: 10940–10944.
39. Salmona M, Morbin M, Massignan T, Colombo L, Mazzoleni G, et al. (2003) Structural properties of Gerstmann-Straussler-Scheinker disease amyloid protein. J Biol Chem 278: 48146–48153.
40. Petchanikow C, Saborio GP, Anderes L, Frossard MJ, Olmedo MI, et al. (2001) Biochemical and structural studies of the prion protein polymorphism. FEBS Lett 509: 451–456.
41. Dettin M, Pegoraro S, Rovero P, Bicciato S, Bagno A, et al. (1997) SPPS of difficult sequences. A comparison of chemical conditions, synthetic strategies and on-line monitoring. J Pept Res 49: 103–111.
42. Sohma Y, Hayashi Y, Kimura M, Chiyomori Y, Taniguchi A, et al. (2005) The 'O-acyl isopeptide method' for the synthesis of difficult sequence-containing peptides: application to the synthesis of Alzheimer's disease-related amyloid beta peptide (A-beta) 1–42. J Pept Sci 11: 441–451.
43. Garcia-Martin F, Quintanar-Audelo M, Garcia-Ramos Y, Cruz LJ, Gravel C, et al. (2006) ChemMatrix, a poly(ethylene glycol)-based support for the solid-phase synthesis of complex peptides. J Comb Chem 8: 213–220.
44. Grillo-Bosch D, Rabanal F, Giralt E (2011) Improved Fmoc-based solid-phase synthesis of homologous peptides fragments of human and mouse prion proteins. J Pept Sci 17: 32–38.
45. LeVine H (1993) Thioflavine T interaction with synthetic Alzheimer's disease beta-amyloid peptides: detection of amyloid aggregation in solution. Protein Sci 2: 404–410.
46. Itkin A, Dupres V, Dufrêne YF, Bechinger B, Ruysschaert JM, et al. (2011) Calcium ions promote formation of amyloid β-peptide (1–40) oligomers causally implicated in neuronal toxicity of Alzheimer's disease. PLoS One 6: e18250.
47. Baskakov I, Disterer P, Breydo L, Shaw M, Gill A, et al. (2005) The presence of valine at residue 129 in human prion protein accelerates amyloid formation. FEBS Lett 579: 2589–2596.
48. Ostapchenko VG, Sawaya MR, Makarava N, Savtchenko R, Nilsson KP, et al. (2010) Two amyloid States of the prion protein display significantly different folding patterns. J Mol Biol 400: 908–921.
49. Makarava N, Ostapchenko VG, Savtchenko R, Baskakov IV (2009) Conformational switching within individual amyloid fibrils. J Biol Chem 284: 14386–14395.
50. Apostol MI, Sawaya MR, Cascio D, Eisenberg D (2010) Crystallographic studies of prion protein (PrP) segments suggest how structural changes encoded by polymorphism at residue 129 modulate susceptibility to human prion disease. J Biol Chem 285: 29671–29675.
51. Lisa S, Meli M, Cabello G, Gabizon R, Colombo G, et al. (2010) The structural intolerance of the PrP alpha-fold for polar substitution of the helix-3 methionines. Cell Mol Life Sci 67: 2825–2838.
52. Smith JL, Thompson A (1998) Reactivity of selenomethionine-dents in the magic bullet? Structure 6: 815–819.
53. Dahlgren KN, Manelli AM, Stine WB, Baker LK, Krafft GA, et al. (2002) Oligomeric and fibrillar species of amyloid-beta peptides differentially affect neuronal viability. J Biol Chem 277: 32046–32053.
54. Fioriti L, Angeretti N, Colombo L, De Luigi A, Colombo A, et al. (2007) Neurotoxic and gliotrophic activity of a synthetic peptide homologous to Gerstmann-Sträussler-Scheinker disease amyloid protein. J Neurosci 27: 1576–1583.
55. Duennwald ML, Jagadish S, Muchowski PJ, Lindquist S (2006) Flanking sequences profoundly alter polyglutamine toxicity in yeast. Proc Natl Acad Sci U S A 103: 11045–50.
56. Sawaya MR, Sambashivan S, Nelson R, Ivanova MI, Sievers SA, et al. (2007) Atomic structures of amyloid cross-β spines reveal varied steric zippers. Nature 447: 453–457.
57. Krause RJ, Elfarra AA (2009) Reduction of L-methionine selenoxide to seleno-L-methionine by endogenous thiols, ascorbic acid, or methimazole. Biochem Pharmacol 77: 134–140.

58. Bergström AL, Chabry J, Bastholm L, Heegaard PM (2007) Oxidation reduces the fibrillation but not the neurotoxicity of the prion peptide PrP106–126. Biochim Biophys Acta 1774: 1118–1127.
59. Lee YJ, Savtchenko R, Ostapchenko VG, Makarava N, Baskakov IV (2011) Molecular structure of amyloid fibrils controls the relationship between fibrillar size and toxicity. PLoS One 6: e20244.
60. Sánchez L, Madurga S, Pukala T, Vilaseca M, López-Iglesias C, et al. (2011) Aβ40 and Aβ42 amyloid fibrils exhibit distinct molecular recycling properties. J Am Chem Soc 133: 6505–6508.
61. Bishop MF, Ferrone FA (1984) Kinetics of nucleation-controlled polymerization. A perturbation treatment for use with a secondary pathway. Biophys J 46: 631–644.

Artículo 4. Failure of prion protein oxidative folding guides the formation of toxic transmembrane forms.

Las enfermedades priónicas se caracterizan por un cambio estructural, mecanísticamente complejo y en etapas, que sufre PrP^C al pasar de un estado conformacional mayoritario de α-hélice a uno con mayor número de láminas-β (207, 286, 421). La presencia de mutaciones en la cadena polipeptídica presupone un incremento en la tendencia a este cambio (363, 445), sin embargo, los estudios biofísicos han puesto de manifiesto que dichas mutaciones no producen grandes alteraciones en la estructura y estabilidad del plegamiento α de PrP (Ver **tabla 5**). No obstante, algunas mutaciones patogénicas impactan en el metabolismo celular de PrP y producen alteraciones significativas (123, 336, 446). Esta aparente contradicción apunta a posibles diferencias entre las rutas de plegamiento *in vitro* e *in vivo* y un posible papel de esta última en el proceso de conversión debido a la multitud de elementos implicados en la misma (447-449). De todas las mutaciones de la cadena de PrP, artificiales y patogénicas, sólo las sustituciones M206S y M213S, solas o en combinación, provocan estados conformacionalmente lábiles *in vitro* (450) y por ello constituyen el modelo adecuado para estudiar su efecto *in vivo*.

En este trabajo, se describe el efecto de las mutaciones M206S y M213S sobre el metabolismo de PrP. Mi contribución ha sido la generación y caracterización de todos los mutantes *in vivo*, el diseño y optimización de metodologías de transfección, de asignación de topologías, de cuantificación de viabilidades celulares y de determinación del estado *in vivo* de puentes disulfuro.

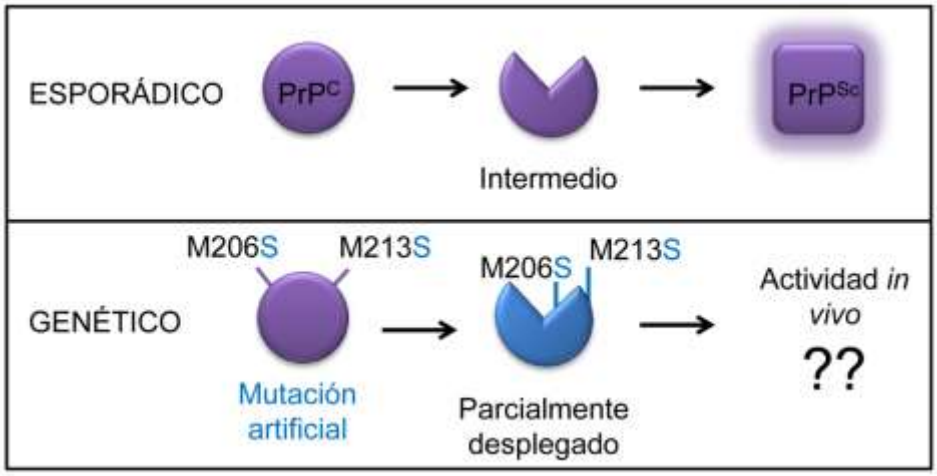

THE JOURNAL OF BIOLOGICAL CHEMISTRY VOL. 287, NO. 44, pp. 36693–36701, October 26, 2012

Failure of Prion Protein Oxidative Folding Guides the Formation of Toxic Transmembrane Forms*

Received for publication, July 6, 2012, and in revised form, September 6, 2012 Published, JBC Papers in Press, September 6, 2012, DOI 10.1074/jbc.M112.398776

Silvia Lisa[‡1], Beatriz Domingo[§], Javier Martínez[‡1], Sabine Gilch[¶], Juan F. Llopis[§], Hermann M. Schätzl[¶], and María Gasset[‡2]

From the [‡]Instituto Química-Física "Rocasolano," Consejo Superior de Investigaciones Científicas, Serrano 119, 28006 Madrid, Spain, the [§]Centro Regional de Investigaciones Biomédicas and Facultad de Medicina, Universidad de Castilla-La Mancha, 02006 Albacete, Spain, and the [¶]Departments of Veterinary Sciences and Molecular Biology, University of Wyoming, Laramie, Wyoming 82071

Background: *In vivo* folding could play an essential role in prion neurodegenerations.
Results: Artificial mutants causing labile PrP folds when expressed in cells originate toxic CtmPrP featured by the absence of the intramolecular disulfide bond.
Conclusion: Oxidative folding impairment facilitates the formation of the toxic PrP forms.
Significance: Unveiling the mechanism facilitating the formation of toxic PrP forms is crucial for the understanding and prevention of prion disorders.

The mechanism by which pathogenic mutations in the globular domain of the cellular prion protein (PrP^C) increase the likelihood of misfolding and predispose to diseases is not yet known. Differences in the evidences provided by structural and metabolic studies of these mutants suggest that *in vivo* folding could be playing an essential role in their pathogenesis. To address this role, here we use the single or combined M206S and M213S artificial mutants causing labile folds and express them in cells. We find that these mutants are highly toxic, fold as transmembrane PrP, and lack the intramolecular disulfide bond. When the mutations are placed in a chain with impeded transmembrane PrP formation, toxicity is rescued. These results suggest that oxidative folding impairment, as on aging, can be fundamental for the genesis of intracellular neurotoxic intermediates key in prion neurodegenerations.

Prion disorders are dominant gain-of-function neurodegenerations whose pathogenesis is linked to misfolded forms of the cellular prion protein (PrP^C),[3] including the prion PrP^{Sc} and the neurotoxic CtmPrP (1–4). PrP^{Sc} is an aggregated and protease-resistant β-sheet-enriched conformer of PrP^C, which self-perpetuates by the templating the conversion of cell surface PrP^C (1, 4). In contrast, CtmPrP is an intracellular transmembrane form generated at the ER with neurotoxic properties (1, 5, 6). Despite that CtmPrP formation was associated with features of the ER translocation process several pathogenic mutations in the C-terminal domain such as H187R and E200K enhance its levels, suggesting a yet unexplored *in vivo* interplay between folding and the accumulation and action of this neurotoxic form (6–8).

Since the enunciation of the prion hypothesis, research has focused on the mechanism by which a native PrP^C structure reorganizes and acquires self-propagative features like those of PrP^{Sc} (9–11). The PrP^C native state was assigned to the fold adopted by the chain lacking the signal sequences and containing the disulfide bond and used as reference for testing the effect of pathogenic mutations and its conversion into active prions (10, 12–16). However, the *in vivo* folding of proteins segregating into the secretory route such as PrP is a complex process participated by the ER folding machinery. This machinery coordinates processing (signal sequences removal, addition of covalent modifications, binding of cofactors, etc.), avoids undesired aggregations, and permits the acquisition of correct structure. This global process involves multiple transient protein-protein interactions with the nascent chains that can sense alterations resulting from environmental changes to the presence of mutations (17–19). Any variation in the sequence of events can impact the final product, as for the doses of secretory and transmembrane PrP forms, and its fate (6, 7, 20–33).

Metabolic studies addressing the effect of pathogenic mutations in the C-terminal domain of PrP as disease predisposition factors have reported a wide range of alterations in processing, trafficking, aggregation, accumulation, and toxicity which varied among experimental setups, as the cell line used and the background expression of wild-type (WT) PrP^C (20, 21, 23–26, 28, 29, 31, 33). These aberrancies contrast with structural reports in which the same pathogenic mutations do not impede the correct *in vitro* folding, but variably modify the stability, dynamics, and surface reactivity of the native state (12–16, 34, 35). Indeed, aging factors such as oxidative modifications and

* This work was supported by the Spanish Ministerio de Economía y Competitividad Grant BFU2009-07971 (to M. G.), a Fundación Cien-Fundación Reina Sofía grant (to M. G.), and an Alberta Prions Research Institute grant (to H. M. S.).
[1] Supported by Formación del Personal Investigador Ph.D. grants.
[2] To whom correspondence should be addressed. Tel.: 34917459500 (ext. 1312); Fax: 34915642431; E-mail: mgasset@iqfr.csic.es.
[3] The abbreviations used are: PrP, prion protein, CtmPrP, transmembrane PrP^C; Endo H, endo-β-*N*-acetylglucosaminidase H; ER, endoplasmic reticulum; GPI, glycosylphosphatidylinositol; PIPLC, phosphatidylinositol phospholipase C; PK, proteinase K; PNGase F, peptide:*N*-glycosidase F; PrP^C, cellular PrP; PrP^{Sc}, aggregated and protease-resistant β-sheet-enriched conformer of PrP^C; PrPDS, PrP chain containing the combined M206S and M213S (M205S and M212S in mouse) substitution; PDI, protein disulfide isomerase; βCOP, β-coatomer protein.

TABLE 1
Primers used for mutagenesis

Mutation	Template	Primer (forward, 5′-3′)
M134S	MoPrP	ATGCTGGGGAGCGCCAGTAGCAGGCCCATGATC
M154S	MoPrP	TACTACCGTGAAAACAGTTACCGCTACCCTAAC
M205S	MoPrP	ACCGATGTGAAGATGAGTGAGCGCGTGGTGGAG
M212S	MoPrP	CGCGTGGTGGAGCAGAGTTGCGTCACCCAGTAC
M205S,M212S	MoPrP M205S	CGCGTGGTGGAGCAGAGTTGCGTCACCCAGTAC
M134S	HaPrP HaPrP-YFP	CTGGGGAGTGCCTCCTCTAGACCCATG
M154S	HaPrP HaPrP-YFP	CTACCGTGAAAACTCCAATCGATACCC
M206S	HaPrP HaPrP-YFP	GACATCAAGATATCCGAGCGCGTGG
M213S	HaPrP HaPrP-YFP	GTGGTGGAGCAGTCCTGTACCACCCAG
M206S,M213S	HaPrP M206S HaPrP-YFP-M206S	GTGGTGGAGCAGTCCTGTACCACCCAG
M213L	HaPrP HaPrP-YFP	GTGGTGGAGCAGCTCTGTACCACCCAG
A117V	HaPrP HaPrP-YFP	GCCGGCGCTGCTGTGGCAGGGGCC
C214A	HaPrP HaPrP-YFP	GAGCGCGTGGTGGAGCAGATGGCTACCACCCAGTATCAG
G123P	HaPrP HaPrP-YFP HaPrPDS HaPrP- YFPDS	GCCGTGGTGCCGGGCCTTGGTG

exhaustion of the ER folding machinery which are not considered in structural studies may play fundamental roles in the formation of pathogenic PrP.

Of the different mutations in the globular domain experimentally tested, substitutions of conserved methionines in α-helix 3 (hitherto PrPα3M) provoked the largest α-fold destabilization (36). In particular, singly or combined M206S and M213S replacements in rHaPrP(23–231) yielded extremely labile folds with enhanced aggregation capacity (36). These mutations also mimicked the flexibility distortions impinged by sulfoxidation of such methionines found in the PrP chains in the conversion pathway (12–14, 36–39). Despite these interesting results, the effect of these substitutions had not been addressed in living systems.

Here, we have used various cultured cells expressing PrPα3M mutants to investigate and model the role of *in vivo* folding in the synthesis and accumulation of PrP forms. Unexpectedly, we found that the PrPα3M expression is highly toxic and that such toxicity relates to the exclusive formation of CtmPrP due to impeded disulfide bond formation.

EXPERIMENTAL PROCEDURES

Plasmid Construction and PrP Mutant Preparation—The pcDNA3.1-MoPrP(1–254, 3F4-tagged), pcDNA4.1-HaPrP(1–254) (40, 41), and pHaPrP-YFP (42) were used as templates for the generation of MoPrP M134S, MoPrP M154S, MoPrP M205S, MoPrP M212S, MoPrP M205S,M212S, HaPrP M134S, HaPrP M154S, HaPrP M206S, HaPrP M213S, HaPrP M206S,M213S, HaPrP M213L, HaPrP A117V, HaPrP C214A, HaPrP G123P. and HaPrP G123P,M206S,M213S mutants. Site-directed mutagenesis was carried out using QuikChange protocols with the oligonucleotides summarized in Table 1.

Cell Culture, Transfections, and Viability Assays—The cell lines HpL 3.14 ($PrP^{-/-}$, mouse hypothalamic), GpL ($PrP^{-/-}$ mouse glial), N2a (mouse neuroblastoma), and CHO (Chinese hamster ovary) cells were kept in Opti-MEM containing 10% fetal bovine serum and penicillin/streptomycin (40, 43–45). Transient transfections with the different PrP-coding plasmid, pEGFP-rab9 (positive control for transfection), and pcDNA3.1/pcDNA4.1 (mock control) were performed using FuGENE 6 transfection reagent (Roche Applied Science) according to the manufacturer's instructions. Typically, 24 h after transfection the medium was exchanged and allowed for other 24 h before analysis. For viability assays, cells were harvested using trypsin/EDTA in PBS followed by centrifugation and stained with 0.4% trypan blue for 5 min at room temperature. Total and viable cells were determined using the TC10 automated cell counter (Bio-Rad) using duplicate independent readings of experiments performed in duplicates. Displayed data are the mean ± S.D. of three independent experiments. Statistical analyses were performed using the *t* test, with significance set to $p < 0.05$. For other analysis, cells were harvested by either *in situ* lysis in cold radioimmune precipitation assay buffer (10 mM Tris-HCl, pH 7.5, 100 mM NaCl, 10 mM EDTA, 0.5% Triton X-100, 0.5% deoxycholate) or by detachment with PBS containing 10 mM EDTA.

Immunoblot Analysis—Samples were diluted in Laemmli sample buffer (4% SDS, 20% glycerol, 10% 2-mercaptoethanol, 0.004% bromphenol blue, and 0.125 M Tris-HCl), heated at 95 °C for 5 min, and then resolved by SDS-PAGE (12% gel). Proteins were electrophoretically transferred onto either PVDF or nitrocellulose membranes, and the membranes were blocked for 1 h in 5% (w/v) nonfat dried skimmed milk powder in Tris-buffered saline containing 0.05% Tween 20. After incubation with appropriate primary and horseradish peroxidase (HRP)-conjugated secondary antibodies, signals were revealed using enhanced chemiluminescence (Amersham Biosciences) and visualized using the ChemiDoc detector (Bio-Rad). The primary antibodies were: mouse anti-PrP 3F4(109–112) HaPrP region, 1:20,000; Signet), 6D11 (1:10,000; 90–100 region; Covance); anti-β-actin (1:5000; Sigma-Aldrich), anti-CHOP (1:1000; Santa Cruz Biotechnology), anti-GRP78 (1:1000; Santa Cruz

Biotechnology), anti-protein disulfide isomerase (1:1000; Abcam), and anti-fluorescein (1:10,000; Invitrogen). The secondary antibodies were: goat anti-mouse HRP (1:5000; Sigma-Aldrich), goat anti-rabbit HRP (1:5000; Chemicon). Quantitative densitometry of protein bands was performed using Quantity One software (Bio-Rad).

Expression Analysis, Detergent Solubility Assay, and Proteinase K Treatments—Cell lysates were cleared by a centrifugation of 5 min at 500 × *g*, supplemented with 0.5 mM Pefabloc, and then precipitated with 5 volumes of methanol at −20 °C. Samples were centrifuged at 10,000 × *g* for 30 min, and the pellets were redissolved in TNE buffer (50 mM Tris-HCl, pH 7.5, 150 mM NaCl, 5 mM EDTA). For expression studies, aliquots of the TNE-resuspended samples were diluted with Laemmli buffer and analyzed by immunoblotting. For solubility assay, the cleared cell lysates were supplemented with sarkosyl to 1% and centrifuged for 1 h at 100,000 × *g*, 4 °C, in a Beckman Optima™ Max centrifuge. Soluble fractions (supernatant) were precipitated with methanol and then together with the insoluble fractions (pellet) were analyzed by immunoblotting. For protease digestions, aliquots of cleared lysates prepared in the absence of Pefabloc were incubated for 30 min at 37 °C with 20 μg/ml proteinase K (PK; Promega); the proteolysis was stopped by addition of 5 mM protease inhibitor PMSF. Samples were precipitated with methanol and analyzed by immunoblotting. For protease protection assays, detached cells were homogenized in 10 mM Tris-HCl, pH 7.4, 0.1 M sodium acetate, 2 mM $MgCl_2$ and centrifuged at 1000 × *g* at 4 °C for 10 min. The supernatants were then centrifuged for 1 h at 100,000 × *g* at 4 °C, and the resulting pellets (microsomes) were resuspended in 50 mM Hepes, pH 7.4, 0.1 M sodium acetate, 2 mM $MgCl_2$, 0.25 M sucrose. Microsome suspensions were split in three equal parts and incubated in the absence and presence of PK (5 μg/ml), both with and without 0.5% Triton X-100, for 30 min at 25 °C. Reactions were stopped by adding 0.5 mM PMSF and analyzed by immunoblotting.

Post-translational Covalent Modification Analysis: Glycosylation, GPI Addition, and Disulfide Bonding—Enzymatic digestions with PNGase F (New England Biolabs), Endo H (New England Biolabs), and phosphatidylinositol phospholipase C (PIPLC) (Sigma-Aldrich) were performed for 1 h at 37 °C on the methanol-precipitated cell lysates, following the manufacturer's instructions. After digestion, reactions were stopped by the addition of Laemmli buffer, and PrP was analyzed by immunoblotting using 3F4 antibody. For analysis of disulfide bonds, cells were lysed in 50 mM Tris-HCl, pH 8, 1% SDS, cleared by a slow speed centrifugation, and then supplemented with or without 200 mM DTT. Both reduced and nonreduced lysates were then incubated with 100 mM Oregon Green 488 iodoacetamide (Invitrogen) for 15 min, diluted with 10 volumes of radioimmune precipitation assay buffer, and incubated with protein A-Sepharose beads (GE Healthcare) for 60 min at 4 °C. After centrifugation, supernatants were incubated with mAb 3F4 for 10 h at 4 °C. Protein A-Sepharose beads were then added, and after a 90-min incubation at 4 °C, the protein-antibody complexes bound to protein A-agarose were sedimented by centrifugation. Pellets were washed with a buffer containing 150 mM NaCl, 10 mM Tris-HCl, pH 7.8, 0.1% sarkosyl, and 0.1% Pefabloc, and bound proteins were eluted by boiling in SDS-sample buffer. Precipitates were analyzed by SDS-PAGE and developed with goat anti-fluorescein/Oregon Green Ab (Invitrogen).

Fluorescence Microscopy Imaging—Cells were seeded on to poly-L-lysine-coated glass coverslips, transfected with the plasmids coding for HaPrP WT, HaPrP-YFP WT, and their mutants, and grown for 36 h to 60% confluence. For immunofluorescence analysis, cells were fixed with 4% paraformaldehyde in PBS containing 5% sucrose for 10 min at room temperature and washed three times with PBS. Cells were permeabilized and blocked in PBS containing 0.5% saponin, 0.1% Triton X-100, and 2% bovine serum albumin for 10 min at room temperature. Cells were incubated with anti-PrP mAb 3F4 (1:600) and with anti-β coatomer protein (1:600) for 1 h at room temperature. After washing with blocking buffer, samples were incubated with Alexa Fluor 488-conjugated goat anti-mouse IgG (1:800), Alexa Fluor 647-conjugated anti-rabbit IgG (1:800), and Hoechst 33342 (10 μg/ml) in for 30 min at room temperature. Once washed, the coverslips were mounted on glass slides with ProLong Gold antifade reagent (Invitrogen). Images were captured with a confocal microscope (Leica TCS-SP-AOBS-UV) as described (40). For living cell analysis, imaging was performed as described previously (42).

RESULTS

PrPα3M Mutants Are Highly Toxic in Cultured Cells—To determine the role of α3M mutations on PrP folding in living cells we generated Met to Ser substitutions in the α-helix 3 both in HaPrP (M206S, M213S, DS) and MoPrP (M205S, M212S, DS) (Fig. 1*A*). We also generated control substitutions at other conserved methionines (M134S and M154S), a substitution that preserves both the conformation and stability of the recombinant chain (M213L) and a pathogenic mutant known to alter *in vivo* PrP folding (A117V) (2, 3, 6, 36) (Fig. 1*A*). We expressed all of these constructs in $PrP^{-/-}$ cells (HpL and GpL) to avoid interference from endogenous WT PrP chains (Fig. 1*A*). Transient expression of HaPrP constructs revealed specific cytotoxicity of PrPα3M mutants in both cell types (Fig. 1*B*). HaPrP WT and the control M134S, M154S, and M213L mutations all had no effect on cell viability, whereas HaPrPα3M mutants caused approximately 40% cell death in both HpL and GpL cells upon transient transfection (Fig. 1*B*). Interestingly, HaPrP A117V also induced 30% cell death, suggesting possible similarities in the pathogenic process (Fig. 1*B*). PrPα3M mutations generated as HaPrP-YFP fusions (42) showed the same cell loss as those on HaPrP background, arguing that YFP does not interfere in the lethal process (Fig. 1*B*). Next, we tested the toxicity of PrPα3M mutants using MoPrP sequence. As with the HaPrP constructs, we found that the three PrPα3M mutants induced approximately 40–50% cell death (Fig. 1*C*). Thus, the scaffold sequence had no effect on PrPα3M toxicity, further supporting the crucial role of these conserved residues on the *in vivo* PrP folding. Importantly, toxicity increases with the dose of PrPα3M expression, as shown for variation of cell death relative to the normalized HaPrPDS signal as a function of the time after transfection (Fig. 1*D*).

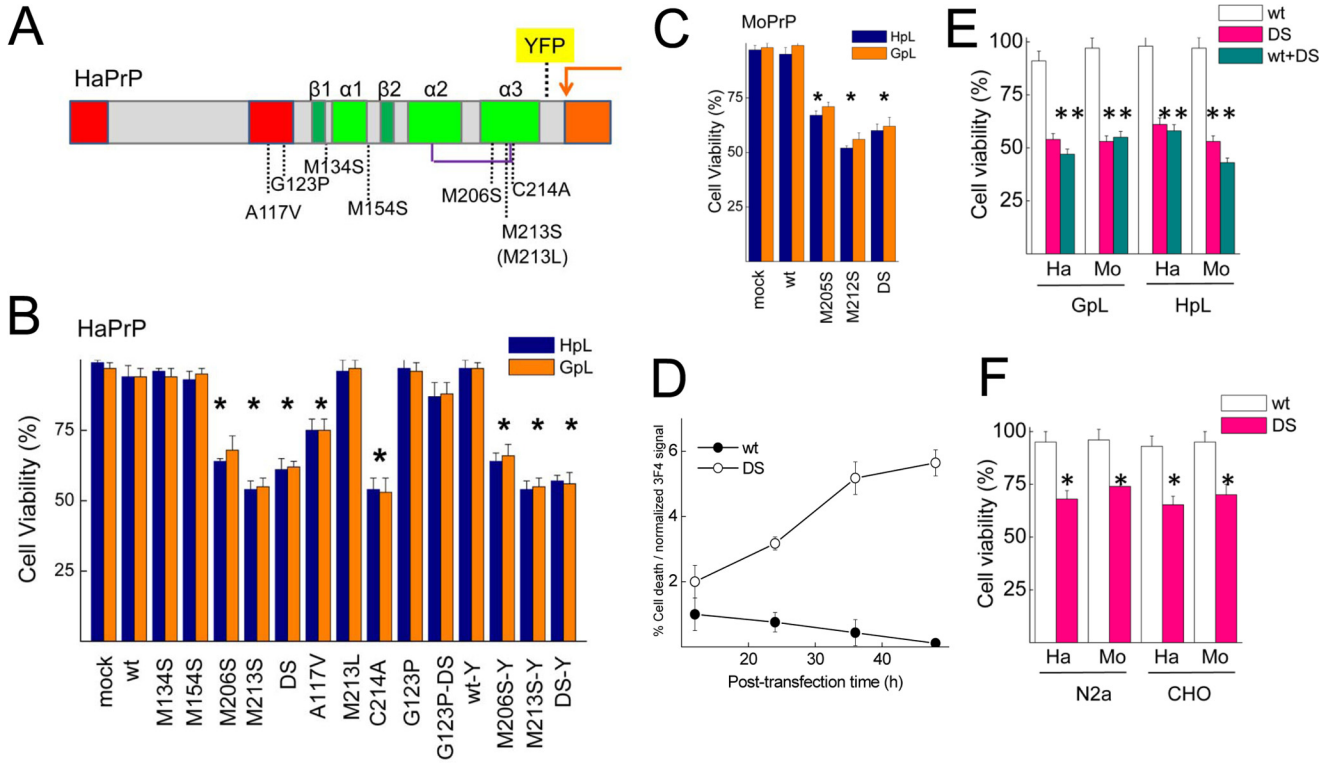

FIGURE 1. **The expression of the PrP α-fold impairing α3M mutations is highly toxic for mammalian PrP$^{-/-}$ cells.** *A*, schematic represents PrP mutants used in this study. *Red rectangles*, translocation-controlling regions (N-terminal signal sequence and hydrophobic region); *green rectangles*, secondary structure elements of the globular fold (α, α-helix; β, β-strand); *purple line*, disulfide bond; *orange arrow*, site of GPI anchor addition; *yellow rectangle*, insertion site of YFP for fluorescence fusions. *B*, transient expression of HaPrP WT and of its mutants on HpL (*blue*) and GpL (*orange*) impacts viability. *C*, transient expression of WT and mutant MoPrP affects HpL (*blue*) and GpL (*orange*) viability. *D*, variation of cell death was normalized to 3F4 signal with the post-transfection time for HaPrP WT and HaPrPDS. Percentage of cell death was obtained from viability assays, and 3F4 signal was obtained from immunoblots after normalization to the signal of β-actin band. *E*, co-expression of WT PrP and PrPα3M mutants preserved mutant toxicity. *F*, PrPα3M mutants retain the toxicity in both N2a and nonneural CHO cells. Displayed data are the mean ± S.D. (*error bars*) of at least three independent experiments performed in duplicate. Statistical analyses were performed using the *t* test, with significance set to $p < 0.05$.

Having seen that PrPα3M mutants are highly toxic to culture cells not expressing an endogenous PrP, we wanted to study whether expression of WT PrP affects this phenotype. We co-expressed HaPrP and MoPrP bearing the double mutant (PrPDS) with the corresponding WT PrP in a 1:1 ratio in GpL and HpL cells to determine whether this could ameliorate the toxic effect. Fig. 1*E* shows that PrP WT had no or little effect on PrPDS toxicity in this setup. Next, we transiently expressed both HaPrPDS and MoPrPDS in N2a cells, which express MoPrP^{C}, and in nonneuronal CHO cells, which lack detectable PrP (Fig. 1*F*). Again, there was substantial toxicity in tested cells, which was apparently independent of endogenous WT PrP expression and cell type used. Altogether, these results indicate that PrPα3M mutants exert a very high level of cell toxicity upon transient expression which is not influenced by cell type and co-expression of WT PrP.

PrPα3M Mutants Are Processed Abnormally during Biogenesis—After determining that PrPα3M mutants are highly toxic, we set out to characterize the molecular basis of such toxicity. Expression of WT and the control M134S and M154S mutants produced the classical 24–38-kDa banding pattern for both HaPrP and MoPrP constructs and in both PrP$^{-/-}$ cell lines (Fig. 2*A*). However, expression of PrPα3M mutants yielded single bands of approximately 30 kDa (Fig. 2*A*). This feature has been described previously for PrP pathogenic mutants with immature glycosylation (6, 20, 22, 25, 30, 32, 46, 47). This stimulated us to study the glycosylation of PrPα3M mutants, focusing on HaPrPDS as a model. Indeed, whereas WT HaPrP was sensitive to PNGase F and resistant to Endo H digestions, the glycan attached to HaPrPDS was sensitive to both PNGase F and Endo H digestion (Fig. 2*B*). These results indicate an immature glycosylation of the PrPDS mutant. To test for the presence of a GPI anchor, the PNGase F-deglycosylated products were further digested with PIPLC. The upward shift in the bands of WT HaPrP and HaPrPDS after PIPLC treatment indicates the removal of the hydrophobic moiety and supported the presence of the GPI anchor in both chains (Fig. 2*B*). Also, the size similarity of WT HaPrP and HaPrPDS bands upon combined PNGase F and PIPLC digestion indicates that in both PrP chains the N-terminal signal sequence has been removed. Taken together, the post-translational processing of HaPrPDS, representative here of PrP3αM mutants, indicates removal of the N-terminal signal sequence, immature glycosylation, and the presence of a GPI anchor.

PrPα3M Mutants Accumulate as CtmPrP—The above biochemical features were reminiscent of previously described *de novo* formation of either PrP^{Sc}-like or CtmPrP forms (6, 40, 41, 48). To assess the conformation adopted by PrPα3M mutants, we analyzed the detergent solubility and the resistance to proteases of HaPrPDS (1, 6). Fig. 2*C* shows that WT HaPrP proved completely soluble in detergents whereas HaPrPDS partitioned almost entirely into the insoluble fraction. Nonetheless, both

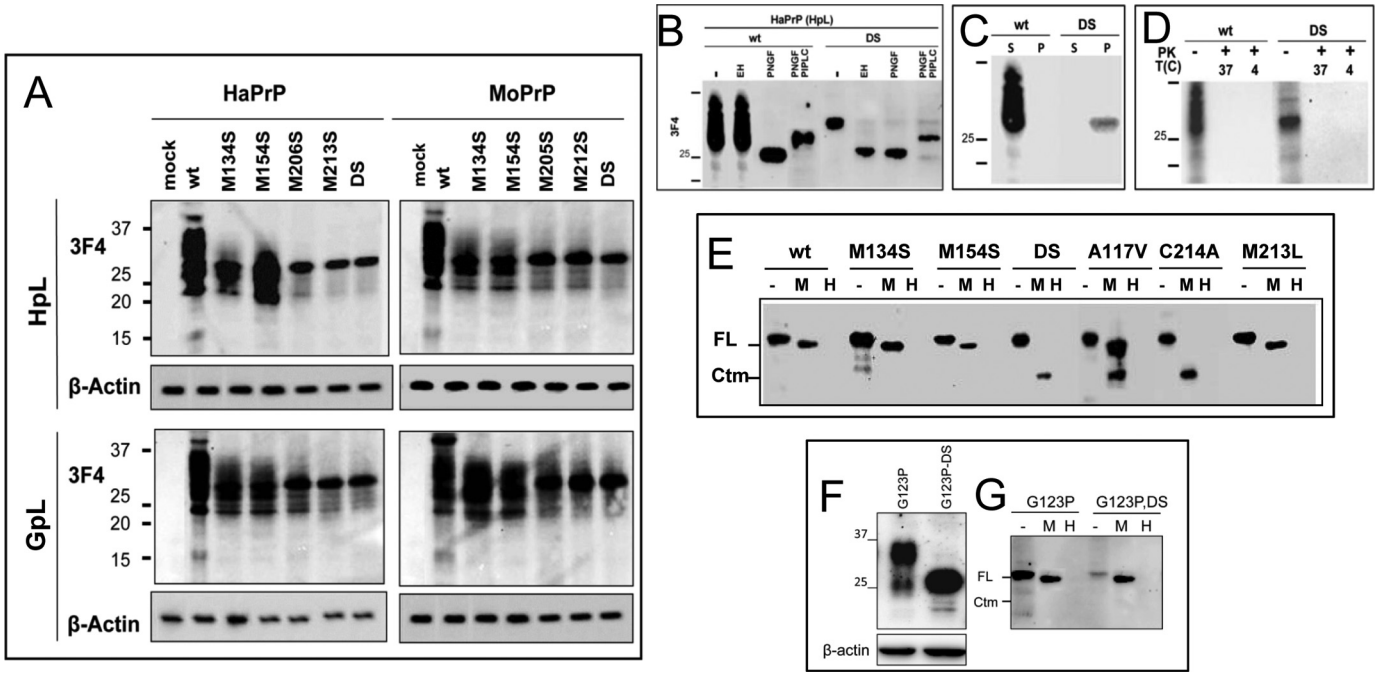

FIGURE 2. **Molecular features of PrP mutants in mammalian cells.** *A*, transient expression of HaPrP and MoPrP WT and mutants in HpL and GpL cells. The signal corresponding to β-actin is displayed at the *bottom* of each membrane. *B*, PNGase F, Endo H, and PIPLC digestions of HaPrP WT and HaPrPDS expressed in HpL cells. *C*, differences in the detergent solubility of HpL-expressed HaPrP WT and HaPrPDS determined by partitioning between the soluble and pellet fraction of an ultracentrifugation. *D*, protease sensitivity at 37 and 4 °C of HpL-expressed HaPrP WT and HaPrPDS probed by PK digestion. *E*, PK protection of PrP chains in intact (*M*) and lysed (*H*) microsomes isolated from HpL-expressed HaPrP WT, M134S, M154S, DS, C214A, M213L, and A117V, this last taken as positive control for CtmPrP topology. *F*, transient expression of HaPrPG123P and HaPrPG123PDS in HpL cells. The signal corresponding to β-actin is displayed at the *bottom*. *G*, PK protection of PrP chains in intact (*M*) and lysed (*H*) microsomes isolated from HpL transiently expressing HaPrPG123P and HaPrPG123PDS mutants. PrP immunoblotting was performed with mAb 3F4.

proteins were fully digested by PK under harsh (37 °C) and mild (4 °C) digestion conditions, supporting the absence of prototypic PrP^{Sc} characteristics (Fig. 2*D*).

Once discarded the generation of *bona fide* and PK-resistant PrP^{Sc}, we next analyzed the membrane topology of HaPrPα3M, using HaPrPA117V as control for acquiring CtmPrP topology. For this, we purified microsomes from transfected cells to carry out protease protection assays (Fig. 2*E*). HaPrP WT and its M134S, M154S, and M213L mutants were fully protected under mild conditions (PK digestion without detergent) but completely digested in the presence of detergents, supporting the production of the secretory PrP form. In contrast, under mild digestion conditions HaPrP A117V revealed a protease-protected fragment of approximately 21 kDa, corresponding to the ER-localized C-terminal domain characteristic of CtmPrP (7). Digestion of microsomes from cells expressing HaPrPM206S, HaPrP213S, and HaPrPDS yielded the same 21-kDa fragment as identified for HaPrP A117V. In summary, these results indicate that HaPrPα3M folding results in acquisition of a transmembrane CtmPrP topology.

PrPα3M Mutants Are Retained Intracellularly and Exert ER Stress—Because CtmPrP is mainly an intracellular conformer and has been proposed to elicit an ER stress response, we then tested these properties for HaPrPα3M (6, 8, 49). First, we performed indirect fluorescence microscopy studies to address the subcellular location upon transient transfection into HpL cells. As expected, WT HaPrP and its control M134S and M213L mutants were located along the secretory pathway in route to the plasma membrane (Fig. 3, *A–C*). In contrast, HaPrPα3M mutants were found mostly intracellularly, with a punctuate distribution overlapping partially the Golgi (co-staining with the marker βCOP) and ER (co-staining with the marker PDI; data not shown) membranes (Fig. 3, *E–G*). We also analyzed the distribution of the corresponding YFP fusion constructs. Again, WT HaPrP-YFP, HaPrPM134S-YFP, and HaPrPM213L-YFP were found mainly at the plasma membrane with some Golgi staining indicating a normal behavior (Fig. 3, *J–L*). However, the HaPrP HaPrPα3M-YFP fusions, which retained toxicity (see Fig. 1*B*), accumulated intracellularly displaying an excess of intracellular vesicle structures containing PrP which most likely represent ER compartments (Fig. 3, *N–P*). Thus, the abnormal intracellular distribution of PrPα3M mutants observed here by microscopy is in line with our biochemical analysis showing immature glycosylation, tendency to aggregate, and CtmPrP topology.

To test whether this intracellular PrP distribution was associated with ER stress, we tested the levels of key components of the unfolded protein response pathway following the expression of HaPrP mutants. Expression of WT HaPrP and of its control M134S, M154S, and M213L mutants did not affect the levels of ER chaperone BiP/Grp78 and of the apoptosis inducer transcription factor CHOP (GADD153) (Fig. 4). However, expression of all PrPα3M mutants along with the A117V construct resulted in a significant increase of BiP/Grp78 and CHOP levels (Fig. 4). We also analyzed the levels of PDI, an ER chaperone that catalyzes thiol-disulfide exchanges and assists in disulfide bridge formation during the folding of secretory proteins. We found that the levels of PDI did not differ signifi-

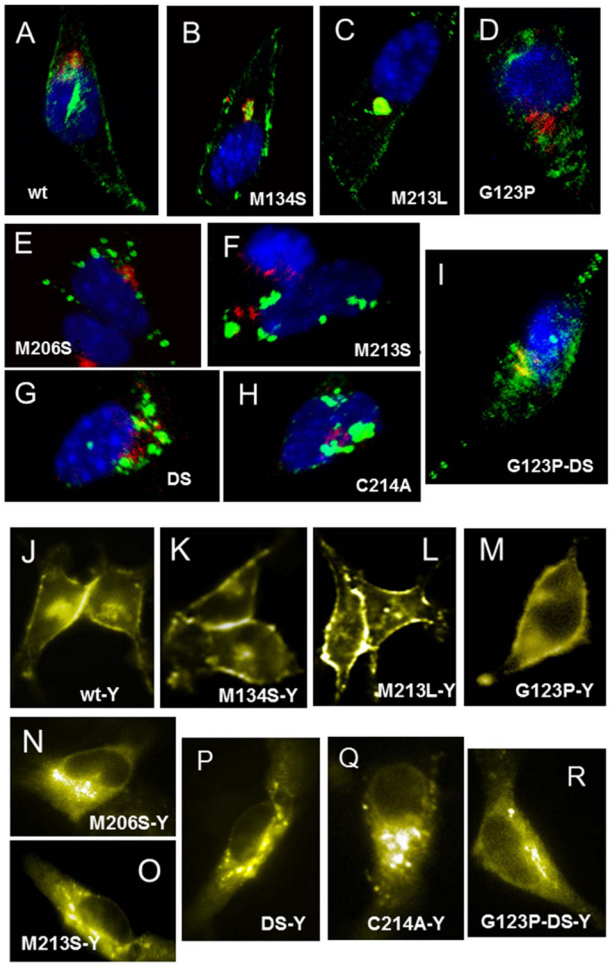

FIGURE 3. **PrPα3M accumulates intracellularly.** Subcellular distribution of WT HaPrP (*A* and *J*) and of its M134S (*B* and *K*), M213L (*C* and *L*), G123P (*D* and *M*), M206S (*E* and *N*), M213S (*F* and *O*), DS (*G* and *P*), C214A (*H* and *Q*), and G123PDS (*I* and *R*) mutants expressed in HpL cells is shown. *Panels A–I* correspond to immunofluorescence detection in fixed cells. PrP (*green*) was stained using 3F4 mAb, nuclei (*blue*) were stained with Hoescht and Golgi (*red*) with anti-βCOP antibody. *Panels J–R* display the fluorescence of the corresponding YFP fusion PrPs in living cells. Mutants M134S, M154S, and M213L were used as negative controls; G123P and A117V as negative and positive controls for CtmPrP, and C214A as control for forms lacking intramolecular disulfide bond.

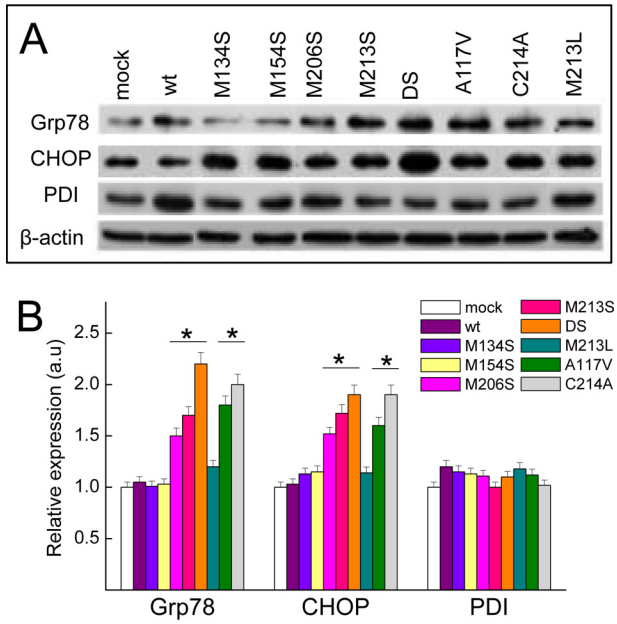

FIGURE 4. **PrPα3M elicit an ER stress response.** *A*, immunoblot analysis of Grp78, CHOP, and PDI ER stress markers associated with the expression of HaPrP mutants. β-Actin signal was used as control for quantification. *B*, relative quantification of Grp78, CHOP, and PDI levels in HpL cells after 48 h of transfection with WT HaPrP and its M134S, M154S, M206S, M213S, DS, M213L, A117V, and C214A mutants. Mutants M134S, M154S, and M213L were used as negative controls; A117V as control for CtmPrP and C214A as control for forms lacking intramolecular disulfide bond.

cantly between WT HaPrP and all of the mutants tested (Fig. 4). Taken together these results show the selective activation of the ER stress response upon accumulation of CtmPrP conformers.

PrPα3M Mutants Lack the Conventional Intramolecular Disulfide Bond—A similar toxicity as observed here for the PrPα3M mutants has been described previously for the MoPrPC213A mutant and ascribed to a failure of the oxidative folding (30, 50). Indeed, this mutant lacks the intramolecular disulfide bond which is a key determinant for the stability of the α2–α3 subdomain both *in vivo* and *in vitro* (22, 30, 32, 51, 52).

To understand better the similarities between the mutant lacking the disulfide bond and the PrPα3M mutants here, we generated the HaPrPC214A mutant, analyzed its toxicity, and tested whether it accumulates as CtmPrP. Fig. 2*A* shows that expression HaPrPC214A is as cytotoxic as that of HaPrPα3M mutants, in agreement with previous observations (30). On the other hand, Fig. 2*E* shows that microsomes of cells expressing HaPrPC214A behaved in the protein protection assay as microsomes from PrPα3M and A117V mutants. These data support that the high toxicity of all these mutants is related to the adoption of CtmPrP topologies.

Then, we analyzed the state of the intramolecular disulfide bond for the PrPα3M mutants using the differential reactivity of free and oxidized thiol groups with Oregon Green-iodoacetamide (Fig. 5*A*). Lysates of transfected cells which we first denatured in the absence and presence of DTT were then treated with Oregon Green-iodoacetamide for the irreversible labeling of free thiol groups. Next, PrP was immunoprecipitated with mAb 3F4 and immunoblotted with anti-Oregon Green/fluorescein antibody to detect only the fraction with free thiols. This assay clearly showed that WT HaPrP and its M134S, M154S, and M213L mutants formed stable disulfide bonds and did not interact with Oregon Green-iodoacetamide in the absence of DTT (Fig. 5). In contrast, the PrPα3M, A117V, and C214A mutants were labeled with Oregon Green-iodoacetamide in the absence of DTT (Fig. 5*B*). Thus, these data suggest that a key structural feature of toxic mutants forming CtmPrP could be the presence of free thiols. To confirm this observation, we studied the effect of the DS mutation on HaPrPG123P, a mutant with described impaired capacity to generate transmembrane forms (6, 20). HaPrPG123PDS shared with HaPrPDS the expression as a single band, but behaved as HaPrPG123P in topology assay (Figs. 2, *F* and *G*, 3, and 4). Importantly, HaPrPG123PDS expression produced cell viability values similar to those of WT HaPrP and HaPrPG123P. Taken together, these data support a direct relation between the lack of intramolecular disulfide bond and the formation of toxic CtmPrP.

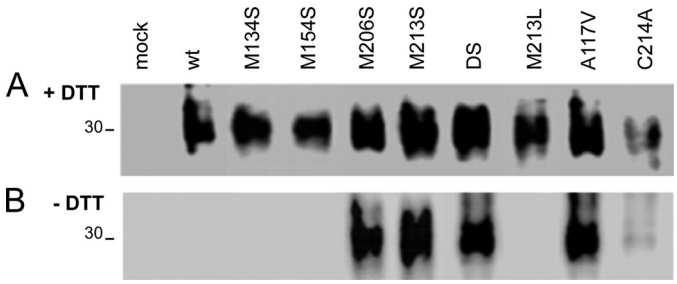

FIGURE 5. **Detection of free thiols in HaPrPα3M and other mutants forming CtmPrP.** Oregon Green-iodoacetamide labeling of PrP in cell lysates pretreated in the (*A*) presence and (*B*) absence of DTT shown by mAb 3F4 capture and anti-Oregon Green development. DTT pretreatment permits labeling of all PrP chains (both disulfide-bonded and -free species), whereas labeling in the absence of DTT selects PrP chains containing thiol-free groups. Mutants M134S, M154S, and M213L were used as negative controls; A117V as control for CtmPrP and C214A as control for forms lacking intramolecular disulfide bond.

DISCUSSION

The efficient production of secreted PrP^C starts with the co-translational translocation to the ER followed by a series of concerted processing including the cleavage of the N-terminal signal sequence, the addition of glycan chains at two facultative sites, the formation of an intramolecular disulfide bond, and a transamidation at the C terminus to add the GPI moiety (1). Of these post-translational modifications, glycosylation and disulfide bond formation depend on the cellular redox state (22, 27). Impairing the ER oxidative environment or mutating the cysteines yields intracellular, diglycosylated PrP chains lacking the disulfide bond, which resembles the PrPα3M mutants described here (22, 27, 30, 32). In this work we demonstrated the interplay between oxidative folding and the formation of the toxic CtmPrP. Introduction of polar substitutions at the α3 methionines, singly or combined, precluded the formation of the intramolecular disulfide bond and dictated the stabilization of highly toxic CtmPrP topologies that killed cells. Importantly, the absence of the disulfide bond in CtmPrP and its escape from the quality control checkpoints support the impairment of the oxidative folding as key pathogenic event for the of toxic PrP forms during normal aging.

CtmPrP has been traditionally viewed as a transmembrane form whose translocation is governed by the hydrophobic region, resulting in a cytosolic N-terminal domain containing the signal sequence (2, 3, 49). However, recent experiments in cell cultures showed that CtmPrP lacked the N-terminal signal sequence, supporting a model of transbilayer post-translocation slippage as observed with recombinant PrP lacking disulfide bond and lipid vesicles (6, 53, 54). Conditions favoring the slippage by trapping the hydrophobic region at the translocon as in A117V may either kinetically delay or impose a distance constraint impeding the formation of the disulfide bond. Also, mutations that may hinder oxidoreductase recognition such as α3M and Y216A may favor the insertion of the N-terminal domain as shown with recombinant chains lacking a disulfide bond (30, 53, 54).

Our results also suggest that conditions preventing PrP oxidative folding may favor the formation of CtmPrP and, consequently, promote its deleterious effects. Indeed, both maintenance of the levels and activity of ER oxidoreductases such as Grp58 and PdIa protect against the toxicity of misfolded PrP forms (55, 56). On aging, both levels and activity of ER chaperones cause a decline of oxidative folding (57). Because PrP3αM mutants were tailored to mimic the effects of Met sulfoxidation, conditions favoring such modification on nascent chains would also facilitate the formation of CtmPrP. In this line, ER stress exhaustion concurs with an overproduction of reactive oxygen species which are the major oxidants of Met residues, as those exposed in nascent unfolded chains (58). Taken together, both decreased efficiency of the oxidative folding and increased probability of sulfoxidation of Met may then explain the aging-associated accumulation of CtmPrP forms in sporadic and inherited diseases.

The role of disulfide bonds in PrP biology has mainly focused on their contribution to the generation of prions. The analysis of highly pure preparations of PrP27–30, the protease-resistant core of PrP^{Sc}, indicated that all Cys were forming disulfide bonds (2, 59). But those samples lack CtmPrP forms due to the proteinase K digestion step used in the purification. The first evidence indirectly suggesting a pathogenic role for free thiols was provided by deletion mutants (60). Mice expressing PrPΔ177-200 and PrPΔ201–217 that are unable to forms intramolecular disulfide bonds developed signs and lesions characteristic of neuronal storage disorders. In these mice, truncated PrP was detergent-insoluble in detergent, PK-sensitive, and with migration properties resembling those of PrPα3M mutants. Also, Cys mutants used in cellular studies resulted in PrP forms sharing key properties with PrPα3M mutants, but their topology and toxicity were not addressed (22, 27, 30, 32).

The finding that free thiols lead to the formation of CtmPrP has several implications. From the structural point of view, the C-terminal domain has to expand its known conformational repertoire to accommodate the absence of the α2–α3 constraint and a double tether to the membrane (51, 52, 61). Also, the fibrillation of CtmPrP may be impeded by the diglycosylation (52, 62). But the detergent insolubility of CtmPrP suggests that it may populate distinct aggregate states, adding more structural complexity. Functionally, the aggregation of PrPα3M mutants suggests that CtmPrP may exert its toxic function through an oligomeric thiol trap. Such traps have been described in the regulation of IgM and adiponectin secretions (63–69). Importantly, given the validation of the PrP chains by the ER quality control systems the assembly of such oligomeric traps must take place upon delivery to a different environment (20). Whether other components participate in their assembly and/or stabilization and whether these factors display different affinities for the WT or mutant chains remains to be elucidated (6). Additionally, this unknown lipid-bound conformation of thiol-free PrP could indeed function as the seed for the conversion of PrP^C into PrP^{Sc}, even in traces amounts (70, 71). This could provide a mechanistic explanation for the spontaneous generation of pathogenic forms of PrP in sporadic human diseases.

Acknowledgments—We thank Rosa Sánchez for technical assistance and Silvia Zorrilla for advice.

REFERENCES

1. Aguzzi, A., and Calella, A. M. (2009) Prions: protein aggregation and infectious diseases. *Physiol. Rev.* **89,** 1105–1152
2. Hegde, R. S., Mastrianni, J. A., Scott, M. R., DeFea, K. A., Tremblay, P., Torchia, M., DeArmond, S. J., Prusiner, S. B., and Lingappa, V. R. (1998) A transmembrane form of the prion protein in neurodegenerative disease. *Science* **279,** 827–834
3. Hegde, R. S., Tremblay, P., Groth, D., DeArmond, S. J., Prusiner, S. B., and Lingappa, V. R. (1999) Transmissible and genetic prion diseases share a common pathway of neurodegeneration. *Nature* **402,** 822–826
4. Prusiner, S. B. (2001) Shattuck lecture: neurodegenerative diseases and prions. *N. Engl. J. Med.* **344,** 1516–1526
5. Chakrabarti, O., Ashok, A., and Hegde, R. S. (2009) Prion protein biosynthesis and its emerging role in neurodegeneration. *Trends Biochem. Sci.* **34,** 287–295
6. Emerman, A. B., Zhang, Z. R., Chakrabarti, O., and Hegde, R. S. (2010) Compartment-restricted biotinylation reveals novel features of prion protein metabolism *in vivo*. *Mol. Biol. Cell* **21,** 4325–4337
7. Kim, S. J., and Hegde, R. S. (2002) Cotranslational partitioning of nascent prion protein into multiple populations at the translocation channel. *Mol. Biol. Cell* **13,** 3775–3786
8. Wang, X., Shi, Q., Xu, K., Gao, C., Chen, C., Li, X. L., Wang, G. R., Tian, C., Han, J., and Dong, X. P. (2011) Familial CJD-associated PrP mutants within transmembrane region induced Ctm-PrP retention in ER and triggered apoptosis by ER stress in SH-SY5Y cells. *PLoS One* **6,** e14602
9. Gasset, M., Baldwin, M. A., Lloyd, D. H., Gabriel, J. M., Holtzman, D. M., Cohen, F., Fletterick, R., and Prusiner, S. B. (1992) Predicted α-helical regions of the prion protein when synthesized as peptides form amyloid. *Proc. Natl. Acad. Sci. U.S.A.* **89,** 10940–10944
10. Makarava, N., Kovacs, G. G., Savtchenko, R., Alexeeva, I., Budka, H., Rohwer, R. G., and Baskakov, I. V. (2011) Genesis of mammalian prions: from noninfectious amyloid fibrils to a transmissible prion disease. *PLoS Pathog.* **7,** e1002419
11. Pan, K. M., Baldwin, M., Nguyen, J., Gasset, M., Serban, A., Groth, D., Mehlhorn, I., Huang, Z., Fletterick, R. J., and Cohen, F. E. (1993) Conversion of α-helices into β-sheets features in the formation of the scrapie prion proteins. *Proc. Natl. Acad. Sci. U.S.A.* **90,** 10962–10966
12. Apetri, A. C., Surewicz, K., and Surewicz, W. K. (2004) The effect of disease-associated mutations on the folding pathway of human prion protein. *J. Biol. Chem.* **279,** 18008–18014
13. Liemann, S., and Glockshuber, R. (1999) Influence of amino acid substitutions related to inherited human prion diseases on the thermodynamic stability of the cellular prion protein. *Biochemistry* **38,** 3258–3267
14. Meli, M., Gasset, M., and Colombo, G. (2011) Dynamic diagnosis of familial prion diseases supports the $\beta2$–$\alpha2$ loop as a universal interference target. *PLoS One* **6,** e19093
15. Riek, R., Hornemann, S., Wider, G., Billeter, M., Glockshuber, R., and Wüthrich, K. (1996) NMR structure of the mouse prion protein domain PrP(121–231). *Nature* **382,** 180–182
16. van der Kamp, M. W., and Daggett, V. (2010) Pathogenic mutations in the hydrophobic core of the human prion protein can promote structural instability and misfolding. *J. Mol. Biol.* **404,** 732–748
17. Anelli, T., and Sitia, R. (2008) Protein quality control in the early secretory pathway. *EMBO J.* **27,** 315–327
18. Hartl, F. U., and Hayer-Hartl, M. (2009) Converging concepts of protein folding *in vitro* and *in vivo*. *Nat. Struct. Mol. Biol.* **16,** 574–581
19. Kim, P. S., and Arvan, P. (1998) Endocrinopathies in the family of endoplasmic reticulum (ER) storage diseases: disorders of protein trafficking and the role of ER molecular chaperones. *Endocr. Rev.* **19,** 173–202
20. Ashok, A., and Hegde, R. S. (2009) Selective processing and metabolism of disease-causing mutant prion proteins. *PLoS Pathog.* **5,** e1000479
21. Campana, V., Sarnataro, D., Fasano, C., Casanova, P., Paladino, S., and Zurzolo, C. (2006) Detergent-resistant membrane domains but not the proteasome are involved in the misfolding of a PrP mutant retained in the endoplasmic reticulum. *J. Cell Sci.* **119,** 433–442
22. Capellari, S., Zaidi, S. I., Urig, C. B., Perry, G., Smith, M. A., and Petersen, R. B. (1999) Prion protein glycosylation is sensitive to redox change. *J. Biol. Chem.* **274,** 34846–34850
23. Drisaldi, B., Stewart, R. S., Adles, C., Stewart, L. R., Quaglio, E., Biasini, E., Fioriti, L., Chiesa, R., and Harris, D. A. (2003) Mutant PrP is delayed in its exit from the endoplasmic reticulum, but neither wild-type nor mutant PrP undergoes retrotranslocation prior to proteasomal degradation. *J. Biol. Chem.* **278,** 21732–21743
24. Ivanova, L., Barmada, S., Kummer, T., and Harris, D. A. (2001) Mutant prion proteins are partially retained in the endoplasmic reticulum. *J. Biol. Chem.* **276,** 42409–42421
25. Kiachopoulos, S., Bracher, A., Winklhofer, K. F., and Tatzelt, J. (2005) Pathogenic mutations located in the hydrophobic core of the prion protein interfere with folding and attachment of the glycosylphosphatidylinositol anchor. *J. Biol. Chem.* **280,** 9320–9329
26. Lorenz, H., Windl, O., and Kretzschmar, H. A. (2002) Cellular phenotyping of secretory and nuclear prion proteins associated with inherited prion diseases. *J. Biol. Chem.* **277,** 8508–8516
27. Orsi, A., and Sitia, R. (2007) Interplays between covalent modifications in the endoplasmic reticulum increase conformational diversity in nascent prion protein. *Prion* **1,** 236–242
28. Rosenmann, H., Talmor, G., Halimi, M., Yanai, A., Gabizon, R., and Meiner, Z. (2001) Prion protein with an E200K mutation displays properties similar to those of the cellular isoform PrP^{C}. *J. Neurochem.* **76,** 1654–1662
29. Schiff, E., Campana, V., Tivodar, S., Lebreton, S., Gousset, K., and Zurzolo, C. (2008) Coexpression of wild-type and mutant prion proteins alters their cellular localization and partitioning into detergent-resistant membranes. *Traffic* **9,** 1101–1115
30. Tabrett, C. A., Harrison, C. F., Schmidt, B., Bellingham, S. A., Hardy, T., Sanejouand, Y. H., Hill, A. F., and Hogg, P. J. (2010) Changing the solvent accessibility of the prion protein disulfide bond markedly influences its trafficking and effect on cell function. *Biochem. J.* **428,** 169–182
31. Vetrugno, V., Malchow, M., Liu, Q., Marziali, G., Battistini, A., and Pocchiari, M. (1999) Expression of wild-type and V210I mutant prion protein in human neuroblastoma cells. *Neurosci. Lett.* **270,** 41–44
32. Yanai, A., Meiner, Z., Gahali, I., Gabizon, R., and Taraboulos, A. (1999) Subcellular trafficking abnormalities of a prion protein with a disrupted disulfide loop. *FEBS Lett.* **460,** 11–16
33. Yin, S., Pham, N., Yu, S., Li, C., Wong, P., Chang, B., Kang, S. C., Biasini, E., Tien, P., Harris, D. A., and Sy, M. S. (2007) Human prion proteins with pathogenic mutations share common conformational changes resulting in enhanced binding to glycosaminoglycans. *Proc. Natl. Acad. Sci. U.S.A.* **104,** 7546–7551
34. Calzolai, L., Lysek, D. A., Guntert, P., von Schroetter, C., Riek, R., Zahn, R., and Wüthrich, K. (2000) NMR structures of three single-residue variants of the human prion protein. *Proc. Natl. Acad. Sci. U.S.A.* **97,** 8340–8345
35. Zahn, R., Liu, A., Lührs, T., Riek, R., von Schroetter, C., López García, F., Billeter, M., Calzolai, L., Wider, G., and Wüthrich, K. (2000) NMR solution structure of the human prion protein. *Proc. Natl. Acad. Sci. U.S.A.* **97,** 145–150
36. Lisa, S., Meli, M., Cabello, G., Gabizon, R., Colombo, G., and Gasset, M. (2010) The structural intolerance of the PrP α-fold for polar substitution of the helix-3 methionines. *Cell. Mol. Life Sci.* **67,** 2825–2838
37. Canello, T., Engelstein, R., Moshel, O., Xanthopoulos, K., Juanes, M. E., Langeveld, J., Sklaviadis, T., Gasset, M., and Gabizon, R. (2008) Methionine sulfoxides on PrPSc: a prion-specific covalent signature. *Biochemistry* **47,** 8866–8873
38. Canello, T., Frid, K., Gabizon, R., Lisa, S., Friedler, A., Moskovitz, J., and Gasset, M. (2010) Oxidation of helix-3 methionines precedes the formation of PK-resistant PrP. *PLoS Pathog.* **6,** e1000977
39. Colombo, G., Meli, M., Morra, G., Gabizon, R., and Gasset, M. (2009) Methionine sulfoxides on prion protein helix-3 switch on the α-fold destabilization required for conversion. *PLoS One* **4,** e4296
40. Juanes, M. E., Elvira, G., García-Grande, A., Calero, M., and Gasset, M. (2009) Biosynthesis of prion protein nucleocytoplasmic isoforms by alternative initiation of translation. *J. Biol. Chem.* **284,** 2787–2794
41. Rane, N. S., Yonkovich, J. L., and Hegde, R. S. (2004) Protection from cytosolic prion protein toxicity by modulation of protein translocation. *EMBO J.* **23,** 4550–4559

42. Domingo, B., Gasset, M., Durán-Prado, M., Castaño, J. P., Serrano, A., Fischer, T., and Llopis, J. (2010) Discrimination between alternate membrane protein topologies in living cells using GFP/YFP tagging and pH exchange. *Cell. Mol. Life Sci.* **67,** 3345–3354
43. Kuwahara, C., Takeuchi, A. M., Nishimura, T., Haraguchi, K., Kubosaki, A., Matsumoto, Y., Saeki, K., Matsumoto, Y., Yokoyama, T., Itohara, S., and Onodera, T. (1999) Prions prevent neuronal cell-line death. *Nature* **400,** 225–226
44. Nishimura, T., Sakudo, A., Xue, G., Ikuta, K., Yukawa, M., Sugiura, K., and Onodera, T. (2008) Establishment of a new glial cell line from hippocampus of prion protein gene-deficient mice. *Biochem. Biophys. Res. Commun.* **377,** 1047–1050
45. Birkett, C. R., Hennion, R. M., Bembridge, D. A., Clarke, M. C., Chree, A., Bruce, M. E., and Bostock, C. J. (2001) Scrapie strains maintain biological phenotypes on propagation in a cell line in culture. *EMBO J.* **20,** 3351–3358
46. Stewart, R. S., Drisaldi, B., and Harris, D. A. (2001) A transmembrane form of the prion protein contains an uncleaved signal peptide and is retained in the endoplasmic reticulum. *Mol. Biol. Cell* **12,** 881–889
47. Stewart, R. S., and Harris, D. A. (2005) A transmembrane form of the prion protein is localized in the Golgi apparatus of neurons. *J. Biol. Chem.* **280,** 15855–15864
48. Resenberger, U. K., Winklhofer, K. F., and Tatzelt, J. (2011) Neuroprotective and neurotoxic signaling by the prion protein. *Top. Curr. Chem.* **305,** 101–119
49. Harris, D. A. (2003) Trafficking, turnover and membrane topology of PrP. *Br. Med. Bull.* **66,** 71–85
50. Riemer, J., Bulleid, N., and Herrmann, J. M. (2009) Disulfide formation in the ER and mitochondria: two solutions to a common process. *Science* **324,** 1284–1287
51. Adrover, M., Pauwels, K., Prigent, S., de Chiara, C., Xu, Z., Chapuis, C., Pastore, A., and Rezaei, H. (2010) Prion fibrillization is mediated by a native structural element that comprises helices H2 and H3. *J. Biol. Chem.* **285,** 21004–21012
52. Lee, S., and Eisenberg, D. (2003) Seeded conversion of recombinant prion protein to a disulfide-bonded oligomer by a reduction-oxidation process. *Nat. Struct. Biol.* **10,** 725–730
53. Shin, J. I., Shin, J. Y., Kim, J. S., Yang, Y. S., Shin, Y. K., and Kweon, D. H. (2008) Deep membrane insertion of prion protein upon reduction of disulfide bond. *Biochem. Biophys. Res. Commun.* **377,** 995–1000
54. Shin, J. Y., Shin, J. I., Kim, J. S., Yang, Y. S., Shin, Y. K., Kim, K. K., Lee, S., and Kweon, D. H. (2009) Disulfide bond as a structural determinant of prion protein membrane insertion. *Mol. Cells* **27,** 673–680
55. Hetz, C., Russelakis-Carneiro, M., Wälchli, S., Carboni, S., Vial-Knecht, E., Maundrell, K., Castilla, J., and Soto, C. (2005) The disulfide isomerase Grp58 is a protective factor against prion neurotoxicity. *J. Neurosci.* **25,** 2793–2802
56. Watts, J. C., Huo, H., Bai, Y., Ehsani, S., Jeon, A. H., Won, A. H., Shi, T., Daude, N., Lau, A., Young, R., Xu, L., Carlson, G. A., Williams, D., Westaway, D., and Schmitt-Ulms, G. (2009) Interactome analyses identify ties of PrP and its mammalian paralogs to oligomannosidic *N*-glycans and endoplasmic reticulum-derived chaperones. *PLoS Pathog.* **5,** e1000608
57. Nuss, J. E., Choksi, K. B., DeFord, J. H., and Papaconstantinou, J. (2008) Decreased enzyme activities of chaperones PDI and BiP in aged mouse livers. *Biochem. Biophys. Res. Commun.* **365,** 355–361
58. Gregersen, N., and Bross, P. (2010) Protein misfolding and cellular stress: an overview. *Methods Mol. Biol.* **648,** 3–23
59. Turk, E., Teplow, D. B., Hood, L. E., and Prusiner, S. B. (1988) Purification and properties of the cellular and scrapie hamster prion proteins. *Eur. J. Biochem.* **176,** 21–30
60. Muramoto, T., DeArmond, S. J., Scott, M., Telling, G. C., Cohen, F. E., and Prusiner, S. B. (1997) Heritable disorder resembling neuronal storage disease in mice expressing prion protein with deletion of an α-helix. *Nat. Med.* **3,** 750–755
61. Maiti, N. R., and Surewicz, W. K. (2001) The role of disulfide bridge in the folding and stability of the recombinant human prion protein. *J. Biol. Chem.* **276,** 2427–2431
62. Bosques, C. J., and Imperiali, B. (2003) The interplay of glycosylation and disulfide formation influences fibrillization in a prion protein fragment. *Proc. Natl. Acad. Sci. U.S.A.* **100,** 7593–7598
63. Anelli, T., Alessio, M., Bachi, A., Bergamelli, L., Bertoli, G., Camerini, S., Mezghrani, A., Ruffato, E., Simmen, T., and Sitia, R. (2003) Thiol-mediated protein retention in the endoplasmic reticulum: the role of ERp44. *EMBO J.* **22,** 5015–5022
64. Anelli, T., Ceppi, S., Bergamelli, L., Cortini, M., Masciarelli, S., Valetti, C., and Sitia, R. (2007) Sequential steps and checkpoints in the early exocytic compartment during secretory IgM biogenesis. *EMBO J.* **26,** 4177–4188
65. Fra, A. M., Fagioli, C., Finazzi, D., Sitia, R., and Alberini, C. M. (1993) Quality control of ER synthesized proteins: an exposed thiol group as a three-way switch mediating assembly, retention and degradation. *EMBO J.* **12,** 4755–4761
66. Guenzi, S., Fra, A. M., Sparvoli, A., Bet, P., Rocco, M., and Sitia, R. (1994) The efficiency of cysteine-mediated intracellular retention determines the differential fate of secretory IgA and IgM in B and plasma cells. *Eur. J. Immunol.* **24,** 2477–2482
67. Reddy, M. M., and Bell, C. L. (1996) Distinct cellular mechanisms of cholinergic and β-adrenergic sweat secretion. *Am. J. Physiol.* **271,** C486–494
68. Sitia, R., Neuberger, M., Alberini, C., Bet, P., Fra, A., Valetti, C., Williams, G., and Milstein, C. (1990) Developmental regulation of IgM secretion: the role of the carboxy-terminal cysteine. *Cell* **60,** 781–790
69. Wang, Y., Lam, K. S., Yau, M. H., and Xu, A. (2008) Post-translational modifications of adiponectin: mechanisms and functional implications. *Biochem. J.* **409,** 623–633
70. Lucassen, R., Nishina, K., and Supattapone, S. (2003) *In vitro* amplification of protease-resistant prion protein requires free sulfhydryl groups. *Biochemistry* **42,** 4127–4135
71. Wang, F., Wang, X., Yuan, C. G., and Ma, J. (2010) Generating a prion with bacterially expressed recombinant prion protein. *Science* **327,** 1132–1135

Discusión General

En ciertos momentos, la única forma de tener razón es perdiéndola

(José Bergamín)

Las prionopatías son el conjunto de enfermedades resultantes de las alteraciones en el metabolismo de PrP^{C} (116-123). Estas alteraciones se manifiestan por la aparición y acumulación sostenida de confórmeros de PrP^{C}, entre los que se encuentran las formas propagativas tipo PrP^{Sc} y las formas citotóxicas de tipo ^{Ctm}PrP (118, 119, 273, 331, 332, 415, 416). Dado que en las prionopatías hereditarias, en las cuales existe un condicionamiento genético, la patología se produce en paralelo al proceso de envejecimiento, conocer los mecanismos que conducen a la formación de las conformaciones tóxicas permitiría elaborar estrategias preventivas que cronificasen situaciones pre-asintomáticas. En esta memoria se describen los efectos de la oxidación de metioninas, de las mutaciones metabólicas MxSeM y de la eficiencia del plegamiento oxidativo en el proceso de formación de confórmeros patológicos de PrP y, por ello, de su consideración como dianas de intervención terapeútica.

Casi desde el enunciado de la hipótesis de sólo proteína se ha asumido dogmáticamente que la única diferencia existente entre PrP^{C} y PrP^{Sc} era estructural (198, 207, 286, 421). Sin embargo, años más tarde gracias al estudio de la reactividad de un anticuerpo se demostró la presencia de una modificación covalente en la población de PrP^{Sc} (415, 416, 423). El hallazgo de MetO en la región de la α3 como firma covalente del estado patógeno y de sus efectos desestabilizantes sobre el plegamiento α, permitió postular el protagonismo de interruptores covalentes en la conversión de PrP^{C} en PrP^{Sc}, bien como causantes del cambio o como consecuencia de la transformación. Este tipo de proceso basado en interruptores covalentes se ha descrito para otras proteínas que participan en demencias neurodegenerativas. Por ejemplo, la forma de Tau que aparece formando los agregados patógenos es un estado hiperfosforilado inactivo (451-453). No obstante, la sulfoxidación de Met tiene dos características diferenciales a resaltar. En primer lugar es una reacción química, con una especificidad de secuencia vinculada al plegamiento (la eficacia de modificación es mayor cuanto mayor es la exposición al solvente). Por otro, la reacción de oxidación es reversible *in vivo* gracias al complejo sistema metionina sulfóxido reductasas, cuya función decae con el envejecimiento (454, 455).

Con el fín de determinar si la presencia de sulfóxidos en PrP^{Sc} es la causa o la consecuencia de su formación, el primer objetivos de esta memoria se centró en la producción de reactivos y métodos dirigidos a determinar en qué momento de la conversión de PrP^{C} en PrP^{Sc} aparece la modificación. El análisis diferencial de formas celulares y tisulares de PrP^{C} en PrP^{Sc} puso de manifiesto que la sulfoxidación de las Met de la hélice α3 precede a la adquisición de resistencia a proteasas y concurre con la adquisición de características de agregación. Esto es, en un esquema temporal del proceso de conversión la sulfoxidación tendría lugar en los estados iniciales. En este sentido, la conversión de PrP^{C} en PrP^{Sc} se considera un cambio conformacional complejo y en múltiples etapas, que se inicia con una desestabilización del estado nativo, que evoluciona a la adquisición de propiedades de autoasociación y a la manifestación de las mismas en forma de autoensamblaje. En este esquema, los estudios teóricos de dinámica molecular y los estudios biofísicos basados en mutaciones MxS indican que la sulfoxidación de Met de la hélice α3 es incompatible con el estado nativo. Es más, el incremento en la flexibilidad de la cadena, la transmisión del efecto a largo alcance y la labilidad de la estructura terciaria sugieren que esta modificación podría estar separando los dos subdominios que constituyen el núcleo globular y de esta forma, favoreciendo la aparición de propiedades pro-agregantes (393, 450, 456-458). Al igual que en

las formas naturales, en las que la sulfoxidación lleva pareja la agregación, los modelos MxS adoptan estados prefibrilares en condiciones fisiológicas.

Dado el papel de los residuos de Met y sus modificaciones en la génesis de estados proagregantes y su abundancia en la cadena de PrP, el siguiente paso a estudiar fue el efecto de su sustitución por SeMet sobre la formación de confórmeros patógenos. Para ello se eligieron dos secuencias proamiloides conteniendo una (Aβ40) y varias (PrP 106-140) y se sustituyeron en síntesis sus Met por SeMet, sustitución que altera el tamaño de la cadena lateral, la hidrofobicidad y las propiedades redox de la cadena lateral. (431-436),(434, 459, 460). Los estudios de fibrilación y de toxicidad revelaron que esta sustitución regula el proceso de ensamblaje, determinando desde su permisividad hasta la forma de los agregados. Los cambios observados sugieren que esta mutación metabólica, que depende de la dieta, podría desempeñar un papel regulador en las amiloidopatías.

Por otra parte, si bien la información necesaria para la generación de confórmeros patógenos está contenida en la secuencia de la cadena polipeptídica, los estudios realizados con modelos de PrP conteniendo mutaciones patógenas han demostrado diferencias entre aproximaciones *in vitro* e *in vivo*, sugiriendo la importancia de la ruta de plegamiento *in vivo*. A nivel celular, el proceso de plegamiento de las proteínas es más complejo, ya que depende de una maquinaria y está coordinado con el procesamiento post-traduccional (447-449). De hecho, in vivo la biogénesis de PrP comienza en la etapa de translocación co-traduccional al RE (118). Si la cadena polipeptídica es completamente translocada al lumen del RE la secuencia señal del extremos N-terminal es escindida, se le adicionan cadenas de glicanos que adquirirán su forma madura en el AG, se formara el puente disulfuro y finalmente, mediante una reacción de transamidación extremo más distal del dominio C-terminal se escindirá y será reemplazado por un GPI (181). De estas modificaciones, la glicosilación y la formación del puente disulfuro dependen de las condiciones del entorno (461, 462). Por el contrario, los estudios in vitro hacen uso de una cadena carente de las secuencias N- y C- terminales y se induce la formación del puente disulfuro mediante oxidación química. El empleo de las cadenas conteniendo M213S, que mimetizan el efecto de las MetO en α3 de PrP y producen plegamientos lábiles, resulta en formas con una citoxicidad sin precedentes debido a su estabilización como agregados intracelulares. El uso de ensayos de topología y de marcaje de tioles libres, demostró que dichas formas eran ^{Ctm}PrP y que resultaban de los impedimentos de la formación del puente disulfuro. La función del puente disulfuro en PrP se ha centrado principalmente en el papel que cumple en la generación de priones. Hay evidencias indirectas de que la imposibilidad de formar el puente disulfuro provoca el desarrollo de lesiones en ratones transgénicos (463). De hecho, en cultivo celular, los mutantes en los que se ve impedido la formación del puente disulfuro comparten algunas de las propiedades de los mutantes de α3 (461, 462, 464, 465). Además, esta conformación de PrP con tioles libres podría funcionar como semilla para la conversión de PrP^{C} en PrP^{Sc} (466, 467) dando así una explicación mecanística a la generación espontánea de las formas patógenas de PrP en las enfermedades priónicas esporádicas en humanos. Así que tanto la disminución de la eficiencia del plegamiento oxidativo como el aumento en la probabilidad de la sulfoxidación de las metioninas puede explicar la acumulación de las formas CtmPrP asociadas al envejecimiento en las formas esporádicas y genéticas.

En conjunto, los resultados descritos en esta memoria indican que los residuos de Met en PrP pueden estar constituidos en un código que de forma encriptada regula la predisposición y permisividad para la formación de confórmeros con propiedades tóxicas.

Conclusiones

Cada día sabemos más y entendemos menos

(Albert Einstein)

El principio básico de la biología de priones establece que la diferencia entre PrP^{C} y PrP^{Sc} es exclusivamente conformacional. No obstante la identificación de modificaciones oxidativas en las metioninas abre la puerta a la participación de interruptores moleculares y a su posible papel regulador. El trabajo aquí descrito ha contribuido al conocimiento de la biología de PrP y a las proteinopatías relacionadas en:

1) **La oxidación de las metioninas de α3 de PrP, las más enterradas y menos accesibles al solvente, es un proceso metabólico de la ruta de conversión que precede a la adquisición de la resistencia a proteasas y es común a las formas de PrP^{Sc} genéticas e infecciosas.**
2) **La flexibilidad estructural causada por la polaridad de los sulfóxidos de las metioninas de α3 de PrP se reproduce empleando sustituciones M-por-S en los cálculos teóricos.**
3) **Las cadenas de rHaPrP conteniendo las mutaciones artificiales M206S y M213S, independientes o combinadas, adoptan plegamientos α lábiles que permiten la formación de agregados protofibrilares en condiciones nativas.**
4) **La sustitución de M-por-SeM, considerada como una mutación metabólica que depende de la dieta, en secuencias pro-amiloides regula la formación, la forma y la toxicidad de las fibras amiloides con especificidad de sitio.**
5) **La expresión celular de plegamientos α lábiles basados en mutantes artificiales M206S y/o M213S provoca una toxicidad sin precedentes debido a su estabilización como ^{Ctm}PrP.**
6) **Las formas ^{Ctm}PrP presentan sus grupos tioles libres, de manera que aquellas mutaciones y condiciones que impidan la formación del puente disulfuro favorecerán la acumulación de estas formas tóxicas.**

Bibliografía

Libros, caminos y días dan al hombre sabiduría

(Proverbio árabe)

1. Carrell RW & Lomas DA (1997) Conformational disease. *Lancet* 350(9071):134-138.
2. Dobson CM (1999) Protein misfolding, evolution and disease. *Trends Biochem Sci* 24(9):329-332.
3. Kikis EA, Gidalevitz T, & Morimoto RI (2010) Protein homeostasis in models of aging and age-related conformational disease. *Advances in experimental medicine and biology* 694:138-159.
4. Surguchev A & Surguchov A (2010) Conformational diseases: looking into the eyes. *Brain research bulletin* 81(1):12-24.
5. Westermark P*, et al.* (2005) Amyloid: toward terminology clarification. Report from the Nomenclature Committee of the International Society of Amyloidosis. *Amyloid* 12(1):1-4.
6. Carrell RW, Lomas DA, Sidhar S, & Foreman R (1996) Alpha 1-antitrypsin deficiency. A conformational disease. *Chest* 110(6 Suppl):243S-247S.
7. Lomas DA, Evans DL, Finch JT, & Carrell RW (1992) The mechanism of Z alpha 1-antitrypsin accumulation in the liver. *Nature* 357(6379):605-607.
8. Balch WE, Morimoto RI, Dillin A, & Kelly JW (2008) Adapting proteostasis for disease intervention. *Science* 319(5865):916-919.
9. Chiti F & Dobson CM (2006) Protein misfolding, functional amyloid, and human disease. *Annu Rev Biochem* 75:333-366.
10. Cohen FE & Kelly JW (2003) Therapeutic approaches to protein-misfolding diseases. *Nature* 426(6968):905-909.
11. Glenner GG & Wong CW (1984) Alzheimer's disease: initial report of the purification and characterization of a novel cerebrovascular amyloid protein. *Biochem Biophys Res Commun* 120(3):885-890.
12. Kopito RR & Ron D (2000) Conformational disease. *Nat Cell Biol* 2(11):E207-209.
13. Soto C (2001) Protein misfolding and disease; protein refolding and therapy. *FEBS Lett* 498(2-3):204-207.
14. Stefani M & Dobson CM (2003) Protein aggregation and aggregate toxicity: new insights into protein folding, misfolding diseases and biological evolution. *J Mol Med (Berl)* 81(11):678-699.
15. Kelly JW (1996) Alternative conformations of amyloidogenic proteins govern their behavior. *Current opinion in structural biology* 6(1):11-17.
16. Moreno-Gonzalez I & Soto C (2011) Misfolded protein aggregates: mechanisms, structures and potential for disease transmission. *Seminars in cell & developmental biology* 22(5):482-487.
17. Wong E & Cuervo AM (2010) Autophagy gone awry in neurodegenerative diseases. *Nature neuroscience* 13(7):805-811.
18. Calloni G, Zoffoli S, Stefani M, Dobson CM, & Chiti F (2005) Investigating the effects of mutations on protein aggregation in the cell. *J Biol Chem* 280(11):10607-10613.
19. Dobson CM (2003) Protein folding and misfolding. *Nature* 426(6968):884-890.
20. Benson MD*, et al.* (2001) A new human hereditary amyloidosis: the result of a stop-codon mutation in the apolipoprotein AII gene. *Genomics* 72(3):272-277.
21. Deng HX*, et al.* (2011) Mutations in UBQLN2 cause dominant X-linked juvenile and adult-onset ALS and ALS/dementia. *Nature* 477(7363):211-215.
22. Goedert M & Spillantini MG (2001) Tau gene mutations and neurodegeneration. *Biochemical Society symposium* (67):59-71.
23. Hands SL & Wyttenbach A (2010) Neurotoxic protein oligomerisation associated with polyglutamine diseases. *Acta Neuropathol* 120(4):419-437.
24. Hayden MR, Tyagi SC, Kerklo MM, & Nicolls MR (2005) Type 2 diabetes mellitus as a conformational disease. *JOP : Journal of the pancreas* 6(4):287-302.

25. Hernandez D*, et al.* (2005) The dardarin G 2019 S mutation is a common cause of Parkinson's disease but not other neurodegenerative diseases. *Neurosci Lett* 389(3):137-139.
26. Kim HJ*, et al.* (2013) Mutations in prion-like domains in hnRNPA2B1 and hnRNPA1 cause multisystem proteinopathy and ALS. *Nature* 495(7442):467-473.
27. Kwiatkowski TJ, Jr.*, et al.* (2009) Mutations in the FUS/TLS gene on chromosome 16 cause familial amyotrophic lateral sclerosis. *Science* 323(5918):1205-1208.
28. Lagier-Tourenne C, Polymenidou M, & Cleveland DW (2010) TDP-43 and FUS/TLS: emerging roles in RNA processing and neurodegeneration. *Hum Mol Genet* 19(R1):R46-64.
29. Ramos CH & Ferreira ST (2005) Protein folding, misfolding and aggregation: evolving concepts and conformational diseases. *Protein and peptide letters* 12(3):213-222.
30. Rosen DR*, et al.* (1993) Mutations in Cu/Zn superoxide dismutase gene are associated with familial amyotrophic lateral sclerosis. *Nature* 362(6415):59-62.
31. Saraiva MJ (2001) Transthyretin amyloidosis: a tale of weak interactions. *FEBS Lett* 498(2-3):201-203.
32. Sato C*, et al.* (2005) Analysis of the glucocerebrosidase gene in Parkinson's disease. *Movement disorders : official journal of the Movement Disorder Society* 20(3):367-370.
33. Selkoe DJ (2001) Alzheimer's disease results from the cerebral accumulation and cytotoxicity of amyloid beta-protein. *J Alzheimers Dis* 3(1):75-80.
34. Soto C (2003) Unfolding the role of protein misfolding in neurodegenerative diseases. *Nat Rev Neurosci* 4(1):49-60.
35. Spillantini MG*, et al.* (1997) Alpha-synuclein in Lewy bodies. *Nature* 388(6645):839-840.
36. Hashimoto M, Rockenstein E, Crews L, & Masliah E (2003) Role of protein aggregation in mitochondrial dysfunction and neurodegeneration in Alzheimer's and Parkinson's diseases. *Neuromolecular medicine* 4(1-2):21-36.
37. Murphy RM (2002) Peptide aggregation in neurodegenerative disease. *Annual review of biomedical engineering* 4:155-174.
38. Brown IR (2007) Heat shock proteins and protection of the nervous system. *Ann N Y Acad Sci* 1113:147-158.
39. Chaudhuri TK & Paul S (2006) Protein-misfolding diseases and chaperone-based therapeutic approaches. *FEBS J* 273(7):1331-1349.
40. Forman MS, Trojanowski JQ, & Lee VM (2004) Neurodegenerative diseases: a decade of discoveries paves the way for therapeutic breakthroughs. *Nat Med* 10(10):1055-1063.
41. Muchowski PJ & Wacker JL (2005) Modulation of neurodegeneration by molecular chaperones. *Nat Rev Neurosci* 6(1):11-22.
42. Munch C & Bertolotti A (2012) Propagation of the Prion Phenomenon: Beyond the Seeding Principle. *J Mol Biol*.
43. Selkoe DJ (2004) Cell biology of protein misfolding: the examples of Alzheimer's and Parkinson's diseases. *Nat Cell Biol* 6(11):1054-1061.
44. Martin JB (1999) Molecular basis of the neurodegenerative disorders. *N Engl J Med* 340(25):1970-1980.
45. Ben-Zvi A, Miller EA, & Morimoto RI (2009) Collapse of proteostasis represents an early molecular event in Caenorhabditis elegans aging. *Proc Natl Acad Sci U S A* 106(35):14914-14919.
46. Esiri MM (2007) Ageing and the brain. *The Journal of pathology* 211(2):181-187.
47. Head E (2009) Oxidative damage and cognitive dysfunction: antioxidant treatments to promote healthy brain aging. *Neurochemical research* 34(4):670-678.
48. Jellinger KA (2009) Recent advances in our understanding of neurodegeneration. *J Neural Transm* 116(9):1111-1162.

49. Koudinov A, Kezlya E, Koudinova N, & Berezov T (2009) Amyloid-beta, tau protein, and oxidative changes as a physiological compensatory mechanism to maintain CNS plasticity under Alzheimer's disease and other neurodegenerative conditions. *J Alzheimers Dis* 18(2):381-400.
50. Martin LJ (2008) DNA damage and repair: relevance to mechanisms of neurodegeneration. *J Neuropathol Exp Neurol* 67(5):377-387.
51. Acevedo-Torres K*, et al.* (2009) Mitochondrial DNA damage is a hallmark of chemically induced and the R6/2 transgenic model of Huntington's disease. *DNA repair* 8(1):126-136.
52. Aguirre N, Beal MF, Matson WR, & Bogdanov MB (2005) Increased oxidative damage to DNA in an animal model of amyotrophic lateral sclerosis. *Free Radic Res* 39(4):383-388.
53. Alam ZI*, et al.* (1997) Oxidative DNA damage in the parkinsonian brain: an apparent selective increase in 8-hydroxyguanine levels in substantia nigra. *J Neurochem* 69(3):1196-1203.
54. Bogdanov M*, et al.* (2000) Increased oxidative damage to DNA in ALS patients. *Free radical biology & medicine* 29(7):652-658.
55. Dorszewska J*, et al.* (2007) Oxidative DNA damage and level of thiols as related to polymorphisms of MTHFR, MTR, MTHFD1 in Alzheimer's and Parkinson's diseases. *Acta neurobiologiae experimentalis* 67(2):113-129.
56. Lyras L, Cairns NJ, Jenner A, Jenner P, & Halliwell B (1997) An assessment of oxidative damage to proteins, lipids, and DNA in brain from patients with Alzheimer's disease. *J Neurochem* 68(5):2061-2069.
57. Polidori MC, Mecocci P, Browne SE, Senin U, & Beal MF (1999) Oxidative damage to mitochondrial DNA in Huntington's disease parietal cortex. *Neurosci Lett* 272(1):53-56.
58. Yasuhara T, Hara K, Sethi KD, Morgan JC, & Borlongan CV (2007) Increased 8-OHdG levels in the urine, serum, and substantia nigra of hemiparkinsonian rats. *Brain Res* 1133(1):49-52.
59. Harman D (1956) Aging: a theory based on free radical and radiation chemistry. *Journal of gerontology* 11(3):298-300.
60. Brzyska M, Bacia A, & Elbaum D (2001) Oxidative and hydrolytic properties of beta-amyloid. *Eur J Biochem* 268(12):3443-3454.
61. Castellani RJ, Perry G, & Smith MA (2004) Prion disease and Alzheimer's disease: pathogenic overlap. *Acta neurobiologiae experimentalis* 64(1):11-17.
62. Mattson MP (2002) Oxidative stress, perturbed calcium homeostasis, and immune dysfunction in Alzheimer's disease. *Journal of neurovirology* 8(6):539-550.
63. Pogocki D (2003) Alzheimer's beta-amyloid peptide as a source of neurotoxic free radicals: the role of structural effects. *Acta neurobiologiae experimentalis* 63(2):131-145.
64. Raina AK, Zhu X, & Smith MA (2004) Alzheimer's disease and the cell cycle. *Acta neurobiologiae experimentalis* 64(1):107-112.
65. Squier TC (2001) Oxidative stress and protein aggregation during biological aging. *Experimental gerontology* 36(9):1539-1550.
66. van der Vlies D, Woudenberg J, & Post JA (2003) Protein oxidation in aging: endoplasmic reticulum as a target. *Amino acids* 25(3-4):397-407.
67. Ballesteros M, Fredriksson A, Henriksson J, & Nystrom T (2001) Bacterial senescence: protein oxidation in non-proliferating cells is dictated by the accuracy of the ribosomes. *EMBO J* 20(18):5280-5289.
68. Cohen E*, et al.* (2009) Reduced IGF-1 signaling delays age-associated proteotoxicity in mice. *Cell* 139(6):1157-1169.
69. Demontis F & Perrimon N (2010) FOXO/4E-BP signaling in Drosophila muscles regulates organism-wide proteostasis during aging. *Cell* 143(5):813-825.

70. Dukan S*, et al.* (2000) Protein oxidation in response to increased transcriptional or translational errors. *Proc Natl Acad Sci U S A* 97(11):5746-5749.
71. Calamini B*, et al.* (2012) Small-molecule proteostasis regulators for protein conformational diseases. *Nature chemical biology* 8(2):185-196.
72. Gidalevitz T, Prahlad V, & Morimoto RI (2011) The stress of protein misfolding: from single cells to multicellular organisms. *Cold Spring Harb Perspect Biol* 3(6).
73. Morimoto RI (2008) Proteotoxic stress and inducible chaperone networks in neurodegenerative disease and aging. *Genes & development* 22(11):1427-1438.
74. Morimoto RI (2011) The heat shock response: systems biology of proteotoxic stress in aging and disease. *Cold Spring Harbor symposia on quantitative biology* 76:91-99.
75. Goldschmidt L, Teng PK, Riek R, & Eisenberg D (2010) Identifying the amylome, proteins capable of forming amyloid-like fibrils. *Proc Natl Acad Sci U S A* 107(8):3487-3492.
76. Laganowsky A*, et al.* (2012) Atomic view of a toxic amyloid small oligomer. *Science* 335(6073):1228-1231.
77. Nelson R & Eisenberg D (2006) Structural models of amyloid-like fibrils. *Advances in protein chemistry* 73:235-282.
78. Caughey BW*, et al.* (1991) Secondary structure analysis of the scrapie-associated protein PrP 27-30 in water by infrared spectroscopy. *Biochemistry* 30(31):7672-7680.
79. Eanes ED & Glenner GG (1968) X-ray diffraction studies on amyloid filaments. *The journal of histochemistry and cytochemistry : official journal of the Histochemistry Society* 16(11):673-677.
80. Glenner GG (1980) Amyloid deposits and amyloidosis. The beta-fibrilloses (first of two parts). *N Engl J Med* 302(23):1283-1292.
81. Eisenberg D*, et al.* (2006) The structural biology of protein aggregation diseases: Fundamental questions and some answers. *Accounts of chemical research* 39(9):568-575.
82. Klement K*, et al.* (2007) Effect of different salt ions on the propensity of aggregation and on the structure of Alzheimer's abeta(1-40) amyloid fibrils. *J Mol Biol* 373(5):1321-1333.
83. Makarava N & Baskakov IV (2008) The same primary structure of the prion protein yields two distinct self-propagating states. *J Biol Chem* 283(23):15988-15996.
84. Pedersen JS*, et al.* (2006) The changing face of glucagon fibrillation: structural polymorphism and conformational imprinting. *J Mol Biol* 355(3):501-523.
85. Toyama BH, Kelly MJ, Gross JD, & Weissman JS (2007) The structural basis of yeast prion strain variants. *Nature* 449(7159):233-237.
86. Verel R*, et al.* (2008) Polymorphism in an amyloid-like fibril-forming model peptide. *Angew Chem Int Ed Engl* 47(31):5842-5845.
87. Aguzzi A, Heikenwalder M, & Polymenidou M (2007) Insights into prion strains and neurotoxicity. *Nature reviews. Molecular cell biology* 8(7):552-561.
88. Wiltzius JJ*, et al.* (2009) Molecular mechanisms for protein-encoded inheritance. *Nat Struct Mol Biol* 16(9):973-978.
89. Eisenberg D & Jucker M (2012) The amyloid state of proteins in human diseases. *Cell* 148(6):1188-1203.
90. Berson JF*, et al.* (2003) Proprotein convertase cleavage liberates a fibrillogenic fragment of a resident glycoprotein to initiate melanosome biogenesis. *J Cell Biol* 161(3):521-533.
91. Chapman HR & Kirby-Turner N (2002) Visual/verbal analogue scales: examples of brief assessment methods to aid management of child and adult patients in clinical practice. *British dental journal* 193(8):447-450.

92. Chien LF & Kuo TT (2001) Reduction in mitochondrial respiratory capacity in Saccharomyces cerevisiae induced by expression of hepatitis B virus surface antigen. *Microbios* 105(410):29-41.
93. Claessen D*, et al.* (2003) A novel class of secreted hydrophobic proteins is involved in aerial hyphae formation in Streptomyces coelicolor by forming amyloid-like fibrils. *Genes & development* 17(14):1714-1726.
94. Eaglestone SS, Cox BS, & Tuite MF (1999) Translation termination efficiency can be regulated in Saccharomyces cerevisiae by environmental stress through a prion-mediated mechanism. *EMBO J* 18(7):1974-1981.
95. Giaever G*, et al.* (2002) Functional profiling of the Saccharomyces cerevisiae genome. *Nature* 418(6896):387-391.
96. Iconomidou VA, Vriend G, & Hamodrakas SJ (2000) Amyloids protect the silkmoth oocyte and embryo. *FEBS Lett* 479(3):141-145.
97. Saupe SJ, Clave C, & Begueret J (2000) Vegetative incompatibility in filamentous fungi: Podospora and Neurospora provide some clues. *Current opinion in microbiology* 3(6):608-612.
98. Chapman MR*, et al.* (2002) Role of Escherichia coli curli operons in directing amyloid fiber formation. *Science* 295(5556):851-855.
99. Chien P, Weissman JS, & DePace AH (2004) Emerging principles of conformation-based prion inheritance. *Annu Rev Biochem* 73:617-656.
100. Pedersen JS (2010) The nature of amyloid-like glucagon fibrils. *Journal of diabetes science and technology* 4(6):1357-1367.
101. Stein KC & True HL (2011) The [RNQ+] prion: a model of both functional and pathological amyloid. *Prion* 5(4):291-298.
102. Jarrett JT, Berger EP, & Lansbury PT, Jr. (1993) The C-terminus of the beta protein is critical in amyloidogenesis. *Ann N Y Acad Sci* 695:144-148.
103. Jarrett JT & Lansbury PT, Jr. (1993) Seeding "one-dimensional crystallization" of amyloid: a pathogenic mechanism in Alzheimer's disease and scrapie? *Cell* 73(6):1055-1058.
104. Scherzinger E*, et al.* (1999) Self-assembly of polyglutamine-containing huntingtin fragments into amyloid-like fibrils: implications for Huntington's disease pathology. *Proc Natl Acad Sci U S A* 96(8):4604-4609.
105. Soto C, Estrada L, & Castilla J (2006) Amyloids, prions and the inherent infectious nature of misfolded protein aggregates. *Trends Biochem Sci* 31(3):150-155.
106. Wood SJ*, et al.* (1999) alpha-synuclein fibrillogenesis is nucleation-dependent. Implications for the pathogenesis of Parkinson's disease. *J Biol Chem* 274(28):19509-19512.
107. Baskakov IV, Legname G, Prusiner SB, & Cohen FE (2001) Folding of prion protein to its native alpha-helical conformation is under kinetic control. *J Biol Chem* 276(23):19687-19690.
108. Dobson CM & Karplus M (1999) The fundamentals of protein folding: bringing together theory and experiment. *Current opinion in structural biology* 9(1):92-101.
109. Ostapchenko VG*, et al.* (2010) Two amyloid States of the prion protein display significantly different folding patterns. *J Mol Biol* 400(4):908-921.
110. Baskakov IV (2007) Branched chain mechanism of polymerization and ultrastructure of prion protein amyloid fibrils. *FEBS J* 274(15):3756-3765.
111. Cohen SI, Vendruscolo M, Dobson CM, & Knowles TP (2011) Nucleated polymerization with secondary pathways. III. Equilibrium behavior and oligomer populations. *The Journal of chemical physics* 135(6):065107.
112. Aguzzi A (2009) Cell biology: Beyond the prion principle. *Nature* 459(7249):924-925.
113. Clavaguera F*, et al.* (2009) Transmission and spreading of tauopathy in transgenic mouse brain. *Nat Cell Biol* 11(7):909-913.

114. Frost B, Jacks RL, & Diamond MI (2009) Propagation of tau misfolding from the outside to the inside of a cell. *J Biol Chem* 284(19):12845-12852.
115. Ren PH*, et al.* (2009) Cytoplasmic penetration and persistent infection of mammalian cells by polyglutamine aggregates. *Nat Cell Biol* 11(2):219-225.
116. Bolton DC, McKinley MP, & Prusiner SB (1982) Identification of a protein that purifies with the scrapie prion. *Science* 218(4579):1309-1311.
117. Griffith JS (1967) Self-replication and scrapie. *Nature* 215(5105):1043-1044.
118. Hegde RS*, et al.* (1998) A transmembrane form of the prion protein in neurodegenerative disease. *Science* 279(5352):827-834.
119. Hegde RS*, et al.* (1999) Transmissible and genetic prion diseases share a common pathway of neurodegeneration. *Nature* 402(6763):822-826.
120. Kim JI*, et al.* (2010) Mammalian prions generated from bacterially expressed prion protein in the absence of any mammalian cofactors. *J Biol Chem* 285(19):14083-14087.
121. Prusiner SB (1982) Novel proteinaceous infectious particles cause scrapie. *Science* 216(4542):136-144.
122. Prusiner SB (1998) Prions. *Proc Natl Acad Sci U S A* 95(23):13363-13383.
123. Wang X*, et al.* (2011) Familial CJD associated PrP mutants within transmembrane region induced Ctm-PrP retention in ER and triggered apoptosis by ER stress in SH-SY5Y cells. *PLoS One* 6(1):e14602.
124. Prusiner SB, Scott MR, DeArmond SJ, & Cohen FE (1998) Prion protein biology. *Cell* 93(3):337-348.
125. Aguzzi A & Polymenidou M (2004) Mammalian prion biology: one century of evolving concepts. *Cell* 116(2):313-327.
126. Collinge J, Sidle KC, Meads J, Ironside J, & Hill AF (1996) Molecular analysis of prion strain variation and the aetiology of 'new variant' CJD. *Nature* 383(6602):685-690.
127. Will RG*, et al.* (1996) A new variant of Creutzfeldt-Jakob disease in the UK. *Lancet* 347(9006):921-925.
128. Gajdusek DC & Zigas V (1957) Degenerative disease of the central nervous system in New Guinea; the endemic occurrence of kuru in the native population. *N Engl J Med* 257(20):974-978.
129. Gambetti P*, et al.* (1993) Fatal familial insomnia and the widening spectrum of prion diseases. *Br Med Bull* 49(4):980-994.
130. Collinge J & Palmer MS (1994) Molecular genetics of human prion diseases. *Philos Trans R Soc Lond B Biol Sci* 343(1306):371-378.
131. Gambetti P, Kong Q, Zou W, Parchi P, & Chen SG (2003) Sporadic and familial CJD: classification and characterisation. *Br Med Bull* 66:213-239.
132. Gambetti P & Parchi P (1999) Insomnia in prion diseases: sporadic and familial. *N Engl J Med* 340(21):1675-1677.
133. Montagna P, Gambetti P, Cortelli P, & Lugaresi E (2003) Familial and sporadic fatal insomnia. *Lancet Neurol* 2(3):167-176.
134. Tateishi J & Kitamoto T (1995) Inherited prion diseases and transmission to rodents. *Brain Pathol* 5(1):53-59.
135. Will RG (2003) Acquired prion disease: iatrogenic CJD, variant CJD, kuru. *Br Med Bull* 66:255-265.
136. Brown P, Preece MA, & Will RG (1992) "Friendly fire" in medicine: hormones, homografts, and Creutzfeldt-Jakob disease. *Lancet* 340(8810):24-27.
137. Ben-Gedalya T & Cohen E (2012) Quality control compartments coming of age. *Traffic* 13(5):635-642.
138. Aguzzi A & Weissmann C (1996) Spongiform encephalopathies: a suspicious signature. *Nature* 383(6602):666-667.
139. Gajdusek DC (1977) Unconventional viruses and the origin and disappearance of kuru. *Science* 197(4307):943-960.

140. Goldfarb LG*, et al.* (1992) Fatal familial insomnia and familial Creutzfeldt-Jakob disease: disease phenotype determined by a DNA polymorphism. *Science* 258(5083):806-808.
141. Hsiao K*, et al.* (1991) Mutation of the prion protein in Libyan Jews with Creutzfeldt-Jakob disease. *N Engl J Med* 324(16):1091-1097.
142. Prusiner SB (1989) Creutzfeldt-Jakob disease and scrapie prions. *Alzheimer disease and associated disorders* 3(1-2):52-78.
143. Prusiner SB (1989) Scrapie prions. *Annu Rev Microbiol* 43:345-374.
144. Prusiner SB (1994) Inherited prion diseases. *Proc Natl Acad Sci U S A* 91(11):4611-4614.
145. Watts JC, Balachandran A, & Westaway D (2006) The expanding universe of prion diseases. *PLoS Pathog* 2(3):e26.
146. Hetz C & Soto C (2003) Protein misfolding and disease: the case of prion disorders. *Cellular and molecular life sciences : CMLS* 60(1):133-143.
147. Ironside JW & Bell JE (1997) Florid plaques and new variant Creutzfeldt-Jakob disease. *Lancet* 350(9089):1475.
148. Palmer MS & Collinge J (1992) Human prion diseases. *Current opinion in neurology and neurosurgery* 5(6):895-901.
149. Bell JE & Ironside JW (1993) Neuropathology of spongiform encephalopathies in humans. *Br Med Bull* 49(4):738-777.
150. Bendheim PE, Barry RA, DeArmond SJ, Stites DP, & Prusiner SB (1984) Antibodies to a scrapie prion protein. *Nature* 310(5976):418-421.
151. DeArmond SJ, Kristensson K, & Bowler RP (1992) PrPSc causes nerve cell death and stimulates astrocyte proliferation: a paradox. *Prog Brain Res* 94:437-446.
152. Masters CL & Richardson EP, Jr. (1978) Subacute spongiform encephalopathy (Creutzfeldt-Jakob disease). The nature and progression of spongiform change. *Brain* 101(2):333-344.
153. Zlotnik I & Stamp JT (1961) Scrapie disease of sheep. *World Neurol* 2:895-907.
154. Finckh U*, et al.* (2000) High prevalence of pathogenic mutations in patients with early-onset dementia detected by sequence analyses of four different genes. *Am J Hum Genet* 66(1):110-117.
155. Gu Y, Singh A, Bose S, & Singh N (2008) Pathogenic mutations in the glycosylphosphatidylinositol signal peptide of PrP modulate its topology in neuroblastoma cells. *Mol Cell Neurosci* 37(4):647-656.
156. Kitamoto T, Iizuka R, & Tateishi J (1993) An amber mutation of prion protein in Gerstmann-Straussler syndrome with mutant PrP plaques. *Biochem Biophys Res Commun* 192(2):525-531.
157. Liu Z*, et al.* (2010) Creutzfeldt-Jakob disease with PRNP G114V mutation in a Chinese family. *Acta neurologica Scandinavica* 121(6):377-383.
158. Mastrianni JA*, et al.* (1995) Prion disease (PrP-A117V) presenting with ataxia instead of dementia. *Neurology* 45(11):2042-2050.
159. Mouillet-Richard S*, et al.* (1999) Mutation at codon 210 (V210I) of the prion protein gene in a North African patient with Creutzfeldt-Jakob disease. *Journal of the neurological sciences* 168(2):141-144.
160. Nitrini R*, et al.* (1997) Familial spongiform encephalopathy associated with a novel prion protein gene mutation. *Ann Neurol* 42(2):138-146.
161. Pastore M*, et al.* (2005) Creutzfeldt-Jakob disease (CJD) with a mutation at codon 148 of prion protein gene: relationship with sporadic CJD. *Am J Pathol* 167(6):1729-1738.
162. Peoc'h K*, et al.* (2000) Identification of three novel mutations (E196K, V203I, E211Q) in the prion protein gene (PRNP) in inherited prion diseases with Creutzfeldt-Jakob disease phenotype. *Hum Mutat* 15(5):482.

163. Piccardo P*, et al.* (1998) Phenotypic variability of Gerstmann-Straussler-Scheinker disease is associated with prion protein heterogeneity. *J Neuropathol Exp Neurol* 57(10):979-988.
164. Piccardo P*, et al.* (1996) Proteinase-K-resistant prion protein isoforms in Gerstmann-Straussler-Scheinker disease (Indiana kindred). *J Neuropathol Exp Neurol* 55(11):1157-1163.
165. Prusiner SB (1993) Genetic and infectious prion diseases. *Archives of neurology* 50(11):1129-1153.
166. Roeber S*, et al.* (2005) Creutzfeldt-Jakob disease in a patient with an R208H mutation of the prion protein gene (PRNP) and a 17-kDa prion protein fragment. *Acta Neuropathol* 109(4):443-448.
167. Yamazaki M*, et al.* (1999) Variant Gerstmann-Straussler syndrome with the P105L prion gene mutation: an unusual case with nigral degeneration and widespread neurofibrillary tangles. *Acta Neuropathol* 98(5):506-511.
168. Zou WQ*, et al.* (2010) Variably protease-sensitive prionopathy: a new sporadic disease of the prion protein. *Ann Neurol* 68(2):162-172.
169. Kretzschmar HA*, et al.* (1986) Molecular cloning of a human prion protein cDNA. *DNA* 5(4):315-324.
170. Robakis NK*, et al.* (1986) Isolation of a cDNA clone encoding the leader peptide of prion protein and expression of the homologous gene in various tissues. *Proc Natl Acad Sci U S A* 83(17):6377-6381.
171. Sparkes RS*, et al.* (1986) Assignment of the human and mouse prion protein genes to homologous chromosomes. *Proc Natl Acad Sci U S A* 83(19):7358-7362.
172. Mastrangelo P & Westaway D (2001) Biology of the prion gene complex. *Biochem Cell Biol* 79(5):613-628.
173. Basler K*, et al.* (1986) Scrapie and cellular PrP isoforms are encoded by the same chromosomal gene. *Cell* 46(3):417-428.
174. Gabriel JM, Oesch B, Kretzschmar H, Scott M, & Prusiner SB (1992) Molecular cloning of a candidate chicken prion protein. *Proc Natl Acad Sci U S A* 89(19):9097-9101.
175. Lee IY*, et al.* (1998) Complete genomic sequence and analysis of the prion protein gene region from three mammalian species. *Genome Res* 8(10):1022-1037.
176. Li G & Bolton DC (1997) A novel hamster prion protein mRNA contains an extra exon: increased expression in scrapie. *Brain Res* 751(2):265-274.
177. Saeki K, Matsumoto Y, Hirota Y, & Onodera T (1996) Three-exon structure of the gene encoding the rat prion protein and its expression in tissues. *Virus Genes* 12(1):15-20.
178. Westaway D*, et al.* (1994) Structure and polymorphism of the mouse prion protein gene. *Proc Natl Acad Sci U S A* 91(14):6418-6422.
179. Westaway D*, et al.* (1987) Distinct prion proteins in short and long scrapie incubation period mice. *Cell* 51(4):651-662.
180. Yoshimoto J*, et al.* (1992) Comparative sequence analysis and expression of bovine PrP gene in mouse L-929 cells. *Virus Genes* 6(4):343-356.
181. Aguzzi A & Calella AM (2009) Prions: protein aggregation and infectious diseases. *Physiological reviews* 89(4):1105-1152.
182. Ning ZY*, et al.* (2005) Quantification of prion gene expression in brain and peripheral organs of golden hamster by real-time RT-PCR. *Animal biotechnology* 16(1):55-65.
183. Bueler H*, et al.* (1993) Mice devoid of PrP are resistant to scrapie. *Cell* 73(7):1339-1347.
184. Bueler H*, et al.* (1992) Normal development and behaviour of mice lacking the neuronal cell-surface PrP protein. *Nature* 356(6370):577-582.
185. Manson JC*, et al.* (1994) 129/Ola mice carrying a null mutation in PrP that abolishes mRNA production are developmentally normal. *Mol Neurobiol* 8(2-3):121-127.

186. Bremer J*, et al.* (2010) Axonal prion protein is required for peripheral myelin maintenance. *Nature neuroscience* 13(3):310-318.
187. Liao YC, Lebo RV, Clawson GA, & Smuckler EA (1986) Human prion protein cDNA: molecular cloning, chromosomal mapping, and biological implications. *Science* 233(4761):364-367.
188. Levine CG, Mitra D, Sharma A, Smith CL, & Hegde RS (2005) The efficiency of protein compartmentalization into the secretory pathway. *Mol Biol Cell* 16(1):279-291.
189. Rane NS, Yonkovich JL, & Hegde RS (2004) Protection from cytosolic prion protein toxicity by modulation of protein translocation. *EMBO J* 23(23):4550-4559.
190. Stewart RS & Harris DA (2003) Mutational analysis of topological determinants in prion protein (PrP) and measurement of transmembrane and cytosolic PrP during prion infection. *J Biol Chem* 278(46):45960-45968.
191. von Heijne G (1985) Signal sequences. The limits of variation. *J Mol Biol* 184(1):99-105.
192. Brown DR*, et al.* (1997) The cellular prion protein binds copper in vivo. *Nature* 390(6661):684-687.
193. Hodak M, Chisnell R, Lu W, & Bernholc J (2009) Functional implications of multistage copper binding to the prion protein. *Proc Natl Acad Sci U S A* 106(28):11576-11581.
194. Morante S*, et al.* (2004) Inter- and intra-octarepeat Cu(II) site geometries in the prion protein: implications in Cu(II) binding cooperativity and Cu(II)-mediated assemblies. *J Biol Chem* 279(12):11753-11759.
195. Redecke L*, et al.* (2005) Comparative analysis of the human and chicken prion protein copper binding regions at pH 6.5. *J Biol Chem* 280(14):13987-13992.
196. Stockel J, Safar J, Wallace AC, Cohen FE, & Prusiner SB (1998) Prion protein selectively binds copper(II) ions. *Biochemistry* 37(20):7185-7193.
197. Viles JH*, et al.* (1999) Copper binding to the prion protein: structural implications of four identical cooperative binding sites. *Proc Natl Acad Sci U S A* 96(5):2042-2047.
198. Caughey B & Race RE (1992) Potent inhibition of scrapie-associated PrP accumulation by congo red. *J Neurochem* 59(2):768-771.
199. Deleault NR*, et al.* (2005) Protease-resistant prion protein amplification reconstituted with partially purified substrates and synthetic polyanions. *J Biol Chem* 280(29):26873-26879.
200. Gonzalez-Iglesias R*, et al.* (2002) Prion protein interaction with glycosaminoglycan occurs with the formation of oligomeric complexes stabilized by Cu(II) bridges. *J Mol Biol* 319(2):527-540.
201. Hundt C*, et al.* (2001) Identification of interaction domains of the prion protein with its 37-kDa/67-kDa laminin receptor. *EMBO J* 20(21):5876-5886.
202. Ostapchenko VG, Makarava N, Savtchenko R, & Baskakov IV (2008) The polybasic N-terminal region of the prion protein controls the physical properties of both the cellular and fibrillar forms of PrP. *J Mol Biol* 383(5):1210-1224.
203. Warner RG, Hundt C, Weiss S, & Turnbull JE (2002) Identification of the heparan sulfate binding sites in the cellular prion protein. *J Biol Chem* 277(21):18421-18430.
204. Weiss S*, et al.* (1997) RNA aptamers specifically interact with the prion protein PrP. *J Virol* 71(11):8790-8797.
205. Chakrabarti O, Ashok A, & Hegde RS (2009) Prion protein biosynthesis and its emerging role in neurodegeneration. *Trends Biochem Sci* 34(6):287-295.
206. Forloni G*, et al.* (1993) Neurotoxicity of a prion protein fragment. *Nature* 362(6420):543-546.
207. Gasset M*, et al.* (1992) Predicted alpha-helical regions of the prion protein when synthesized as peptides form amyloid. *Proc Natl Acad Sci U S A* 89(22):10940-10944.
208. Wuthrich K & Riek R (2001) Three-dimensional structures of prion proteins. *Advances in protein chemistry* 57:55-82.

209. Lysek DA*, et al.* (2005) Prion protein NMR structures of cats, dogs, pigs, and sheep. *Proc Natl Acad Sci U S A* 102(3):640-645.
210. Green KM*, et al.* (2008) The elk PRNP codon 132 polymorphism controls cervid and scrapie prion propagation. *J Gen Virol* 89(Pt 2):598-608.
211. Palmer MS & Collinge J (1993) Mutations and polymorphisms in the prion protein gene. *Hum Mutat* 2(3):168-173.
212. Kornfeld R & Kornfeld S (1985) Assembly of asparagine-linked oligosaccharides. *Annu Rev Biochem* 54:631-664.
213. Turk E, Teplow DB, Hood LE, & Prusiner SB (1988) Purification and properties of the cellular and scrapie hamster prion proteins. *Eur J Biochem* 176(1):21-30.
214. Englund PT (1993) The structure and biosynthesis of glycosyl phosphatidylinositol protein anchors. *Annu Rev Biochem* 62:121-138.
215. Stahl N*, et al.* (1992) Glycosylinositol phospholipid anchors of the scrapie and cellular prion proteins contain sialic acid. *Biochemistry* 31(21):5043-5053.
216. Taraboulos A, Raeber AJ, Borchelt DR, Serban D, & Prusiner SB (1992) Synthesis and trafficking of prion proteins in cultured cells. *Mol Biol Cell* 3(8):851-863.
217. Vey M*, et al.* (1996) Subcellular colocalization of the cellular and scrapie prion proteins in caveolae-like membranous domains. *Proc Natl Acad Sci U S A* 93(25):14945-14949.
218. Alken M*, et al.* (2009) The sequence after the signal peptide of the G protein-coupled endothelin B receptor is required for efficient translocon gating at the endoplasmic reticulum membrane. *Molecular pharmacology* 75(4):801-811.
219. Juanes ME, Elvira G, Garcia-Grande A, Calero M, & Gasset M (2009) Biosynthesis of prion protein nucleocytoplasmic isoforms by alternative initiation of translation. *J Biol Chem* 284(5):2787-2794.
220. De Fea KA*, et al.* (1994) Determinants of carboxyl-terminal domain translocation during prion protein biogenesis. *J Biol Chem* 269(24):16810-16820.
221. Hay B, Barry RA, Lieberburg I, Prusiner SB, & Lingappa VR (1987) Biogenesis and transmembrane orientation of the cellular isoform of the scrapie prion protein [published errratum appears in Mol Cell Biol 1987 May;7(5):2035]. *Molecular and cellular biology* 7(2):914-920.
222. Hegde RS & Rane NS (2003) Prion protein trafficking and the development of neurodegeneration. *Trends Neurosci* 26(7):337-339.
223. Ma J & Lindquist S (2001) Wild-type PrP and a mutant associated with prion disease are subject to retrograde transport and proteasome degradation. *Proc Natl Acad Sci U S A* 98(26):14955-14960.
224. Ma J, Wollmann R, & Lindquist S (2002) Neurotoxicity and neurodegeneration when PrP accumulates in the cytosol. *Science* 298(5599):1781-1785.
225. Zanusso G*, et al.* (1999) Proteasomal degradation and N-terminal protease resistance of the codon 145 mutant prion protein. *J Biol Chem* 274(33):23396-23404.
226. Ashok A & Hegde RS (2008) Retrotranslocation of prion proteins from the endoplasmic reticulum by preventing GPI signal transamidation. *Mol Biol Cell* 19(8):3463-3476.
227. Harris DA (2003) Trafficking, turnover and membrane topology of PrP. *Br Med Bull* 66:71-85.
228. Haraguchi T*, et al.* (1989) Asparagine-linked glycosylation of the scrapie and cellular prion proteins. *Arch Biochem Biophys* 274(1):1-13.
229. Kaneko K*, et al.* (1997) COOH-terminal sequence of the cellular prion protein directs subcellular trafficking and controls conversion into the scrapie isoform. *Proc Natl Acad Sci U S A* 94(6):2333-2338.
230. Naslavsky N, Stein R, Yanai A, Friedlander G, & Taraboulos A (1997) Characterization of detergent-insoluble complexes containing the cellular prion protein and its scrapie isoform. *J Biol Chem* 272(10):6324-6331.

231. Taraboulos A*, et al.* (1995) Cholesterol depletion and modification of COOH-terminal targeting sequence of the prion protein inhibit formation of the scrapie isoform. *J Cell Biol* 129(1):121-132.
232. Caughey B, Race RE, Ernst D, Buchmeier MJ, & Chesebro B (1989) Prion protein biosynthesis in scrapie-infected and uninfected neuroblastoma cells. *J Virol* 63(1):175-181.
233. Chen SG*, et al.* (1995) Truncated forms of the human prion protein in normal brain and in prion diseases. *J Biol Chem* 270(32):19173-19180.
234. Jimenez-Huete A*, et al.* (1998) Endogenous proteolytic cleavage of normal and disease-associated isoforms of the human prion protein in neural and non-neural tissues. *Am J Pathol* 153(5):1561-1572.
235. Parchi P*, et al.* (1999) Classification of sporadic Creutzfeldt-Jakob disease based on molecular and phenotypic analysis of 300 subjects. *Ann Neurol* 46(2):224-233.
236. Rachidi W*, et al.* (2003) Prion infection impairs copper binding of cultured cells. *J Biol Chem* 278(17):14595-14598.
237. Dron M*, et al.* (2010) Endogenous proteolytic cleavage of disease-associated prion protein to produce C2 fragments is strongly cell- and tissue-dependent. *J Biol Chem* 285(14):10252-10264.
238. Oliveira-Martins JB*, et al.* (2010) Unexpected tolerance of alpha-cleavage of the prion protein to sequence variations. *PLoS One* 5(2):e9107.
239. Vincent B, Cisse MA, Sunyach C, Guillot-Sestier MV, & Checler F (2008) Regulation of betaAPP and PrPc cleavage by alpha-secretase: mechanistic and therapeutic perspectives. *Current Alzheimer research* 5(2):202-211.
240. Yadavalli R*, et al.* (2004) Calpain-dependent endoproteolytic cleavage of PrPSc modulates scrapie prion propagation. *J Biol Chem* 279(21):21948-21956.
241. Mange A*, et al.* (2004) Alpha- and beta- cleavages of the amino-terminus of the cellular prion protein. *Biol Cell* 96(2):125-132.
242. Guillot-Sestier MV, Sunyach C, Druon C, Scarzello S, & Checler F (2009) The alpha-secretase-derived N-terminal product of cellular prion, N1, displays neuroprotective function in vitro and in vivo. *J Biol Chem* 284(51):35973-35986.
243. Guillot-Sestier MV*, et al.* (2012) alpha-Secretase-derived fragment of cellular prion, N1, protects against monomeric and oligomeric amyloid beta (Abeta)-associated cell death. *J Biol Chem* 287(7):5021-5032.
244. Westergard L, Turnbaugh JA, & Harris DA (2011) A naturally occurring C-terminal fragment of the prion protein (PrP) delays disease and acts as a dominant-negative inhibitor of PrPSc formation. *J Biol Chem* 286(51):44234-44242.
245. Parkin ET, Watt NT, Turner AJ, & Hooper NM (2004) Dual mechanisms for shedding of the cellular prion protein. *J Biol Chem* 279(12):11170-11178.
246. Taguchi Y*, et al.* (2009) Specific biarsenical labeling of cell surface proteins allows fluorescent- and biotin-tagging of amyloid precursor protein and prion proteins. *Mol Biol Cell* 20(1):233-244.
247. Hsiao K*, et al.* (1989) Linkage of a prion protein missense variant to Gerstmann-Straussler syndrome. *Nature* 338(6213):342-345.
248. Scott M*, et al.* (1989) Transgenic mice expressing hamster prion protein produce species-specific scrapie infectivity and amyloid plaques. *Cell* 59(5):847-857.
249. Westaway D & Prusiner SB (1986) Conservation of the cellular gene encoding the scrapie prion protein. *Nucleic Acids Res* 14(5):2035-2044.
250. Lauren J, Gimbel DA, Nygaard HB, Gilbert JW, & Strittmatter SM (2009) Cellular prion protein mediates impairment of synaptic plasticity by amyloid-beta oligomers. *Nature* 457(7233):1128-1132.
251. Li A*, et al.* (2007) Neonatal lethality in transgenic mice expressing prion protein with a deletion of residues 105-125. *EMBO J* 26(2):548-558.

252. Caughey B (1993) Scrapie associated PrP accumulation and its prevention: insights from cell culture. *Br Med Bull* 49(4):860-872.
253. Caughey B & Raymond GJ (1993) Sulfated polyanion inhibition of scrapie-associated PrP accumulation in cultured cells. *J Virol* 67(2):643-650.
254. Collinge J*, et al.* (1994) Prion protein is necessary for normal synaptic function. *Nature* 370(6487):295-297.
255. Cordeiro Y*, et al.* (2001) DNA converts cellular prion protein into the beta-sheet conformation and inhibits prion peptide aggregation. *J Biol Chem* 276(52):49400-49409.
256. Dong CF*, et al.* (2008) Molecular interaction between prion protein and GFAP both in native and recombinant forms in vitro. *Medical microbiology and immunology* 197(4):361-368.
257. Jin T*, et al.* (2000) The chaperone protein BiP binds to a mutant prion protein and mediates its degradation by the proteasome. *J Biol Chem* 275(49):38699-38704.
258. Jouvin-Marche E*, et al.* (2006) Overexpression of cellular prion protein induces an antioxidant environment altering T cell development in the thymus. *J Immunol* 176(6):3490-3497.
259. Kuwahara C*, et al.* (1999) Prions prevent neuronal cell-line death. *Nature* 400(6741):225-226.
260. Le Pichon CE*, et al.* (2009) Olfactory behavior and physiology are disrupted in prion protein knockout mice. *Nature neuroscience* 12(1):60-69.
261. Linden R*, et al.* (2008) Physiology of the prion protein. *Physiological reviews* 88(2):673-728.
262. Lopes MH*, et al.* (2005) Interaction of cellular prion and stress-inducible protein 1 promotes neuritogenesis and neuroprotection by distinct signaling pathways. *J Neurosci* 25(49):11330-11339.
263. Mange A, Crozet C, Lehmann S, & Beranger F (2004) Scrapie-like prion protein is translocated to the nuclei of infected cells independently of proteasome inhibition and interacts with chromatin. *J Cell Sci* 117(Pt 11):2411-2416.
264. McLennan NF*, et al.* (2004) Prion protein accumulation and neuroprotection in hypoxic brain damage. *Am J Pathol* 165(1):227-235.
265. Milhavet O & Lehmann S (2002) Oxidative stress and the prion protein in transmissible spongiform encephalopathies. *Brain research. Brain research reviews* 38(3):328-339.
266. Schmitt-Ulms G*, et al.* (2001) Binding of neural cell adhesion molecules (N-CAMs) to the cellular prion protein. *J Mol Biol* 314(5):1209-1225.
267. Striebel JF, Race B, Pathmajeyan M, Rangel A, & Chesebro B (2013) Lack of influence of prion protein gene expression on kainate-induced seizures in mice: studies using congenic, coisogenic and transgenic strains. *Neuroscience* 238:11-18.
268. Tobler I*, et al.* (1996) Altered circadian activity rhythms and sleep in mice devoid of prion protein. *Nature* 380(6575):639-642.
269. Vana K & Weiss S (2006) A trans-dominant negative 37kDa/67kDa laminin receptor mutant impairs PrP(Sc) propagation in scrapie-infected neuronal cells. *J Mol Biol* 358(1):57-66.
270. Vassallo N & Herms J (2003) Cellular prion protein function in copper homeostasis and redox signalling at the synapse. *J Neurochem* 86(3):538-544.
271. Watt NT & Hooper NM (2003) The prion protein and neuronal zinc homeostasis. *Trends Biochem Sci* 28(8):406-410.
272. Zhang CC, Steele AD, Lindquist S, & Lodish HF (2006) Prion protein is expressed on long-term repopulating hematopoietic stem cells and is important for their self-renewal. *Proc Natl Acad Sci U S A* 103(7):2184-2189.
273. Prusiner SB (2001) Shattuck lecture--neurodegenerative diseases and prions. *N Engl J Med* 344(20):1516-1526.

274. Diaz-Espinoza R & Soto C (2010) Generation of prions in vitro and the protein-only hypothesis. *Prion* 4(2):53-59.
275. Baskakov IV (2009) Switching in amyloid structure within individual fibrils: implication for strain adaptation, species barrier and strain classification. *FEBS Lett* 583(16):2618-2622.
276. Weissmann C (2009) Thoughts on mammalian prion strains. *Folia neuropathologica / Association of Polish Neuropathologists and Medical Research Centre, Polish Academy of Sciences* 47(2):104-113.
277. Baskakov IV & Breydo L (2007) Converting the prion protein: what makes the protein infectious. *Biochim Biophys Acta* 1772(6):692-703.
278. Solomon IH, Schepker JA, & Harris DA (2010) Prion neurotoxicity: insights from prion protein mutants. *Current issues in molecular biology* 12(2):51-61.
279. Ayers JI*, et al.* (2011) The strain-encoded relationship between PrP replication, stability and processing in neurons is predictive of the incubation period of disease. *PLoS Pathog* 7(3):e1001317.
280. Legname G*, et al.* (2006) Continuum of prion protein structures enciphers a multitude of prion isolate-specified phenotypes. *Proc Natl Acad Sci U S A* 103(50):19105-19110.
281. Tanaka M, Collins SR, Toyama BH, & Weissman JS (2006) The physical basis of how prion conformations determine strain phenotypes. *Nature* 442(7102):585-589.
282. Collinge J & Clarke AR (2007) A general model of prion strains and their pathogenicity. *Science* 318(5852):930-936.
283. Glockshuber R*, et al.* (1997) Three-dimensional NMR structure of a self-folding domain of the prion protein PrP(121-231). *Trends Biochem Sci* 22(7):241-242.
284. Hornemann S*, et al.* (1997) Recombinant full-length murine prion protein, mPrP(23-231): purification and spectroscopic characterization. *FEBS Lett* 413(2):277-281.
285. Knaus KJ*, et al.* (2001) Crystal structure of the human prion protein reveals a mechanism for oligomerization. *Nat Struct Biol* 8(9):770-774.
286. Pan KM*, et al.* (1993) Conversion of alpha-helices into beta-sheets features in the formation of the scrapie prion proteins. *Proc Natl Acad Sci U S A* 90(23):10962-10966.
287. Riek R*, et al.* (1996) NMR structure of the mouse prion protein domain PrP(121-231). *Nature* 382(6587):180-182.
288. Christen B, Hornemann S, Damberger FF, & Wuthrich K (2009) Prion protein NMR structure from tammar wallaby (Macropus eugenii) shows that the beta2-alpha2 loop is modulated by long-range sequence effects. *J Mol Biol* 389(5):833-845.
289. Christen B, Perez DR, Hornemann S, & Wuthrich K (2008) NMR structure of the bank vole prion protein at 20 degrees C contains a structured loop of residues 165-171. *J Mol Biol* 383(2):306-312.
290. Gossert AD, Bonjour S, Lysek DA, Fiorito F, & Wuthrich K (2005) Prion protein NMR structures of elk and of mouse/elk hybrids. *Proc Natl Acad Sci U S A* 102(3):646-650.
291. Lopez Garcia F, Zahn R, Riek R, & Wuthrich K (2000) NMR structure of the bovine prion protein. *Proc Natl Acad Sci U S A* 97(15):8334-8339.
292. Perez DR, Damberger FF, & Wuthrich K (2010) Horse prion protein NMR structure and comparisons with related variants of the mouse prion protein. *J Mol Biol* 400(2):121-128.
293. Riek R, Hornemann S, Wider G, Glockshuber R, & Wuthrich K (1997) NMR characterization of the full-length recombinant murine prion protein, mPrP(23-231). *FEBS Lett* 413(2):282-288.
294. Wen Y*, et al.* (2010) Unique structural characteristics of the rabbit prion protein. *J Biol Chem* 285(41):31682-31693.
295. Zahn R*, et al.* (2000) NMR solution structure of the human prion protein. *Proc Natl Acad Sci U S A* 97(1):145-150.

296. Gonzalez-Iglesias R*, et al.* (2004) Cu2+ binding triggers alphaBoPrP assembly into insoluble laminar polymers. *FEBS Lett* 556(1-3):161-166.
297. Renner C*, et al.* (2004) Micellar environments induce structuring of the N-terminal tail of the prion protein. *Biopolymers* 73(4):421-433.
298. Valensin G, Molteni E, Valensin D, Taraszkiewicz M, & Kozlowski H (2009) Molecular dynamics study of the Cu2+ binding-induced "structuring" of the N-terminal domain of human prion protein. *J Phys Chem B* 113(11):3277-3279.
299. Zahn R (2003) The octapeptide repeats in mammalian prion protein constitute a pH-dependent folding and aggregation site. *J Mol Biol* 334(3):477-488.
300. Safar J, Roller PP, Gajdusek DC, & Gibbs CJ, Jr. (1993) Thermal stability and conformational transitions of scrapie amyloid (prion) protein correlate with infectivity. *Protein Sci* 2(12):2206-2216.
301. Smirnovas V*, et al.* (2009) Distinct structures of scrapie prion protein (PrPSc)-seeded versus spontaneous recombinant prion protein fibrils revealed by hydrogen/deuterium exchange. *J Biol Chem* 284(36):24233-24241.
302. Tycko R, Savtchenko R, Ostapchenko VG, Makarava N, & Baskakov IV (2010) The alpha-helical C-terminal domain of full-length recombinant PrP converts to an in-register parallel beta-sheet structure in PrP fibrils: evidence from solid state nuclear magnetic resonance. *Biochemistry* 49(44):9488-9497.
303. Antzutkin ON, Leapman RD, Balbach JJ, & Tycko R (2002) Supramolecular structural constraints on Alzheimer's beta-amyloid fibrils from electron microscopy and solid-state nuclear magnetic resonance. *Biochemistry* 41(51):15436-15450.
304. Baxa U*, et al.* (2007) Characterization of beta-sheet structure in Ure2p1-89 yeast prion fibrils by solid-state nuclear magnetic resonance. *Biochemistry* 46(45):13149-13162.
305. Chen M, Margittai M, Chen J, & Langen R (2007) Investigation of alpha-synuclein fibril structure by site-directed spin labeling. *J Biol Chem* 282(34):24970-24979.
306. Ladner CL*, et al.* (2010) Stacked sets of parallel, in-register beta-strands of beta2-microglobulin in amyloid fibrils revealed by site-directed spin labeling and chemical labeling. *J Biol Chem* 285(22):17137-17147.
307. Lin NS*, et al.* (2010) Molecular structure of amyloid fibrils formed by residues 127 to 147 of the human prion protein. *Chemistry* 16(18):5492-5499.
308. Paravastu AK, Leapman RD, Yau WM, & Tycko R (2008) Molecular structural basis for polymorphism in Alzheimer's beta-amyloid fibrils. *Proc Natl Acad Sci U S A* 105(47):18349-18354.
309. Shewmaker F, Wickner RB, & Tycko R (2006) Amyloid of the prion domain of Sup35p has an in-register parallel beta-sheet structure. *Proc Natl Acad Sci U S A* 103(52):19754-19759.
310. Walsh P, Simonetti K, & Sharpe S (2009) Core structure of amyloid fibrils formed by residues 106-126 of the human prion protein. *Structure* 17(3):417-426.
311. Wickner RB, Dyda F, & Tycko R (2008) Amyloid of Rnq1p, the basis of the [PIN+] prion, has a parallel in-register beta-sheet structure. *Proc Natl Acad Sci U S A* 105(7):2403-2408.
312. Fandrich M, Meinhardt J, & Grigorieff N (2009) Structural polymorphism of Alzheimer Abeta and other amyloid fibrils. *Prion* 3(2):89-93.
313. Anderson M*, et al.* (2006) Polymorphism and ultrastructural organization of prion protein amyloid fibrils: an insight from high resolution atomic force microscopy. *J Mol Biol* 358(2):580-596.
314. Cohen FE*, et al.* (1994) Structural clues to prion replication. *Science* 264(5158):530-531.
315. Harper JD & Lansbury PT, Jr. (1997) Models of amyloid seeding in Alzheimer's disease and scrapie: mechanistic truths and physiological consequences of the time-dependent solubility of amyloid proteins. *Annu Rev Biochem* 66:385-407.

316. Lansbury PT (1994) Mechanism of scrapie replication. *Science* 265(5178):1510.
317. Soto C, Saborio GP, & Anderes L (2002) Cyclic amplification of protein misfolding: application to prion-related disorders and beyond. *Trends Neurosci* 25(8):390-394.
318. Barria MA, Mukherjee A, Gonzalez-Romero D, Morales R, & Soto C (2009) De novo generation of infectious prions in vitro produces a new disease phenotype. *PLoS Pathog* 5(5):e1000421.
319. Makarava N, Savtchenko R, & Baskakov IV (2013) Selective amplification of classical and atypical prions using modified protein misfolding cyclic amplification. *J Biol Chem* 288(1):33-41.
320. Morales R, Duran-Aniotz C, Diaz-Espinoza R, Camacho MV, & Soto C (2012) Protein misfolding cyclic amplification of infectious prions. *Nature protocols* 7(7):1397-1409.
321. Pastrana MA*, et al.* (2006) Isolation and characterization of a proteinase K-sensitive PrPSc fraction. *Biochemistry* 45(51):15710-15717.
322. Weber P*, et al.* (2007) Generation of genuine prion infectivity by serial PMCA. *Veterinary microbiology* 123(4):346-357.
323. Sailer A, Bueler H, Fischer M, Aguzzi A, & Weissmann C (1994) No propagation of prions in mice devoid of PrP. *Cell* 77(7):967-968.
324. Brandner S, Isenmann S, Kuhne G, & Aguzzi A (1998) Identification of the end stage of scrapie using infected neural grafts. *Brain Pathol* 8(1):19-27.
325. Brandner S*, et al.* (1996) Normal host prion protein (PrPC) is required for scrapie spread within the central nervous system. *Proc Natl Acad Sci U S A* 93(23):13148-13151.
326. Chesebro B*, et al.* (2005) Anchorless prion protein results in infectious amyloid disease without clinical scrapie. *Science* 308(5727):1435-1439.
327. Hetz C, Maundrell K, & Soto C (2003) Is loss of function of the prion protein the cause of prion disorders? *Trends in molecular medicine* 9(6):237-243.
328. Kessels HW, Nguyen LN, Nabavi S, & Malinow R (2010) The prion protein as a receptor for amyloid-beta. *Nature* 466(7308):E3-4; discussion E4-5.
329. Kudo W*, et al.* (2012) Cellular prion protein is essential for oligomeric amyloid-beta-induced neuronal cell death. *Hum Mol Genet* 21(5):1138-1144.
330. Sorice M*, et al.* (2012) Trafficking of PrPc to mitochondrial raft-like microdomains during cell apoptosis. *Prion* 6(4):354-358.
331. Ma J & Lindquist S (2002) Conversion of PrP to a self-perpetuating PrPSc-like conformation in the cytosol. *Science* 298(5599):1785-1788.
332. Stewart RS, Piccardo P, Ghetti B, & Harris DA (2005) Neurodegenerative illness in transgenic mice expressing a transmembrane form of the prion protein. *J Neurosci* 25(13):3469-3477.
333. Norstrom EM, Ciaccio MF, Rassbach B, Wollmann R, & Mastrianni JA (2007) Cytosolic prion protein toxicity is independent of cellular prion protein expression and prion propagation. *J Virol* 81(6):2831-2837.
334. Roucou X, Guo Q, Zhang Y, Goodyer CG, & LeBlanc AC (2003) Cytosolic prion protein is not toxic and protects against Bax-mediated cell death in human primary neurons. *J Biol Chem* 278(42):40877-40881.
335. Rane NS, Kang SW, Chakrabarti O, Feigenbaum L, & Hegde RS (2008) Reduced translocation of nascent prion protein during ER stress contributes to neurodegeneration. *Developmental cell* 15(3):359-370.
336. Emerman AB, Zhang ZR, Chakrabarti O, & Hegde RS (2010) Compartment-restricted biotinylation reveals novel features of prion protein metabolism in vivo. *Mol Biol Cell* 21(24):4325-4337.
337. Kovacs GG*, et al.* (2002) Mutations of the prion protein gene phenotypic spectrum. *J Neurol* 249(11):1567-1582.

338. Tateishi J, Kitamoto T, Hoque MZ, & Furukawa H (1996) Experimental transmission of Creutzfeldt-Jakob disease and related diseases to rodents. *Neurology* 46(2):532-537.
339. Lopez CD, Yost CS, Prusiner SB, Myers RM, & Lingappa VR (1990) Unusual topogenic sequence directs prion protein biogenesis. *Science* 248(4952):226-229.
340. Stewart RS & Harris DA (2001) Most pathogenic mutations do not alter the membrane topology of the prion protein. *J Biol Chem* 276(3):2212-2220.
341. Yost CS, Lopez CD, Prusiner SB, Myers RM, & Lingappa VR (1990) Non-hydrophobic extracytoplasmic determinant of stop transfer in the prion protein. *Nature* 343(6259):669-672.
342. Capellari S*, et al.* (2000) Effect of the E200K mutation on prion protein metabolism. Comparative study of a cell model and human brain. *Am J Pathol* 157(2):613-622.
343. Chasseigneaux S*, et al.* (2006) V180I mutation of the prion protein gene associated with atypical PrPSc glycosylation. *Neurosci Lett* 408(3):165-169.
344. Chen SG*, et al.* (1997) Allelic origin of the abnormal prion protein isoform in familial prion diseases. *Nat Med* 3(9):1009-1015.
345. Daidone I, Di Nola A, & Smith JC (2011) Molecular origin of Gerstmann-Straussler-Scheinker syndrome: insight from computer simulation of an amyloidogenic prion peptide. *Biophys J* 100(12):3000-3007.
346. Eigenbrod S*, et al.* (2011) Comprehensive neuropathologic analysis of genetic prion disease associated with the E196K mutation in PRNP reveals phenotypic heterogeneity. *J Neuropathol Exp Neurol* 70(3):192-200.
347. Gerum C, Schlepckow K, & Schwalbe H (2010) The unfolded state of the murine prion protein and properties of single-point mutants related to human prion diseases. *J Mol Biol* 401(1):7-12.
348. Grasbon-Frodl E*, et al.* (2004) Loss of glycosylation associated with the T183A mutation in human prion disease. *Acta Neuropathol* 108(6):476-484.
349. Gsponer J, Ferrara P, & Caflisch A (2001) Flexibility of the murine prion protein and its Asp178Asn mutant investigated by molecular dynamics simulations. *J Mol Graph Model* 20(2):169-182.
350. Gu Y, Verghese S, Bose S, Mohan M, & Singh N (2007) Mutant prion protein D202N associated with familial prion disease is retained in the endoplasmic reticulum and forms 'curly' intracellular aggregates. *J Mol Neurosci* 32(1):90-96.
351. Guo J, Ren H, Ning L, Liu H, & Yao X (2012) Exploring structural and thermodynamic stabilities of human prion protein pathogenic mutants D202N, E211Q and Q217R. *J Struct Biol* 178(3):225-232.
352. Heske J, Heller U, Winklhofer KF, & Tatzelt J (2004) The C-terminal globular domain of the prion protein is necessary and sufficient for import into the endoplasmic reticulum. *J Biol Chem* 279(7):5435-5443.
353. Hsiao KK*, et al.* (1991) A prion protein variant in a family with the telencephalic form of Gerstmann-Straussler-Scheinker syndrome. *Neurology* 41(5):681-684.
354. Jeong BH*, et al.* (2010) Creutzfeldt-Jakob disease with the V203I mutation and M129V polymorphism of the prion protein gene (PRNP) and a 17 kDa prion protein fragment. *Neuropathol Appl Neurobiol* 36(6):558-563.
355. Kiachopoulos S, Bracher A, Winklhofer KF, & Tatzelt J (2005) Pathogenic mutations located in the hydrophobic core of the prion protein interfere with folding and attachment of the glycosylphosphatidylinositol anchor. *J Biol Chem* 280(10):9320-9329.
356. Kitamoto T*, et al.* (1993) A new inherited prion disease (PrP-P105L mutation) showing spastic paraparesis. *Ann Neurol* 34(6):808-813.
357. Krebs B*, et al.* (2005) Creutzfeldt-Jakob disease associated with an R148H mutation of the prion protein gene. *Neurogenetics* 6(2):97-100.

358. Mishra RS, Bose S, Gu Y, Li R, & Singh N (2003) Aggresome formation by mutant prion proteins: the unfolding role of proteasomes in familial prion disorders. *J Alzheimers Dis* 5(1):15-23.
359. Mishra RS*, et al.* (2002) Cell surface accumulation of a truncated transmembrane prion protein in Gerstmann-Straussler-Scheinker disease P102L. *J Biol Chem* 277(27):24554-24561.
360. Parchi P*, et al.* (1998) Different patterns of truncated prion protein fragments correlate with distinct phenotypes in P102L Gerstmann-Straussler-Scheinker disease. *Proc Natl Acad Sci U S A* 95(14):8322-8327.
361. Petersen RB, Parchi P, Richardson SL, Urig CB, & Gambetti P (1996) Effect of the D178N mutation and the codon 129 polymorphism on the metabolism of the prion protein. *J Biol Chem* 271(21):12661-12668.
362. Shi Q*, et al.* (2012) The diversities of PrP(Sc) distributions and pathologic changes in various brain regions from a Chinese patient with G114V genetic CJD. *Neuropathology* 32(1):51-59.
363. Swietnicki W, Petersen RB, Gambetti P, & Surewicz WK (1998) Familial mutations and the thermodynamic stability of the recombinant human prion protein. *J Biol Chem* 273(47):31048-31052.
364. van der Kamp MW & Daggett V (2010) Pathogenic mutations in the hydrophobic core of the human prion protein can promote structural instability and misfolding. *J Mol Biol* 404(4):732-748.
365. Vanik DL & Surewicz WK (2002) Disease-associated F198S mutation increases the propensity of the recombinant prion protein for conformational conversion to scrapie-like form. *J Biol Chem* 277(50):49065-49070.
366. Vetrugno V*, et al.* (1999) Expression of wild-type and V210I mutant prion protein in human neuroblastoma cells. *Neurosci Lett* 270(1):41-44.
367. Watzlawik J*, et al.* (2006) Prion protein helix1 promotes aggregation but is not converted into beta-sheet. *J Biol Chem* 281(40):30242-30250.
368. Zuegg J & Gready JE (1999) Molecular dynamics simulations of human prion protein: importance of correct treatment of electrostatic interactions. *Biochemistry* 38(42):13862-13876.
369. Wang X, Wang F, Sy MS, & Ma J (2005) Calpain and other cytosolic proteases can contribute to the degradation of retro-translocated prion protein in the cytosol. *J Biol Chem* 280(1):317-325.
370. Helmus JJ, Surewicz K, Nadaud PS, Surewicz WK, & Jaroniec CP (2008) Molecular conformation and dynamics of the Y145Stop variant of human prion protein in amyloid fibrils. *Proc Natl Acad Sci U S A* 105(17):6284-6289.
371. Helmus JJ, Surewicz K, Surewicz WK, & Jaroniec CP (2010) Conformational flexibility of Y145Stop human prion protein amyloid fibrils probed by solid-state nuclear magnetic resonance spectroscopy. *Journal of the American Chemical Society* 132(7):2393-2403.
372. Jones EM*, et al.* (2011) Structural polymorphism in amyloids: new insights from studies with Y145Stop prion protein fibrils. *J Biol Chem* 286(49):42777-42784.
373. Kundu B*, et al.* (2003) Nucleation-dependent conformational conversion of the Y145Stop variant of human prion protein: structural clues for prion propagation. *Proc Natl Acad Sci U S A* 100(21):12069-12074.
374. Lee S & Eisenberg D (2003) Seeded conversion of recombinant prion protein to a disulfide-bonded oligomer by a reduction-oxidation process. *Nat Struct Biol* 10(9):725-730.
375. Shin JI*, et al.* (2008) Deep membrane insertion of prion protein upon reduction of disulfide bond. *Biochem Biophys Res Commun* 377(3):995-1000.
376. Shin JY*, et al.* (2009) Disulfide bond as a structural determinant of prion protein membrane insertion. *Mol Cells* 27(6):673-680.

377. Hebert DN, Foellmer B, & Helenius A (1995) Glucose trimming and reglucosylation determine glycoprotein association with calnexin in the endoplasmic reticulum. *Cell* 81(3):425-433.
378. Ben-Zaken O*, et al.* (2003) Cellular heparan sulfate participates in the metabolism of prions. *J Biol Chem* 278(41):40041-40049.
379. Horonchik L*, et al.* (2005) Heparan sulfate is a cellular receptor for purified infectious prions. *J Biol Chem* 280(17):17062-17067.
380. Lee CI & Chang NY (2010) Characterizing the denatured state of human prion 121-230. *Biophys Chem* 151(1-2):86-90.
381. Papy-Garcia D*, et al.* (2011) Glycosaminoglycans, protein aggregation and neurodegeneration. *Curr Protein Pept Sci* 12(3):258-268.
382. Tang JL, Wu PJ, Wang SC, & Lee CI (2012) Insights into structural properties of denatured human prion 121-230 at melting temperature studied by replica exchange molecular dynamics. *J Phys Chem B* 116(10):3305-3312.
383. Chakrabarti O, Rane NS, & Hegde RS (2011) Cytosolic aggregates perturb the degradation of nontranslocated secretory and membrane proteins. *Mol Biol Cell* 22(10):1625-1637.
384. Davies MJ (2005) The oxidative environment and protein damage. *Biochim Biophys Acta* 1703(2):93-109.
385. Wong BS, Wang H, Brown DR, & Jones IM (1999) Selective oxidation of methionine residues in prion proteins. *Biochem Biophys Res Commun* 259(2):352-355.
386. Levine RL, Berlett BS, Moskovitz J, Mosoni L, & Stadtman ER (1999) Methionine residues may protect proteins from critical oxidative damage. *Mech Ageing Dev* 107(3):323-332.
387. Levine RL, Mosoni L, Berlett BS, & Stadtman ER (1996) Methionine residues as endogenous antioxidants in proteins. *Proc Natl Acad Sci U S A* 93(26):15036-15040.
388. Taggart C*, et al.* (2000) Oxidation of either methionine 351 or methionine 358 in alpha 1-antitrypsin causes loss of anti-neutrophil elastase activity. *J Biol Chem* 275(35):27258-27265.
389. Radzicka A, Pedersen L, & Wolfenden R (1988) Influences of solvent water on protein folding: free energies of solvation of cis and trans peptides are nearly identical. *Biochemistry* 27(12):4538-4541.
390. Kumar RA, Koc A, Cerny RL, & Gladyshev VN (2002) Reaction mechanism, evolutionary analysis, and role of zinc in Drosophila methionine-R-sulfoxide reductase. *J Biol Chem* 277(40):37527-37535.
391. Moskovitz J*, et al.* (2001) Methionine sulfoxide reductase (MsrA) is a regulator of antioxidant defense and lifespan in mammals. *Proc Natl Acad Sci U S A* 98(23):12920-12925.
392. Moskovitz J, Weissbach H, & Brot N (1996) Cloning the expression of a mammalian gene involved in the reduction of methionine sulfoxide residues in proteins. *Proc Natl Acad Sci U S A* 93(5):2095-2099.
393. Wolschner C*, et al.* (2009) Design of anti- and pro-aggregation variants to assess the effects of methionine oxidation in human prion protein. *Proc Natl Acad Sci U S A* 106(19):7756-7761.
394. Choi J*, et al.* (2006) Oxidative damage of DJ-1 is linked to sporadic Parkinson and Alzheimer diseases. *J Biol Chem* 281(16):10816-10824.
395. Binger KJ, Griffin MD, & Howlett GJ (2008) Methionine oxidation inhibits assembly and promotes disassembly of apolipoprotein C-II amyloid fibrils. *Biochemistry* 47(38):10208-10217.
396. Brot N & Weissbach H (1991) Biochemistry of methionine sulfoxide residues in proteins. *Biofactors* 3(2):91-96.

397. Gonias SL, Swaim MW, Massey MF, & Pizzo SV (1988) cis-dichlorodiammineplatinum (II) as a selective modifier of the oxidation-sensitive reactive-center methionine in alpha 1-antitrypsin. *J Biol Chem* 263(1):393-397.
398. Vogt W (1995) Oxidation of methionyl residues in proteins: tools, targets, and reversal. *Free Radic Biol Med* 18(1):93-105.
399. Klee CB, Draetta GF, & Hubbard MJ (1988) Calcineurin. *Adv Enzymol Relat Areas Mol Biol* 61:149-200.
400. Michaelis ML*, et al.* (1996) Decreased plasma membrane calcium transport activity in aging brain. *Life Sci* 59(5-6):405-412.
401. Yao Y*, et al.* (1996) Oxidative modification of a carboxyl-terminal vicinal methionine in calmodulin by hydrogen peroxide inhibits calmodulin-dependent activation of the plasma membrane Ca-ATPase. *Biochemistry* 35(8):2767-2787.
402. Cui ZJ, Han ZQ, & Li ZY (2012) Modulating protein activity and cellular function by methionine residue oxidation. *Amino Acids* 43(2):505-517.
403. Lim JC, Kim G, & Levine RL (2013) Stereospecific oxidation of calmodulin by methionine sulfoxide reductase A. *Free radical biology & medicine* 61C:257-264.
404. Anbanandam A*, et al.* (2005) Mediating molecular recognition by methionine oxidation: conformational switching by oxidation of methionine in the carboxyl-terminal domain of calmodulin. *Biochemistry* 44(27):9486-9496.
405. Martin SF*, et al.* (2007) Coenzyme Q and protein/lipid oxidation in a BSE-infected transgenic mouse model. *Free Radic Biol Med* 42(11):1723-1729.
406. Yun SW, Gerlach M, Riederer P, & Klein MA (2006) Oxidative stress in the brain at early preclinical stages of mouse scrapie. *Exp Neurol* 201(1):90-98.
407. Freixes M, Rodriguez A, Dalfo E, & Ferrer I (2006) Oxidation, glycoxidation, lipoxidation, nitration, and responses to oxidative stress in the cerebral cortex in Creutzfeldt-Jakob disease. *Neurobiol Aging* 27(12):1807-1815.
408. Pamplona R*, et al.* (2008) Increased oxidation, glycoxidation, and lipoxidation of brain proteins in prion disease. *Free Radic Biol Med* 45(8):1159-1166.
409. Brown DR (2005) Neurodegeneration and oxidative stress: prion disease results from loss of antioxidant defence. *Folia Neuropathol* 43(4):229-243.
410. Fernaeus S, Reis K, Bedecs K, & Land T (2005) Increased susceptibility to oxidative stress in scrapie-infected neuroblastoma cells is associated with intracellular iron status. *Neurosci Lett* 389(3):133-136.
411. Lee DW*, et al.* (1999) Alteration of free radical metabolism in the brain of mice infected with scrapie agent. *Free Radic Res* 30(6):499-507.
412. Milhavet O*, et al.* (2000) Prion infection impairs the cellular response to oxidative stress. *Proc Natl Acad Sci U S A* 97(25):13937-13942.
413. Wong BS*, et al.* (2000) Prion disease: A loss of antioxidant function? *Biochem Biophys Res Commun* 275(2):249-252.
414. Requena JR*, et al.* (2004) Oxidation of methionine residues in the prion protein by hydrogen peroxide. *Arch Biochem Biophys* 432(2):188-195.
415. Canello T*, et al.* (2008) Methionine sulfoxides on PrPSc: a prion-specific covalent signature. *Biochemistry* 47(34):8866-8873.
416. Stahl N*, et al.* (1993) Structural studies of the scrapie prion protein using mass spectrometry and amino acid sequencing. *Biochemistry* 32(8):1991-2002.
417. Colombo G, Meli M, Morra G, Gabizon R, & Gasset M (2009) Methionine sulfoxides on prion protein Helix-3 switch on the alpha-fold destabilization required for conversion. *PLoS One* 4(1):e4296.
418. Aguzzi A (2006) Prion diseases of humans and farm animals: epidemiology, genetics, and pathogenesis. *J Neurochem* 97(6):1726-1739.
419. Rutishauser D*, et al.* (2009) The comprehensive native interactome of a fully functional tagged prion protein. *PLoS One* 4(2):e4446.

420. Sigurdson CJ*, et al.* (2009) De novo generation of a transmissible spongiform encephalopathy by mouse transgenesis. *Proc Natl Acad Sci U S A* 106(1):304-309.
421. Gasset M, Baldwin MA, Fletterick RJ, & Prusiner SB (1993) Perturbation of the secondary structure of the scrapie prion protein under conditions that alter infectivity. *Proc Natl Acad Sci U S A* 90(1):1-5.
422. Oien DB*, et al.* (2009) Detection of oxidized methionine in selected proteins, cellular extracts and blood serums by novel anti-methionine sulfoxide antibodies. *Arch Biochem Biophys* 485(1):35-40.
423. Canello T*, et al.* (2010) Oxidation of Helix-3 methionines precedes the formation of PK resistant PrP. *PLoS Pathog* 6(7):e1000977.
424. Kelly JW (1998) The alternative conformations of amyloidogenic proteins and their multi-step assembly pathways. *Current opinion in structural biology* 8(1):101-106.
425. Butterfield DA & Boyd-Kimball D (2005) The critical role of methionine 35 in Alzheimer's amyloid beta-peptide (1-42)-induced oxidative stress and neurotoxicity. *Biochim Biophys Acta* 1703(2):149-156.
426. Butterfield DA & Bush AI (2004) Alzheimer's amyloid beta-peptide (1-42): involvement of methionine residue 35 in the oxidative stress and neurotoxicity properties of this peptide. *Neurobiology of aging* 25(5):563-568.
427. Clementi ME*, et al.* (2005) Abeta(31-35) and Abeta(25-35) fragments of amyloid beta-protein induce cellular death through apoptotic signals: Role of the redox state of methionine-35. *FEBS Lett* 579(13):2913-2918.
428. Johansson AS*, et al.* (2007) Attenuated amyloid-beta aggregation and neurotoxicity owing to methionine oxidation. *Neuroreport* 18(6):559-563.
429. Maiti P, Lomakin A, Benedek GB, & Bitan G (2010) Despite its role in assembly, methionine 35 is not necessary for amyloid beta-protein toxicity. *J Neurochem* 113(5):1252-1262.
430. Naslund J*, et al.* (1994) Relative abundance of Alzheimer A beta amyloid peptide variants in Alzheimer disease and normal aging. *Proc Natl Acad Sci U S A* 91(18):8378-8382.
431. Budisa N*, et al.* (1998) Atomic mutations in annexin V--thermodynamic studies of isomorphous protein variants. *Eur J Biochem* 253(1):1-9.
432. Gassner NC, Baase WA, Hausrath AC, & Matthews BW (1999) Substitution with selenomethionine can enhance the stability of methionine-rich proteins. *J Mol Biol* 294(1):17-20.
433. Hakansson K, Broder D, Wang AH, & Miller CG (2000) Crystallization of peptidase T from Salmonella typhimurium. *Acta crystallographica. Section D, Biological crystallography* 56(Pt 7):924-926.
434. Le DT*, et al.* (2008) Analysis of methionine/selenomethionine oxidation and methionine sulfoxide reductase function using methionine-rich proteins and antibodies against their oxidized forms. *Biochemistry* 47(25):6685-6694.
435. Wernimont AK*, et al.* (2003) Crystal structure and dimerization equilibria of PcoC, a methionine-rich copper resistance protein from Escherichia coli. *Journal of biological inorganic chemistry : JBIC : a publication of the Society of Biological Inorganic Chemistry* 8(1-2):185-194.
436. Yamniuk AP, Ishida H, Lippert D, & Vogel HJ (2009) Thermodynamic effects of noncoded and coded methionine substitutions in calmodulin. *Biophysical journal* 96(4):1495-1507.
437. Griffiths NM, Stewart RD, & Robinson MF (1976) The metabolism of [75Se]selenomethionine in four women. *The British journal of nutrition* 35(3):373-382.
438. Rayman MP (2008) Food-chain selenium and human health: emphasis on intake. *The British journal of nutrition* 100(2):254-268.

439. Schrauzer GN (2000) Selenomethionine: a review of its nutritional significance, metabolism and toxicity. *The Journal of nutrition* 130(7):1653-1656.
440. Yokoyama S (2003) Protein expression systems for structural genomics and proteomics. *Current opinion in chemical biology* 7(1):39-43.
441. Butterfield DA & Boyd-Kimball D (2004) Amyloid beta-peptide(1-42) contributes to the oxidative stress and neurodegeneration found in Alzheimer disease brain. *Brain Pathol* 14(4):426-432.
442. Maiti P, Piacentini R, Ripoli C, Grassi C, & Bitan G (2011) Surprising toxicity and assembly behaviour of amyloid beta-protein oxidized to sulfone. *Biochem J* 433(2):323-332.
443. Arteel GE, Briviba K, & Sies H (1999) Protection against peroxynitrite. *FEBS Lett* 445(2-3):226-230.
444. Assmann A, Briviba K, & Sies H (1998) Reduction of methionine selenoxide to selenomethionine by glutathione. *Arch Biochem Biophys* 349(1):201-203.
445. Zhang Y, Swietnicki W, Zagorski MG, Surewicz WK, & Sonnichsen FD (2000) Solution structure of the E200K variant of human prion protein. Implications for the mechanism of pathogenesis in familial prion diseases. *J Biol Chem* 275(43):33650-33654.
446. Kim SJ & Hegde RS (2002) Cotranslational partitioning of nascent prion protein into multiple populations at the translocation channel. *Mol Biol Cell* 13(11):3775-3786.
447. Anelli T & Sitia R (2008) Protein quality control in the early secretory pathway. *EMBO J* 27(2):315-327.
448. Hartl FU & Hayer-Hartl M (2009) Converging concepts of protein folding in vitro and in vivo. *Nat Struct Mol Biol* 16(6):574-581.
449. Kim PS & Arvan P (1998) Endocrinopathies in the family of endoplasmic reticulum (ER) storage diseases: disorders of protein trafficking and the role of ER molecular chaperones. *Endocr Rev* 19(2):173-202.
450. Lisa S*, et al.* (2010) The structural intolerance of the PrP alpha-fold for polar substitution of the helix-3 methionines. *Cellular and molecular life sciences : CMLS* 67(16):2825-2838.
451. Iqbal K, Liu F, Gong CX, Alonso Adel C, & Grundke-Iqbal I (2009) Mechanisms of tau-induced neurodegeneration. *Acta Neuropathol* 118(1):53-69.
452. Kopke E*, et al.* (1993) Microtubule-associated protein tau. Abnormal phosphorylation of a non-paired helical filament pool in Alzheimer disease. *J Biol Chem* 268(32):24374-24384.
453. Sun Q & Gamblin TC (2009) Pseudohyperphosphorylation causing AD-like changes in tau has significant effects on its polymerization. *Biochemistry* 48(25):6002-6011.
454. Oien DB & Moskovitz J (2008) Substrates of the methionine sulfoxide reductase system and their physiological relevance. *Curr Top Dev Biol* 80:93-133.
455. Stadtman ER (2006) Protein oxidation and aging. *Free Radic Res* 40(12):1250-1258.
456. Hart T*, et al.* (2009) Folding kinetics of the human prion protein probed by temperature jump. *Proc Natl Acad Sci U S A* 106(14):5651-5656.
457. Hirschberger T*, et al.* (2006) Structural instability of the prion protein upon M205S/R mutations revealed by molecular dynamics simulations. *Biophysical journal* 90(11):3908-3918.
458. Winklhofer KF*, et al.* (2003) Determinants of the in vivo folding of the prion protein. A bipartite function of helix 1 in folding and aggregation. *J Biol Chem* 278(17):14961-14970.
459. Krause RJ & Elfarra AA (2009) Reduction of L-methionine selenoxide to seleno-L-methionine by endogenous thiols, ascorbic acid, or methimazole. *Biochemical pharmacology* 77(1):134-140.
460. Smith JL & Thompson A (1998) Reactivity of selenomethionine--dents in the magic bullet? *Structure* 6(7):815-819.

461. Capellari S*, et al.* (1999) Prion protein glycosylation is sensitive to redox change. *J Biol Chem* 274(49):34846-34850.
462. Orsi A & Sitia R (2007) Interplays between covalent modifications in the endoplasmic reticulum increase conformational diversity in nascent prion protein. *Prion* 1(4):236-242.
463. Muramoto T*, et al.* (1997) Heritable disorder resembling neuronal storage disease in mice expressing prion protein with deletion of an alpha-helix. *Nat Med* 3(7):750-755.
464. Tabrett CA*, et al.* (2010) Changing the solvent accessibility of the prion protein disulfide bond markedly influences its trafficking and effect on cell function. *Biochem J* 428(2):169-182.
465. Yanai A, Meiner Z, Gahali I, Gabizon R, & Taraboulos A (1999) Subcellular trafficking abnormalities of a prion protein with a disrupted disulfide loop. *FEBS Lett* 460(1):11-16.
466. Lucassen R, Nishina K, & Supattapone S (2003) In vitro amplification of protease-resistant prion protein requires free sulfhydryl groups. *Biochemistry* 42(14):4127-4135.
467. Wang F, Wang X, Yuan CG, & Ma J (2010) Generating a prion with bacterially expressed recombinant prion protein. *Science* 327(5969):1132-1135.

Apéndice 1

Introduction

Prion disorders are dominant gain-of-function neurodegenerations whose pathogenesis is linked to misfolded forms of the cellular prion protein (PrPC), including the prion PrP^{Sc} and the neurotoxic ^{Ctm}PrP (1-4). PrP^{Sc} is an aggregated and protease resistant β-sheet-enriched conformer of PrP^{C}, which self-perpetuates by the templating the conversion of cell surface PrP^{C} (1, 4). In contrast, ^{Ctm}PrP is an intracellular transmembrane form generated at the ER with neurotoxic properties (1, 5, 6).

The long-standing hypothesis of prion biology is that the distinct biological and physicochemical properties separating PrP^{C} and PrP^{Sc} relate only to the conformational differences of the C-terminal domain, which adopts a major globular α-fold in PrP^{C} and displays a high content of β-sheet structure in PrP^{Sc} (7-15). However, the populations of PrP^{C} and PrP^{Sc} also differ in the redox state the methionines of Helix-3, suggesting a posible role for these residues in facilitating the structural change (16-19). The fact that these specific Met residues are oxidized in PrP^{Sc} is particularly intriguing since they are the most buried residues among methionines in the 3D PrP α-fold and thus are less accessible to reactive oxygen species (ROS) (20). However, if and when they are oxidized, Helix-3 Met residues may not be targeted by the methionine reductase (Msr) system, which reverses oxidation of accessible Met residues (21, 22). Theoretical investigations have predicted that the polarity increase of Met 206 and 213 residues upon sulfoxidation may induce destabilization of the PrP helical conformation (17). This destabilization in turn determines a decrease in the internal dynamic coordination of the native state, favoring the transition to alternative conformational states.

Aims

Since the enunciation of the prion hypothesis, research has focused on the mechanism by which a native PrP^{C} structure reorganizes and acquires either the self-propagative features like those of PrP^{Sc} or the cytotoxic properties (10, 14, 23). With such background, in this work we have pursued:

1. To design and generate immunological reagents for the in vivo metabolic timing of Met oxidation moment along conversion from PrP^{C} to PrP^{Sc} conversion.

2. To design and generation of methionine sulfoxide (MetO) models for their used in recombinant chains to experimentally test their effect on PrP conformation and stability.

3. To design and generate models to evaluate the effect of Met/ SeMet metabolic mutations on amyloid formation.

4. To design and generate models of PrP with labile folds to determine the role of *the in vivo* folding pathway of toxic PrP formation.

Results and Discusion

Design and generation of immunological reagents for the in vivo metabolic timing of Met oxidation moment along conversion from PrP^{C} to PrP^{Sc} conversion. We generated specific Ab

to reduced and sulfoxidized Helix-3 PrP forms. For that, we immunized rabbits with several KLH-coupled peptides with an array of small PrP peptides to determine the recognition site of each antibody on the protein sequence by competition, and then tested against prion-infected samples. The antiserum raised against the KLH-conjugated and oxidized TC peptide (pAb RTC) and the antiserum raised against the reduced VC peptide (pAb RVC) recognized Mo and Hu PrP^{C}, although they did not recognize Ha and Bo PrP's. Then, we examined the capacity of the RTC and RVC pAbs to recognize PrP^{Sc} forms. The pAb RVC could not detect all of $HuPrP^{Sc}$ and detected only low levels of $MoPrP^{Sc}$ after PK digestion. When we used MMA treatment (specific MetO reducing agent (24)), the pAb RVC easily recognized both human and mouse PrP^{Sc} at detection levels similar to those of the α-PrP mAb 6H4 both before and after MMA treatment.

Once obtained, the immunological reagent were used to establish whether oxidation of Met residues is essential for the conversion of PrP^{C} to PrP^{Sc}. We asked whether MetO occurs first on PrP^{C} or whether oxidation is a delayed effect related to the long-term accumulation and reduced clearance of PK resistant and misfolded prion protein in the brains of the affected subjects. To separate these mechanistic possibilities, we studied by pAb RVC the oxidation status of newly formed PK resistant PrP^{Sc} generated in cells permanently infected with prions (these cells constantly proliferate, PrP^{Sc} produced by them can be considered relatively new). pAb RVC failed to detect PK resistant PrP forms in any of the infected cell systems and barely detected bands characteristic for PrP^{Sc} before PK digestion. These results indicate that newly made PrP^{Sc} may be quantitatively oxidized. Similar to brain PrP^{Sc}, detection of cell PrP^{Sc} by the pAb RVC could be restored in both cell lines when samples were reduced by MMA before being subjected to immunoblotting. This finding is consistent with the notion that the lack of PrP^{Sc} recognition by RVC indeed relates to the oxidative state.

Previous studies on prion-infected cells demonstrated that the formation of PrP^{Sc} from PrP^{C} is a slow multistep process, which may include a variety of intermediate PrP states (25, 26). To investigate whether PrP Helix-3 Met oxidation occurs before the acquisition of PK resistance, we examined the oxidation state of putative PK sensitive intermediate forms. With the pAb RVC, no PrP forms were detected in any of the intermediate or heavy fractions, except low levels of mouse PrP^{Sc} in the heaviest fraction. Following PK digestion, the PrP signal mostly disappeared form all infected fractions, except traces in the last fraction of the mouse gradient. Similar results were obtained for brain samples from sporadic CJD patients. Since the lack of recognition of PrP by the pAb RVC in the intermediate gradient fractions indicates that PrP^{Sc}-sen forms are as oxidized as the PrP^{Sc}-res forms, we conclude that oxidation of PrP accompanies the conformational change required for PrP aggregation and precedes the acquisition of PK resistance during PrP^{Sc} formation.

The pAb raised against the HuPrP peptide containing E at position 200 (pAb RGM) did not recognize PK sensitive PrP forms expressed in fibroblasts from homozygous E200K patients, suggesting that the pAb RGM specifically detected wt PrP as opposed to the mutant E200K form (27). Due to the general belief at the time that no covalent modification separates PrP^{C} from PrP^{Sc} and that the only difference between the mutant and wt PrP proteins could be the mutation itself, it was concluded that in heterozygous E200K patients only the mutant protein (K at codon 200) acquires the PK resistance property during disease (27). Based on the results described above for the pAb RVC (failed to detect PK PrP form in brains of heterozygous E200K PrP fCJD patients), we now investigated whether pAb RGM does not recognize E200K PrP^{Sc} specifically or otherwise cannot detect all forms of human PrP^{Sc}, as described above for pAb RVC. We found that the activity of pAb RGM, which detected only mouse and human PrP, was totally inhibited by several peptides covering the Helix-3 Met residues, including the one

comprising the 203–211 PrP sequence. This prevents the residue at codon 200, regardless E or K, from forming part of the pAb RGM epitope, indicating that the lack of recognition of the mutant PrP by pAb RGM is not related to the presence of K instead of E at position 200. In addition, and since the epitope of this antibody does not comprise M213, these results constitute the first direct evidence that oxidation of M206 (and/or M205) can also be considered as a covalent signature of PrP^{Sc}, as predicted by the theoretical studies (17). In addition, the rHuPrP E200K was recognized by pAb DZS18, a pAb raised against a MetO rich maize repetitive sequence, which was shown to recognize enriched PrP^{Sc} as well as other oxidized proteins (28). These results suggest that Helix-3 methionines in PrP E200K may undergo facilitated or spontaneous oxidation both in cells (27) and in its α-folded recombinant form. Indeed, the monomers of wt and E200K HuPrP (23–231) are indistinguishable by far ultraviolet CD spectroscopy at 25 ºC and pH 4.5, but they differ in their thermal denaturation profile. Curve fitting yielded Tm values of 60 ± 0.5 ºC and 54.5 ± 1 ºC for the wt and E200K chains, which agrees with previously reported destabilization of this mutant PrP under a different setup (29). These results, as well as previous experiments showing charged-induced alterations of E200K PrP (30) suggest that changed dynamics of Helix-3 in the mutated protein might favor transient exposures of the contained methionines to ROS.

Design and generation of methionine sulfoxide (MetO) models for their used in recombinant chains to experimentally test their effect on PrP conformation and stability. To generate MetO models we proposed M-to-S mutations because Ser provide the polar change of the sulfoxidation of methionine side chains while retaining the secondary structure propensities (31). To determine whether this polar substitution also behaves as a structural destabilizer, we first analyzed the impact of the mutations on the dynamic evolution of the C-terminal domain α-fold via MD simulations in HuPrP(125-229) and compared the results with those previously obtained for the sulfóxido variants (17). Summarizing, the theorical studies show that the M-to-S substitutions indeed trigger transmissible structural signals as found for the oxidative modifications (17). Then, the polarity increase in the side chain provided by the M-to-S replacement perturbs the global coordination and essential dynamics of the α-fold native state. However, its destabilizing potency differs from that observed for the sulfoxidation of equivalent methionines.

Based on the previous considerations, we generated the full-length M206S, M213S, and M206S-M213S mutants using the HaPrP(23–231) wt chain as a template. We included the M134S and M154S mutations, as these residues are also conserved and flank secondary structure elements (Strand-1 and Helix-1, respectively). In addition, we prepared the mutant M213L as a control for site substitution. We began the study of the effect of the M-to-S mutations on the conformation and stability of the HaPrP(23–231) α-fold using dynamic light scattering (DLS). At pH 4.5 and at 15 ºC, all proteins being studied yield an Rh of about 3.7 ± 0.5 nm. Therefore, they can be described essentially as monomers. However, only the M206S, M213S, and M206S-M213S mutants permit the detection of an additional minor species (amounting to about 15% of the total) featured by a higher Rh (9.2 ± 0.4 nm), suggesting the presence of soluble oligomers. Experiments performed at pH 6.5 yielded essentially similar results.

Then, to study the conformational features of HaPrP(23–231) wt and its M-to-S mutants were used far- and near-UV CD to probe the secondary and tertiary structures, respectively. At pH 4.5 and pH 6.5, a comparison of the far-UV CD spectra shows that only M206S and M213S mutations, singly or in combination, cause a drastic change. This change is characterized by an increase in the H205/H220 ratio (from 1.07 up to 2.0) and indicates the

presence of non-native secondary structures. As in the previous spectral region, the M206S and M213S mutations, both singly or combined, also altered the near-UV spectrum. This is not true for the M134S and M154S mutations. Here the observed spectral changes, in which the aromatic bands but not the disulfide bond region (around 260 nm) are affected, show the disruption of the native tertiary structure. The CD studies taken together indicate that the replacement of M by S at positions 206, 213, and both, but not at positions M134 or M154, preclude the adoption of the conventional α-fold and induce partially unstructured states. Interestingly, replacing M213 by L rather than S retains the conformational features of the wt supporting the importance of the polarity of the side chain for the observed perturbations. In addition, the Helix-3 M-to-S mutants displayed an enhanced binding of bis-ANS, indicating an increase in their solvent-exposed hydrophobic surfaces and again their partially structured state. Given that structural changes have large impacts on stability, we further probed the effect of the M-to-S substitutions using thermal denaturation experiments. Under the conditions used, the thermal unfolding of the wt, M134S, M154S, and M213L proteins was similar at pH 6.5 (about 57 ± 1 ºC), whereas at pH 4.5 the M134S and M154S mutants unfold at a lower Tm than the wt (56 ± 0.5 and 61 ± 0.5 ºC, respectively). Conversely, the thermal denaturation of M206S, M213S, and the M206S-M213S HaPrP(23–232) was less cooperative and occurred at significantly lower temperatures (38 and 40 ºC at both pH 6.5 and 4.5, respectively). Taken together, these results indicate that the M-to-S substitutions in Helix-3 do indeed prevent the adoption of the conventional α-fold and induce a partially structured state.

Bearing in mind that partially structured states are key precursors for the formation of amyloid fibrils through their allowance for rearrangement of ‘‘amyloid-prone sequence regions’’ (7, 9, 32-34), we then asked whether the structural states formed by M-to-S replacement in Helix 3 could permit or facilitate oligomerization pathways that are impeded to the native fold. The aggregation kinetics, followed by turbidity measurements, show that all proteins at concentrations above 13 μM undergo a time-dependent aggregation upon increasing the ionic strength to 0.35 M NaCl. However, the turbidity increase was significantly larger for the Helix-3 methionine mutants than for the wt, M134S, M154S, and M213L mutants. Under similar conditions, the kinetics of ThT binding reveal the occurrence of a significant fibrillation process in the M206S, M213S, and M206S-M213S mutants. This process was negligible in the wt, M134S, M154S, and M213L HaPrP(23–231) forms. Analyzing the topographical images of the Helix-3 methionine mutants revealed the presence of aggregates constituted by irregular rod-like structures with diameters of about 25–50 nm. In conclusion, these results indicate that under denaturant-free conditions, the partially structured state that is induced by the M-to-S substitution in Helix-3 undergoes a polymerization process leading to the formation of amyloid protofibrils.

Design and generation of models to evaluate the effect of Met/ SeMet metabolic mutations on amyloid formation. We used synthetic peptides to evaluate the ability of SeM to modify the aggregation properties of pro-amyloid peptides like Aβ40 (M35) and HuPrP(106-140) (M109, M112, M129 and M134). We started with set up a ThT binding kinetics assay. To this end, either wt Aβ40 (Met35) or [SeM35]Aβ40 were incubated at 20–40 mM concentration in PBS in the presence of 15 mM ThT and the increase in fluorescence emission as consequence of its binding to cross β-sheets was monitored. Wt Aβ40 at 20 μM and 30 ºC provokes a time-dependent increase in ThT fluorescence compatible with the known fibrillation process (35). In contrast, incubation of [SeM35]Aβ40 under similar conditions did not cause any detectable change in ThT fluorescence. Increasing [SeM35]Aβ40 concentration up to 200 μM and the incubation time up to 1 week did not provoke any significant or additional change. By Atomic Force Microscopy (AFM), as expected from the ThT fluorescence readings, Aβ40 assembles into long (>200 nm length) and thin (7 nm height and about 2640 nm diameter) fibrils. In

contrast, [SeM35]Aβ40 uniquely yields globular aggregates characterized by 3.5–7 nm height and 35 nm average diameter, corroborating the impairment of the fibrillation process.

In HuPrP(106-140) we investigated a non-oxidizable version (all-V, all four Met replaced by Val), as well as single SeM replacements with Val at the other positions. At 30 ºC, 20 mM concentration in PBS and with mild orbital shaking, both all-M and all-V HuPrP(106–140) undergo fibrillation, though with notable kinetic differences. Thus, all-M HuPrP(106–140) exhibits the kinetic profile of a highly cooperative process, characterized by an average lag time of 33.8 ± 2.0 h and a final arbitrary ThT fluorescence intensity of 60 ± 5, whereas fibrillation of the all-V variant is characterized by a lag-phase of about 16.4 ± 2.0 h and a final ThT intensity reading of 40 ± 4. Placing SeM at position 109 slightly reduces both the lag phase and the final ThT intensity of the fibrillation kinetics. However, the absence of a clear statistical significance in these changes suggests that SeM109 behaves as an all-Val variant. On the contrary, placing SeM at position 112 significantly increases the lag time to 19.7 ± 1.2 h with no effects in the maximum ThT intensity. Surprisingly, the introduction of SeM at position 129 drastically impairs the fibrillation process. Prolonged incubations (up to 1 week) yielded ThT intensity increases below 2.5 with averaged lag phases of >72 h. Along similar lines but to a lesser extent, placing SeM at position 134 allowed a slight fibrillation process featured by a final ThT intensity of 8 and a lag time of 31.5 ± 2.0 h. To confirm these findings we analyzed by AFM the products of the aggregation reactions. In agreement with the ThT kinetics, the all-M, all-V, SeM109 and SeM112 versions of HuPrP(106–140) yielded fibrillar structures, of which those formed by SeM112 differed notably from the others by appearing as regular straight rods with a high homogeneity in length. On the contrary, the reaction product of the SeM129 analog yielded mainly amorphous aggregates with rarely the presence of fibrillar aggregates. The SeM134 peptide displayed an intermediate behaviour, showing few but detectable fibrillar assemblies. Taken together these data indicate that, as for the case of Aβ40, SeM incorporation also impairs HuPrP(106–140) fibrillation, but in this case the inhibitory process is highly dependent on the replacement site.

By far-UV CD for comparison with previous reports (36), the fibrillar aggregates of All-M, all-V and SeM109 peptides shared a common spectrum, featured by a double minimum at 208 and 220 nm suggesting an altered β-sheet structure. On the contrary, the spectrum of the SeM112 analog displayed the features of a pure β-sheet structure. The results thus support that, depending on its incorporation site, SeM can modulate the secondary structure and subsequently sculpture its self-assembly shape. Consistent with the previous findings and with the fact that Met substitution by SeM would be hardly ever quantitative under physiological conditions, we next tested the capacity of the SeM containing sequences to modulate the amyloid formation process of the unlabelled sequences. Co-incubation of [SeM35]Aβ40 with Aβ40 and with its longer and more fibrillogenic form Aβ42 impaired their fibrillation process. Similarly, in the HuPrP(106–140) case, co-incubation of 10 Mm SeM129 analog with 10 µM of either all-M or all-V peptides inhibited amyloid formation. On the other hand, SeM109 and SeM112 when mixed 1:1 with either all-V or all-M peptides altered the ThT binding kinetics, imposing their characteristic lag-phase and allowing the final ThT intensity of the SeM-free peptide.

To investigate the structure–activity relationship of the SeM substitutions we analyzed the effect of the aggregation reaction products on the viability of rodent primary cortical neurons. All peptides except [SeM35]Aβ40 and the SeM129 and SeM134-analogs of HuPrP(106–140) and their mixtures have completed their fibrillation process as judged by parallel ThT reading, and the untreated cells yielded cell viability values that amounted to 97.5 ± 1%. [SeM35]Aβ40 reduced cell death to 3± 1.5%, thereby excluding any relationship between

its assemblies and the highly neurotoxic nonfibrillar oligomers formed by Aβ peptides [27]. SeM129 and to a lesser extent SeM134 caused minor effects on cell viability (1.1 ± 0.5 and 4 ± 0.6, respectively). Mixing SeM129 1:1 with either all-M or all-V decreases cell death extent to almost abrogation, and the effect cannot be explained solely in terms of the reduction all-M and all-V concentration as shown by the concentration controls. On the contrary, mixing the SeM134 analog 1:1 with either all-M or all-V reproduces the cell death percentage of diluted all-M and all-V peptides.

Design and generation of models of PrP with labile folds to determine the role of *the in vivo* folding pathway of toxic PrP formation. We used α3M mutants like models of labile structures PrP. To determine the role of this mutations in living cells we generated Met to Ser substitutions in the α-helix 3 both in HaPrP (M206S, M213S, DS) and MoPrP (M205S, M212S, DS). We also generated control substitutions at other conserved methionines (M134S and M154S), a substitution that preserves both the conformation and stability of the recombinant chain (M213L) and a pathogenic mutant known to alter *in vivo* PrP folding (A117V) (2, 3, 6, 37). Transient expression of HaPrP and MoPrP constructs revealed specific cytotoxicity of PrPα3M mutants. WT and the control M134S, M154S, and M213L mutations all had no effect on cell viability, whereas HaPrPα3M mutants caused approximately ≥ 40% cell death (independent of specie and cell type). In addition, PrPWT had no or little effect on PrPDS toxicity in this setup. Interestingly, HaPrP A117V also induced 30% cell death, suggesting possible similarities in the pathogenic process. Altogether, these results indicate that PrPα3M mutants exert a very high level of cell toxicity upon transient expression which is not influenced by cell type and co-expression of WT PrP.

After determining that PrPα3M mutants are highly toxic, we set out to characterize the molecular basis of such toxicity. Expression of WT and the control M134S and M154S mutants produced the classical 24–38 kDa banding pattern for both HaPrP and MoPrP constructs and in both $PrP^{-/-}$ cell lines. However, expression of PrPα3M mutants yielded single bands of approximately 30 kDa. WT HaPrP was sensitive to PNGase F and resistant to Endo H digestions, the glycan attached to HaPrPDS was sensitive to both PNGase F and Endo H digestion. These results indicate an immature glycosylation of the PrPDS mutant. To test for the presence of a GPI anchor, the PNGase F deglycosylated products were further digested with PIPLC. The upward shift in the bands of WT HaPrP and HaPrPDS after PIPLC treatment indicates the removal of the hydrophobic moiety and supported the presence of the GPI anchor in both chains. Also, the size similarity ofWTHaPrP and HaPrPDS bands upon combined PNGase F and PIPLC digestion indicates that in both PrP chains the N-terminal signal sequence has been removed. To assess the conformation adopted by PrPα3M mutants, we analyzed the detergent solubility and the resistance to proteases of HaPrPDS (1, 6). WTHaPrP was completely soluble in detergents whereas HaPrPDS partitioned almost entirely into the insoluble fraction. Nonetheless, both proteins were fully digested by PK under harsh (37 °C) and mild (4 °C) digestion conditions, supporting the absence of prototypic PrP^{Sc} characteristics.

Once discarded the generation of *bona fide* and PK-resistant PrP^{Sc}, we next analyzed the membrane topology of HaPrPα3M, using HaPrPA117V as control for acquiring ^{Ctm}PrP topology. Digestion of microsomes from cells expressing HaPrPM206S, HaPrP213S, HaPrPDS and HaPrPC214A yielded the same 21-kDa fragment as identified for HaPrP A117V. In summary, these results indicate that HaPrPα3M folding results in acquisition of a transmembrane ^{Ctm}PrP topology, mainly an intracellular conformer. We performed indirect fluorescence microscopy studies to address the subcellular location upon transient transfection into HpL cells. As expected, WT HaPrP and its control M134S and M213L mutants were located along the secretory pathway in route to the plasma membrane. In contrast,

HaPrPα3M and HaPrPC214A mutants were found mostly intracellularly displaying an excess of intracellular vesicle structures containing. Thus, the abnormal intracellular distribution of PrPα3M mutants observed here by microscopy is in line with our biochemical analysis showing immature glycosylation, tendency to aggregate, and ^{Ctm}PrP topology.

A similar toxicity as observed here for the PrPα3M mutants has been described previously for the MoPrPC213A mutant and ascribed to a failure of the oxidative folding (38, 39). Indeed, this mutant lacks the intramolecular disulfide bond which is a key determinant for the stability of the α2–α3 subdomain both *in vivo* and *in vitro* (39-43). We analyzed the state of the intramolecular disulfide bond for the PrPα3M mutants this assay clearly showed that WT HaPrP and its M134S, M154S, and M213L mutants formed stable disulfide bonds unlike the PrPα3M, A117V, and C214A mutants. Thus, these data suggest that a key structural feature of toxic mutants forming ^{Ctm}PrP could be the presence of free thiols.

Conclusions

1. Oxidation of helix-3 methionines of PrP, the most buried methionine residues, is a metabolic process taking place in the conversion pathway conversion. Oxidation precedes the acquisition of resistance to proteases, and is common to all forms of genetic and infectious PrP^{Sc}.

2. Structural flexibility caused by the polarity of the methionines sulfoxides of helix-3 PrP substitutions reproduced using M-to-S theoretical calculations.

3. Recombinant HaPrP chains with the artificial mutations M206S and M213S, singly or combined, adopt labile α folds that easily evolve to protofibrils aggregate under native conditions.

4. Substitution of M-to-SeM, a metabolic mutation depending on diet, on pro-amyloid sequences regulates the formation, the shape and toxicity of amyloid fibers with site-specific.

5. Cellular expression based on labile folding artificial mutants M206S and/or M213S causes an unprecedented toxicity due to its stabilization as ^{Ctm}PrP, as a consequence of oxidative folding impairement.

Bibliography

1. Aguzzi A & Calella AM (2009) Prions: protein aggregation and infectious diseases. *Physiological reviews* 89(4):1105-1152.
2. Hegde RS*, et al.* (1998) A transmembrane form of the prion protein in neurodegenerative disease. *Science* 279(5352):827-834.
3. Hegde RS*, et al.* (1999) Transmissible and genetic prion diseases share a common pathway of neurodegeneration. *Nature* 402(6763):822-826.
4. Prusiner SB (2001) Shattuck lecture--neurodegenerative diseases and prions. *N Engl J Med* 344(20):1516-1526.

5. Chakrabarti O, Ashok A, & Hegde RS (2009) Prion protein biosynthesis and its emerging role in neurodegeneration. *Trends Biochem Sci* 34(6):287-295.
6. Emerman AB, Zhang ZR, Chakrabarti O, & Hegde RS (2010) Compartment-restricted biotinylation reveals novel features of prion protein metabolism in vivo. *Mol Biol Cell* 21(24):4325-4337.
7. Baskakov IV & Breydo L (2007) Converting the prion protein: what makes the protein infectious. *Biochim Biophys Acta* 1772(6):692-703.
8. Caughey BW*, et al.* (1991) Secondary structure analysis of the scrapie-associated protein PrP 27-30 in water by infrared spectroscopy. *Biochemistry* 30(31):7672-7680.
9. Colby DW*, et al.* (2009) Design and construction of diverse mammalian prion strains. *Proc Natl Acad Sci U S A* 106(48):20417-20422.
10. Gasset M*, et al.* (1992) Predicted alpha-helical regions of the prion protein when synthesized as peptides form amyloid. *Proc Natl Acad Sci U S A* 89(22):10940-10944.
11. McKinley MP*, et al.* (1991) Scrapie prion rod formation in vitro requires both detergent extraction and limited proteolysis. *J Virol* 65(3):1340-1351.
12. Meyer RK*, et al.* (1986) Separation and properties of cellular and scrapie prion proteins. *Proc Natl Acad Sci U S A* 83(8):2310-2314.
13. Oesch B*, et al.* (1985) A cellular gene encodes scrapie PrP 27-30 protein. *Cell* 40(4):735-746.
14. Pan KM*, et al.* (1993) Conversion of alpha-helices into beta-sheets features in the formation of the scrapie prion proteins. *Proc Natl Acad Sci U S A* 90(23):10962-10966.
15. Sigurdson CJ*, et al.* (2009) De novo generation of a transmissible spongiform encephalopathy by mouse transgenesis. *Proc Natl Acad Sci U S A* 106(1):304-309.
16. Canello T*, et al.* (2008) Methionine sulfoxides on PrPSc: a prion-specific covalent signature. *Biochemistry* 47(34):8866-8873.
17. Colombo G, Meli M, Morra G, Gabizon R, & Gasset M (2009) Methionine sulfoxides on prion protein Helix-3 switch on the alpha-fold destabilization required for conversion. *PLoS One* 4(1):e4296.
18. Stahl N*, et al.* (1993) Structural studies of the scrapie prion protein using mass spectrometry and amino acid sequencing. *Biochemistry* 32(8):1991-2002.
19. Wolschner C*, et al.* (2009) Design of anti- and pro-aggregation variants to assess the effects of methionine oxidation in human prion protein. *Proc Natl Acad Sci U S A* 106(19):7756-7761.
20. Requena JR & Levine RL (2001) Thioredoxin converts the Syrian hamster (29-231) recombinant prion protein to an insoluble form. *Free radical biology & medicine* 30(2):141-147.
21. Binger KJ, Griffin MD, & Howlett GJ (2008) Methionine oxidation inhibits assembly and promotes disassembly of apolipoprotein C-II amyloid fibrils. *Biochemistry* 47(38):10208-10217.
22. Moskovitz J*, et al.* (2001) Methionine sulfoxide reductase (MsrA) is a regulator of antioxidant defense and lifespan in mammals. *Proc Natl Acad Sci U S A* 98(23):12920-12925.
23. Makarava N*, et al.* (2011) Genesis of mammalian prions: from non-infectious amyloid fibrils to a transmissible prion disease. *PLoS Pathog* 7(12):e1002419.
24. Houghten RA & Li CH (1979) Reduction of sulfoxides in peptides and proteins. *Analytical biochemistry* 98(1):36-46.
25. Borchelt DR, Rogers M, Stahl N, Telling G, & Prusiner SB (1993) Release of the cellular prion protein from cultured cells after loss of its glycoinositol phospholipid anchor. *Glycobiology* 3(4):319-329.

26. Caughey B, Race RE, Ernst D, Buchmeier MJ, & Chesebro B (1989) Prion protein biosynthesis in scrapie-infected and uninfected neuroblastoma cells. *J Virol* 63(1):175-181.
27. Gabizon R*, et al.* (1996) Insoluble wild-type and protease-resistant mutant prion protein in brains of patients with inherited prion disease. *Nat Med* 2(1):59-64.
28. Oien DB*, et al.* (2009) Detection of oxidized methionine in selected proteins, cellular extracts and blood serums by novel anti-methionine sulfoxide antibodies. *Arch Biochem Biophys* 485(1):35-40.
29. Swietnicki W, Petersen RB, Gambetti P, & Surewicz WK (1998) Familial mutations and the thermodynamic stability of the recombinant human prion protein. *J Biol Chem* 273(47):31048-31052.
30. Zhang Y, Swietnicki W, Zagorski MG, Surewicz WK, & Sonnichsen FD (2000) Solution structure of the E200K variant of human prion protein. Implications for the mechanism of pathogenesis in familial prion diseases. *J Biol Chem* 275(43):33650-33654.
31. Ostapchenko VG, Makarava N, Savtchenko R, & Baskakov IV (2008) The polybasic N-terminal region of the prion protein controls the physical properties of both the cellular and fibrillar forms of PrP. *J Mol Biol* 383(5):1210-1224.
32. Kelly JW (1998) The alternative conformations of amyloidogenic proteins and their multi-step assembly pathways. *Current opinion in structural biology* 8(1):101-106.
33. Nelson R & Eisenberg D (2006) Structural models of amyloid-like fibrils. *Advances in protein chemistry* 73:235-282.
34. Jahn TR, Parker MJ, Homans SW, & Radford SE (2006) Amyloid formation under physiological conditions proceeds via a native-like folding intermediate. *Nat Struct Mol Biol* 13(3):195-201.
35. LeVine H, 3rd (1993) Thioflavine T interaction with synthetic Alzheimer's disease beta-amyloid peptides: detection of amyloid aggregation in solution. *Protein Sci* 2(3):404-410.
36. Ostapchenko VG*, et al.* (2010) Two amyloid States of the prion protein display significantly different folding patterns. *J Mol Biol* 400(4):908-921.
37. Lisa S*, et al.* (2010) The structural intolerance of the PrP alpha-fold for polar substitution of the helix-3 methionines. *Cellular and molecular life sciences : CMLS* 67(16):2825-2838.
38. Riemer J, Bulleid N, & Herrmann JM (2009) Disulfide formation in the ER and mitochondria: two solutions to a common process. *Science* 324(5932):1284-1287.
39. Tabrett CA*, et al.* (2010) Changing the solvent accessibility of the prion protein disulfide bond markedly influences its trafficking and effect on cell function. *Biochem J* 428(2):169-182.
40. Adrover M*, et al.* (2010) Prion fibrillization is mediated by a native structural element that comprises helices H2 and H3. *J Biol Chem* 285(27):21004-21012.
41. Capellari S*, et al.* (1999) Prion protein glycosylation is sensitive to redox change. *J Biol Chem* 274(49):34846-34850.
42. Lee S & Eisenberg D (2003) Seeded conversion of recombinant prion protein to a disulfide-bonded oligomer by a reduction-oxidation process. *Nat Struct Biol* 10(9):725-730.
43. Yanai A, Meiner Z, Gahali I, Gabizon R, & Taraboulos A (1999) Subcellular trafficking abnormalities of a prion protein with a disrupted disulfide loop. *FEBS Lett* 460(1):11-16.